Structural evolution of the Taiwan fold-and-thrust belt gleaned from balanced cross sections and tectono-metamorphic studies in the Central Range

Dissertation

zur Erlangung des akademischen Grades doctor rerum naturalium

(Dr. rer. nat.)

vorgelegt dem Rat der Chemisch-Geowissenschaftlichen Fakultät der

Friedrich-Schiller-Universität Jena

von M.Sc. Yiqiong Zhang

geboren am 29.12.1990 in Xinjiang

Gutachter:

1. Prof. Dr. Kamil Ustaszewski, Friedrich-Schiller-Universität Jena
2. Prof. Dr. Nikolaus Froitzheim, Rheinische Friedrich-Wilhelms-Universität Bonn

Tag der öffentlichen Verteidigung: 13.01.2021

Zusammenfassung

Taiwan liegt entlang einer aktiven Plattengrenze zwischen der Eurasischen Platte und der Philippinischen Platte, wobei die Konvergenzrate bei etwa 80 mm/a liegt. Die anhaltende Konvergenz führt zu einer fortschreitenden Gebirgsbildung, die eine besonders komplexe Struktur aufweist. Diese Studie konzentriert sich hauptsächlich auf die strukturelle und tektonische Entwicklung des taiwanesischen Gebirgsgürtels und seines östlichen metamorphen Yuli Belt. Die Analysen und Ergebnisse in den Kapiteln 2, 3 und 4 sind im Folgenden zusammengefasst:

Die Arbeit dokumentiert die inneren strukturellen Geometrien des taiwanesischen Berggürtels sowie paläogeographische Rekonstruktionen des Eurasischen Kontinentalrands. Auf Grundlage der Ergebnisse regionaler Kartierungen und Strukturanalysen wurden drei krustenmaßstäbliche geologische Profilschnitte in verschiedenen Breiten des taiwanesischen Gebirgszuges erstellt. Die Grenzflächen zwischen Kruste und Mantel wurden auf Basis eines kürzlich erstellten 3D-Modells unter Verwendung seismologischer Daten berücksichtigt. Das im Tananao-Komplex aufgeschlossene Grundgebirge umfasst zwei Einschaltungen aus vorrangig Eurasischem Grundgebirge (Tailuko- und Yuli- Belt), die auf die känozoischen Einheiten des passiven Kontinentalrandes aufgeschoben wurden und ihrerseits tektonisch von der aus der oberen Platte stammenden sogenannten Coastal Range überlagert werden. Die Bilanzierung der Profilschnitte ergibt eine Verkürzung in den Einheiten des passiven Eurasischen Kontinentalrandes von mindestens 120 km, wobei etwa 50% des Grundgebirges, auf dem das akkretierte Material lagerte, bereits unter die Philippinische Platte subduziert wurde.

Die Dissertation befasst sich mit dem seit langem bestehenden Problem der strukturellen Geometrien und der Kinematik der tektonischen Kontakte des Yuli Belts zu den angrenzenden Einheiten. Der Yuli Belt ist im Retro-wedge des östlichen Teils des taiwanesischen Orogens aufgeschlossen. Er beinhaltet Bruchstücke einer heterogenen Einheit aus Blauschiefer-faziellen Gesteinen, die von einer stark deformierten metasedimentären Einheit mit niedrigerem Metamorphosegrad umgeben sind. Feldarbeit und mikrostrukturelle Analysen weisen auf drei Deformationsphasen im Yuli Belt hin. Auf der Grundlage von Profilschnitten und einer Überprüfung der verfügbaren P-T-t-Daten gehen wir davon aus, dass während einer ersten Deformationsphase D1 Blauschiefer-fazielle Einheiten auf niedriggradigere, Grünschiefer-

fazielle metasedimentäre Einheiten geschoben wurden. Diese Anordnung wurde später während einer zweiten Deformationsphase D2 über den zu Eurasien gehörenden Tailuko Belt entlang der Shoufeng-Verwerfung geschoben, was W-tauchende Streckungslineare auf störungsparallelen Foliationsebenen zeigen. D3 erzeugte E-vergente Falten mit W- bis NW-abtauchenden Faltenachsenebenen, die frühere Foliationen sowie den D1-Deckenkontakt verfalteten. Diese E-vergente Faltung könnte mit dem entlang der Shoufeng-Verwerfung beobachteten Top-E-Rückschub zusammenhängen, der die Umorientierung von einem anfänglich E-tauchenden zu einem gegenwärtig W-tauchenden Kontakt mit sich brachte. Auf Basis geochemischer Gesamtgesteinsanalysen stellt die Blauschiefer-fazielle Einheit des Yuli Belts ein mittelmiozänes Fragment der ozeanischen Kruste und des Mantels dar, das im Südchinesischen Meer entstanden ist. Der Yuli Belt könnte daher als Teil der Sutur zwischen der Eurasischen und der Philippinischen Platte betrachtet werden.

Die Deformation des Yuli Belt und der südwestlich angrenzenden Einheit, der Chulai Formation, im östlichen Zentralbereich von Taiwan wurde ebenfalls untersucht. Metamorphe Maximaltemperaturen in beiden Einheiten basierend auf Raman-spektroskopischer Geothermometrie in Verbindung mit Strukturanalysen zeigen, dass der Yuli Belt Temperaturen von ca. 400-550 °C über denen der angrenzenden Einheiten aufweist. Temperaturen > 500 °C im Yuli Belt liegen in der Nähe von drei tektonischen Hochdruckblöcken. Der Temperaturunterschied zwischen dem Yuli Belt und der Chulai-Formation erreicht über 100 °C. Es ist wahrscheinlich, dass beide Einheiten Störungsgebunden sind und dass sie nach der E-vergenten Rückfaltungsphase die gleiche Verformungsgeschichte durchlaufen haben.

Summary

Taiwan is situated along an active plate boundary between the Eurasian Plate and the Philippine Sea Plate, with a convergence rate at about 80 mm/yr. The convergence results in an ongoing mountain building that displays a structure particularly complex. This dissertation mainly focuses on the structural and tectonic evolution of the Taiwan fold-and-thrust belt and its eastern metamorphic Yuli Belt in the Central Range. The study involves geological mapping, cross-section construction and balancing, whole-rock geochemistry analysis, Raman spectroscopic geothermometry, and palaeogeographic reconstructions. Analyses and results in Chapters 2, 3, and 4 are summarized below.

Chapters 2: This work documents the internal structural geometries of the Taiwan fold-and-thrust belt and palaeogeographic reconstructions of the Eurasian margin. Three crustal-scale geological cross-sections at various latitudes of the Taiwan fold-and-thrust belt were constructed, based on results from regional mapping and structure analysis. The crust-mantle interfaces were constrained by seismological data. We interpreted three basal thrusts, namely the Pilu Tunnel Thrust (PTT), the Infra-Pilu Tunnel Thrust (IPT), and the Shoufeng Fault (SFF), which are inversion of Eurasian deep-seated rift-related extensional faults, separating the three basement imbricates. The largely Eurasian basement overthrust the Cenozoic passive margin series and which are, in turn, tectonically overlain by the upper-plate-derived Coastal Range series. The restoration of cross sections yields a minimum shortening of ca. 120 km in the Eurasian passive margin series, with about 50% of the basement, on top of which the accreted material was initially sitting, already subducted below the Philippine Sea Plate. In the paleogeographic maps, the Eurasian passive margin likely formed a slightly eastward-convex salient prior to plate convergence that created the Taiwan orogen.

Chapters 3: The thesis addresses long-standing problems of the structural geometries and kinematics of the Yuli Belt's tectonic contacts with its adjacent units. The Yuli Belt exposed is in the retro-wedge of the eastern part of the Taiwan Central Range. It hosts slivers of a heterogeneous unit of blueschist-facies metamorphic rocks that are surrounded by an intensely deformed metasedimentary unit of lower metamorphic grade. Fieldwork and microstructural analyses indicate three deformation phases in the Yuli Belt. Based on cross sections and a review of available P-T-t data, we suggest that blueschist-facies units were emplaced on top of the Yuli Belt metasedimentary unit along a thrust during a first deformation phase D1. This

assembly was later thrust over the Eurasian-derived Tailuko Belt along the Shoufeng Fault during D2, as suggested by W-plunging stretching lineations on fault-parallel foliation planes. D3 produced E-vergent folds with W- to NW-dipping axial planes, refolding earlier foliations as well as the D1 nappe contact. This E-vergent folding could be related to top-E backthrusting observed along the Shoufeng Fault, involving its reorientation from an initially E-dipping to a presently W-dipping contact. On the basis of the whole-rock geochemical data with MORB affinity, the blueschist-facies metamorphic unit of the Yuli Belt likely represents a mid-Miocene fragment formed in the South China Sea. The Yuli Belt hence could be considered as part of the suture between the Eurasian and the Philippine Sea plates.

Chapters 4: The deformation of the Yuli Belt and its southwesterly adjacent unit, the Chulai Formation, in the eastern Taiwan Central Range was also investigated. New estimates of peak metamorphic temperatures in both units using Raman spectroscopic geothermometry in relation to structural analyses show that the Yuli Belt metasedimentary unit experienced temperatures of ca. 400–550 °C higher than those of adjacent units (the Tailuko belt and the Chulai Formation). Temperatures > 500 °C in the Yuli Belt metasediments are close to three tectonic blocks that are characterized by high-pressure metamorphism. The temperature difference between the Yuli Belt and Chulai Formation reaches more than 100 °C, indicating the contact between these two units chould be a fault. The Yuli Belt schist has experienced greenschist to amphibolite facies metamorphism at deeper levels, with higher estimated temperatures than the phyllitic Chulai Formation. On the basis of surface structural data and RSCM data, we interpreted an overall synformal structural position of the Yuli Belt with respect to the easterly and westerly adjacent units. This synformal geometry is likely as results of E-vergent backfolding of the Taiwan Central Range.

Contents

List of figures

Chapter 1

General Introduction

Chapter 2

Cross section balancing across the Taiwan fold-and-thrust belt for improving palaeogeographic reconstructions of the Eurasian passive margin

Chapter 3

The Yuli Belt in Taiwan: part of the suture zone separating Eurasian and Philippine Sea plates

Chapter 4

Thermal evolution of the metamorphism in the eastern Taiwan: implications for blueschist exhumation

List of tables

Chapter 1

General Introduction

1.1 Tectonic setting

Collision between oceanic island-arc terranes and passive continental margins (i.e., arc-continent collision) has been one of the most important tectonic processes in the formation of mountain belts throughout much of Earth's history (e.g., Condie, 1989; Brown and Ryan, 2011). During arc-continent collision, volcanic arcs are obducted onto continents, creating ophiolites, which are preserved along suture zones and mark the position of former oceans (e.g., Gansser, 1980; Condie, 2016). Situated in an active arc-continent collision, the Taiwan orogen is among the most studied orogens and is well known for its active and oblique collision between the Luzon Arc and the Eurasian continental margin (Figs. 1-1) (e.g., Biq, 1971; Barrier and Muller, 1984; Suppe, 1984a; Angelier, 1986; Malavieille at al., 2002). Two plates are involved in the complex tectonic setting that surrounds the Taiwan orogen (Figs. 1-1, 1-2, 1-3, 1-4): the Philippine Sea Plate to the east and the Eurasian Plate to the west. Northeast of the Taiwan area,

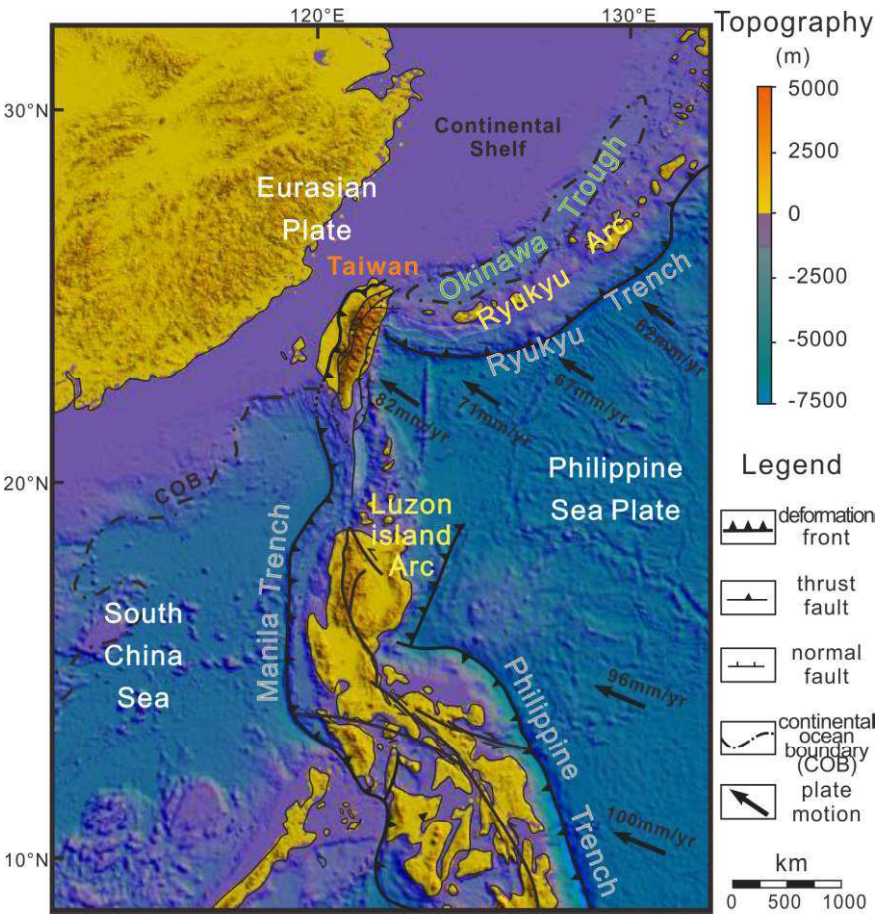

Fig. 1-1: Plate tectonic framework around the Taiwan-Luzon arc-continent collision. The Philippine Sea Plate moves towards the Eurasian Plate at a rate of ca. 60-90 mm/yr (e.g., Seno, 1977; Yu et al., 1997) and subducts underneath it along the Ryukyu trench. The South China Sea (part of Eurasian Plate) subducts beneath the Philippine Sea Plate along the Manila Trench.

the Philippine Sea Plate is being subducted beneath the Ryukyu arc which belongs to the Eurasian continental margin. The Okinawa backarc basin of the Ryukyu arc is developed to the north (e.g., Letouzey and Kimura, 1985) and is associated with extension and recent volcanism (e.g., Sibuet et al., 1999). South of the Taiwan island, the oceanic lithosphere of the South China Sea subducts beneath the Philippine Sea Plate, inducing the volcanism of the Luzon arc (e.g., Chen et al., 1992; Yang et al., 1995). The relative motion between the Philippine Sea Plate and the Eurasian Plate has resulted in the progressive subduction of the Chinese continental margin (Fig. 1-2) (Ustaszewski et al., 2012; Wu and Suppe, 2018), the development of the Taiwan orogen (Lee et al., 2015), and the major faults that accommodate the deformation (Wu et al., 2008b) (Fig. 1-3).

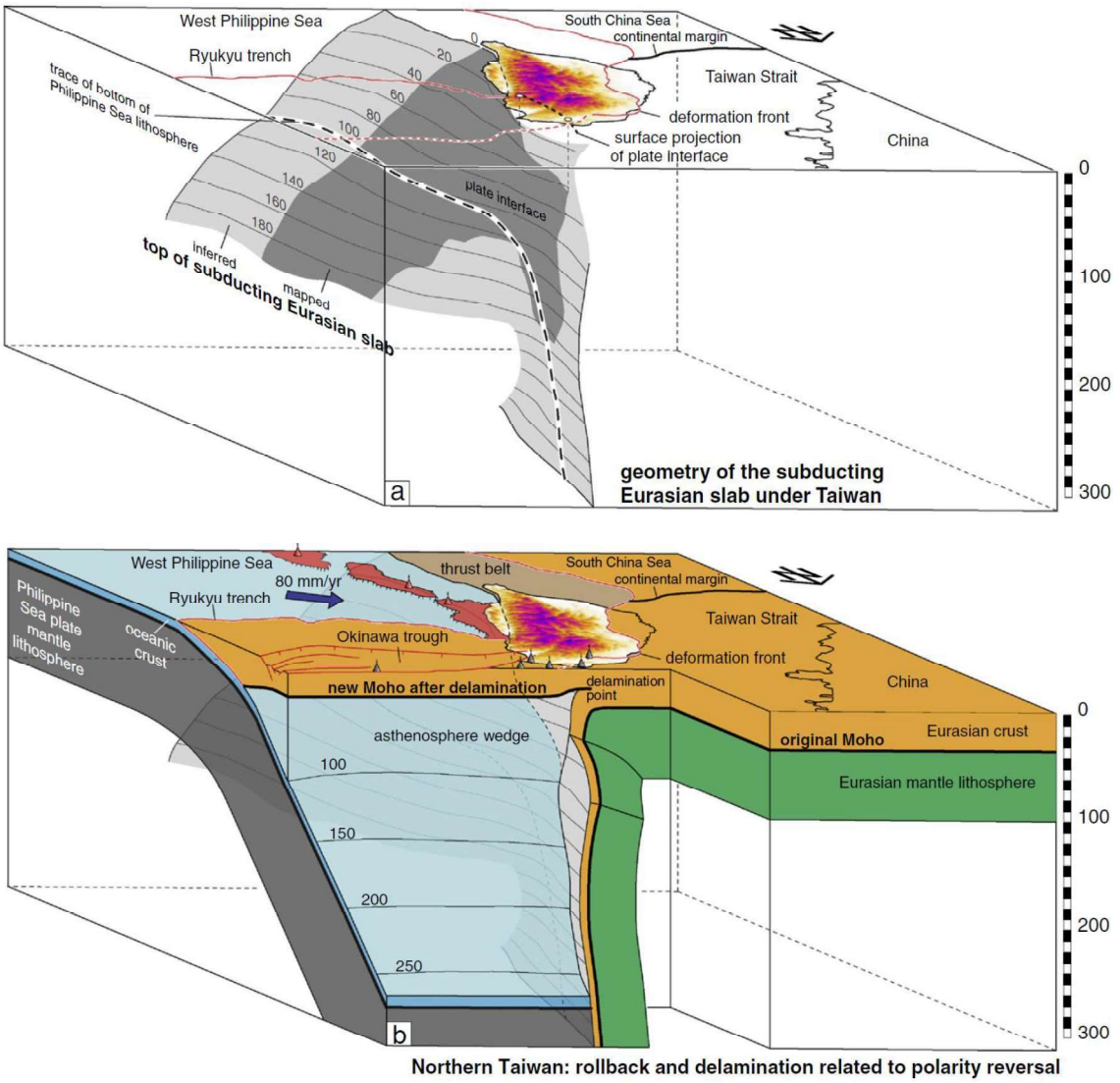

Fig. 1-2: Schematic lithosphere-scale block diagrams illustrating along-strike changes in the geometry of various crust–mantle boundaries under Taiwan (after Ustaszewski et al. 2012). Depth is given in km. (a) Geometry of the plate interface separating the Eurasian and Philippine Sea plates. The plate interface progressively steepens from south to north. (b) Section at the northern tip of Taiwan, illustrating the rollback and delamination of the subducting Eurasian lithosphere. This creates the space required for the Philippine Sea Plate to subduct northward. The deactivation of the deformation front occurs at the hinge of the subducting and delaminating Eurasian lithosphere.

The six roughly North-South oriented morpho-tectonic units of Taiwan are separated by major thrust/shear zones (Ho, 1986; Fig. 1-5). From west to east the provinces are the Coastal Plain, the Western Foothills, the Hsuehshan Range, the Backbone Slates, the Tananao Complex, and the Coastal Range. Taiwan is divided into two parts by the Longitudinal Valley Fault (LVF). West of the Longitudinal Valley Fault is the lithotectonic belts belonging to the Eurasian Plate.

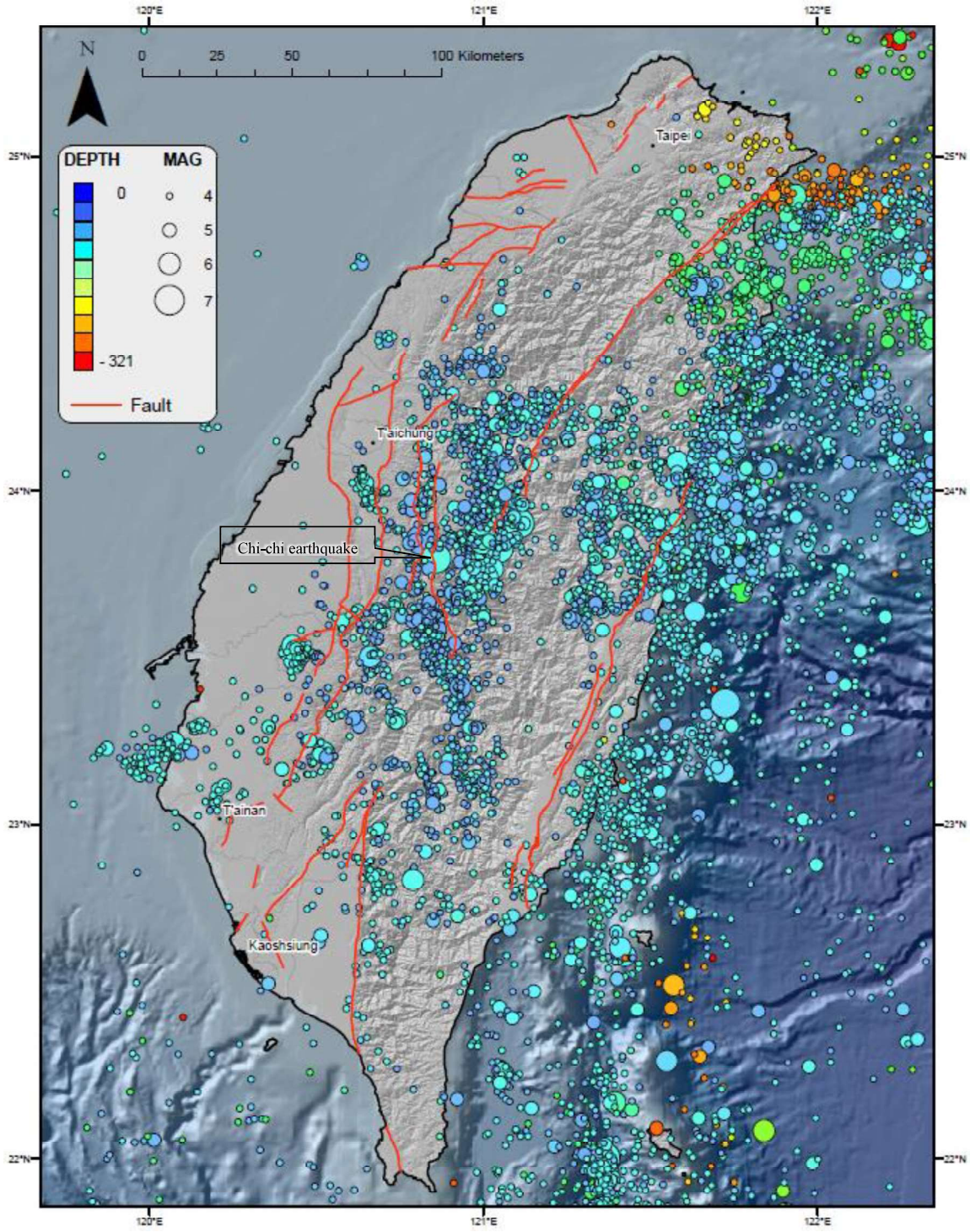

Fig. 1-3: Taiwan earthquakes in the year of 1991-2017 (modified after Lee et al., 2002; Wu et al., 2008a,b). The depth and magnitude of earthquakes are from the USGS and plotted in scale. Major faults are shown in red. They may be active and responsible for earthquakes in Taiwan or regional detachment faults exist at depth (e.g., Chang et al., 1998; Shyu et al., 2005).

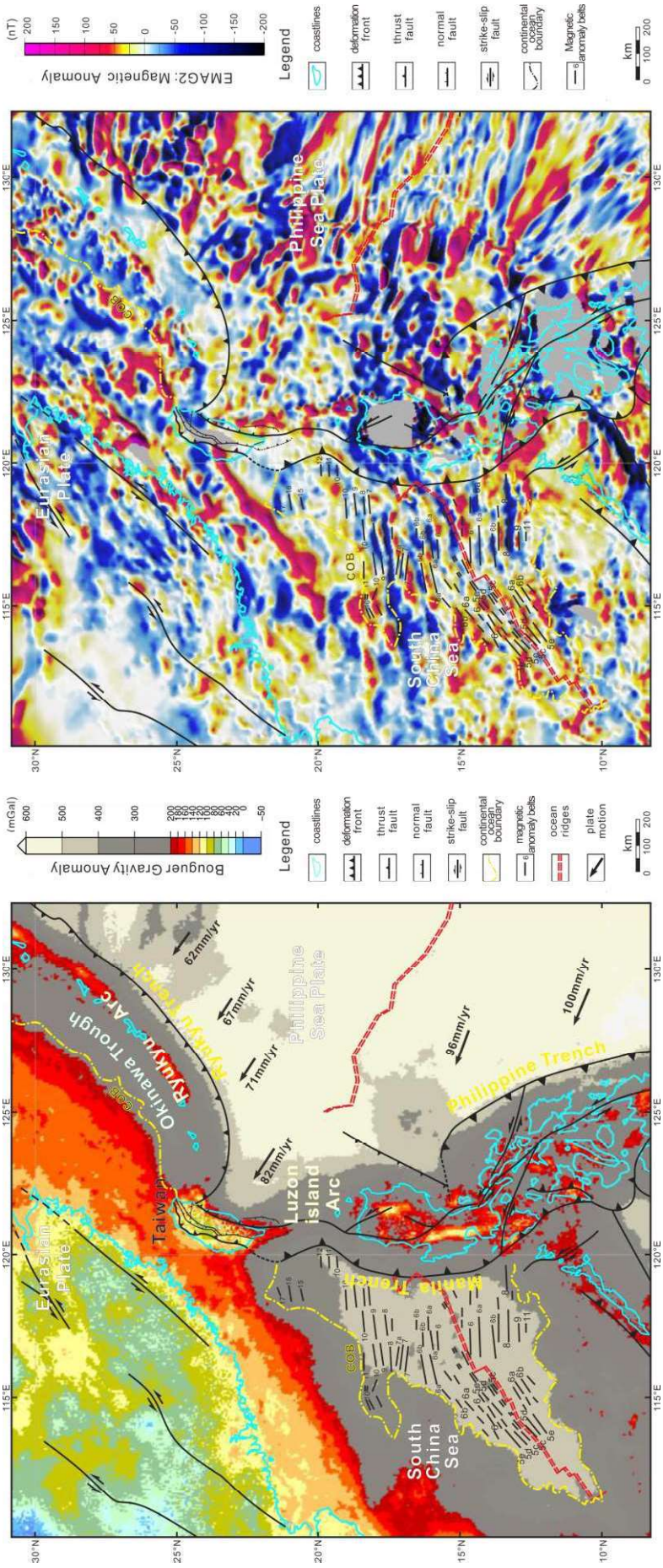

Fig. 1-4: Bouguer gravity anomaly map (left) and magnetic anomaly map (right) of Taiwan and its greater surroundings. Data sources: EMAG2 (Earth Magnetic Anomaly Grid in 2-arc-minute resolution; Wan, K., 2017; Briais et al., 1993) and World Gravity Map (WGM; Bowvalot et al., 2012).

East of the Longitudinal Valley Fault is the Coastal Range incorporating the accreted volcanic arc and belongs to the Philippine Sea Plate. The Taiwan mountain building process is very much alive and can be well illustrated by the rugged topography, rapid uplift and denudation, young tectonic landforms, active faulting, and numerous earthquakes (Fig. 1-3). The latest major earthquake is the devastating 1999 Chi-chi earthquake (Mw=7.6) with surface rupture of about 100 km in length that occurs primarily along the pre-existing Chelungpu Fault in the Western Foothills (e.g., Lee et al., 2002; Yue et al., 2005; Chapter 2, Fig. 2-6).

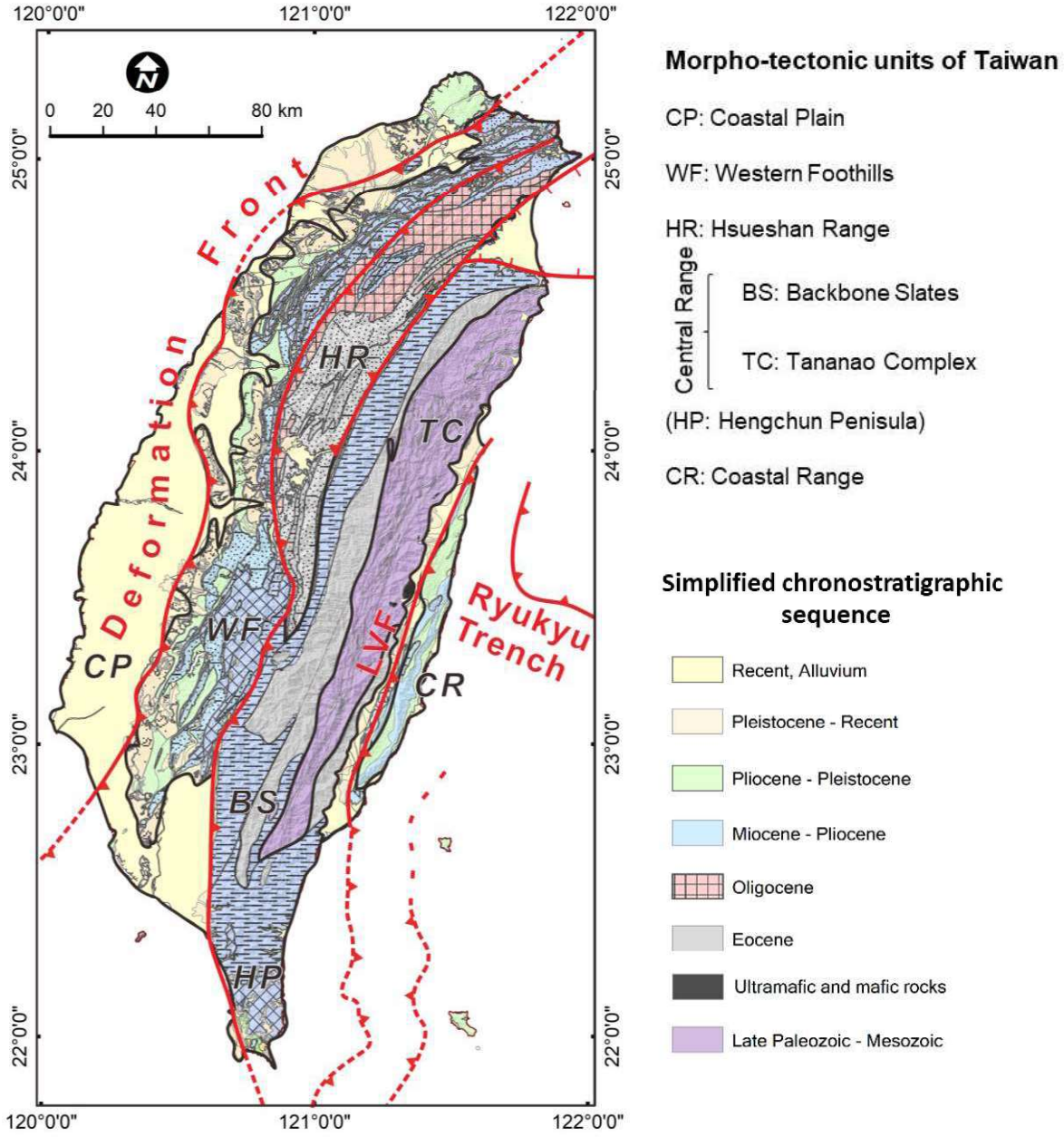

Fig. 1-5: Tectonic map of Taiwan (modified after Lin and Chen, 2016). Six morpho-tectonic units of Taiwan are labeled. The Tananao Complex (TC) is composed of the Tailuko Belt in the west and the Yuli Belt in the east. LVF: Longitudinal Valley Fault. See Appendix D for the GIS digital supplemental map.

Subduction of the Eurasian passive margin below the Philippine Sea Plate is believed to have started from the trailing edge of the Eurasian passive margin at its transition into the South China Sea. This gave rise to pressure-dominated metamorphism, relics of which are preserved in a tectonic mélange within in the Yuli Belt (e.g., Tsai et al., 1977; Angelier, 1986; Ustaszewski et al., 2012; Figs. 1-5, 1-6), yielding the so far youngest age for blueschists worldwide (5.1 ± 1.7 Ma; Sandmann et al., 2015). The Yuli Belt therefore is a key element in any reconstruction of the collision process of Taiwan (e.g., Zhang et al., 2020). It contains lithologically heterogeneous blueschist-facies rocks in what is referred to as tectonic or exotic blocks (e.g., Liou et al., 1977; Liou, 1981; Yui et al., 2012; Tsai et al., 2013). The high-pressure assemblages are surrounded by an intensely deformed metasedimentary unit of lower metamorphic grade metapelitic schists (e.g., Stanley et al. 1981).

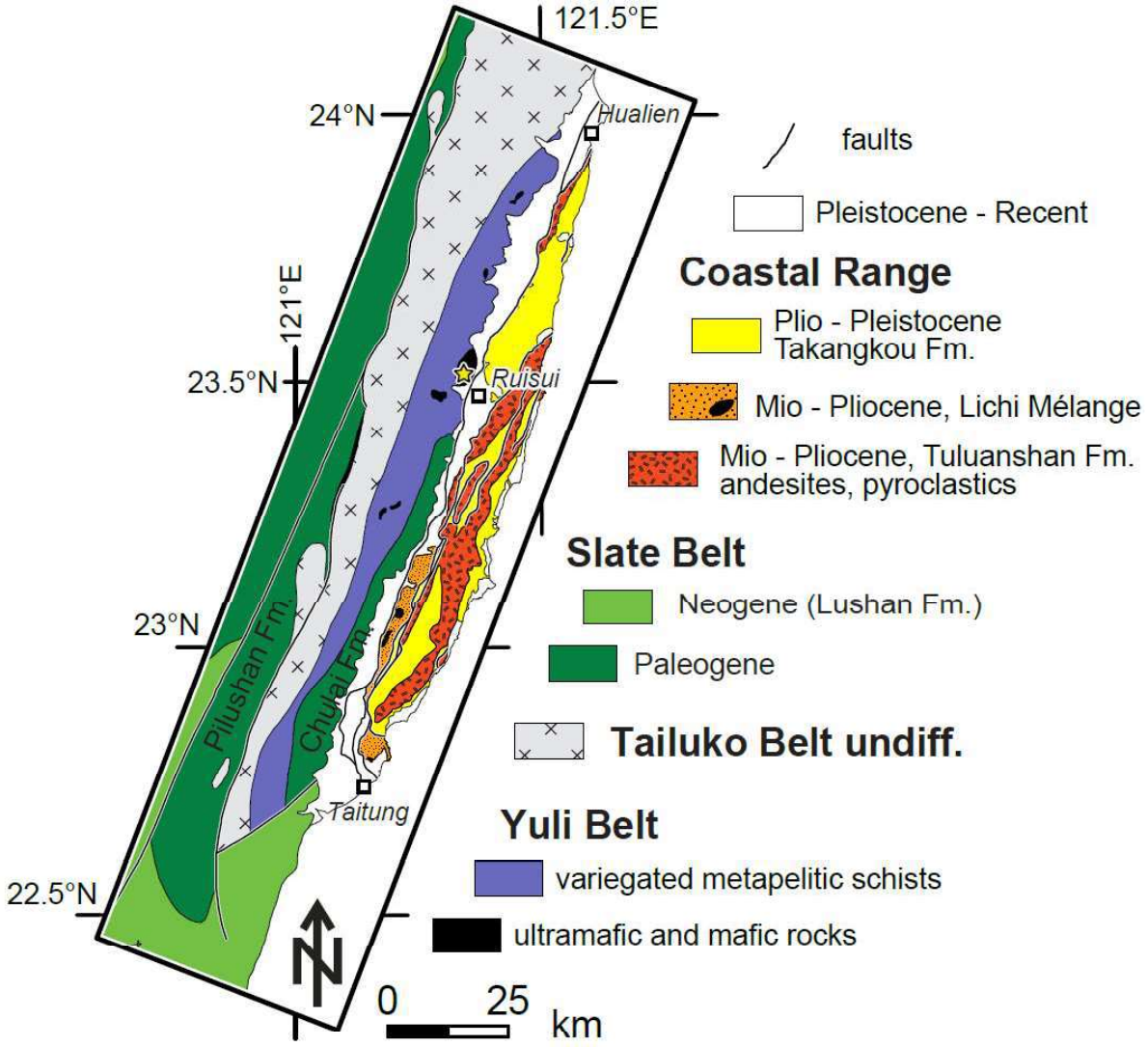

Fig. 1-6: Geological map of central eastern Taiwan showing the main lithological units within the Yuli Belt and adjacent units (modified after Ho, 1988; Sandmann et al., 2015). The Chulai Formation of the Backbone Slates is exposed in the eastern range adjacent to the Yuli Belt. The Lichi Mélange flanks the southernwestern borber of the Coastal Range, which is composed of accreted Luzon volcanic arc edifices and deformed allochthonous forearc sedimentary sequences (e.g., Huang et al., 2006).

1.2 Motivation

Owing to oblique convergence between the Eurasian passive margin and the Luzon island arc of the Philippine Sea Plate, spatial changes across this system can be viewed as a temporal evolution from intraoceanic to continental subduction and finally continent-arc collision (e.g., Biq, 1971; Chai, 1972; Suppe, 1981). The Taiwan orogen is therefore a natural laboratory for studying the structural, metamorphic, and thermal evolution of a collision mountain belt. My research aims to better understand improperly understood aspects of the Taiwan orogeny and accretion, subduction and collision processes. There are several important questions addressed in this study, outlined in the following.

(A) Structures of the internal orogen are only very cursorily known

The structures of the Taiwan mountain belt is often presented as an imbricate fold-and-thrust belt developed in a forward breaking sequence above a shallow, east dipping basal detachment (e.g., Suppe, 1980, 1984a; Carena et al. 2002; Yue et al., 2005; Malavieille and Trullenque, 2007). The abundant data for this structural interpretation come from surface geological observations, shallow reflection seismics, borehole data, upper-crustal geophysical studies, and modeling (e.g., Suppe, 1981; Namson 1983, 1984; Yue et al., 2005; McIntosh et al., 2005). Despite the advances that have been made on the basis of surface geology (e.g., Chen and Chuang, 1989; Brown et al. 2012), upper-crustal geophysical studies (e.g., McIntosh et al., 2005), and modeling (e.g., Malavieille et al., 2019), there is still great uncertainty about the detailed structural architecture of the orogen. The structures of the internal parts of the eastern Taiwan orogen exposing metamorphic basement in the so-called Tananao Complex (including Tailuko and Yuli schists belts) have not been treated in much detail (Stanley, 1981; Yang and Wang, 1985; Fisher et al., 1999, 2007; Ho and Lo, 2015), although the western part of the Taiwan fold-and-thrust belt has been well-documented (e.g., Suppe, 1981, 1984a; Namson 1983, 1984; Suppe 1986; Mouthereau et al., 2001; Huang et al., 2004; Yue et al., 2005; Yang et al., 2006, 2007). To our knowledge, even today there are no published geological cross-sections covering the entire Taiwan orogeny that depict the structures in the Central Range in greater detail.

(B) Numerous aspects of the tectonic evolution of the Yuli Belt remain unclear

(1) The kinematics of the Shoufeng Fault, the tectonic contact between the Yuli Belt and the westerly adjacent Tailuko unit are little investigated. Because of lithologic characteristics and geographic proximity, the Shoufeng Fault was previously suggested to tentatively correlate

with the Median Tectonic Line of southwestern Japan (Yen, 1963; Ernst and Jahn 1987; Fig. 1-6). Lin et al. (1984) described the Shoufeng Fault as an NNE-striking and 70°~80° W-dipping and topographically discernible feature, but no outcrop-scale faults were found. The recent geologic map published by Lin and Chen (2016) shows that the trace of the Shoufeng Fault has hardly been changed after Lin (1984) and Ho (1986). Chen et al. (2017) revised the fault trace ca. 60 km shorter in the south, but without providing clear arguments for this reinterpretation.

(2) The tectonic relationship between blueschist-facies units and metasedimentary rocks in the Yuli Belt is still largely uncertain. The collision of the Luzon arc with the Chinese passive margin in the Late Miocene–Early Pliocene (Ernst and Jahn, 1987; Lin et al., 2003; Mesalles et al., 2014) resulted in the exhumation of suites of differing lithologies including high-pressure mineral assemblages (Beyssac et al., 2008; Lin et al., 1984; Liou, 1981; Tsai et al., 2013; Yui and Lo, 1989). These suites have been interpreted as tectonic mélanges (Lin et al., 1984; Tsai et al., 2013). Alternatively, other researchers suggest that the tectonic blocks are allochthonous thrust sheets (Yang and Wang, 1985; Lin, 1999).

(3) Whole-rock geochemical data of the blueschist-facies assemblages yield partly intriguing results concerning the geodynamic environment in which the protoliths were formed (Island Arc or Mid Oceanic Ridge origin; e.g., Jahn et al. 1981).

(4) The tectonic relationship between the Yuli Belt high-pressure rocks and the East Taiwan Ophiolite is a matter of debate. Recent studies have contributed with a mid-Miocene protolith crystallisation age for the high-pressure metamafic blocks in the Yuli Belt (15.6 ± 0.3 Ma; Chen et al., 2017), suggesting very similar early Middle Miocene protolith ages as for the mafic rocks in the East Taiwan Ophiolite of the Lichi Mélange in the Coastal Range (14~17 Ma; Shao 2015; Hsieh et al. 2017; Huang et al. 2018; Lin et al. 2019; Fig. 1-6). As the Yuli Belt high-pressure rocks and the East Taiwan Ophiolite situated at two sides of the Longitudinal Valley Fault, the suture fault of Taiwan (Fig. 1-6), the question regarding the relationship between these two units remains.

(C) It is still debated if the Chulai Formation to the east is part of the Yuli Belt

The greenschist facies Chulai Formation of the Backbone Slates is exposed in the eastern range adjacent to the Yuli Belt (e.g., Chow and Lin, 1974; Stanley et al., 1981; Ho, 1986; Fig. 1-6). Geochronological studies on metasediments in both the Yuli Belt of the Tananao Complex (Chen et al., 2017) and its eastern adjacent Chulai Formation of the Backbone Slates (Mesalles et al., 2020) yield a youngest age peak at ca. 10-12 Ma. The two units present a stratigrpahically coherent sedimentary succession but different lithologies and maximum metamorphic

temperatures. How did the Yuli Belt and the Chulai Formation form and what is the relationship between them? Notably the nature of the depositional contact (i.e., nonconformity? angular unconformity? fault?) is critical to understand the timing of the initial stage of deformation in the Central Range.

1.3 Methodology

This dissertation presents the new interpretation of three crustal-scale cross sections of the fold-and-thrust belt across the entire island of Taiwan, providing quantitative estimates on the amount of shortening that the former passive margin of the South China Sea underwent prior to its involvement in arc-continent collision at about 4 to 6 Ma ago (e.g., Chang and Chi, 1983; Suppe, 1984a; Teng, 1990; **Chapter 2**). Besides, this dissertation reinvestigated the tectonic evolution of the Yuli Belt with particular emphasis on the structural relationships between its blueschist-facies rocks, the metasedimentary unit, the westerly adjacent Tailuko Belt, and the east adjacent Chulai Formation (**Chapters 3 and 4**). Analyses and methods are summarized in the following (Fig. 1-7).

(1) Meso- and Microscale structural analysis

Structural analyses of ductile fabrics include measuring the orientation of planar and linear fabrics in the field (foliations, cleavages, stretching and intersection lineations, fold axes and axial planes) in order to determine the orientation of the finite strain ellipsoid and to deduce the kinematics of the deformation (Simpson and Schmid, 1983). Polarized light microscopy on thin sections from oriented samples (Prior et al., 1987) provides information on additional kinematic information and the succession of deformational and metamorphic events (pre-, syn- and post-tectonic mineral growth; Misch, 1969). These techniques allow us to reconstruct the relative age, conditions and kinematics of deformation (Spry, 1969) of the Taiwan fold-and-thrust belt.

(2) Geological mapping and cross-sections

The cross sections, oriented perpendicular to the regional strike of structures (bedding, thrusts, and major fold traces), were constructed using standard construction techniques (e.g., Dahlstrom, 1969; Maltman, 1990; Groshong, 2006). The thicknesses of the formation were estimated from the surface geological map, and orientations of bedding and cleavage are projected into the subsurface using dip data measured along the section. Where possible, additional constraints were placed on the structure and the stratigraphic thicknesses from published borehole data (e.g., Yue et al., 2005), Vp tomography (e.g., Wang et al., 2006; Wu et al., 2008a), as well as reflection seismic profiles (e.g., Lee J.-C. et al. 2002). The dip data of geological units were taken from geological maps and projected into the cross sections.

(3) Balanced and restored cross sections

Balancing cross sections is the most useful strategy in the interpretation of fold-thrust belts (e.g., Dahlstrom, 1969; Mitra and Namsom, 1989; Mitra, 1992). All available data are constructed and analyzed to ensure they are geometrically possible and geologically admissible, given reasonable assumptions about the pre-deformation setting and how rocks behave during deformation in a particular tectonic environment (Groshong, 2006). This strategy allows us to directly compare the restored upper-crustal stratigraphy, paleo-environments, paleogeography and structures of the restored upper crust with the underlying crustal thickness of the unfolded tomography across the shelf-slope-rise transition. Data of the aforementioned methods were used here for subsequent interpretation and synthesised in map-view restorations of the Eurasian passive margin prior to arc-continent collision.

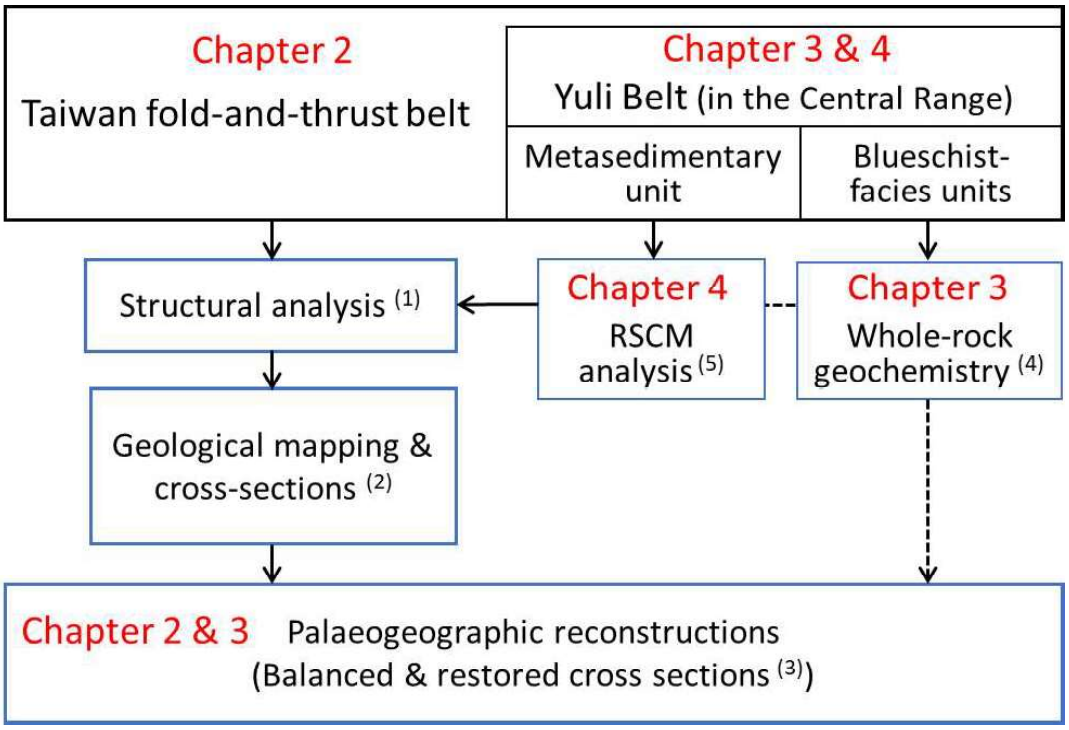

Fig. 1-7: Flow chart of research methodologies (labeled (1) ~ (5)) presented in this thesis. RSCM: Raman spectroscopy of carbonaceous material. See text for descriptions.

(4) Whole-rock geochemistry analysis

Whole-rock geochemical analyses (sixteen samples) were determined at the Institute of Geological Sciences at the Friedrich-Schiller University Jena. Major elements were determined by using ICP-OES (Inductively coupled plasma - optical emission spectrometry) after fusion with lithium borate flux. Trace elements, including the REE (rare earth elements), were analyzed by ICP-MS (Inductively coupled plasma mass spectrometry) with additional lithium

tetraborate fusion. The REE patterns and trace element compositions are essentially unaffected by metamorphism (e.g., Muecke et al., 1979; Spandler et al., 2003) in order to classify and identify the geochemical affinity and tectonic environment of the Yuli Belt high-pressure rocks. This facilitated our understanding of the modes of fore-arc subduction.

(5) Raman spectroscopy of carbonaceous material analysis

Raman spectroscopy on carbonaceous matter (RSCM) is being increasingly used as a quantitative geothermometer to estimate the maximum metamorphic temperature of the host sediments (e.g., Wopenka and Pasteris,1993; Yui et al., 1996; Beyssac et al., 2002; Lahfid et al., 2010; Henry et al. 2019). Some studies employing RSCM across the Tananao Schist complex (e.g., Beyssac et al., 2007; Kouketsu et al., 2019) have been published, but they did not systematically include the Yuli Belt. Sixteen black metapelites/phyllites samples were collected along selected transects in the Yuli Belt and the Chulai Formation of the eastern Taiwan Central Range. RSCM was used to quantify the degree of thermal alteration of carbonaceous matter within the metasediments.

Chapter 2

Cross section balancing across the Taiwan fold-and-thrust belt for improving palaeogeographic reconstructions of the Eurasian passive margin

This manuscript is in preparation for submission.
This study was funded by the Deutsche Forschungsgemeinschaft (DFG number 380155214; granted to K. Ustaszewski, Jena and N. Froitzheim, Bonn; “Cross section balancing across the Taiwan fold-and-thrust belt”).

Abstract:

Taiwan is located along an active plate boundary between the Eurasian and Philippine Sea Plates, with convergence rates amounting to about 80 mm/yr. The island has since long served as a cradle for many tectonic concepts. Yet, the internal parts of the Taiwan fold-and-thrust belt are still improperly understood in terms of fault kinematics, internal geometries and the amount of shortening they underwent since the onset of arc-continent collision in the Mio- to Pliocene. As a consequence, geometrical restorations of the Eurasian passive margin prior to continental subduction are often guesses rather than quantitative estimates. We constructed three new crustal-scale geological cross-sections at various latitudes of the Taiwan fold-and-thrust belt, on the basis of the surface geology and crust-mantle interfaces constrained from a 3D-model employing seismological data. We interpreted three basal thrusts, namely the Pilu Tunnel Thrust (PTT), the Infra-Pilu Tunnel Thrust (IPT), and the Shoufeng Fault (SFF), which are inversion of deep-seated rift-related extensional faults, separating the pre-Cenozoic basement imbricates. The three basement imbricates overthrust the Cenozoic passive margin series and which are, in turn, tectonically overlain by the upper-plate-derived Coastal Range series. The restoration of cross sections yields a minimum shortening of 120 km in the Eurasian passive margin series, with about 50% of the basement, on top of which the accreted material was initially sitting, already subducted below the Philippine Sea Plate. When put into paleogeographic maps, these findings imply that the Eurasian passive margin likely formed a slightly eastward-convex salient prior to plate convergence that created the Taiwan fold-and-thrust belt.

Keywords: Taiwan fold-thrust belt; crustal-scale geometry; Eurasian passive margin; subduction; palaeogeographic reconstruction

2.1 Introduction

Taiwan is located along an active plate boundary between the Eurasian and Philippine Sea Plates, which converge at about 80 mm/yr (e.g., Seno, 1977; Yu et al., 1997; Fig. 2-1). Taiwan's high-rising mountains have since long been inspiring for the development of modern ideas in structural geology, such as, e.g., the concepts of fault-related folding (Suppe and Namson, 1979), the consideration of fold-and-thrust belts as critically tapered wedges (Suppe, 1981), or links between tectonics and erosion (e.g., Willett et al., 2003; Dadson et al., 2003). Yet, the structures in the internal parts of the fold-and-thrust belt, involving the imbrication of the Eurasian distal passive margin, are still improperly understood in terms of their internal geometries and the amount of shortening they underwent since the Mio- to Pliocene. As a consequence, geometrical restorations of the Eurasian passive margin prior to continental subduction are at best educated guesses, but do not rely on quantitative estimates of thrust belt shortening (e.g., Lallemand et al., 2001; Sibuet and Hsu, 2004; Malavieille and Trullenque, 2007; von Hagke et al., 2016).

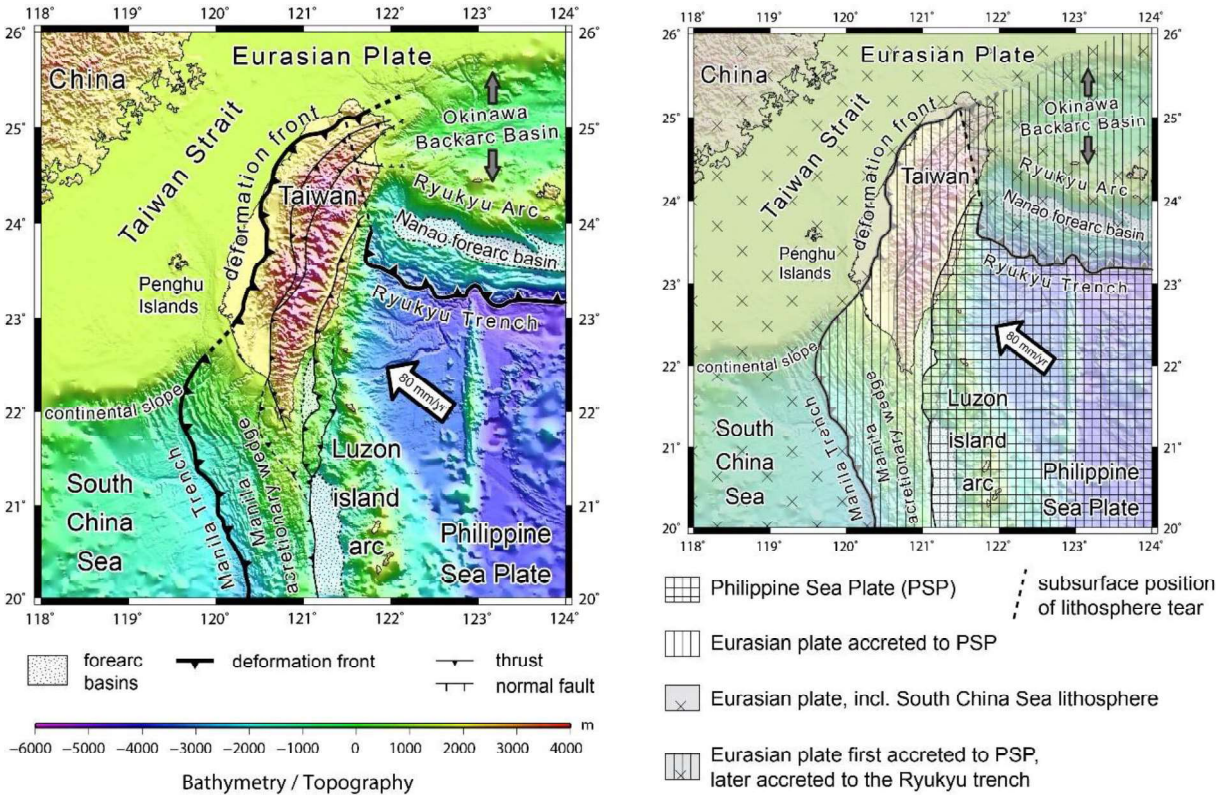

Fig. 2-1: Right: geotectonic setting around Taiwan (modified after Ustaszewski et al. (2012)). Note the progressive northward disappearance of the fore-arc basins west of the Luzon island arc. Left: plate tectonic framework around the Taiwan–Luzon arc-continent collision. The subsurface position of the lithosphere tear is taken from Ustaszewski et al. (2012). The Philippine Sea Plate is converging at a rate of ~80 mm/yr relative to Eurasia, with most of the shortening occurring within the width of the island of Taiwan (e.g., Yu et al., 1997).

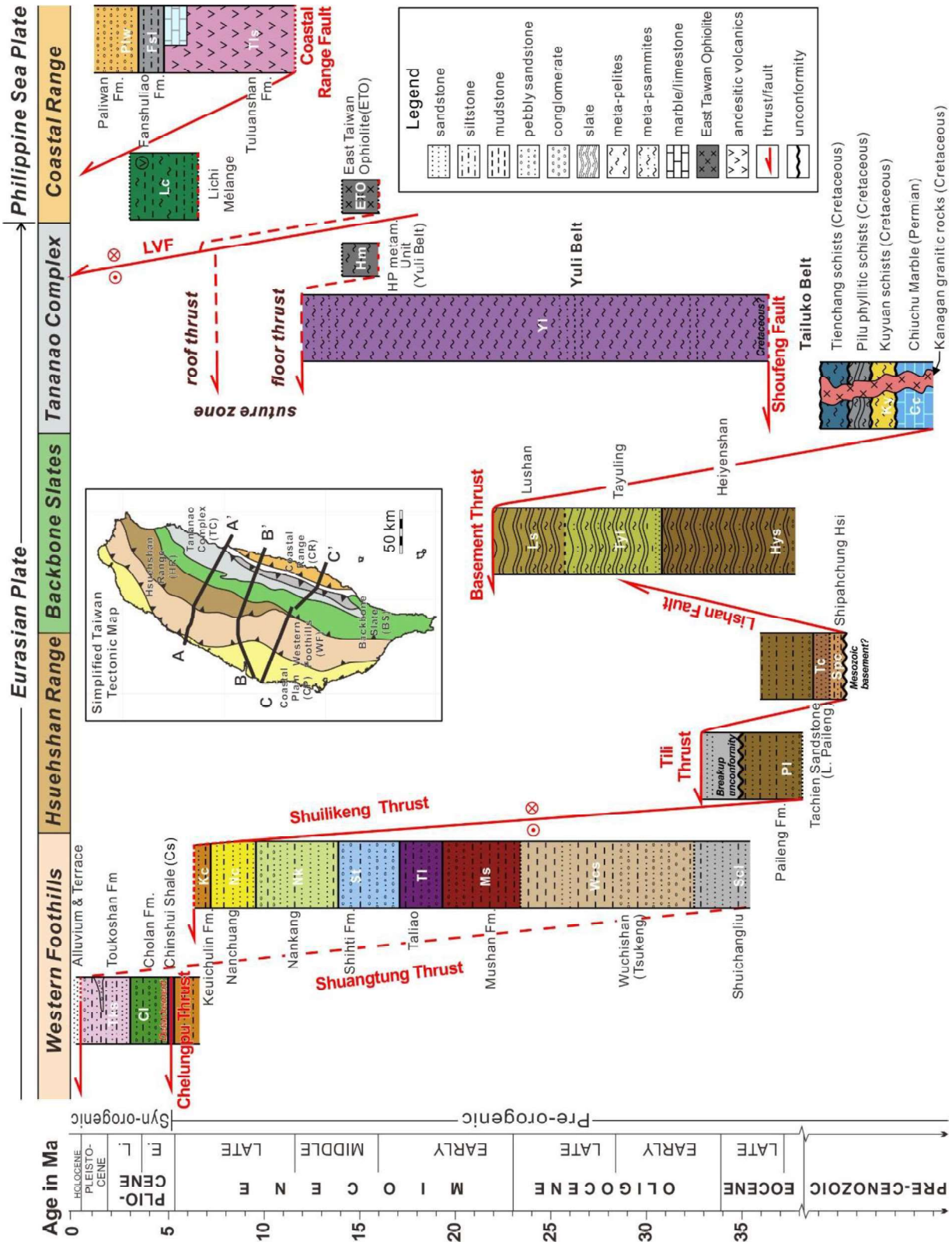

Fig. 2-2: Schematic tectonostratigraphic columns portraying the tectonic units shown in the cross section B-B' of this study (modified after Brown et al. (2012)). Vertical scale is according to the time. The solid lines of Formation are constrained by previous studies of seismic, borehole, paleontological and chronostratigraphic data (e.g., Yue et al., 2005; Brown et al., 2012; Chen et al., 2017; Huang et al., 2018, and references therein). The dashed lines and the Formation without borderlines indicate unknown information and are inferred based on the geological cross sections from this paper. We conceptually treat the blueschist-facies rocks of the Yuli Belt as occupying the position of part of the suture zone separating Eurasian and Philippine Sea plates, bound by a floor thrust and roof thrust. The Longitudinal Valley Fault possibly overprinted the earlier roof thrust. High-res images are enclosed in the supplement.

In spite of an almost overwhelming amount of published studies on the Taiwan tectonics, the knowledge of present-day crustal- to lithospheric-scale geometries (e.g., Ustaszewski et al., 2012; Brown et al., 2012; Biete et al., 2018), on the petrology (e.g., Wintsch et al., 2011; Tsai et al., 2013; Baziotis et al., 2016; Keyser et al. 2016) or the geochronological evolution of Taiwan (e.g., Simoes et al., 2012; Chen et al., 2017), the structures in the internal parts of the orogen exposing metamorphic basement in the so-called Tailuko and Yuli schists belts (Fig. 2-2), are only very cursorily known (Stanley, 1981; Fisher et al., 2007; Conand et al., 2020), particularly when compared with its well-documented westernmost part of the thrust belt (e.g., Suppe, 1980, 1984a,b, 1986; Namson 1983, 1984; Mouthereau et al., 2001; Huang et al., 2004; Yue et al., 2005; Yang et al., 2006, 2007). To our knowledge, there are no published geological cross-sections covering the entire Taiwan orogeny that depict the structures in the Central Range, the metamorphic core of Taiwan, in greater detail.

In this paper we build on this theme, presenting the results of new geological mapping of the fold-and-thrust belt across the entire Taiwan, providing quantitative estimates on the amount of shortening that the former passive margin of the South China Sea underwent prior to its involvement in arc-continent collision at about 4 to 6 Ma ago (Chang and Chi, 1983; Suppe, 1984a; Teng, 1990; Yu and Chou, 2001; Lin et al., 2003; Lee et al., 2015). We go on to propose how these areas of along-strike structural change can be related to the preexisting structure of the Eurasian continental margin.

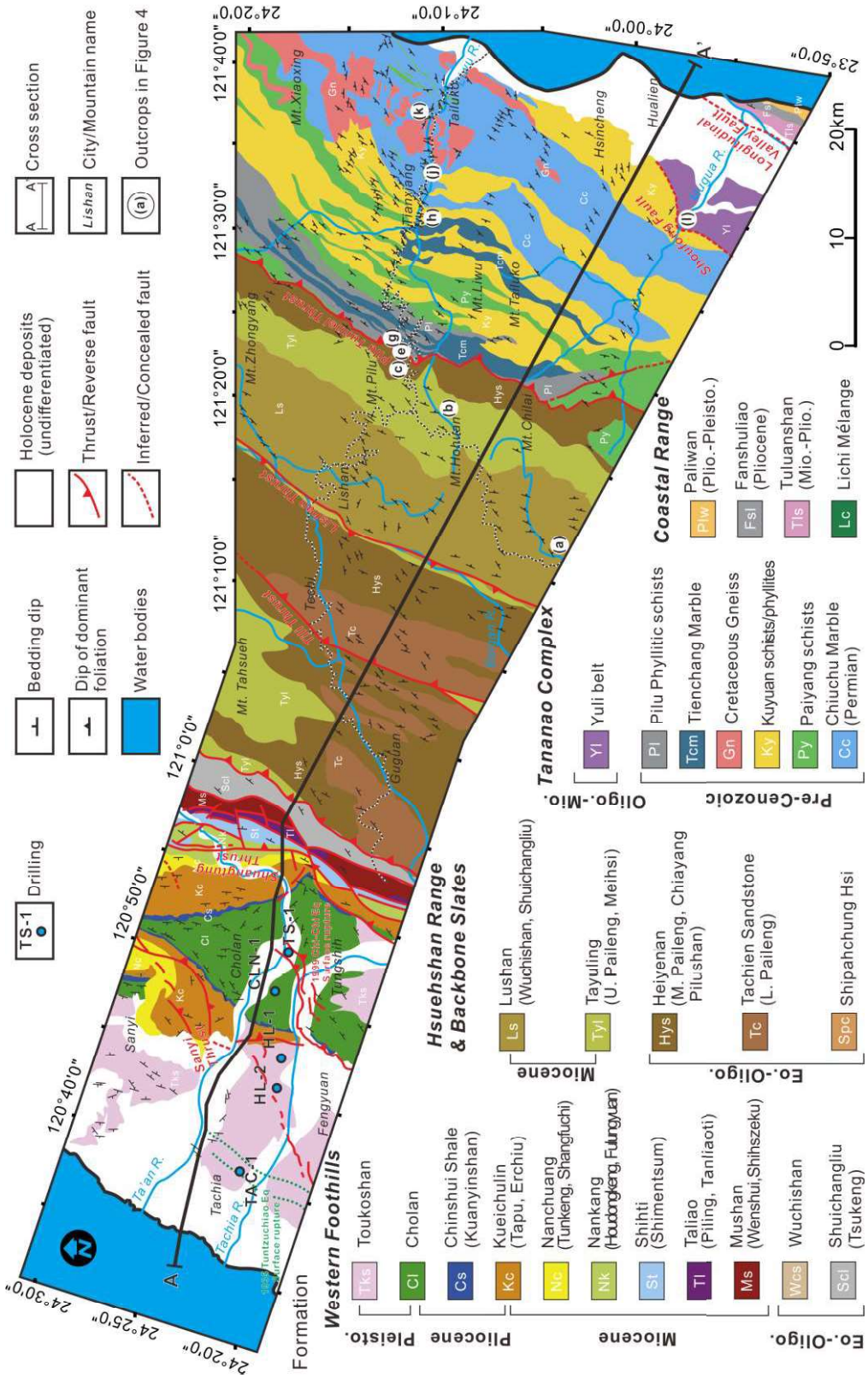

Fig. 2-3: Geological swath map across the Central Cross-island Highway of Taiwan (A-A'). The tectonic units from west to east are Coastal Plain, Western Foothills, Hsuehshan Range, Backbone Slates, Tananao Complex, and Coastal Range. Letters (a)-(l) show the localities of the outcrops in Fig.2-4 and measurements in Fig. 2-5. Roads of the Central Cross-island Highway are shown in the black-white dashed line. High-res images are enclosed in the supplement.

2.2 Regional geology

2.2.1 Plate tectonic setting

Tectonics in the Taiwan region is characterized by the two opposite subduction systems within two plates: the eastward subduction of the South China Sea oceanic crust (on the Eurasian Plate) beneath the Philippine Sea Plate along the N-S-trending the Manila Trench, and the northward subduction of the Philippine Sea Plate beneath the Eurasian Plate along the E-W-trending Ryukyu Trench (e.g., Suppe, 1984a; Fig. 2-1). The conversion from the passive into the active margin of the Eurasian continental margin was caused by an arc-continent collision (e.g., Wu et al., 2016; Chen W.S. at al., 2017). The Eurasian continental margin (trending N 60°E) is oblique to the N-oriented Luzon Arc, and the Philippine Sea Plate moves toward 310°-305°, hence the point of the diagonal arc-continent collision migrated southward (at the rate of 84 km/m.y.; Suppe, 1984a). The onset of the collision is constrained in the late Neogene, at ~4-6.5 Ma, based on records in the foreland and intra-arc basins (Chi et al., 1981; Lin et al., 2003). The exhumation and uplift of the central part of the range since ~5-6 Ma (Lee et al., 2015; Hsu et al., 2016; Chen et al., 2018; Chen et al., 2019). Successive phases of increased exhumation rates are deduced at 5, 2-1.5 and 0.5 Ma (Mesalles et al., 2014; Lee et al., 2015; Hsu et al., 2016). The punctuated growth of the Taiwan mountains possible reveals complex relationships between the accreted South China Sea margin, the accretion of the Luzon arc/forearc as well as changes in the erosion and plate kinematics.

2.2.2 Stratigraphy

The six roughly N-S oriented morpho-tectonic units of Taiwan are separated by major thrust/shear zones (Ho, 1986; Fig. 2-2). From west to east the provinces are the Coastal Plain, the Western Foothills, the Hsuehshan Range, the Backbone Slates, the Tananao Complex, and the Coastal Range. Taiwan is divided into two parts by the Longitudinal Valley Fault (LVF) (Fig. 2-2). West of the Longitudinal Valley Fault is the lithotectonic belts belonging to the Eurasian Plate. East of the Longitudinal Valley Fault is the Coastal Range incorporating the accreted volcanic arc and belongs to the Philippine Sea Plate. Below we give an overview of the outcropping stratigraphy in the morpho-tectonic units.

(1) Coastal Plain and Western Foothills

Seismic investigations over the offshore Taiwan Strait and the inland Coastal Plain show that there are Paleogene rifting basins bounded by normal faults (e.g., Huang C. Y. et al., 2000). The Coastal Plain consists of Quaternary uplifted but undeformed poorly consolidated sediments (Figs. 2-2, 2-3). The parautochthonous strata of the Western Foothills comprises Eocene through Miocene clastic sediments of the Eurasian platform margin and latest Miocene

to Pliocene through Holocene synorogenic sediments (e.g., Teng, 1992; Fig. 2-2). The Coastal Plain and Western Foothills expose a foreland basin sequence (Lin and Watts, 2002), which deformed into generally west-verging imbricate thrust sheets and folds (e.g., Suppe 1986; Ho, 1986; Figs. 2-6, 2-9, 2-13). Because of differences in the naming and discrimination of individual formations between the 1:50,000 geological maps in the study area (e.g., Appendix A- Fig. S4), in this study we suggest the eleven sequences of Western Foothills in the central Taiwan (Figs. 2-3, 2-8) and ten sequences in the southern Taiwan (Fig. 2-11).

(2) Hsuehshan Range and Backbone Slates

The stratigraphy of the Hsuehshan Range is primarily composed of argillite, slate and sandstone. The rocks in the Hsuehshan Range are assigned to the prehnite–pumpellyite metamorphic facies with an Eocene and Oligocene age (e.g., Ho, 1986; Teng et al., 1991; Chen and Wang, 1995). It is originated from eastward-deepening grabens on the outer part of the Chinese continental margin (Teng, 1990) and complicated by a complex structure and the almost complete lack of fossils (e.g., Chen C.-T. et al., 2011; Brown at al., 2012). The Backbone Slates comprises a metamorphosed Cenozoic sedimentary slate cover, i.e., Heiyenshan/Pilushan, Tayuling and Lushan formations (Figs. 2-2, 2-3, 2-4(a)~(f), 2-8, 2-11). It is bordered to the southeast by the Longitudinal Valley Fault, the suture fault between the accreted Luzon arc and the Eurasian Plate (e.g., Conand et al., 2020). To the west, the Lishan Fault separates it from the Hsuehshan Range (e.g., Lee et al., 1997). To the east, the Basement Fault (the Pilu Tunnel Thrust, in this study) separates it from the Tananao Complex (Figs. 2-2, 2-6, 2-9, 2-13). In this study, we propose a chronostratigraphic correlation that link different rock units and facies together on the basis of age. From our mapping and cross sections stratigraphic units of the Hsuehshan Range match to the present day Heiyenshan Formation in the Backbone Slates (e.g., Teng et al., 1991), and separated to its west by the Lishan Fault, an east vergent backthrust with little offsets (Clark et al., 1993; Lee et al., 1997; Brown at al., 2012).

(3) Tananao Complex

The geological history of the Tananao Complex can be traced back to the Paleozoic and involves multiple crustal basement deformation and metamorphism in the Mesozoic and Tertiary (Ernst and Jahn, 1987). In the western part, the Tananao Complex is exposed in several thrust sheets (Tailuko Belt) with the composition of pre-Cenozoic schist and marble (Figs. 2-2; 2-4(h)~(k)). A high-grade metamorphism of upper amphibolite facies coupled with granitoid intrusions occurred during 110 to 77 Ma (e.g., Jahn et al., 1986; Fig. 2-4(k)). This thermal event is generally correlated to the westward subduction of a paleo Pacific plate beneath the Asian continental margin (e.g., Liou, 1981; Ernst et al.,1981). The tectonic contact between the

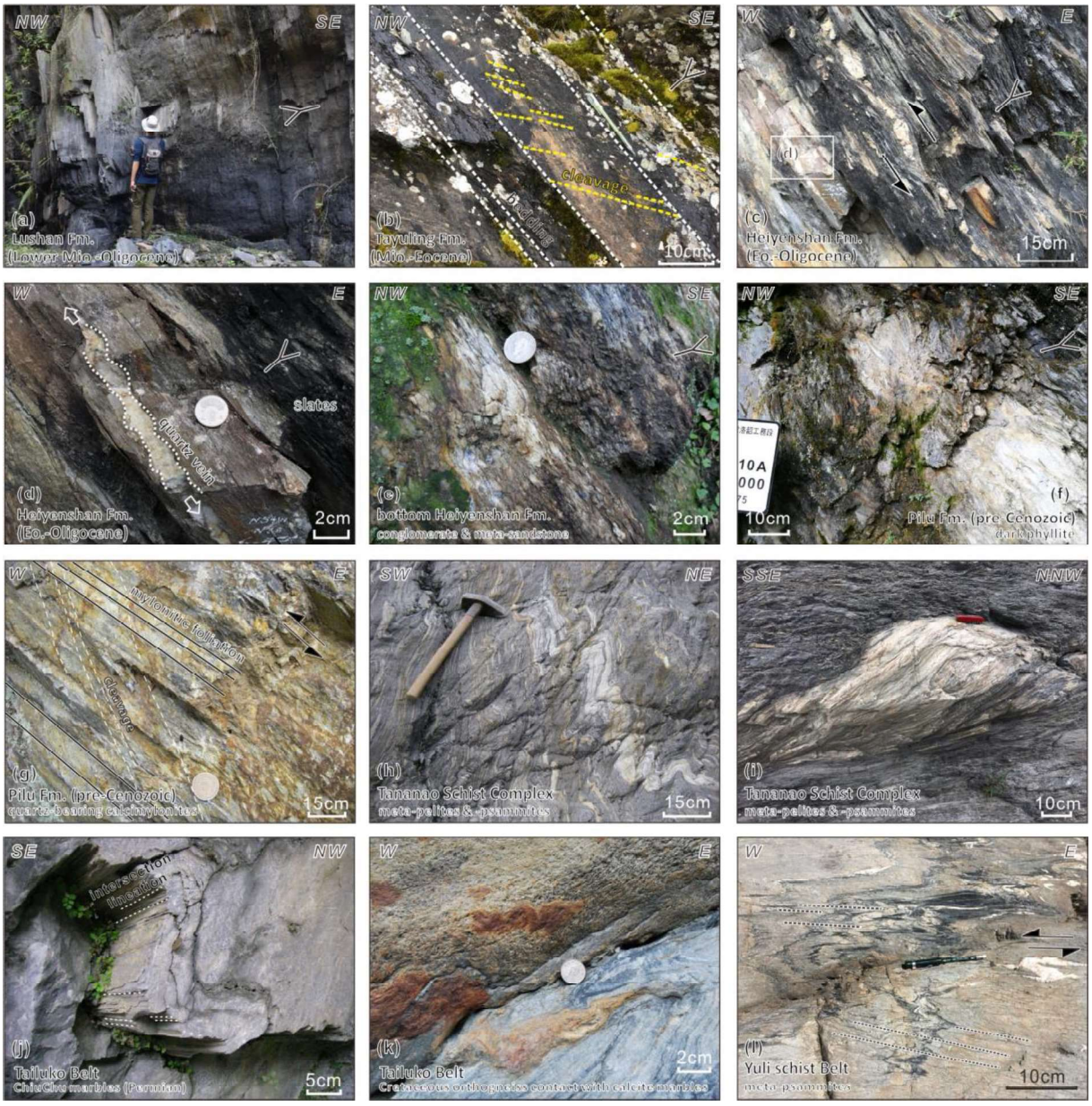
NW
SE
(a)
Lushan Fm.
(Lower Mio.-Oligocene)
Cleavage
Bedding
(b)
Tayuling Fm.
(Mio.-Eocene)
10cm
W
E
(d)
(c)
Heiyenshan Fm.
(Eo.-Oligocene)
15cm
slates
quartz vein
(d)
Heiyenshan Fm.
(Eo.-Oligocene)
2cm
(e)
bottom Heiyenshan Fm.
conglomerate & meta-sandstone
2cm
10A
000
10cm
(f)
Pilu Fm. (pre-Cenozoic)
dark phyllite
mylonitic foliation
Cleavage
(g)
Pilu Fm. (pre-Cenozoic)
quartz-bearing calcschist/meta-s
15cm
SW
NE
(h)
Tananao Schist Complex
meta-pelites & -psammites
15cm
SSE
NNW
(i)
Tananao Schist Complex
meta-pelites & -psammites
10cm
Intersection lineation
(j)
Tailuko Belt
ChinChu marbles (Permian)
5cm
(k)
Tailuko Belt
Cretaceous orthogneiss contact with calcite marbles
2cm
(l)
Yuli schist Belt
meta-psammites
10cm

Fig. 2-4: Outcrops across various tectonics units along the Central Cross Island Highway (transect A-A', Fig. 2-3) considered representative for map-scale structures. The symbol "Y" points stratigraphically young direction from top to bottom. High-res images are enclosed in the supplement.

(a) Steeply southeast-dipping alternations of low-grade slates and thin intercalations of sandstones in the Lushan Formation. Location: Northeast Puli town, 24.006239°N, 121.111208°E.

(b) Black, low-grade metamorphic slate in the Tayuling Formation in an overturned limb, as implied by bedding-cleavage relationships (bedding dips steeper than slaty cleavage). Location: Hehuanshan east peak, 24.188053°N, 121.343847°E.

(c) Quartz veins crosscutting bedding planes (108/67) in the Heiyenshan Formation, showing deformation structures indicative of top-to-the W shear. The plunge/trend of quartz stretching lineations in quartz layers is 123/40. Location: east Tayuling, 24.180594°N, 121.357468°E.

(d) An enlargement from the square box in (c). A pinch-and-swell structure in a quartz vein indicative of layer-parallel extension in the inverted limb.

(e) Quartz-rich conglomerate with elongated quartz aggregates in bottom Heiyenshan Formation, contacting east to pre-Cenozoic formation (f). The pebbles in the conglomerate are mostly quartz, chert and feldspar with up to 1cm size. Weak foliation developed due to pressure solution. The conglomerate layer indicates the clasts might be transported from an area of high relief of a rifted continental margin. The dip direction/angle of dominant foliation is 165/51 (S1) and the plunge/trend of the elongated quartz is 155/50. Location: road bends near Bilu tunnel, 24.179117°N, 121.365897°E.

(f) Strongly foliated slaty cleavage in dark phyllites of the pre-Cenozoic Pilu Formation, marking the Pilu Tunnel Thrust. Location: road bends at east Bilu tunnel, 24.179117°N, 121.365897°E.

(g) The east-facing refolding metamorphic foliation (slaty cleavage, S1) of quartzite and sericite mylonites in the pre-Cenozoic Pilu Formation. The dip direction/angle of dominant foliation is 134/18 and the dip direction/angle of cleavage layer is 164/56. Location: road bends at west Bilu tunnel, 24.177321°N, 121.372440°E.

(h) and (i) Meta-pelites and quartzose metasandstones in the Tailuko Belt. Note how the pronounced compositional layering (S2) and stretching lineations are affected by D2 E-facing backfolding. Location: Tianxiang gorge, 24.181728°N, 121.496292°E.

(j) Refolded compositional layering (S2) of Chiuchu massive calcite marbles in the Tailuko Belt. The intersection lineations of S1 and S2 foliations are highlighted in dashed line, with plunge/trend of 217/02. Location: road bends at Lushui, 24.181068°N, 121.508318°E.

(k) The irregular contact between Chiuchu calcite marble (right) to Kanagan orthogneiss (left) in the Tailuko Belt. Marble and schist enclaves are commonly observed within the granitic rocks, suggesting intrusion into the Chiuchu Formations. Location: near Xipan, 24.170258°N, 121.578786°E.

(l) Veined meta-pelitic schists and metasandstones in the Yuli Belt affected by D2 refolding. The crenulation cleavage compositional layering (S2) are commonly observed. Location: Shoufong River, 23.837992°N, 121.388542°E.

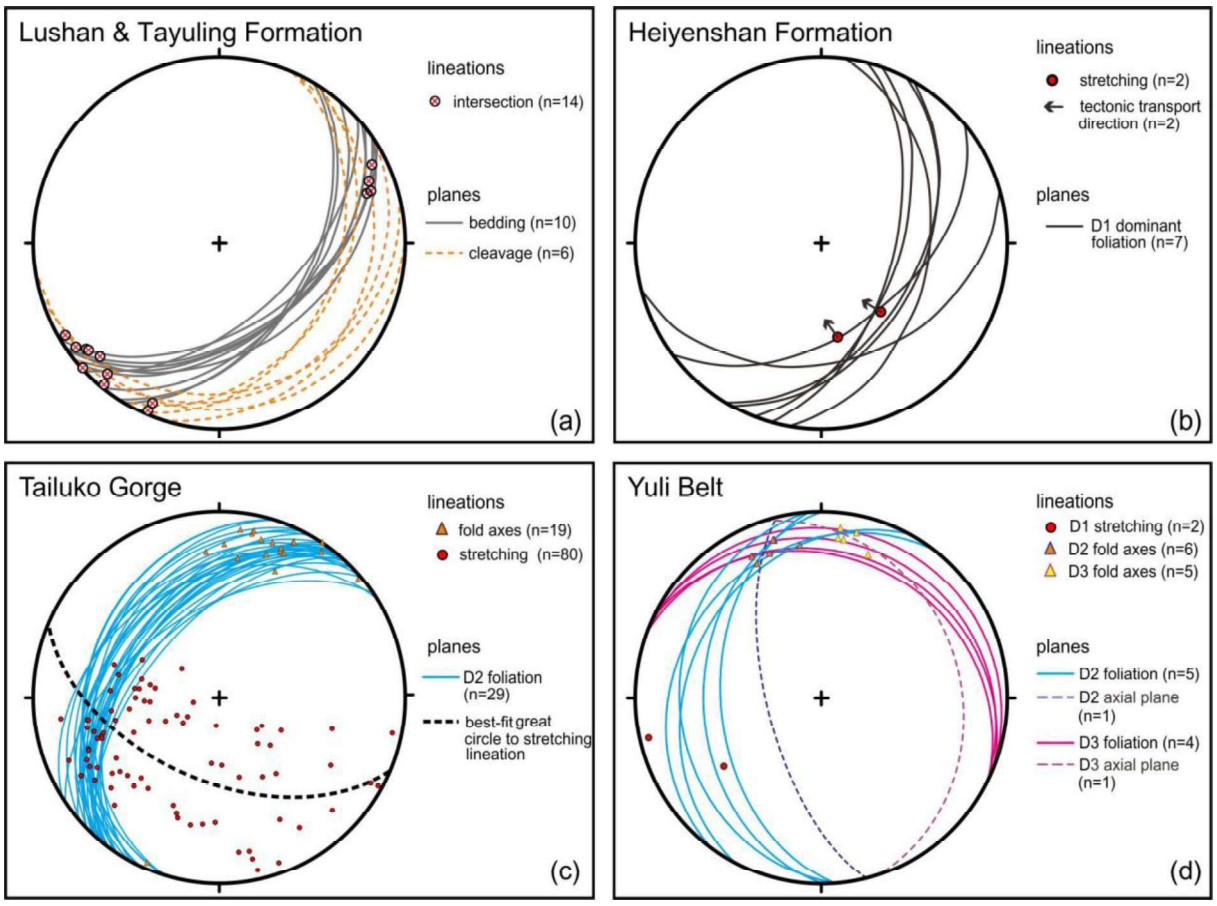

Fig. 2-5: Equal area, lower hemisphere ("Schmidt net") projections of fabric elements across various tectonic units considered representative for the map-scale structures along the Central Cross-island Highway (Transect A-A'). Compare with Fig. 2-4 for actual outcrop geometries.

(a) Southeast-dipping bedding in the Lushan and Tayuling Formations, respectively, affected by D1 slaty cleavage. Bedding steeper than cleavage indicates overturned stratigraphy in the eastern limb of a broad syncline. Location of Lushan Formation: 24.006239°N, 121.111208; Location of Tayuling Formation: 24.188053°N, 121.343847°E.

(b) Southeast-dipping dominant foliation in the Heiyenshan Formation (D1) with top-to-the NW shear sense of the hanging wall. Location: 24.180594°N, 121.357468°E.

(c) West-dipping D2 foliation in the Tailuko Belt refolding D1 compositional layering and stretching lineations considered to have accommodated W-directed shear during D1. Compare with Figure 5 (h) and (i). Location: 24.181728°N, 121.496292°E.

(d) West dipping dominant foliation (D2) locally overprinted by north-dipping foliation (D3) in meta-sediments of the Yuli Belt along the Shoufong Hsi river. Location: 23.837992°N, 121.388542°E.

Tailuko Belt and the easterly adjacent Yuli Belt is the Shoufeng Fault (Yen, 1963). The Yuli Belt of the Tananao Complex is exposed and forms the most internal tectonic unit of the Central Range (Liou, 1981). It hosts blueschist-facies metamorphic igneous rocks embedded in an intensely deformed metasedimentary succession (e.g., Tsai et al., 2013; Keyser et al., 2016; Figs. 2-2; 2-4(i); 2-12(q)). Recent detrital zircon age spectra from metasediments of the Yuli Belt and found that they resemble Cretaceous, Eocene-Oligocene, and Miocene sediments of Taiwan (e.g., Chen et al., 2017; Mesalles et al., 2020). Consequently, they suggest that the youngest sediments in the Yuli Belt are Miocene, and that the belt represents a Miocene-age accretionary complex.

(4) Coastal Range

The Coastal Range in eastern Taiwan is the Neogene Luzon calc-alkaline arc and associated volcanogenic sediments as well as the Luzon trough forearc basin deposits (e.g., Huang et al., 2018). It comprises an upper Miocene arc basement (the Tuluanshan Formation, > 2 km thick), with a patchy occurrence of limestone at its top (the Kankou Limestone), the Late Miocene Fanshuliao Formation with less slate chips in the lower part (Chang, 1969), and the Pliocene Paliwan Formation with more slate chips disconformably in the upper part (Teng, 1979) (Fig. 2-2). A thin slice of tectonic mélange, the Lichi Mélange is exposed along the tectonic suture on the overriding plate (Biq, 1971). Remnants of oceanic facies (the East Taiwan Ophiolite, Hsu, 1956) that formerly lay between the Asian continental margin and the volcanic arc are preserved in exotic blocks of the Lichi Mélange (e.g., Page and Suppe, 1981; Ernst et al., 1985; Lin et al., 2019).

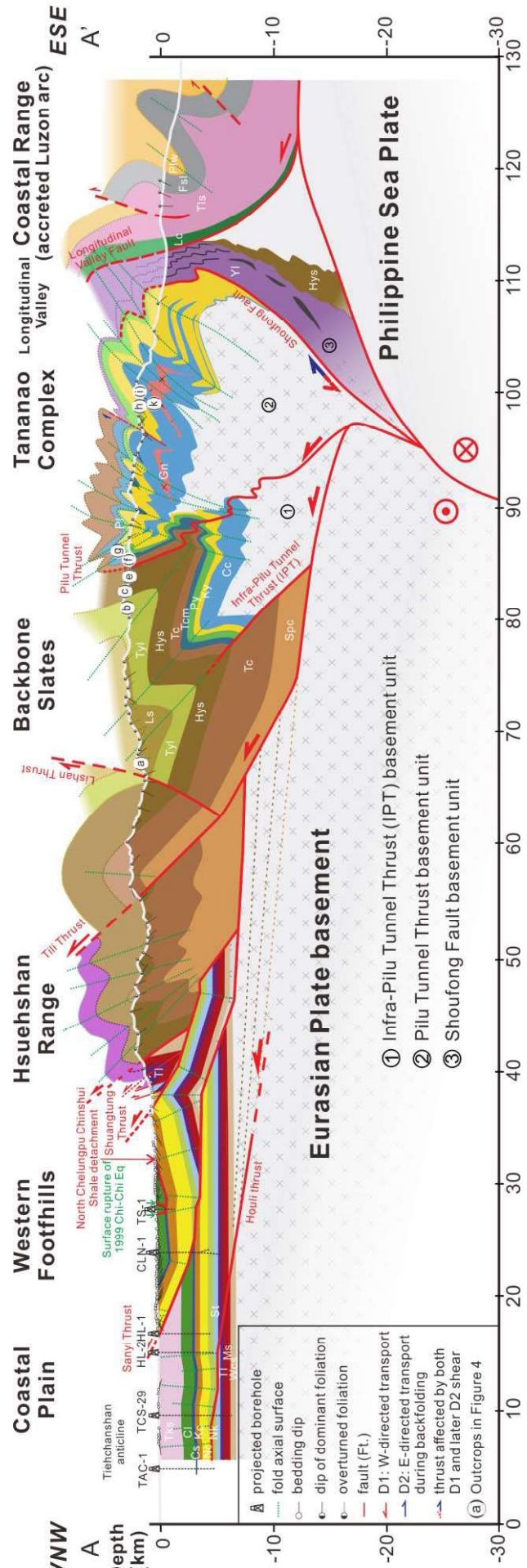

Fig. 2-6: Crustal-scale geological cross section across the Central Cross-island Highway of Taiwan (A-A'), modified and extended after Lee J.-C. et al. (2002). Color-coding of geological units follows that of Fig. 2-3. The D1 west-directed transport sheets are Houli thrust, Sanyi thrust, Shuangtung thrust and Tili thrust from west to east, respectively. The Infra-Pilu Thrust (IPT) is interpreted as a revived half-graben normal fault, indicated by the thickness differences of both sides in the Backbone Slates unit. Pilu Tunnel Thrust divides Heiyenshan Formation of the Backbone Slates and pre-Cenozoic Pilu Formation of the Tananao Complex (with outcrop evidences in Fig.2-5 (e) and (f)). Three thrusted imbricates of the internal basement were involved in crustal-scale D2 back-folding in the retro wedge of the Taiwan orogen. High-res images are enclosed in the supplement.

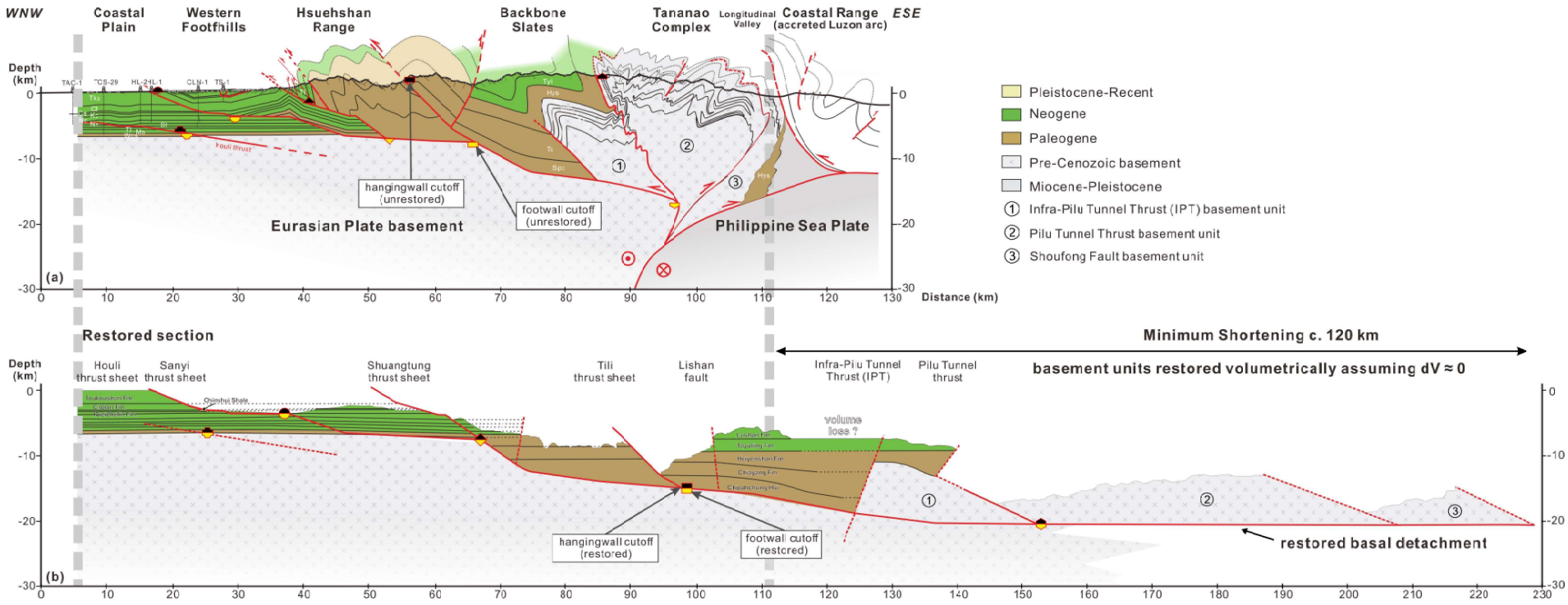

Fig. 2-7: (a) Crustal scale transect across the Central Cross-island Highway of Taiwan (A-A'). See Fig. 2-3 for section trace. (b) First-order restoration of the section A-A' with minimum shortening estimates. High-res images are enclosed in the supplement.

2.3 Structural geometry

The structural analyses and interpretations that follow are based on our new geological mapping (Figs. 2-3, 2-8, 2-11). This mapping is the continuation of previous work in the western and central Taiwan (e.g., Chi et al., 1981; Lee J.-C. et al. 2002; Huang S.-T. et al., 2004; Yue et al., 2005; Sandmann et al., 2015; Lin and Chen, 2016). Field mapping dataset was carried out at 1:50,000 scale using the geological maps of the Central Geological Survey of Taiwan (e.g., Yi et al., 2012) as a base. Major thrusts and stratigraphic contacts (Ho, 1986; Lin and Chen, 2016) have been correlated along strike. Three transects that are geometrically constrained from the surface geological data are presented for the middle part of Taiwan in Figs. 2-6, 2-9, 2-13. The cross sections, oriented perpendicular to the regional strike of structures (bedding, thrusts, and major fold traces), were constructed using standard construction techniques (e.g., Dahlstrom, 1969). The thicknesses of the brittle deformation are taken directly from the surface geological map, and bedding and cleavage are projected into the subsurface using dip data measured along the section. Where possible, additional constraints were placed on the structure and the stratigraphic thicknesses from published borehole data (e.g., Yue et al., 2005). The location of the basal detachment and the deep structure are determined using the geometric controls provided by the stratigraphy and wedge mechanics (e.g., Carena et al. 2002; Naylor and Sinclair 2007), Vp tomography (Wu Y.-M. et al., 2008a; Appendix A- Figs. S1-S3), as well as reflection seismic profiles (e.g., Lee J.-C. et al. 2002). In the description of the structure that follows, the study area has been divided into two deformation types with representative outcrops and structures (Figs. 2-4, 2-5, 2-12).

2.3.1 D1: west-facing folding & transport

In the pro-wedge side of the orogen, the structure of western Taiwan is similar to most compressive mountain belts in that it displays large horizontal contraction strain overlying a décollement. It has a buried thrust front (e.g., the Holi Thrust in A-A'; Fig. 2-6; the Changhua Thrust in B-B'; Fig. 2-9) and all major thrusts are interpreted to extend westward into the offshore where they form a marine accretionary complex. The surface structure of the study area is that of an imbricate westward fold-and-thrust system (D1), but with a distinct north-south change in structural architecture that is presented in detail below. In the Central Cross-island Highway of Taiwan (A-A'), the transect comprises four thrust sheets: the Holi, Sanyi, Shuangtung, and Tili thrust sheets (Figs. 2-3, 2-6); in the central Taiwan (B-B') it consists Changhua, Chelungpu, Shuangtung, and Tili thrust sheets (Figs. 2-8, 2-9); in the Southern Cross-island Highway of Taiwan (C-C'), the extensional fault system of the Eurasian continental margin are oriented at a high angle to develop imbricated fold-and-thrust belts,

consisting Chuku, Lunhou, Tatou, Hsianlin, Changshan thrust sheets (Figs. 2-11, 2-13). The west-vergent folding is a result of the bending of the thrust sheets as they ride over steps along décollements (the fault-bend folding, e.g., Suppe, 1979). A large-scale pop-up structure in the Central Cross-island Highway of Taiwan (A-A') buttresses against the Western Foothills to the west along the Tili Thrust and juxtaposed to the Backbone Slates to the east by the backthrust Lishan Fault (Fig. 2-6).

On the basis of our surface structural data (Figs. 2-3, 2-8), we interpret the Backbone Slates in the central Taiwan to be forming an over-20 km-length synclinorium structure (Figs. 2-6, 2-9), which is in good agreement with significant changes of the Vp tomography (Wu Y.-M. et al., 2008a; Appendix A- Figs. S1-S2) and the rock type. A steep to gently east to southeast dipping monocline in the slate dominated Lushan Formation (Lower Miocene) represents the western limb of the regional synclinorium in the Backbone Slates (Figs. 2-4(a), 2-6). East of the Hehuan Mountain, black, low-grade metamorphic slates of the Tayuling Formation (Oligocene-Miocene), implies an east-dipping overturned limb of the large synclinorium, where bedding dips steeper than slaty cleavage (Figs. 2-3, 2-4(b), 2-5(a), 2-6). The Heiyenshan Formation (Eocene-Oligocene) is exposed in the inverted limb at east of the Pilu Mountain and the Chilai Mountain (Fig. 2-3), showing deformation structures indicative of top-to-the W/NW shear and layer-parallel extension (Figs. 2-4(c)(d), 2-5(b), 2-6). Quartz-rich conglomerate with elongated quartz aggregates in bottom Heiyenshan Formation (Fig. 2-4(e)), contacting east to the strongly foliated Pilu Formation (pre-Cenozoic) (Fig. 2-4(f)), indicates the clasts might be transported from an area of high relief of a rifted continental margin. The westward transport direction (D1) provides important kinematic information for the Pilu Tunnel Thrust in our structural model (Figs. 2-4(g)). To maintain structural consistency in the Backbone Slates, we use the Pilushan Formation (Eocene-Oligocene), that consists of both the Tayuling and Heiyenshan Formations in the Southern Cross-island Highway of Taiwan (C-C'; Fig. 2-11). The westward transport direction (D1) is observed in the east of Yakou, showing deformation structures indicative of top-to-the WNW shear (Fig. 2-12(m) (o)), kinematically similar to the central Taiwan.

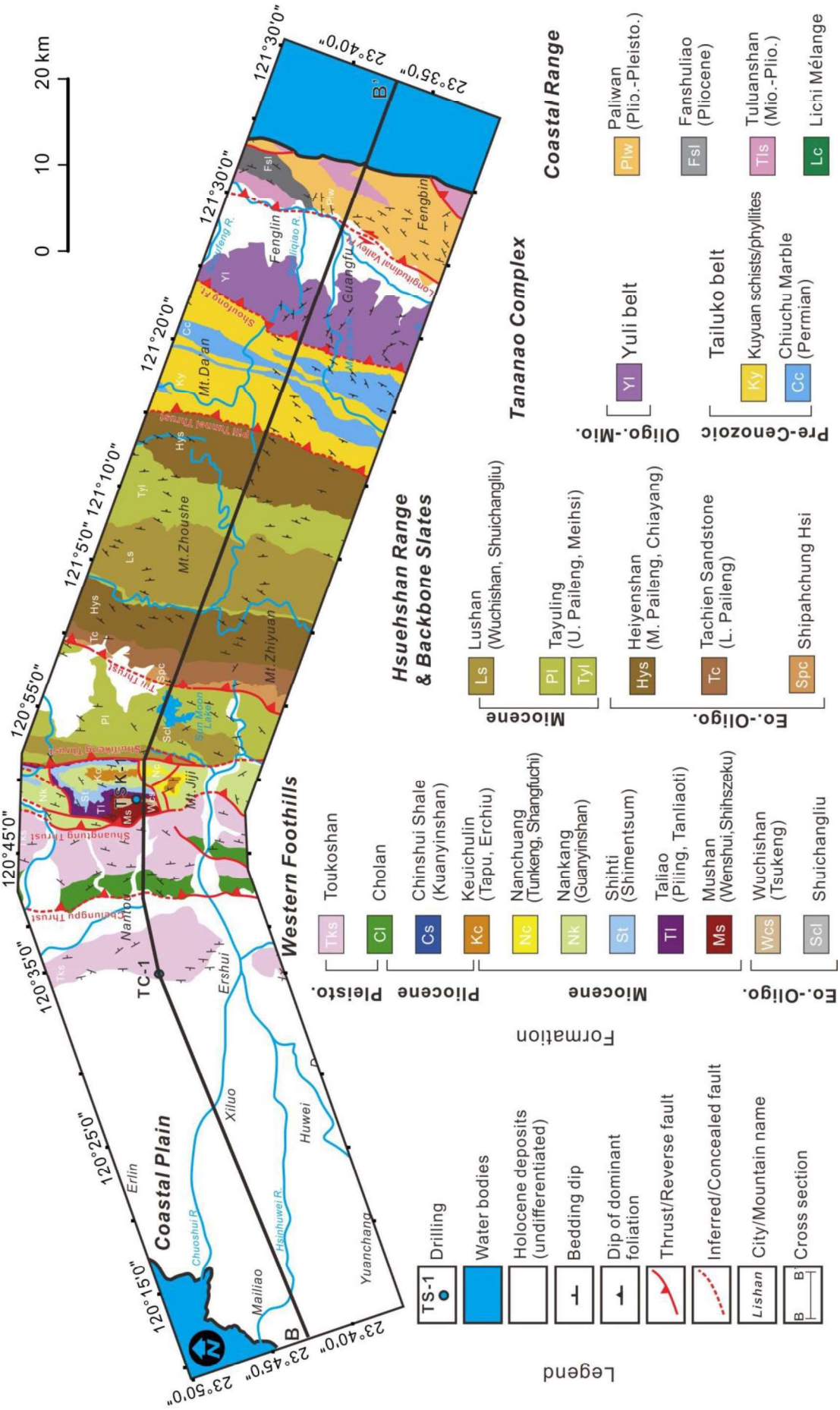

Fig. 2-8: Geological swath map across the central Taiwan (B-B'). High-res images are enclosed in the supplement.

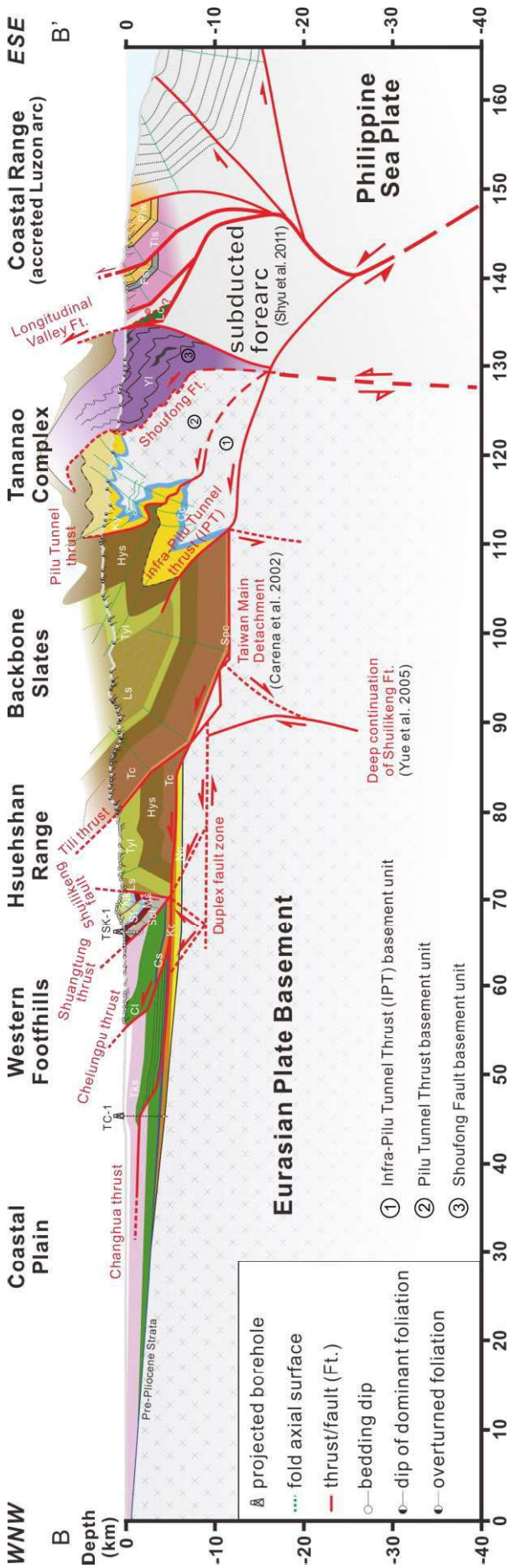

Fig. 2-9: Crustal-scale geological cross section across the central Taiwan (B-B'), modified and extended after Yue et al. (2005) and Sandmann et al. (2015). Color-coding of geological units follows that of Fig. 2-8. High-res images are enclosed in the supplement.

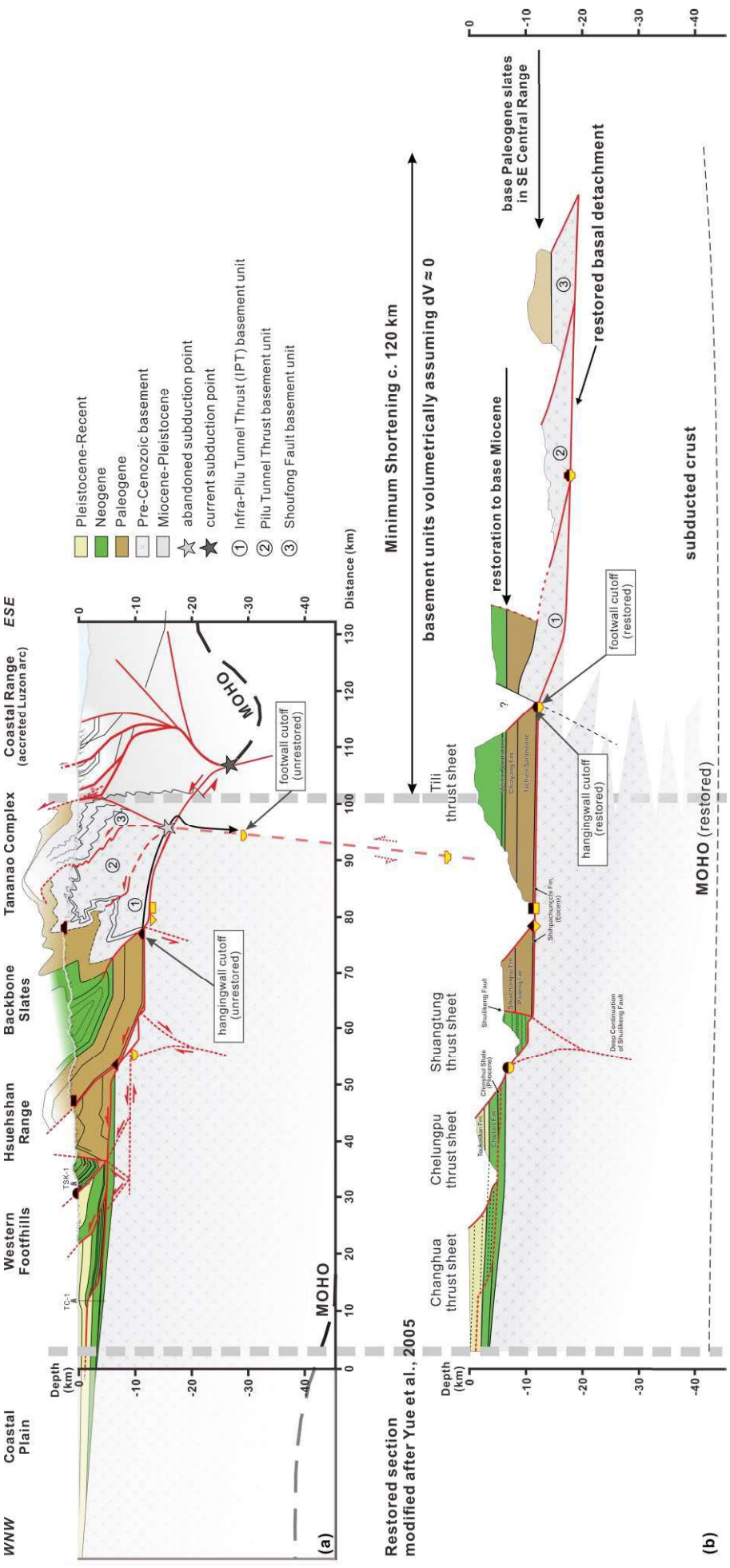

Fig. 2-10: (a) Crustal scale transect across the central Taiwan (B-B'). See Fig. 2-3 for section trace. (b) First-order restoration of the section B-B' with minimum shortening estimates. High-res images are enclosed in the supplement.

2.3.2 D2: east-facing folding & transport

In contrast, the retro-wedge of the Taiwan orogen contains different orientations of cleavages. Rocks in the Tananao Complex that are exposed within the retro-wedge record the early deformation history (D1) which is the same as that in the pro-wedge, but the later history involves eastward backfolding and thrusting (D2), evidenced by the new developing foliations (S1) overprinting earlier foliated planes (S1) during crenulation (Figs. 2-4(h)(l), 2-5(c)(d), 2-11(p)(q), 2-12 (n)(p)(q)). In the western Central Range (Hsuehshan Range and Backbone Slates), the pervasive slaty cleavage (S1) associated with the west-vergent folds is gently southeast-dipping with NE-SW strike. Moreover, the slaty cleavage (S1) dips to the southeast but steepens near the divide or the axis of the range (Figs. 2-6, 2-9, 2-13). In the eastern Central Range (Tananao Complex), the pronounced compositional layering is tightly refolded and transposed into parallelism with S2, which dips to the west. A detailed D2 structural analysis in the Tananao Complex is presented and discussed in the Chapter 3.

2.3.3 Basement imbricates

Three crustal scale imbricates (basement units), bounded by three basal thrusts and the Longitudinal Valley Fault, are proposed in this study (Figs. 2-6, 2-9, 2-13). We interpret basal thrusts, namely the Pilu Tunnel Thrust (PTT), the Infra-Pilu Tunnel Thrust (IPT), and the Shoufeng Fault (SFF), are inversion of deep-seated rift-related extensional faults. The structural model is consistent with the consensus that the former passive margin was segmented into rift grabens and adjacent shoulders, revealing Eocene to Oligocene sedimentary successions of highly contrasting sedimentary facies and thickness in the western Central Range (Teng et al., 1991; Tilmann et al., 1992; Brown et al., 2012; Alvarez-Marron et al., 2014; Camanni et al., 2014). Below we give a description of each basal accretion unit, followed by an interpretation of the kinematic reconstructions (Figs. 2-7, 2-10, 2-14) in Section 2.4.

① The Infra-Pilu Tunnel Thrust basement unit is bounded by the buried Infra-Pilu Tunnel Thrust in the west and the Pilu Tunnel Thrust (Figs. 2-4(f)) in the east. It contains buried pre-Cenozoic Eurasian continental margin basement, that is overlain by Eocene to Oligocene sedimentary successions (i.e., Heiyenshan, Tayuling, and Lishan Formations) (Fig. 2-7). ② The Pilu Tunnel Thrust basement unit is bounded in the west by the Pilu Tunnel Thrust and in the east by the Shoufeng Fault. It is composed of predominately pre-Cenozoic Tailuko Belt in the study area, with a minor amount of Paleogene Pilu Formation cropping out in the Southern Cross-island Highway of Taiwan (C-C') (Figs. 2-11, 2-13, 2-14). We interpret the Pilu Formation to be forming the core of an east-vergent synformal structure in the transect C-C'. ③ The Shoufeng Fault basement unit is bounded by the Shoufeng Fault in the west, by the

Longitudinal Valley Fault in the northeast (Fig. 2-9) and by the Chulai Fault in the southeast (Fig. 2-13). We interpret the Shoufeng Fault basement unit comprises tightly refolded (and faulted) rocks of the Yuli Belt (Figs. 2-7, 2-10, 2-14), although the details of this area may be more complex with Miocene ages on detrital zircons (e.g., Chen et al. 2017) and the interaction between the high-pressure metamorphic units and the basal thrusts (e.g., Chapter 3 and 4). Following nappe stacking, these basement units were later involved in orogen-scale back-folding, leading to the development of a second, vertical to steeply W-dipping younger cleavage (S2) that overprinted older nappe-stacking related foliations (S1).

2.3.4 Normal faults and strike-slip faults

Most orogenic belts result from oblique convergence, which can result in both margin-normal (thrust faulting) and margin-parallel (strike-slip faulting) displacements. In the Taiwan orogenic belt, the along-strike extension has been observed within the eastern Central Range and interpreted as non-coaxial left lateral shear related to the strain partitioning (e.g., Faure et al. 1991; Fisher, 1999; Conand et al., 2020) or sub-horizontal lateral extrusion associated with an arcward-dipping backstop (Fisher et al. 2002; Wintsch et al. 1999). In the Yuli Belt region, the normal faults dip to the southwest or northeast and could be related to the latest shallow extension of exhumation processes. We assume that any late-stage (e.g., post penetrative strain) structures (e.g., normal or strike-slip faulting) are insignificant in the crustal-scale of this study.

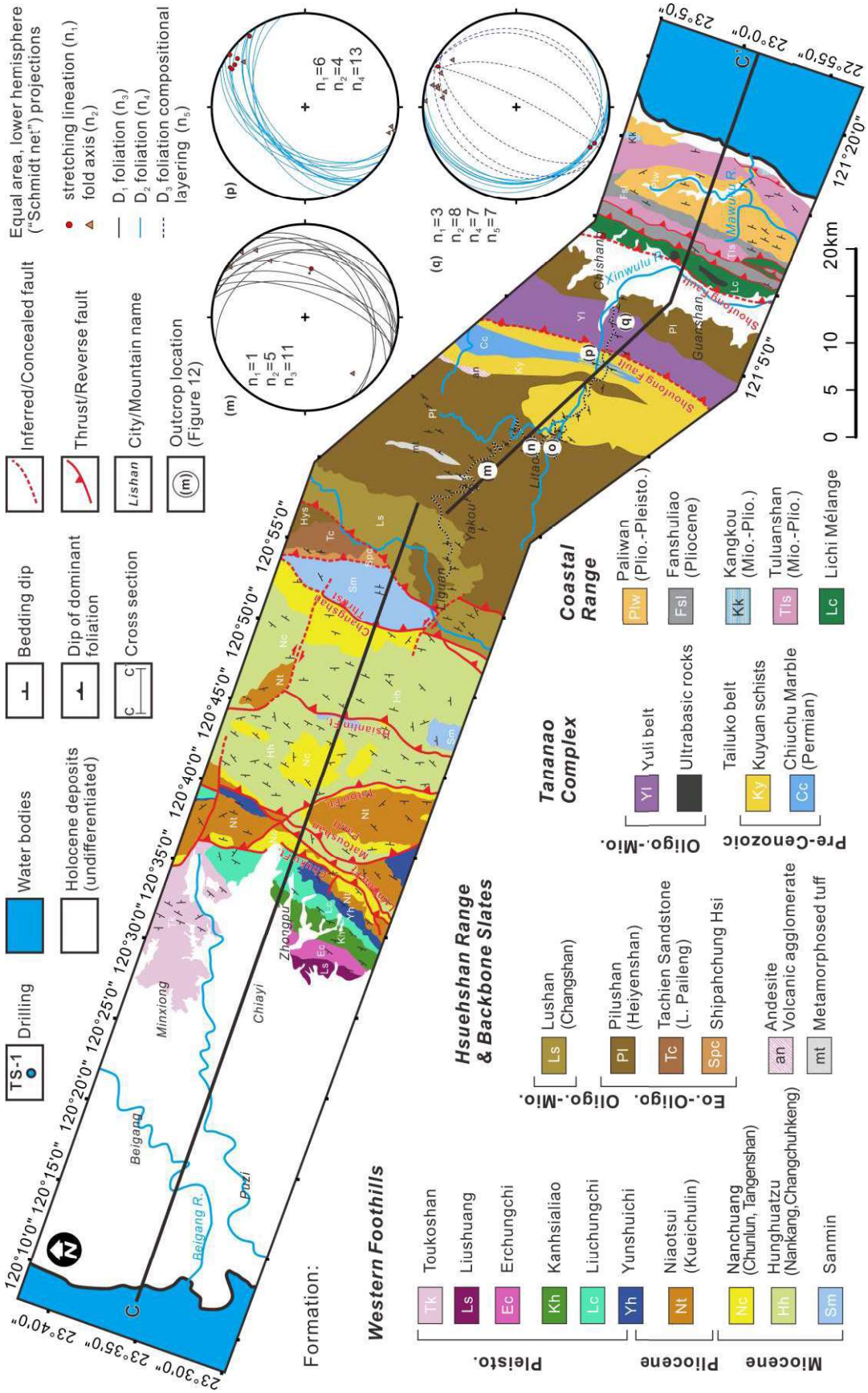

Fig. 2-11: Geological swath map across the Southern Cross-island Highway of Taiwan (C-C'). Letters (m)-(q) show the localities of the outcrops in Fig. 2-12 and measurements projected in the " Schmidt net" . Roads of the Southern Cross-island Highway are shown in the black-white dashed line. High-res images are enclosed in the supplement.

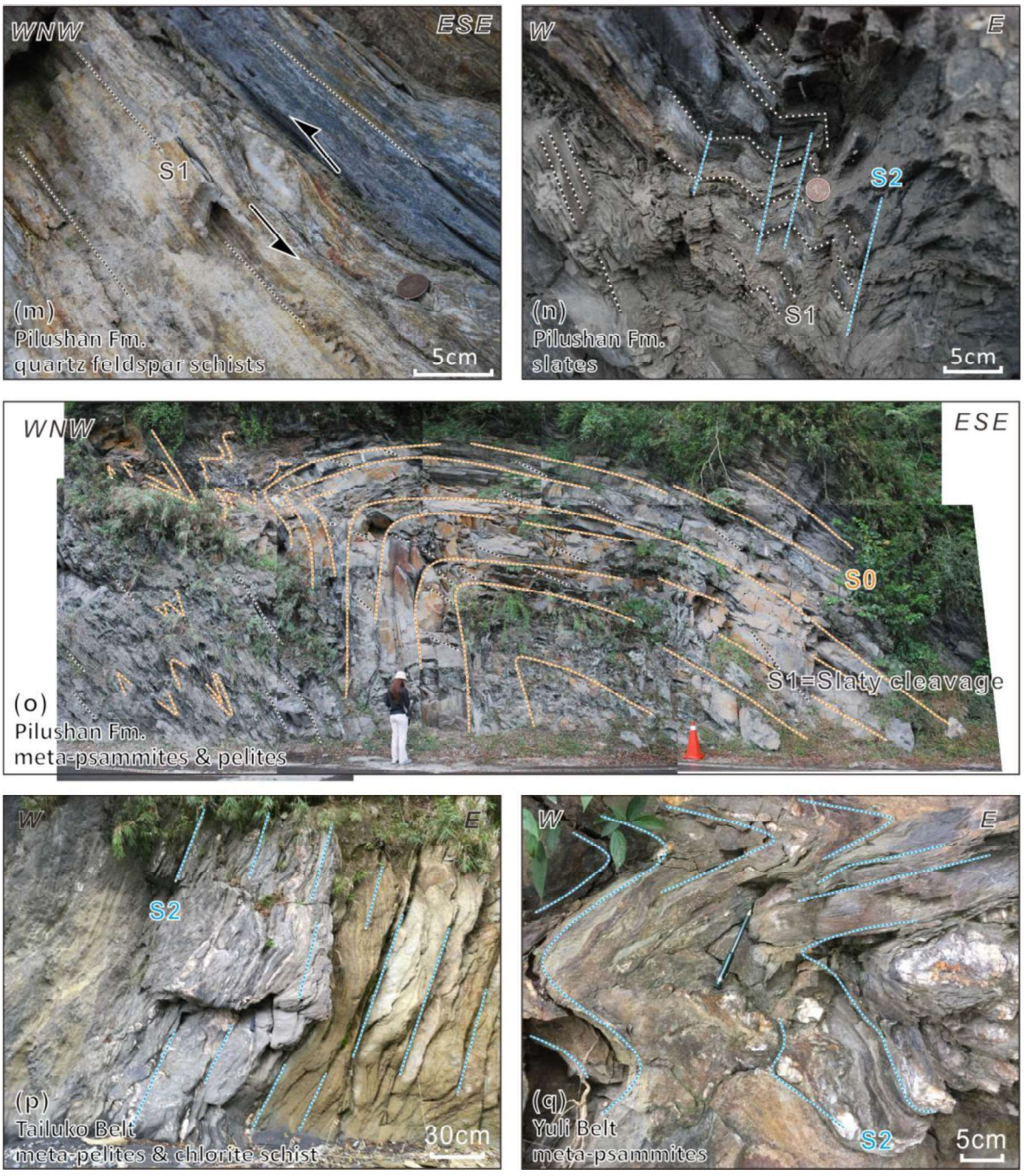

Fig. 2-12: Outcrops across various tectonics units along the Southern Cross Island Highway (transect C-C', Fig. 2-11) considered representative for map-scale structures.

(m) East-dipping veined quartz feldspar schists in the Pilushan Formation affected by D1 folding, showing deformation structures indicative of top-to-the WNW shear, similar to Fig. 2-4(c). Location: west Litao, 23.242931°N, 120.991406°E.

(n) The east-facing refolding metamorphic foliation (slaty cleavage, S1) of quartzite slate and dark phyllites in the Pilushan Formation. The refolded S2 foliation dips to the west. Location: east Litao, 23.191908°N, 121.018261°E.

(o) Folded bedding (S0) of black, low-grade metamorphic slate in the Pilushan Formation. An over 10 m-wavelength overturned anticline exposed at the roadside of east Litao, as implied by bedding-cleavage relationships. The fold axial plan is east-dipping. Location: 23.191908°N, 121.018261°E.

(p) WNW-dipping meta-pelites of Yuli Belt contact with epidote chlorite schists in the Tailuko Belt. Both Formations show the same dip of S2 foliation. Location: 200m east of Xinwu Bridge, 23.1359°N, 121.114°E.

(q) Veined meta-pelitic schists and metasandstones in the Yuli Belt affected by D2 refolding, similar to Figure 4 (l). Location: SE Chulai village along raod 20, 23.1285°N, 121.116°E.

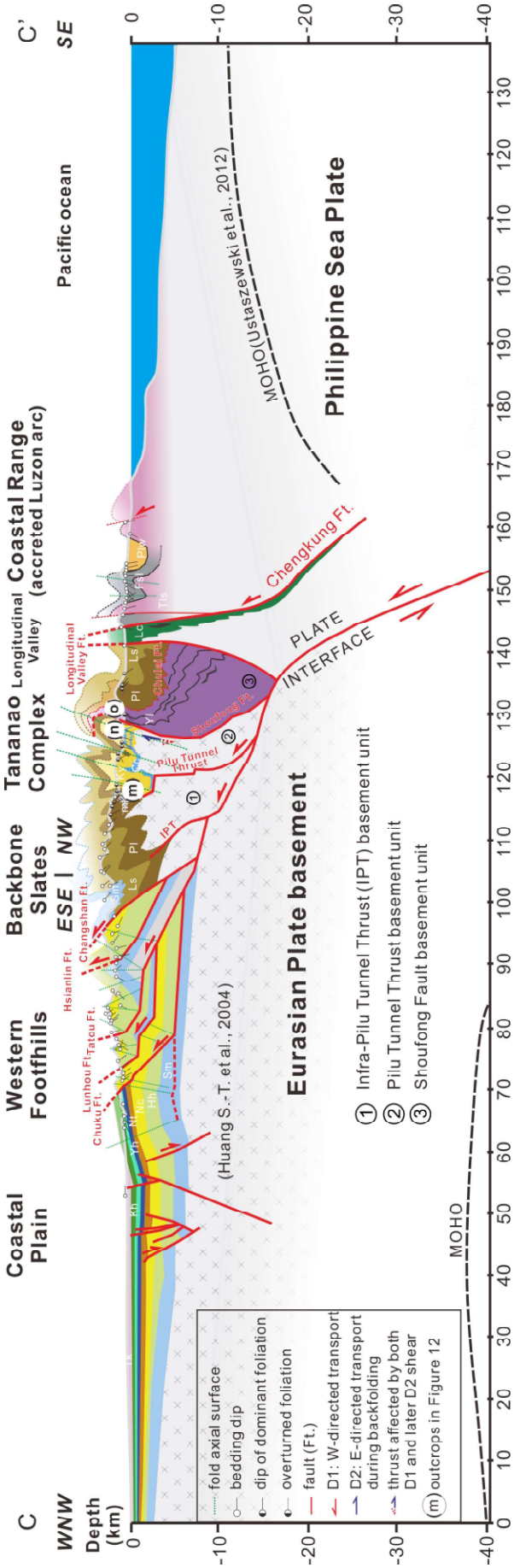

Fig. 2-13: Crustal-scale geological cross section across the Southern Cross-island Highway of Taiwan (C-C'), modified and extended after Huang S.-T. et al. (2004) and Chi et al. (1981). Color-coding of geological units follows that of Fig. 2-11. Crust-mantle boundaries after Ustaszewski et al. (2012). High-res images are enclosed in the supplement.

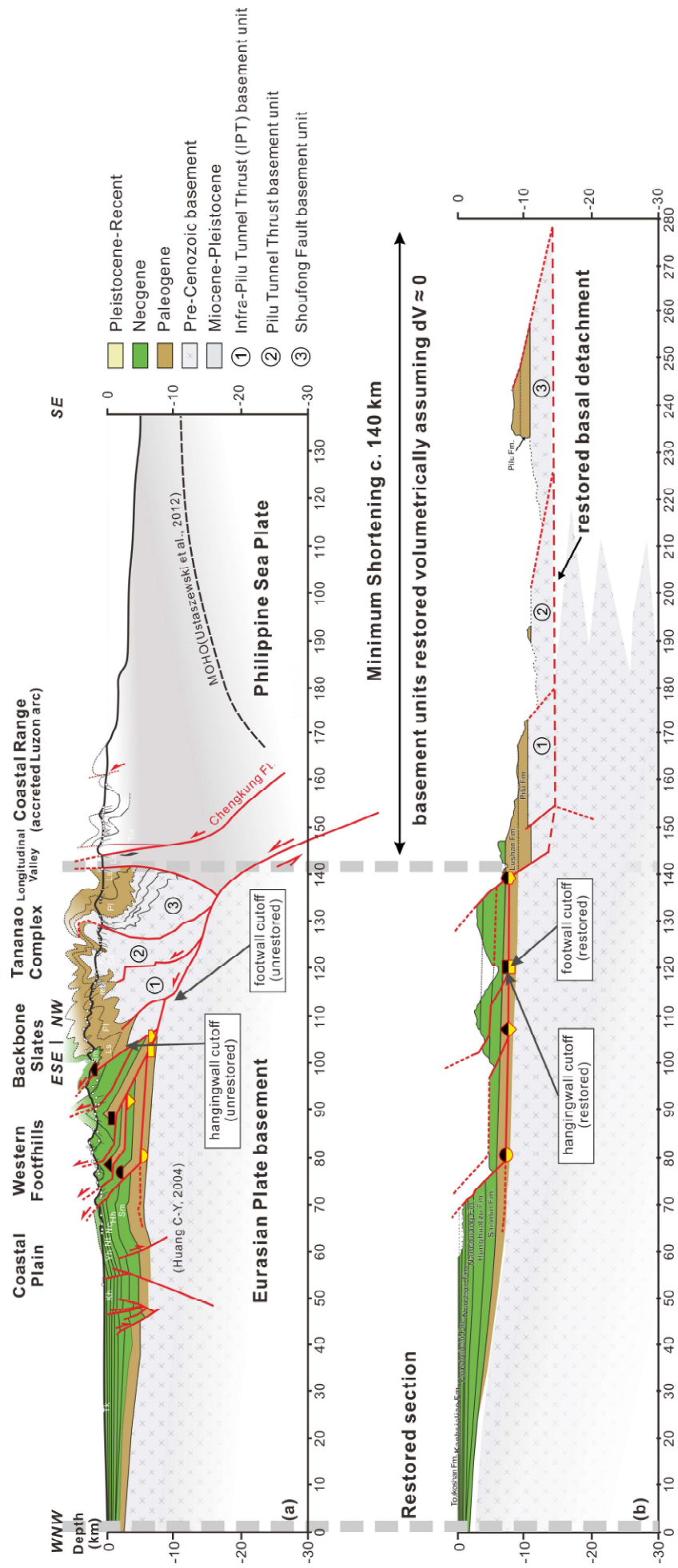

Fig. 2-14: (a) Crustal scale transect across the Southern Cross-island Highway of Taiwan (C-C'). See Fig. 2-11 for section trace. (b) First-order restoration of the section C-C' in with minimum shortening estimates. High-res images are enclosed in the supplement.

2.4 Palaeogeographic reconstructions of the Eurasian margin

We construct balanced and restored cross sections (Figs. 2-7, 2-10, 2-14) using classical line-length (in brittle units) and equal area-balancing (in ductile units) approaches aim to assure the viability of the structural interpretation. Minimum shortening estimations in the three cross sections, which is a by-product of their balancing and restoration, are also presented (Figs. 2-14, 2-15, 2-16). The reactivation and inversion of faults derived from the Eurasian continental margin have been shown to be particularly crucial in Taiwan orogeny (e.g., Mouthereau et al., 2006). Based on the analysis of the Cenozoic stratigraphy in Hsuehshan Range, Backbone Slates, and Tananao Complex (Fig. 2-2), the rifting phase predates the Late Oligocene to Miocene break-up and drifting in the South China Sea (Teng and Lin, 2004). Contraction was triggered by subduction of the Eurasian passive margin below the Philippine Sea Plate (Tsai et

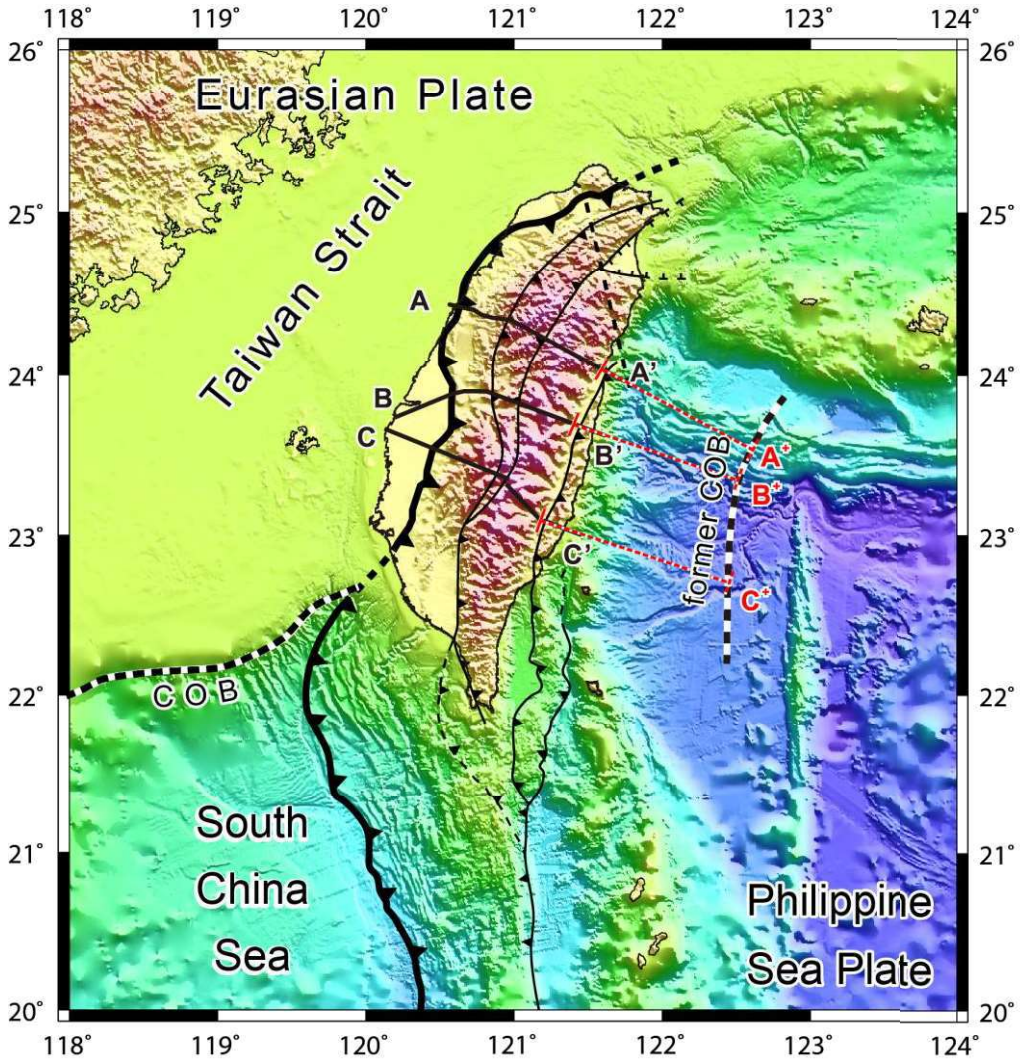

Fig. 2-15: The extended lines (A-A+,B-B+,C-C+) of three restorations of the Eurasian section in Figs. 2-7, 2-10, 2-14 with minimum shortening estimates derived from line-length and area-balancing in the Cenozoic and pre-Cenozoic succession. The former continent-ocean boundary (COB) is reconstructed on the basis of shortening estimates of the three transects. The topography base map follows that of Fig. 2-1.

al., 1977; Angelier, 1986; Lallemand et al., 2001; Ustaszewski et al., 2012). A number of extensional faults in this study that developed along the outer part of the margin and its slope can be traced on land (e.g., the Sanyi, Shuangtung, and Tili thrusts in Figs. 2-7, 2-10, 2-14; Yang et al., 2006, 2016), where they have been shown to affect the structure of the foreland thrust-and-fold belt (Alvarez-Marron et al., 2014; Brown et al., 2017; Camanni et al., 2016; Rodriguez-Roa & Wiltschko, 2010; Suppe, 1986; Yang et al., 2007, 2016). Our own interpretation considers the Tailuko and Yuli belts as comprising two crustal scale imbricates of Eurasian basement that form the tectonically highest units and which overthrust the Cenozoic passive margin series (Figs. 2-7, 2-10, 2-14). They were juxtaposed along a West-vergent thrust contact soon after collision.

The restored version of three cross sections yields the shortening amount of the former passive margin of Eurasia at least ~120 km, ~120 km, and ~140 km in A-A', B-B', and C-C', respectively (Fig. 2-15). The position of the plate interface along this transect, constrained from geophysical data (Ustaszewski et al., 2012; Fig. 2-1), implies that over half of the basement, on top of which the accreted material was initially sitting, has entered subduction ("subducted crust"). Therefore, the former continent-ocean boundary (COB) is reconstructed before subducting in Fig. 2-16, which is consistent with the underlying unfolded passive margin tomography (e.g., Chen, 1995, Rau and Wu, 1995). In the paleogeographic maps, the Eurasian passive margin likely formed a slightly eastward-convex salient prior to plate convergence that created the Taiwan fold-and-thrust belt.

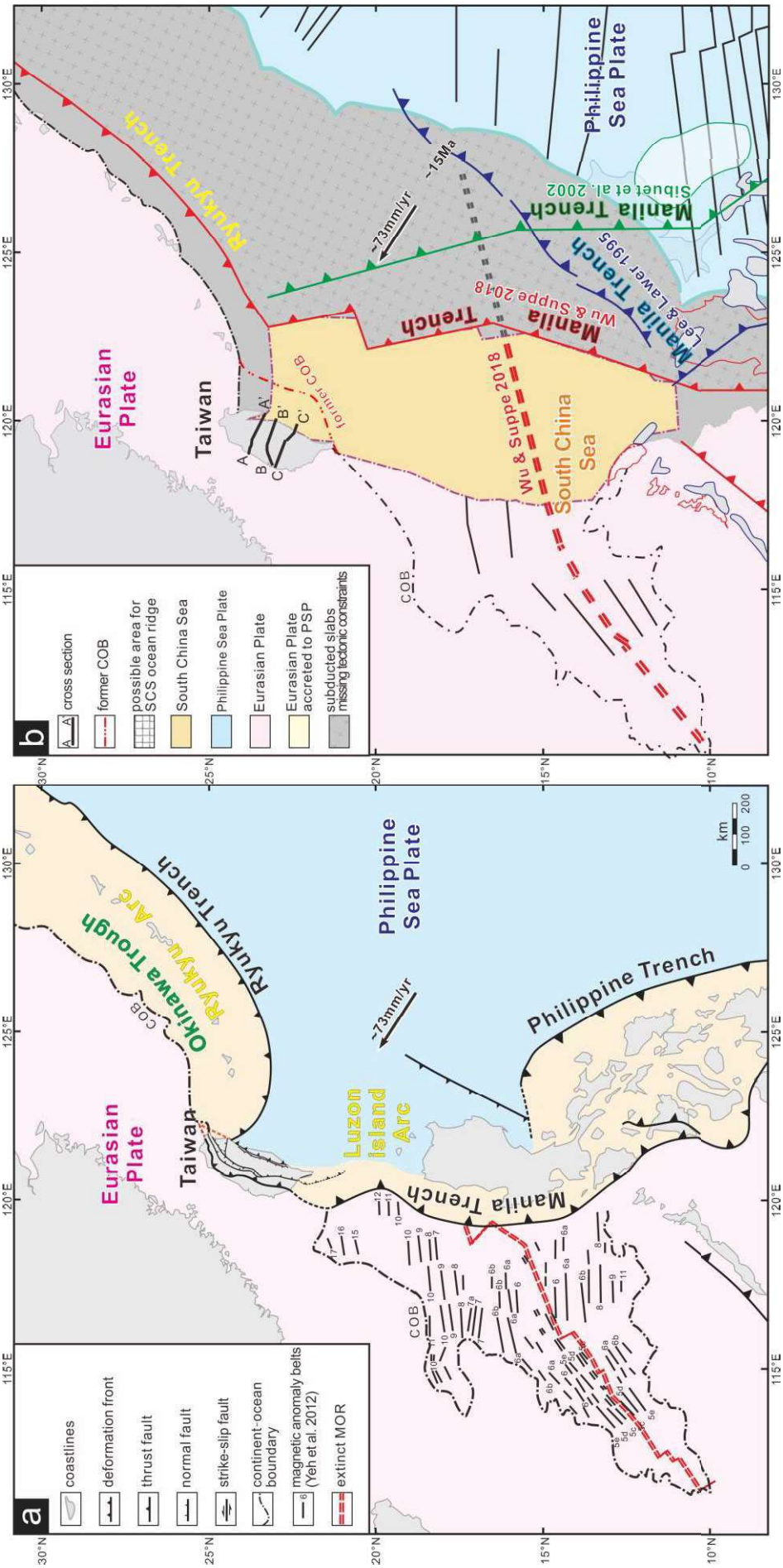

Fig. 2-16: Palaeogeographic reconstructions of the Eurasian passive margin in the map view. The former continent-ocean boundary (COB) is reconstructed on the basis of shortening estimates of the three transects (A-A' , B-B' , C-C'). a: Present-day plate tectonic map around Taiwan. b: Paleogeographic reconstruction for 15 Ma (Chapter 3). We selected the framework of a global plate reconstruction of Wu and Suppe (2018) using a hybrid absolute reference frame that includes moving Indian/Atlantic hotspots and a true polar wander corrected paleomagnetic-based model (Seton et al., 2012).

2.5 Conclusions

On the basis of our new surface geological mapping, we interpret the structure of three transects across the entire Taiwan to be two deformation types (D1 and D2) with three basement imbricates. D1 type is an imbricate westward fold-and-thrust system, which develops in the Coastal Plain, Western Foothills, Hsuehshan Range and Backbone Slates. In the western Central Range, the pervasive slaty cleavage (S1) associated with the west-vergent folds is gently southeast-dipping with NE-SW strike. D2 type is an east-facing backfolding and backthrusting system in the eastern Central Range, leading to the development of a second, vertical to steeply W-dipping younger cleavage (S2) that overprinted older nappe-stacking related foliations (S1). Three crustal scale basement imbricates are bounded by three basal thrusts and the Longitudinal Valley Fault. Following nappe stacking accretion, these basement units were later involved in orogen-scale D2 backfolding and backthrusting in structural architecture. In our balanced and restored cross sections, we estimate the minimum shortening of the former passive margin of Eurasia to be ~120 km in the central and ~140 km in the south. Over half of the basement, on top of which the accreted material was initially sitting, has entered subduction. In the paleogeographic maps, the Eurasian passive margin likely formed a slightly eastward-convex salient prior to plate convergence that created the Taiwan fold-and-thrust belt.

Chapter 3

The Yuli Belt in Taiwan: part of the suture zone separating Eurasian and Philippine Sea plates

This Chapter is an extended version of the manuscript published in "Terrestrial, Atmospheric and Oceanic Sciences".

Zhang, Y., Tsai, C.-H., Froitzheim, N., Ustaszewski, K. (2020): The Yuli Belt in Taiwan: part of the suture zone separating Eurasian and Philippine Sea plates. Terrestrial, Atmospheric and Oceanic Sciences, 31, 1-18, doi: 10.3319/TAO.2020.06.28.01

Abstract:

The Yuli Belt exposed in the retro-wedge of the eastern part of the Taiwan orogen hosts slivers of a heterogeneous unit of blueschist-facies rocks. However, the question pertaining to its palaeogeographic provenance is still debated despite new geochronological data. This is largely because the structural geometries and kinematics of the Yuli Belt's tectonic contacts with its adjacent units are improperly understood. This paper presents new structural data from field work along several river transects in the Yuli Belt, which we combine with published data into a new tectonic model. Fieldwork and microstructural analyses indicate three deformation phases in the Yuli Belt. Based on cross sections and a review of available P-T-t data, we suspect that blueschist-facies units could have been emplaced on top of greenschist-facies metasedimentary units along a thrust during a first deformation phase D1. This assembly was later thrust over the Eurasian-derived Tailuko Belt along the Shoufeng Fault during D2, as suggested by W-plunging stretching lineations on fault-parallel foliation planes. D3 produced E-vergent folds with W- to NW-dipping axial planes, refolding earlier foliations as well as the D1 nappe contact. We suspect that this E-vergent folding could be related to top-E backthrusting observed along the Shoufeng Fault, involving its reorientation from an initially E-dipping to a presently W-dipping contact. On the basis of the whole-rock geochemical data with MORB affinity, the blueschist-facies metamorphic unit of the Yuli Belt likely represents a mid-Miocene fragment of oceanic crust and mantle issued in the South China Sea. It could hence be considered as part of the suture between the Eurasian and the Philippine Sea plates.

Keywords: Taiwan; Yuli Belt; Shoufeng Fault; South China Sea; blueschists; subduction; exhumation

3.1 Introduction

Sutures or suture zones are variably sized allochthonous tectonic units occurring in every collisional orogen, separating tectonic units of contrasting palaeogeographic origin (Gansser, 1964 and 1980; Dewey, 1987, Grasemann and Huet, 2016). They typically contain ophiolitic fragments that represent relics of formerly larger amounts of oceanic crust and mantle lithosphere initially separating the continental units before subduction (Moores 1970; Moores and Vine 1971; Gansser, 1980; Condie, 2016). Put more simply, sutures are fossil collisional plate boundaries. Quite often, sutures form brittle or mylonitic shear zones that accommodated large amounts of contractional strain, providing testimony of plate convergence. Sutures regularly represent strongly tectonised zones with large lithological and metamorphic heterogeneity of mappable units, which are furthermore often spatially disrupted. Among the many heterogeneous lithologies encountered in suture zones, high-pressure metamorphosed rocks always receive particular attention, because they provide undisputable proof for subduction processes preceding collision (e.g., Stern, 2005). This is also the case for the famous Yuli Belt of Taiwan, a tectonic unit on the eastern side of Taiwan's Central Range (Fig. 3-1). Its occurrences of blueschist-facies rocks have been the focus of continued petrological and geochronological investigations since the pioneering work of Yen (1959). The Yuli Belt contains lithologically heterogeneous blueschist-facies rocks in what is referred to as tectonic or exotic blocks (Table 3-1), which, according to numerous authors (e.g., Liou et al., 1977; Liou, 1981; Yui et al. 2012; Tsai et al. 2013), are surrounded by an intensely deformed metasedimentary unit of lower metamorphic grade (Table 3-1). Internally, some of the high-pressure blocks are considered tectonic mélanges themselves, exhibiting four petrographically different types of glaucophane-bearing rocks (Tsai et al., 2013) with intervening metasediments such as garnet-bearing blackschists (Beyssac et al., 2008) or garnet paragonite mica schists (Keyser et al. 2016). Recent geochronological work on the blueschists has yielded a Lu-Hf age of 5.1 ± 1.7 Ma (Sandmann et al. 2015; see Table 3-2 for an overview of hitherto obtained geochronological data from the Yuli Belt) – rendering it one of the youngest blueschists belts worldwide (Ota and Kaneko 2010).

The metasedimentary unit of the Yuli Belt (i.e., all units other than the aforementioned blueschist-bearing tectonic blocks) has been differentiated into four units, according to Taiwan's Central Geological Survey (Wang 1992; Yi et al. 2012), namely the Hutoushan Schists, Senjung Schists, Hungyeh Schists, and Albite spotted Schists (Juisui Schists). In the case of the first three units, lack of metamorphic index minerals and lithological similarities (mostly metapelitic to metapsammitic schists with variable amounts of carbonaceous matter) make it challenging to map differences between these lower amphibolite- to greenschist-facies

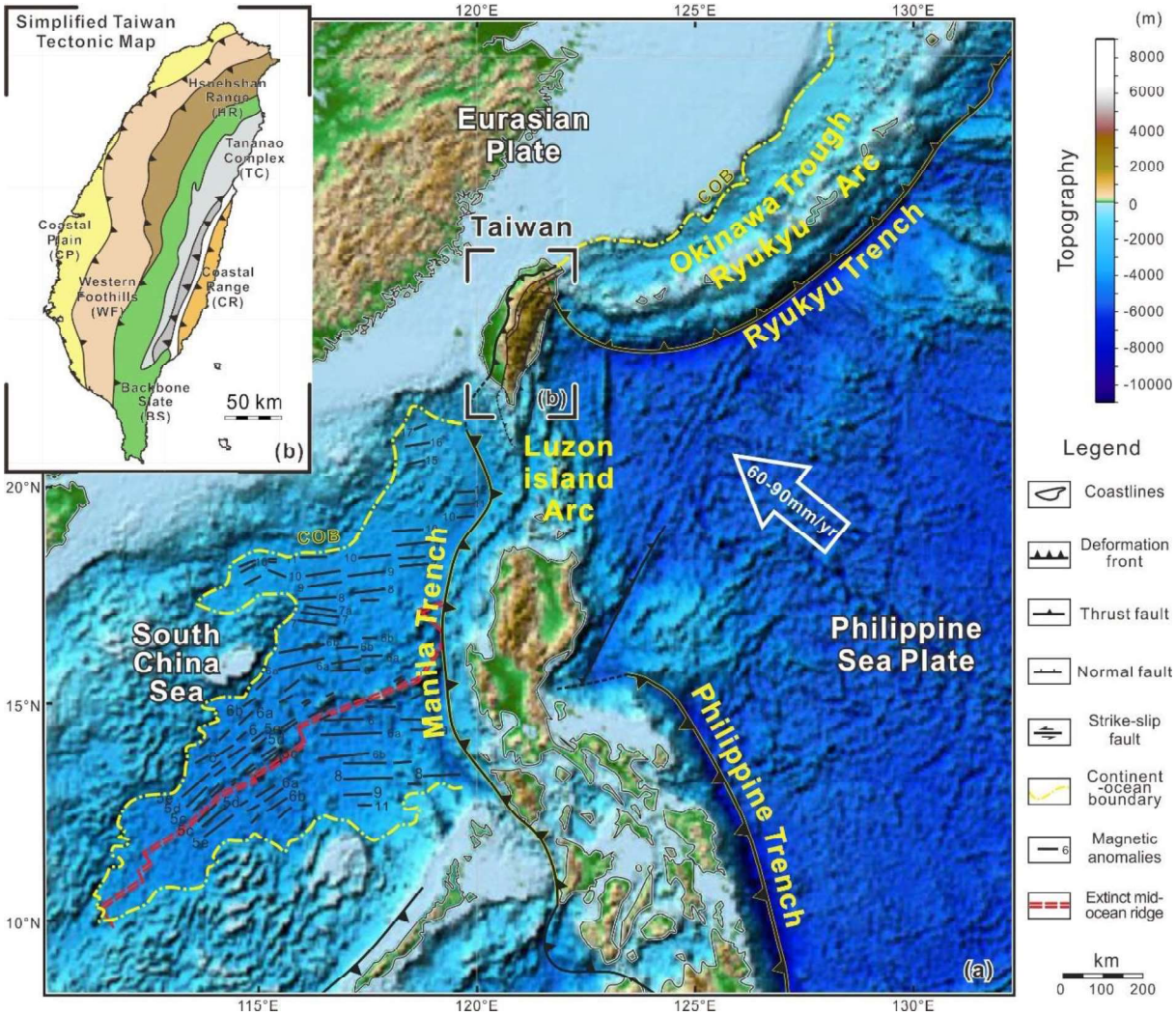

Fig. 3-1: Plate tectonic map of Taiwan and its greater surroundings showing main tectonic units. The Philippine Sea Plate moves towards the Eurasian Plate at a rate of c. 60-90 mm/yr and subducts underneath it along the Ryukyu trench. The South China Sea (part of Eurasian Plate) subducts beneath the Philippine Sea Plate along the Manila Trench. The extinct South China Sea spreading ridge and magnetic lineations after Yeh et al. (2012); global topography model ETOPO1 (Amante and Eakins, 2009); continent-ocean boundary (COB) from Sibuet et al. (2016).

units in terms of their structural position within the Yuli Belt. The sole more diagnostic lithology within the metasedimentary unit are the albite-bearing spotted schists (e.g., Yang and Wang 1985; see Table 3-1 for further references; Fig. 3-4). The Yuli Belt has long been considered an exhumed portion of the Eurasian pre-Cenozoic basement, partly based on geochronological data indicating Cretaceous ages for metamorphism (Jahn and Liou 1977; Jahn et al. 1981; Lo and Yui 1996). However, recently geochronological data called for a reinterpretation (Fig. 3-2; Table 3-2). Chen et al. (2017, 2019) demonstrated that they contain detrital zircons as young as the middle Miocene, suggesting that the whole Yuli Belt schists as a part of Backbone Range extruded and exhumed prior to the arc-continent collision at ~12 Ma, which is much older than the previously determined onset age of Taiwan mountain building of

~4-6 Ma (e.g. Chang and Chi 1983; Lee et al. 2015). With respect to the blueschist-facies rocks that the metasedimentary succession hosting, zircon U-Pb in-situ ICP-MS dating in exotic blueschists, also from Tamayen (Fig. 3-4), yielded protolith ages as young as 15.4~16.0 Ma(Chen et al. 2017; Lo et al. 2020), proving the concept of a pre-Cenozoic age for the Yuli Belt meta-igneous rocks most likely wrong. Lo (2018) also broadcasted the crystallization ages of metaplagiogranite in the Chisui Hsi area with c. 13 ~ 15 Ma by using zircon U-Pb in-situ ICP-MS dating.

Table 3-1: Comparison of the Yuli Belt and the Lichi mélange

	Rock type	Protolith	Age	Inferred Origin	
Yuli Belt					
Matrix	albite-garnet prophyroblastic schists ("spotted schists") [1,2,3,4]	terrigenous clay?	protolith ages unknown		
	paragonite-white mica metapelitic schists[5]	pelagic clay?			
Tectonic blocks	serpentinite[6]	peridotite	protolith ages unknown	Middle-Late Miocene accretionary prism[15,16]	PSP fore-arc[12,17]
	rodingite[6]	metasomatized mafics			
	meta-gabbro[7]	gabbro			
	meta-plagiogranite[8]	plagiogranite			
	epidote amphibolite[7,8,9,10]	gabbro, basalt			
	greenschist[7,8]	basalt			
	garnet-epidote amphibolite[6]	tuff, basalt?			
	glaucophane schists[9,10,11,12,13,14]	tuff, basaltic andesite, Mn-rich pelagic clay?	~15 Ma [16,18]		
Lichi Mélange					
Matrix	Sheared mudstone without stratification		3.5-3.7 Ma [a,b,c]; 3.4-4.3 Ma [i]		
Tectonic blocks	ophiolitic rocks (East Taiwan Ophiolite/ETO), incl. ultramafics (serpentinized harzburgite, serpentinite breccia) [d], gabbro[f], dikes of dolerite and plagiogranite[g], pillow basalts[f]		Mid-Late Miocene [f,h,j]	SCS [d,e,f]	
	sedimentary rocks		Mio-Pliocene [a,b]	SCS [d,e]	

References for Yuli Belt: 1: Yang and Lin 1982; 2: Lin et al. 1984; 3: Yang and Wang 1985; 4: Chiang 2003; 5: Shen and Yang 1996; 6: Lan and Liou 1981; 7: Liou, J. G., 1981; 8: Lan and Liou 1984; 9: Yen 1966; 10: Liou et al. 1975; 11: Jahn and Liou 1977; 12: Jahn et al. 1981; 13: Lo and Yui 1996; 14: Juang and Bellon 1986; 15: Liou and Ernst 1984; 16: Chen et al. 2017; 17: Beyssac et al. 2008; 18: Lo et al. 2020.

References for Lichi Mélange: a: Chi et al. 1981; b: Chang and Chi 1983; c: Barrier and Muller 1984; d: Suppe and Liou 1979; e: Suppe et al. 1984a; f: Lin et al. 2019; g: Shen et al. 1984; h: Suppe et al. 1977; i: Chen et al. 2015; j: Lo et al. 2020.

Table 3-2: Summary of geochronological ages from the Yuli Belt. The tectonic blocks are sorted from N to S.

Area		Rock type	Protolith	Age	Method	Reference
Tectonic blocks	Fengtien	Clinozoisite rock	?	3.3 ± 1.7 Ma (zircon rim)	U-Pb NanoSIMS	Yui et al. 2014
	Wanjung	Omphacite-zoisite-albite-phlogopite- quartz metabasite	?	4.4 ± 0.1 Ma (phlogopite) 109 ± 3 Ma (omphacite)	$^{40}Ar/^{39}Ar$	Lo and Yui 1996
	Juisui	Glaucophane schists	Volcanic arc andesites and manganese rich sediments (Jahn and Liou 1981)	110 ± 3 Ma (glaucophane) 12.2 ± 0.5 Ma (amphibole) 10.4-11.3 Ma (phengite)	$^{40}Ar/^{39}Ar$	Lo and Yui 1996
				8.2-14.3 Ma (whole rock/hornblende-phengite)	Rb-Sr	Jahn and Liou 1981
				5.1 ± 1.7 Ma (whole rock/Garnet)	Lu-Hf	Sandmann et al. 2015
				15.4-16.0 Ma* (zircon)	U-Pb	Chen et al. 2017
		Epidote amphibolites	Gabbro and basalt (MORB like)	78.8 ± 6.6 Ma (whole rock/hornblende-paragonite) 4.6 ± 0.6 Ma (mineral isochron)	Rb-Sr	Jahn and Liou 1981
	Chinsui Hsi	Metaplagiogranites	Plagiogranite	13.1,15.71 Ma* (zircon)	U-Pb	Lo 2018
Meta- sediments matrix	Various localities in Yuli Belt	Pelitic schist	Sediments	Major peaks: 1900-1700 Ma, 1000-900 Ma, 850-700 Ma, 200-65 Ma, 65-8 Ma	U-Pb on detrital zircons	Chen et al. 2017
				Major peaks: ~1874 Ma, >500Ma, ~300 Ma, ~260 Ma, ~200 Ma, ~130 Ma Youngest: 64 Ma	U-Pb on detrital zircons	Wang et al. 2017
				Major peaks: ~ 2500 Ma, ~ 1800 Ma Youngest: 108 ± 22 Ma	U-Pb on detrital zircons	Yui et al. 2012
				1-5 Ma (<2 mm illite / muscovite)	K–Ar	Tsao et al. 1996

*Note: Ages marked with * are considered crystallization ages.*

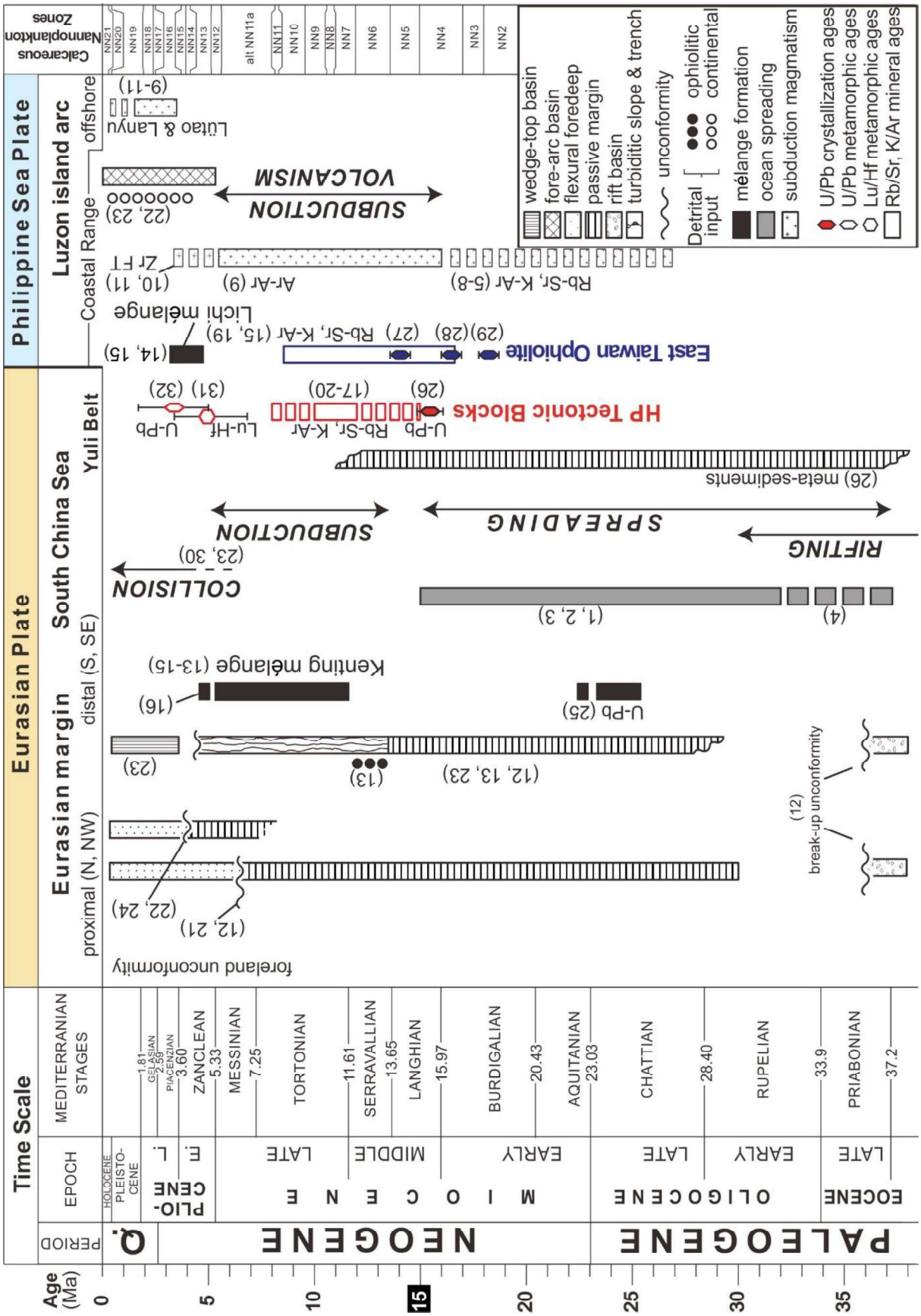
Time Scale
Eurasian Plate
Philippine Sea Plate
Eurasian margin
South China Sea
Yuli Belt
Luzon island arc
proximal (N, NW)
distal (S, SE)
offshore
Coastal Range
Calcareous Nannoplankton Zones
PERIOD
EPOCH
MEDITERRANIAN STAGES
Age (Ma)
Q.
NEOGENE
PALEOGENE
PLIO-CENE
MIOCENE
OLIGOCENE
EOCENE
HOLOCENE
PLEISTO-CENE
L.
E.
LATE
MIDDLE
EARLY
GELASIAN
PIACENZIAN
ZANCLEAN
MESSINIAN
TORTONIAN
SERRAVALLIAN
LANGHIAN
BURDIGALIAN
AQUITANIAN
CHATTIAN
RUPELIAN
PRIABONIAN
1.81
2.59
3.60
5.33
7.25
11.61
13.65
15.97
20.43
23.03
28.40
33.9
37.2
NN21
NN20
NN19
NN18
NN17
NN16
NN15
NN14
NN13
NN12
alt NN11a
NN11
NN10
NN9
NN8
NN7
NN6
NN5
NN4
NN3
NN2
wedge-top basin
fore-arc basin
flexural foredeep
passive margin
rift basin
turbiditic slope & trench
unconformity
Detrital input
ophiolitic
continental
mélange formation
ocean spreading
subduction magmatism
U/Pb crystallization ages
U/Pb metamorphic ages
Lu/Hf metamorphic ages
Rb/Sr, K/Ar mineral ages
RIFTING
SPREADING
SUBDUCTION
COLLISION
SUBDUCTION
VOLCANISM
(1, 2, 3)
(4)
(26) meta-sediments
U-Pb
Rb-Sr, K-Ar
Lu-Hf
U-Pb
(17-20)
(26)
(31) (32)
HP Tectonic Blocks
(23, 30)
East Taiwan Ophiolite
(29)(28) (27) Rb-Sr, K-Ar (15, 19)
(14, 15)
Lichi mélange
(22, 23)
Rb-Sr, K-Ar (5-8)
Ar-Ar (9)
(10, 11)
Zr FT
Lütao & Lanyu
(9-11)
(12, 13, 23)
(13)
(23)
U-Pb (25)
Kenting mélange (13-15)
(16)
(12, 21)
(22, 24)
foreland unconformity
(12)
break-up unconformity

Fig. 3-2: Tectonostratigraphic chart reviewing timing of major geodynamic events around Taiwan. Recent geochronological ages are highlighted. Note discrepancies on the onset of continent-arc collision and uncertainties on the timing of pre-collisional metamorphism in the Yuli Belt. Sources: (1) Taylor and Hayes 1983; (2) Briais et al. 1993; (3) Sibuet et al. 2002; (4) Hsu et al. 2004; (5) Lan et al. 1996; (6) Richard et al. 1986; (7) Juang, 1988; (8) Juang and Chen 1990; (9) Lo et al. 1994; (10) Chen et al. 1992; (11) Yang et al. 1995; (12) Lin and Watts 2002, 2003; (13) Pelletier and Stephan 1986; (14) Page and Lan 1983; (15) Chang and Chi 1983; (16) Huang et al. 1983; (17) Jahn and Liou 1977; (18) Jahn et al. 1981; (19) Juang and Bellon 1986; (20) Lo and Yui 1996; (21) Yu and Chou 2001; (22) Chi et al. 1981; (23) Huang et al. 2006; (24) Chen et al. 2001; (25) Tian et al. 2019; (26) Chen et al. 2017; (27) Hsieh et al. 2017; (28) Lin et al. 2019; (29) Huang et al. 2018; (30) Teng 1990; (31) Sandmann et al. 2015; (32) Yui et al. 2014. Geologic time scale after Gradstein et al. (2012)

Meanwhile, numerous aspects of the tectonics of the Yuli Belt remain unclear. The kinematics of the Shoufeng Fault, the tectonic contact between the Yuli Belt and the westerly adjacent Tailuko unit (Yen, 1963), are little investigated. Lin et al. (1984) described the Shoufeng Fault as an NNE-striking and 70°~80° W-dipping and topographically discernible feature, but no outcrop-scale faults were found. Recent geological maps (e.g., Lin and Chen 2016) depict the Shoufeng Fault essentially unchanged since Ho (1986). Chen et al. (2017) revised the fault trace (Fig. 3-4), but without providing clear arguments for this reinterpretation. Also, the tectonic relationship between blueschist-facies units and the metasedimentary unit is poorly constrained. Furthermore, whole-rock geochemical data of the blueschist-facies assemblages yield partly intriguing results concerning the geodynamic environment in which the protoliths were issued (Island Arc vs. Mid Oceanic Ridge origin; e.g. Jahn et al. 1981).

In this study, we reinvestigated the tectonic evolution of the Yuli Belt with particular emphasis on the structural relationships between its blueschist-facies rocks and the metasedimentary unit. We build on recent geochronological results (e.g. Chen et al., 2017), incorporating own structural data from several river transects. Three new cross-sections across the Yuli Belt were constructed, suggesting that the blueschist-facies unit tectonically overlies the metasedimentary unit along a thrust that was later tightly folded together with the adjacent units of the Yuli Belt. We present more definitive whole rock geochemistry data from three tectonic blocks of Yuli Belt and explore the spatial and temporal relationships among the high-pressure blocks, the East Taiwan Ophiolite of the Lichi Mélange (Table 3-2), the oceanic crust of the South China Sea, and the incipient Luzon arc. Finally, relying on a simple plate tectonic reconstruction, we suggest that the Yuli Belt high-pressure unit could have originated from the oceanic crust of the South China Sea before its subduction below the Philippine Sea Plate. Since this unit at present occupies a structural position between series derived from Eurasia and those from the Philippine Sea Plate, it represents as part of the suture zone.

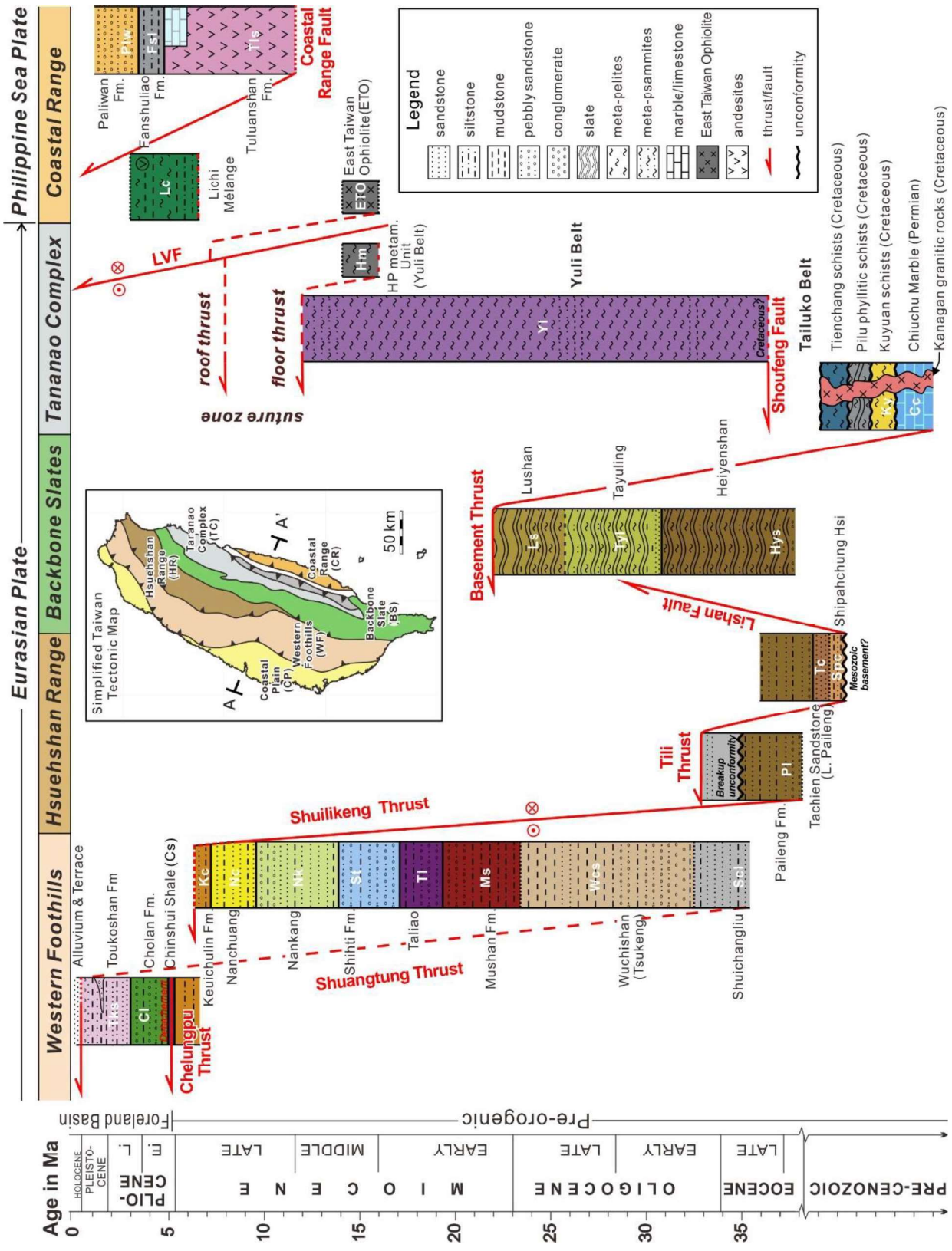

Fig. 3-3: Schematic tectonostratigraphic columns portraying the stratigraphic ranges of the major tectonic units and their mutual fault-bound relationships shown (based and modified after Yue et al., 2005; Brown et al., 2012; Chen et al., 2017; Huang et al., 2018, and references therein). We conceptually treat the blueschist-facies rocks of the Yuli Belt as occupying the position of part of the suture zone separating Eurasian and Philippine Sea plates, bound by a floor thrust and roof thrust. The Longitudinal Valley Fault possibly overprinted the earlier roof thrust.

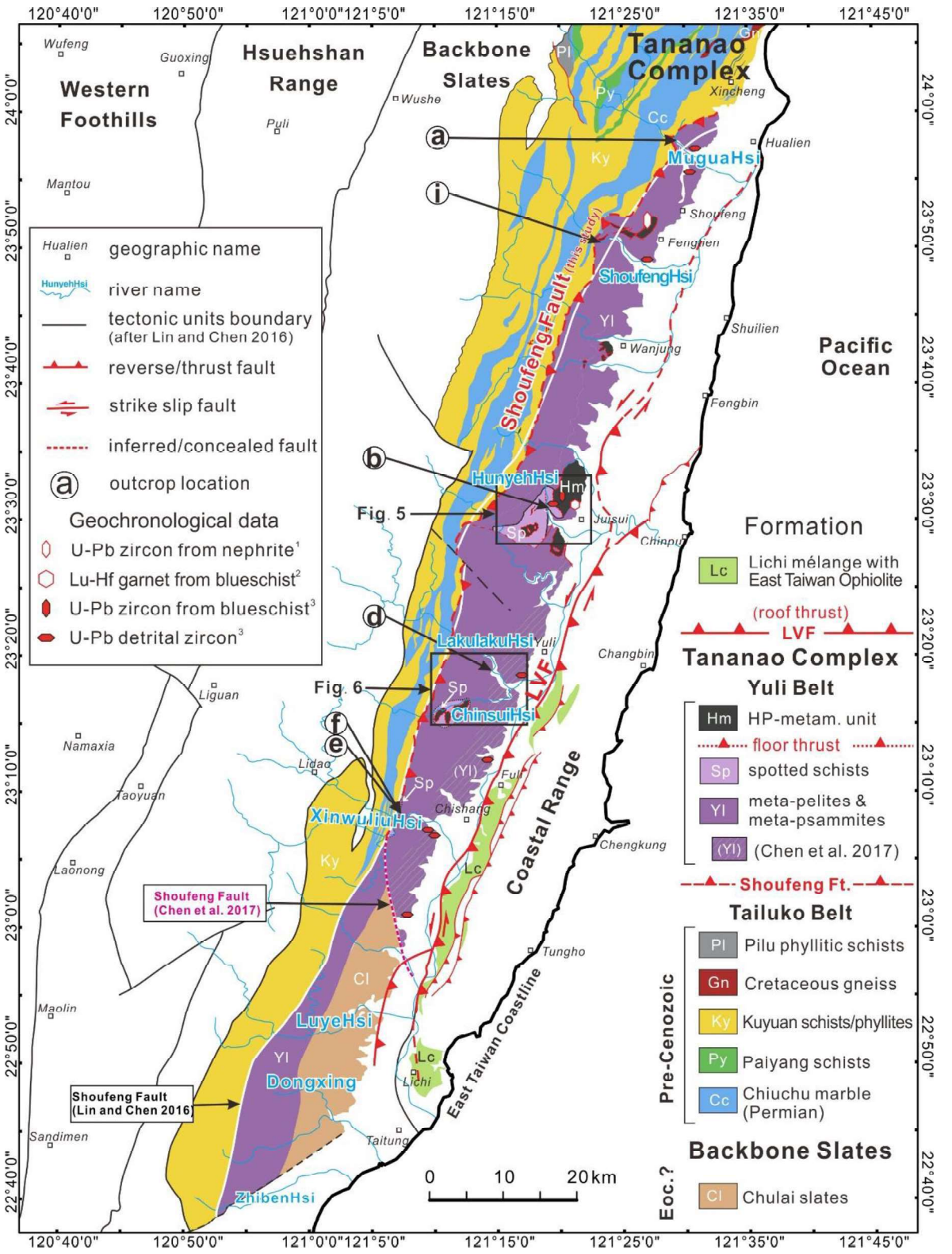

Fig. 3-4: Geological map of the metamorphic units exposed in the eastern part of Taiwan's Central Range (modified after Lin and Chen 2016). The Lichi Mélange is after Huang et al. (2006). The Yuli Belt hosts exotic blueschist-facies meta-igneous and ultramafic rocks (Hm) that we consider tectonically emplaced on top of an amphibolite- to greenschist-facies, polyphasely deformed metasedimentary unit (Yl). The diagonally dashed area of the Yuli Belt is adopted from Chen et al. 2017. Occurrences of spotted schists (Sp) are based on Yi et al. (2012) and Lo (2018). Locations of outcrops in Fig. 3-7 and thin sections in Fig. 3-9 are marked by small letters. Longitudinal Valley Fault (LVF) is from Shyu et al. (2005). Geological units outside Tananao Complex and Chulai Formation are not differentiated. Sources for the geochronological data in superscripts: 1: 3.3 ± 1.7 Ma (Yui et al. 2014); 2: 5.1±1.7 Ma (Sandmann et al. 2015); 3: 15.4-16.0 Ma for blueschist; 1900-1700 Ma, 1000-900 Ma, 850-700 Ma, 200-65 Ma and 65-8 Ma for metasediments (Chen et al. 2017).

3.2 Plate tectonic setting and regional geology

Several geodynamic events have shaped Taiwan throughout the Cenozoic (Fig. 3-2). The collision between the Eurasian passive continental margin and the Luzon island arc of the overriding Philippine Sea Plate (PSP) formed (and keeps forming) the spectacular topography of the Taiwan mountain belt since about 4 to 6 Ma (Chang and Chi 1983; Suppe 1984a; Teng; 1990; Yu and Chou 2001; Lee et al. 2015; Fig. 3-1). The Philippine Sea Plate moves towards NW at 60~90 mm/yr (e.g., Seno 1977; Yu et al. 1997). In the south of Taiwan, Eurasian lithosphere subducts southeastward underneath the Philippine Sea Plate. This geometry is inherited from the intra-oceanic subduction of South China Sea lithosphere underneath the Philippine Sea Plate, which commenced after the end of spreading in the South China Sea at around the early Middle Miocene (c. 16 Ma; Taylor and Hayes 1983; Sibuet et al. 2002; Fig. 3-2). While intra-oceanic subduction still prevails south of Taiwan along the Manila trench (e.g., Angelier 1986; Malavieille et al. 2002; Reed et al. 1992), advanced collisional shortening on the island of Taiwan has already led to the exposure of blueschist-facies rocks in the Yuli Belt of the eastern Central Range (Huang et al. 2006; Yui et al. 2012; Fig. 3-1).

Spreading of the South China Sea commenced at approximately 34 Ma (e.g., IODP Site U1435; Li et al. 2017) and stopped at c. 15.5 Ma (based on magnetic anomalies; Taylor and Hayes 1983; Briais et al. 1993; Sibuet et al. 2002). Subsequently, the oceanic lithosphere of the South China Sea started subducting under the Philippine Sea Plate as early as c. 15~16 Ma (Huang et al. 2006). This was inferred from ages of island arc magmas from Taiwan's Coastal Range, which forms a northward extension of the Luzon arc. Magmatism in the Coastal Range commenced in Early to Middle Miocene, as recorded by Rb-Sr, K-Ar, Ar-Ar, and fission track geochronological studies (e.g., Lo et al. 1994; Richard et al. 1986; Juang and Chen 1990; Chi et al. 1981). This is supported by more recently obtained U-Pb zircon ages of c. 14.2 Ma in the Chimei complex (Shao 2015). Geochronological studies on the East Taiwan Ophiolite (ETO) contained Lichi Mélange yielded U - Pb magmatic zircon ages of 14~17 Ma (Shao 2015; Hsieh et al. 2017; Huang et al. 2018; Lin et al. 2019). Similar ages of 15.6 ± 0.3 and 16.0 Ma were also obtained by the U-Pb dating of zircons from blueschists in the Yuli Belt (Chen et al. 2017), suggesting very similar early Middle Miocene protolith ages as for the mafic rocks in the ETO (Table 3-1).

The five major morphotectonic units making up the Taiwan mountain belt are illustrated as tectonostratigraphic columns in Fig. 3-3 (Ho 1986; Chen and Wang 1995). From west to east and separated by major faults, these are the Western Foothills, the Hsuehshan Range, the Backbone Slates, the Tananao Complex, and the Coastal Range. Tananao Complex and Coastal

Range are separated by the Longitudinal Valley Fault (LVF, Fig. 3-3). Units west of the LVF are derived from the Eurasian Plate. The Western Foothills, the Hsuehshan Range, and the Backbone Slates comprise the imbricated parautochthonous Cenozoic passive margin sequence of sandstones, conglomerates, argillites and slates structurally below the Tananao Complex (e.g., Yue et al. 2005; Beyssac et al. 2008). The deformation of those three imbricates involves the pro-wedge of Taiwan fold-and-thrust belt with the earliest fabrics of east-dipping bedding planes (S0) and slaty cleavage (S1) (e.g., Pelletier and Hu 1984; Fisher et al. 2007; Naylor and Sinclair 2007; Appendix B- Table S1). East of the LVF is the Coastal Range, consisting of Neogene calc-alkaline arc volcanics and associated volcanodetrital sediments, as well as the Huatung forearc basin deposits (e.g., Huang et al. 2018). A progressive increase in continental contamination of andesitic magmas correlates with progressively younger ages in Coastal Range volcanic rocks (e.g., Chi et al. 1981; Dorsey 1992; Shao et al. 2015). The transition from oceanic to incipient continental subduction induced the subduction of a slice of the forearc lithosphere (e.g., Malavieille et al., 2002; Wu et al. 2008; Sandmann et al. 2015). The forearc lithosphere belonging to the Philippine Sea Plate is suspected to subduct beneath the Coastal Range at about 22°N and is probably absent north of 24°N, shortly before the cessation of island-arc magmatism (Kao et al. 2000; Sibuet et al. 2002; Shyu et al., 2011).

The Tananao Complex crops out as a narrow belt west of the LVF and bears evidence of polymetamorphism and multiple deformations (e.g., Ernst and Jahn 1987). Traditional nomenclature subdivides the Tananao Complex into the western Tailuko Belt and the eastern Yuli Belt (Ho 1986; Chen and Wang 1995), separated by the Shoufeng Fault (Yen 1963, Figs. 3-3 and 4). The Tailuko Belt consists of Permian marbles, variegated Mesozoic metapelites, and greenschists (Liou 1981), intruded by the Late Cretaceous Kanagan granitic gneiss (Jahn 1986; Fig. 3-3). The Yuli Belt is dominantly composed of greenschist facies, often highly carbonaceous quartz-mica schists with blocks of metabasites up to blueschist facies (Fig. 3-4). Three larger exposures of these blocks are the Wanjun, Juisui, and Chinsui Hsi areas (Yen 1963; Liou et al. 1975; Liou and Ernst 1984; Tsai et al., 2013; Table 3-2 and Fig. 3-4). The Yuli Belt's eastern contact with the Eocene (?) Chulai/Pilushan Formation of the Backbone Slates is a sharp boundary in terms of lithology and metamorphic grade, previously interpreted as an unconformity (Stanley et al. 1981; Ho 1986). However, based on comparable ages on detrital zircons from the Yuli Belt metasediments and the northern part of the Chulai Formation (Lin and Chen 2016) as young as Miocene, the Chulai Formation has been reinterpreted as part of the metasediments of the Yuli Belt (e.g., Chen et al. 2017; Chen et al. 2019; Conand et al. 2020).

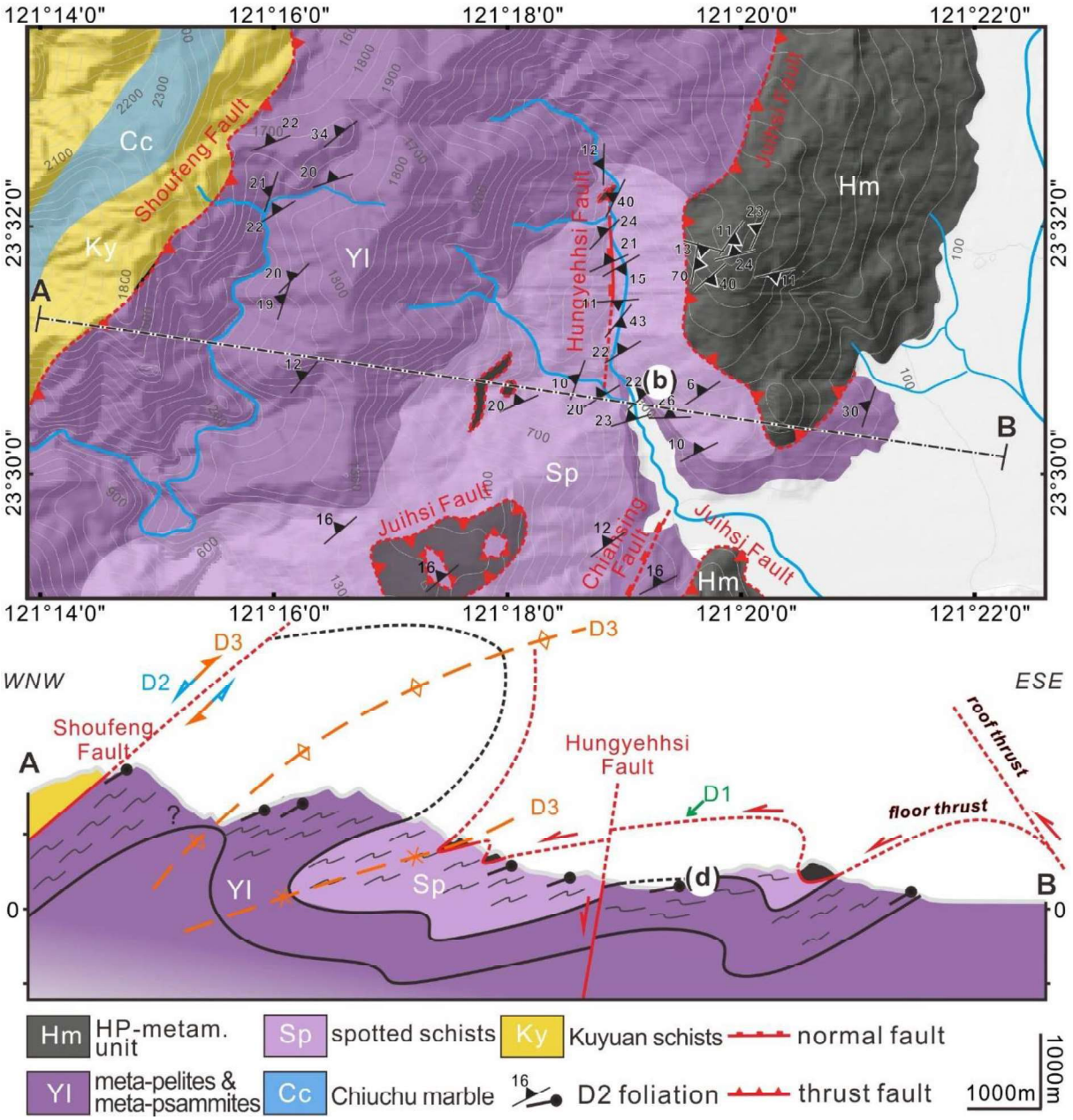

Fig. 3-5: Geological map and the cross-section A-B of the Hunyeh Hsi area. The floor thrust (Juihsi Fault) separates the blueschist-facies units from metasediments and is interpreted as a floor thrust of a suture zone. Topographic contours in this and the following figure in grey. See Fig. 3-4 for location.

3.3 New meso- to microscale observations in the Yuli Belt

3.3.1 Mesoscale structures in the metasedimentary unit

We made new outcrop-scale structural observations in the metasedimentary unit along several rivers crossing the Yuli Belt (Fig. 3-4). Mutual overprinting relationships between the observed structural elements suggest that they were formed during three successive deformation phases, termed D1, D2, and D3 in the following (Figs. 3-5, 6, 7 and 8). The S1 foliation forms a compositional layering, discernible for instance in the often graphite-rich metapelites to metasandstones in the Mugua Hsi area, where it is found to be overprinted by a moderately NW- to W-dipping S2 foliation developing a spaced crenulation or pressure-solution cleavage (Fig. 3-7a and Fig. 3-8a). Closer to the Shoufeng Fault, e.g. along the Shoufeng Hsi itself, S2 foliations usually form a more densely spaced and pervasive W- to NW-dipping compositional layering (Fig. 3-8b), carrying rare WSW-plunging stretching lineations (Fig. 3-8b) that we tentatively interpret as being associated with shear displacement along the Shoufeng Fault itself during deformation phase D2 or D3 (Fig. 3-4).

We found S2 to be often folded during a later deformation phase D3 (Fig. 3-7 b, c, d and Fig. 3-8b). On the outcrop scale, the intensity of this D3 deformation depends on the lithology. S3 foliations form an open axial plane to crenulation cleavage that is well-developed in the metapelitic layers, and absent in the metapsammites (Fig. 3-7b) owing to the competence contrast. In proximity to the Shoufeng fault, axial planes dip clearly to the west (Fig. 3-8 top right). On a regional scale, we interpret S3 to form gently to moderately W-dipping axial planes associated with kilometer-scale E-vergent folding of the entire Yuli Belt succession (Figs. 3-5 and 6), most likely in conjunction with a major phase of E-facing back-folding of eastern parts of the Taiwan orogen (Yeh, 2004; Fisher et al., 2007), termed here D3.

Cross section A-B (Fig. 3-5) also portrays a late-stage brittle normal fault (Hungyeh Hsi Fault), but with only minor offset and hence considered of no importance here. In general, however, late stage brittle faulting is well documented in the eastern Central Range (e.g., Crespi et al. 1996; Appendix B- Table S1).

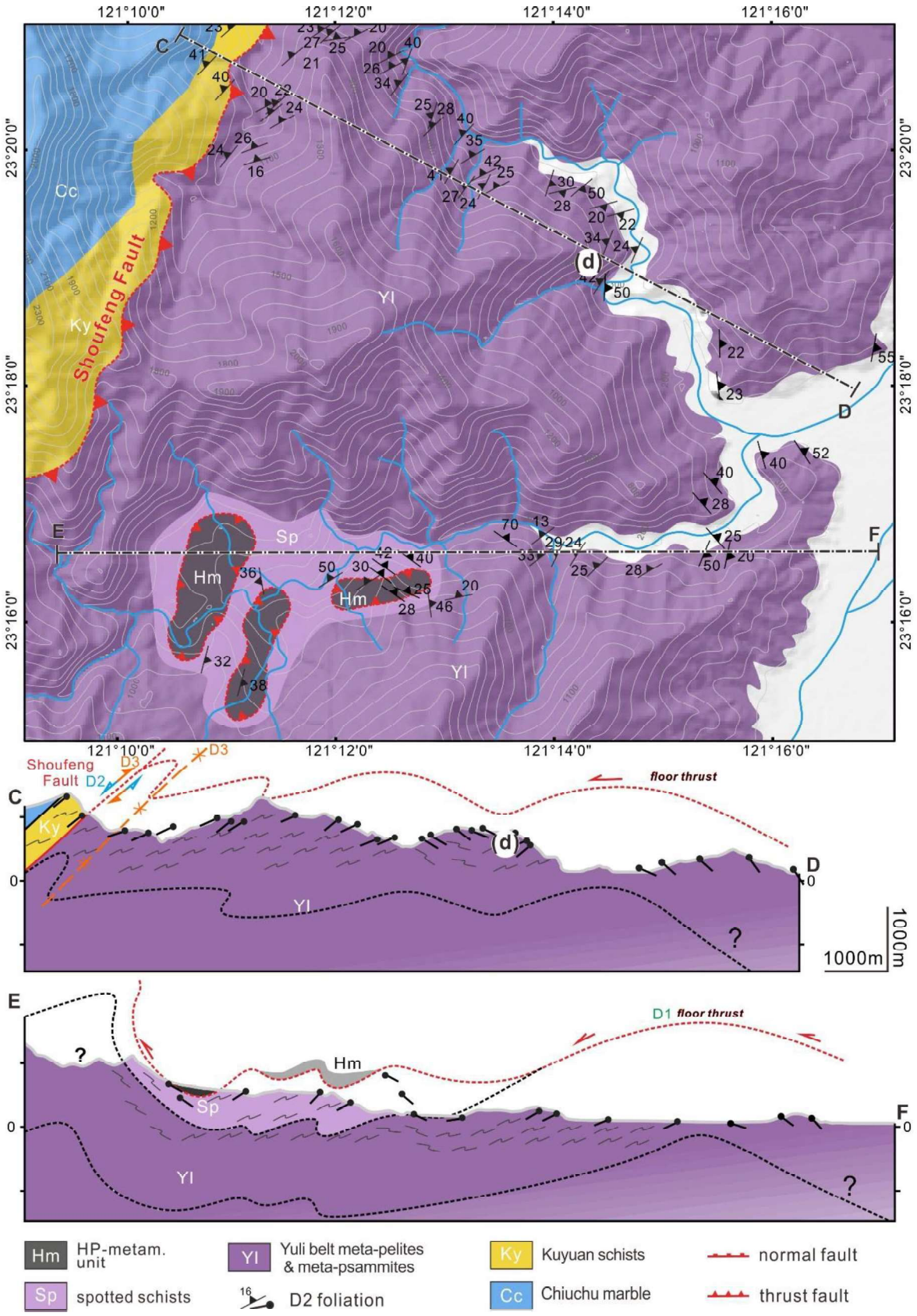

Fig. 3-6: Geological map and cross sections (C-D and E-F) of the Lakulaku Hsi and Chinsui Hsi area. See Fig. 3-4 for location.

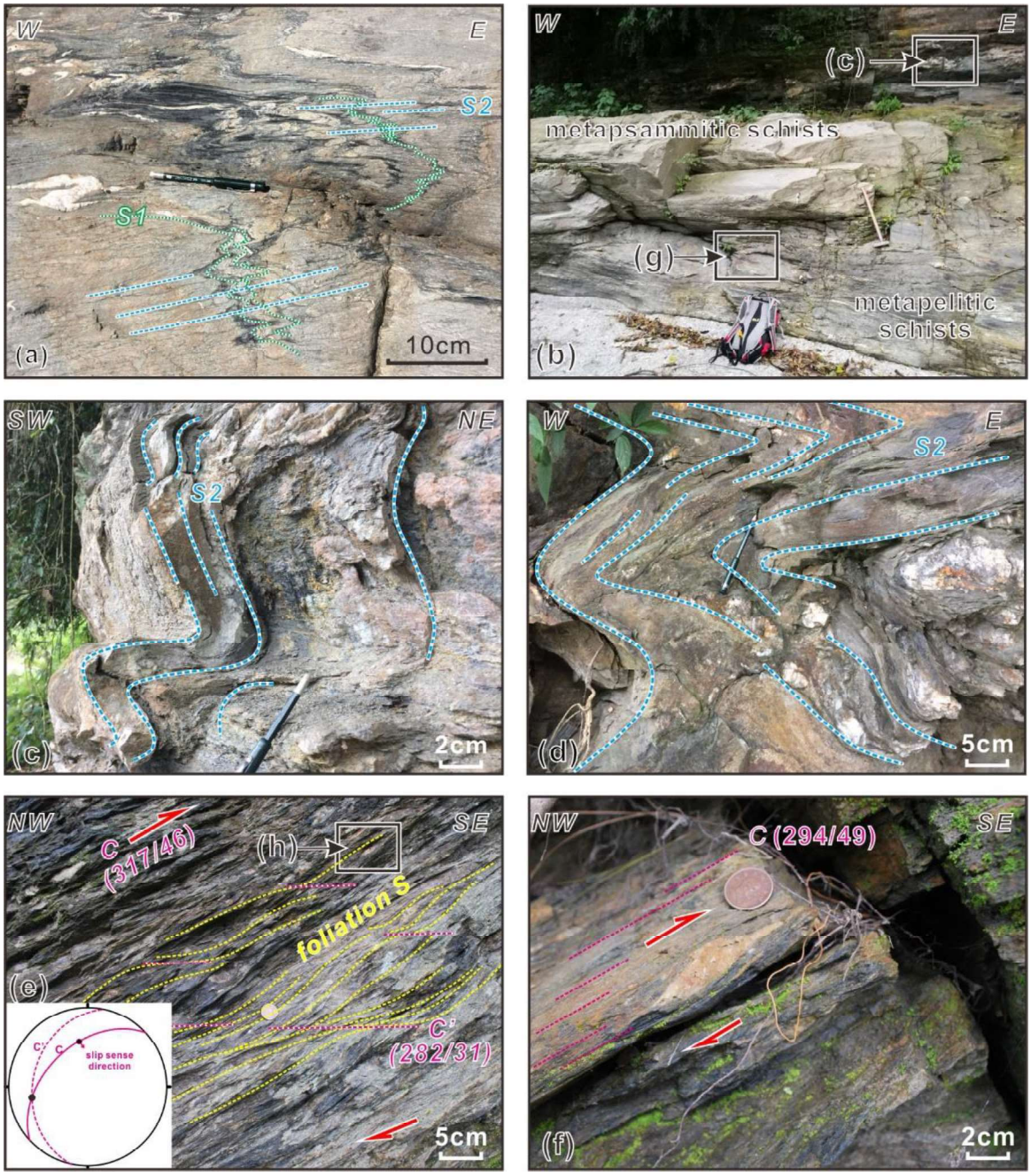

Fig. 3-7: Outcrops of polyphasely deformed metapelites and metapsammites in the Yuli Belt (a-f) considered representative for map-scale structures. Location: (a) Mugua Hsi (23.969540°N, 121.481748°E); (b) and (c) Hunyeh Hsi (23.509600°N, 121.325941°E); (d) Lakulaku Hsi (23.310988°N, 121.248190°E); (e) and (f) Xinwuliu Hsi (23.136959°N, 121.124392°E). (g) and (h) refer to areas where microscopic samples were taken (Fig. 3-9).

3.3.2 Shoufeng Fault

Previous maps have depicted the Shoufeng Fault as a quasi-vertical planar discontinuity separating Tailuko and Yuli Belts. We dare making the remark that such a map pattern was in clear violation of the actually observed gently NW- to W-dipping S2 foliations in several river transects (Figs. 3-4, 5 and 6). We have hence felt it necessary to partly remap the trace of the northern segment of the Shoufeng Fault to better agree with actual foliation dips (Fig. 3-4). The southern part of the Shoufeng Fault as shown in Fig. 3-4 still follows the interpretations of Lin and Chen (2016), but also depicts the alternative trace suggested by Chen et al. (2017; Fig. 3-4, thinly dashed red line). Dip direction and dip of S2 foliations are mostly W- to NW-dipping and remain constant across the contact. Also, the lithological and fabric transitions across this fault (e.g., Kuyuan schist of Tailuko Belt and Yuli Belt metasedimentary unit, along Hunyeh Hsi and Lakulaku Hsi, Fig. 3-4, Fig. 3-6, Fig. 3-8) are gradual. Both Kuyuan Schist and Yuli Belt metasedimentary unit are very similar to undistinguishable in the field as they are mainly composed quartz-mica schists. We suspect that the juxtaposition of Yuli and Tailuko Belts across the Shoufeng Fault may have occurred during an early W-directed transport direction (D2 phase). This interpretation is made on the notion that the Yuli Belt metasediments experienced elevated pressures of up to 1.5 GPa (Conand et al. 2020), which have not been reported in the westerly adjacent Tailuko Belt. We suspect that the Shoufeng Fault became reoriented and reactivated with an opposite slip sense during a later phase of E-vergent backfolding (termed here D3 phase; Fig. 3-7e, f). Evidence for such top-SE shear was found in an outcrop of spotted schists from Xinwuliu Hsi, close to the Shoufeng Fault (Fig. 3-7e, f and Fig. 3-9h). There, S-C' fabrics with a C-foliation (317/46) and C' shear bands (282/31) have accommodated SE directed shear (Fig. 3-7e, f, Fig. 3-9h). We interpret these top-SE senses of shear to also belong to D3 phase of backfolding, which overprints earlier (D2) top-W emplacement fabrics along the Shoufeng fault.

3.3.3 Microstructural observations from the spotted schist subunit

The mineralogically most distinctive unit within the metasedimentary unit of the Yuli Belt is the albite spotted schists, separately mapped in Fig. 3-4, relying on Lin et al. (1984), Yi et al. (2012) and Lo (2018). The spots in these metapelites are formed by albite and - to a smaller amount - garnet and titanite porphyro*blasts* (Yang and Wang 1985; Fig. 3-9). The characteristic mineral assemblage of these schists is albite, garnet, muscovite, chlorite, titanite, ± tourmaline, ± calcite and ± rutile (Chiang 2003), as well as a variable amount of carbonaceous matter. Our observations suggest that the growth of albite porphyro*blasts* with graphitic inclusions predated the formation of the S3 foliation. This is evidenced in a sample from the Juisui/Hunyeh Hsi area (Fig. 3-9 g), which shows that asymmetrically rotated albite with graphitic inclusions and

chlorite in pressure shadows forms a porphyroclast with respect to the older S2 foliation. In the sample from Xinwuliu Hsi, albite and titanite form porphyroclasts that are pre-kinematic with respect to the younger foliation (Fig. 3-9 h). This younger foliation forms pervasive C-planes with enrichment of carbonaceous material. S-C' type of shearing clearly transposes an older compositional layering S that can be identified in isolated microlithons. Chlorite is locally observed to form at the expense of biotite and grows in the main foliation, implying that this fabric formed at greenschist-facies conditions. In combination, these observations suggest that peak-metamorphic conditions in the spotted schists were attained before the D3 event that locally forms the penetrative fabrics observed. This would be in support of our hypothesis portrayed in cross sections (Fig. 3-5 and 6), according to which the nappe structure within the Yuli Belt was refolded during D3.

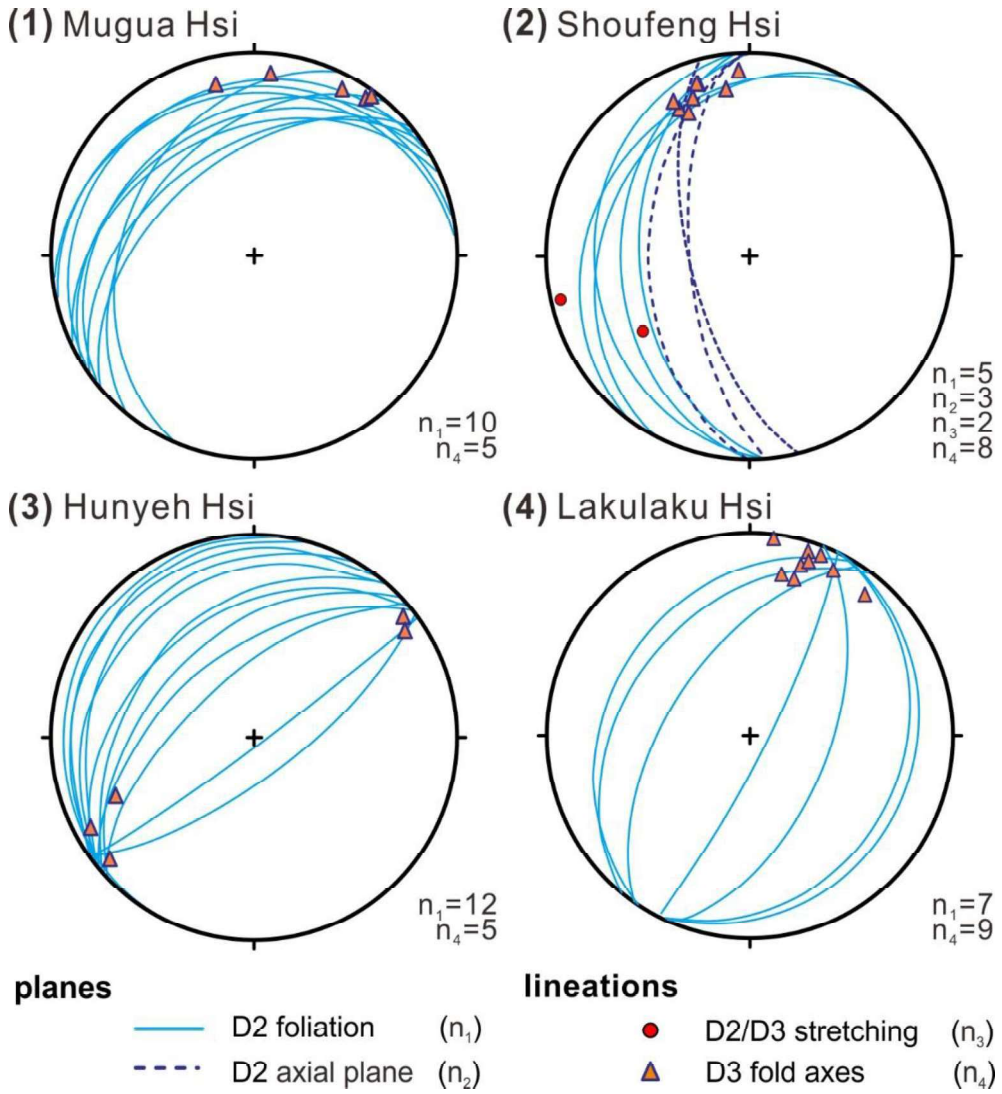

Fig. 3-8: Equal area, lower hemisphere ("Schmidt net") projections of fabric elements across Yuli Belt (1-4) considered representative for the map-scale structures. Compare with Fig. 3-7 for actual outcrop geometries at the corresponding locations. (1)-(a) Mugua Hsi; (2)-(i) Shoufeng Hsi (23.841331°N, 121.380597°E); (3)-(b) Hunyeh Hsi; (4)-(d) Lakulaku Hsi.

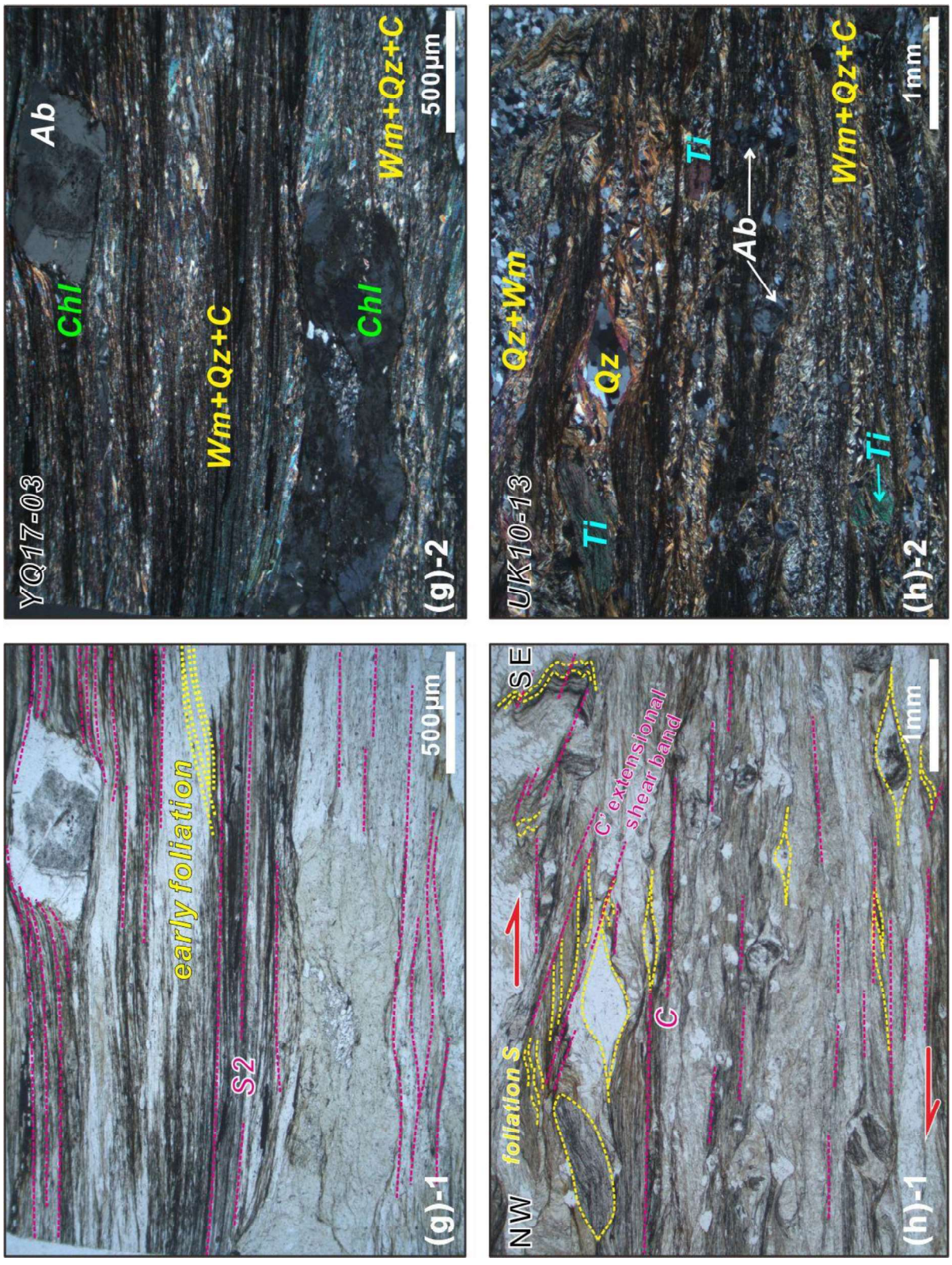

Fig. 3-9: Microscopic features of albite spotted mica schists from the Hunyeh Hsi and Xinwuliu Hsi areas of the Yuli Belt, respectively. (g)-1 and (h)-1 are in plane-polarized light; (g)-2 and (h)-2 in cross-polarized light. (g): albite-chlorite-mica schists in the Hunyeh Hsi area of Fig. 3-7b with pressure solution cleavage affecting an asymmetric albite σ-porphyroclast in metapelites. (h): albite-quartz-mica schists from the Xinwuliu Hsi area of Fig. 3-7e, showing mylonitic foliations with top-to-SE sense of shear during D3. Abbreviations: Ab = albite; C = carbonaceous material; Chl = chlorite; Qz = quartz; Ti = titanite; Wm = white mica.

3.4 Whole-rock geochemistry of the HP metamorphic rocks

3.4.1 Sampling and petrography

Twelve rock samples were collected for this study from three tectonic high pressure metamorphic blocks of Yuli Belt, i.e., Wanjun, Juisui, and Chinsui Hsi areas (Table 3-3; Fig. 3-4; see Appendix B- Fig. S2 for sample localities), to further extend the sample base (e.g., Liou et al. 1975; Jahn et al. 1981; Lin et al. 1984; Sun et al. 1998; Shao 2015) for characterizing geotectonic settings in which they were issued. Most of samples are from the largest tectonic block, Juisui / Tamayan area (e.g., Fig. 3-10(A)); two samples are from Wanjun area (e.g., Fig. 3-11(c)); and one sample is from Chinsui Hsi area (Fig. 3-11(b)).

The rock samples can be classified into five groups according to mineralogical and petrographic studies (e.g., Liou et al. 1975 and this study; Fig. 3-12). In some cases, garnet-rich coarse-grained dark amphibolite are in direct contact with garnet free fine-grained amphibolite (Fig. 3-11(a), Fig. 3-10(C)). Pillow structures are preserved in the massive to foliated amphibolite (Fig. 3-10(B)). (1) Glaucophane schists: Glaucophane-bearing rocks (Type I and Type II after Tsai et al. 2013) occur as layers or irregular meter-scale boulders surrounded by greenschist or amphibolite. Major phases are amphibole (42%), quartz (24%), epidote (21%) and garnet (11%). In these rocks, glaucophane occurs only as rare inclusions within porphyroblastic bluish-green amphibole (Fig. 3-11(g)). (2) Garnet-epidote amphibolites (Type III in Tsai et al. 2013): Major phases are amphiboles (40%), epidote (19%), garnet (12%), and quartz + albite (27%). Garnet is euhedral and zoned. Quartz, epidote, and rare dolomite are present in garnet cores (Fig. 3-11(e), (f)). (3) Epidote amphibolites (glaucophane free Type IV in Tsai et al. 2013): Garnet-absent rocks with major phases of amphiboles (45%), epidote (24%), paragonite (10%), and quartz + albite (18%). (4) Chlorite schists: They were collected from Wanjun area (Fig. 3-11(c), (d)). Major phases are chlorite (45%), albite (40%), amphiboles (6%), epidote (5%), and titanite (1%). (5) Meta-albite rich felsic / albitite rocks: They were collected from Chinsui Hsi area (Fig. 3-11(b), (h)). The albitite consist of euhedral porphyroblastic albite (85%), amphiboles (6%), white mica (3%). They occur as irregular masses or layers surrounded by serpentinite or talc albite chlorite schists (Fig. 3-10(F)).

3.4.2 Analytical methods

After removing weathered surfaces, all samples were crushed in a jaw-crusher, cleaned in an ultrasonic bath with deionized water, sieved and carefully hand-picked under a binocular microscope to avoid the most altered portions of the samples. Selected whole rock chips (~10g) of each sample were ground with a ball mill (sintered corundum) to a grain size < 63 μm for homogenization and dried at 105°C overnight. Major elements (Table 3-3) were measured using

X–ray fluorescence (XRF) and after total digestion, selected trace elements (Table 3-4) were measured using inductively coupled plasma-optical emission spectrometry (ICP–OES) and inductively coupled plasma–mass spectrometry (ICP–MS) at the Institute of Geological Sciences at the Friedrich-Schiller University Jena.

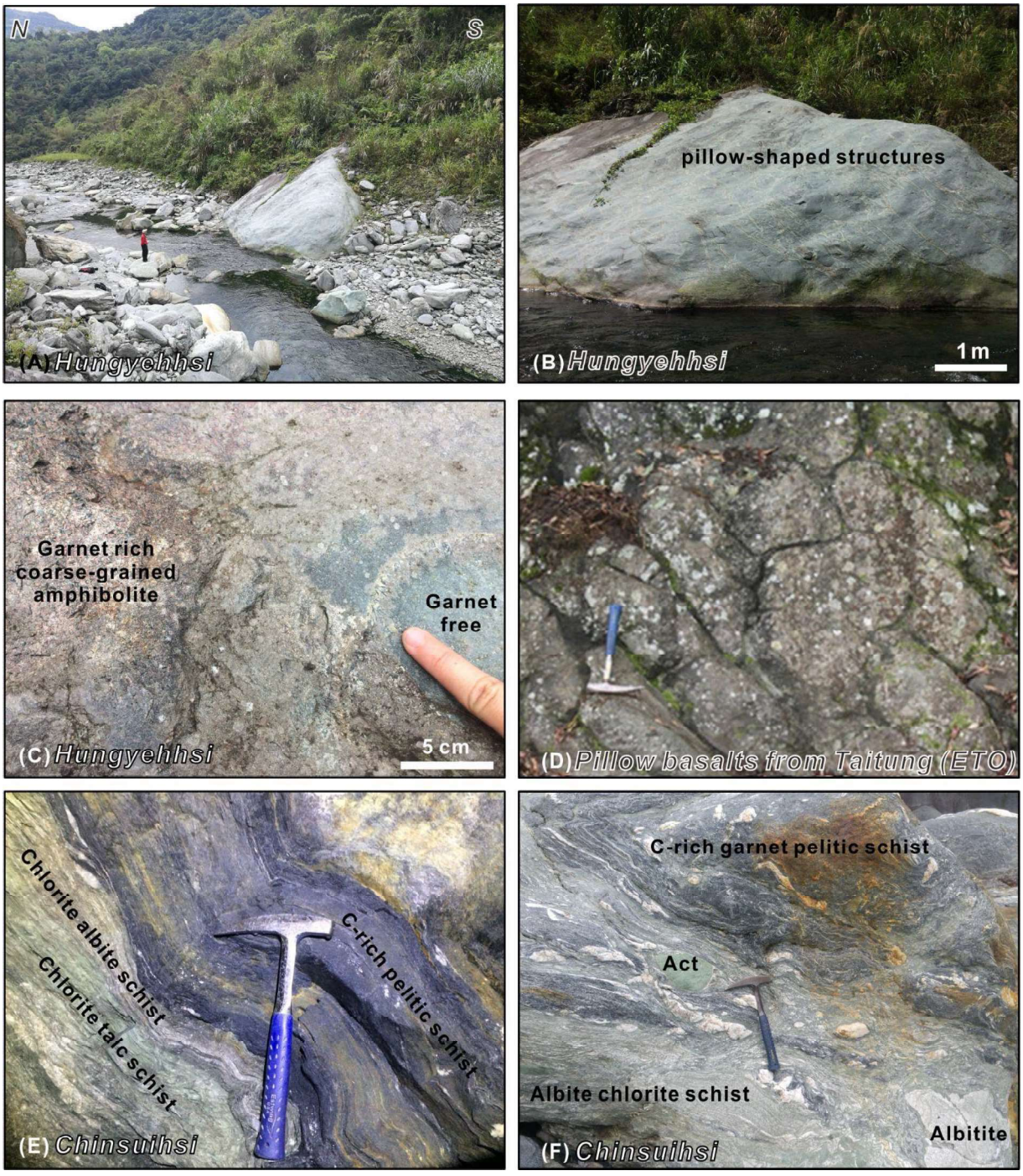

Fig. 3-10: Field occurrences of the high-pressure metamorphic rocks from Yuli Belt. (A)-(C): A slump float in Hungyehhsi/Juisui area. Garnet-free and garnet-rich mafic amphibolite with flattened pillow structures. The medial boundary zone is enriched in coarse-grained, dark-green calcic amphibole and fine-grained yellowish epidote as thin folded layers. (D): Unmetamorphosed Pillow basalts from Taitung (Lin et al. 2019) for comparison. (E): The contact relationships between chlorite talc schists, chlorite albite schists, and carbonaceous (C) -rich pelitic schists from a serpentinite pit mine, Chinsuihsi area. (F): Actinolite (Act) and albitite are included in albite chlorite schists and carbonaceous (C) -rich pelitic schists from Chinsuihsi area.

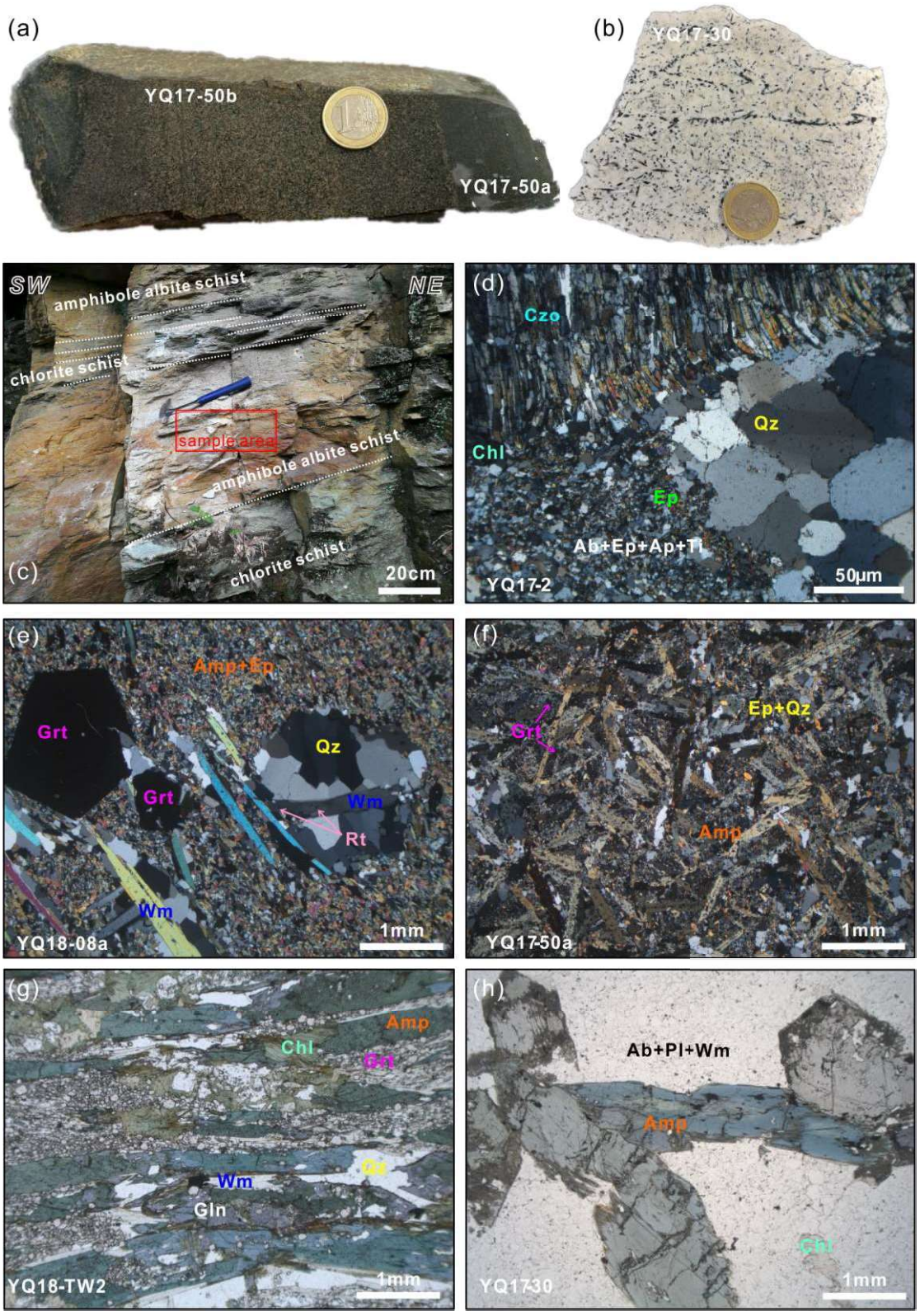

Fig. 3-11: Megascopic and microscopic features of the high-pressure metamorphic rocks from Yuli Belt. The coin is 23.25 mm in diameter for scale in (a) and (b). (d), (e) and (f) are photomicrographs in cross polarized light. (g) and (h) are photomicrographs in plan polarized light. (a): Hand specimen of a garnet-hornblende metagabbro from Juisui area. It is subdivided into the fine-grained amphibolite type (YQ17-50a) and the coarse-grained amphibolite type (YQ17-50b). (b): Hand specimen of an amphibole albitite from Chisuihsi area (YQ17-30). (c): Southwest-dipping foliated and banded amphibole-rich chlorite schists at the mountain path of Wanjung (23°42'38.10"N, 121°24'37.49"E). (d): epidote-clinozoisite-chlorite-amphibole-albite schists from the sample area of (c). (e), (f) and (g) are garnet-epidote-amphibole gneiss/schists from Juisui area. (h): Thin section of sample (b). Abbreviations: Ab=albite; Amp=amphibole; Czo=clinozoisite; Chl=chlorite; Ep=epidote; Grt=garnet; Wm=white mica; Pl=plagioclase; Qz=quartz; Rt=rutile.

3.4.3 Major element compositions

Major element data for sixteen samples from three high-pressure metamorphic units are given in Table 3-3. The analyzed rocks show a wide compositional range on the total alkali-silica (TAS) diagram (Fig. 3-12). The SiO_2 content ranges from 42 to 66 wt.% with a small gap between 59 and 63 wt.% (Bunsen-Daly gap; Bunsen, 1851; Daly, 1925; Bonnefoi et al., 1995), and the $Na_2O + K_2O$ ranges from 0.5 to 10.5 wt.%, dividing the samples into mafic (mostly MgO =2.8-13.0 wt.%) and felsic (mostly MgO =1.50-6.20 wt.%) suites (Table 3-3). Most of meta-mafic rocks (Group (1)-(4)) are in the subalkaline/ tholeiite series, and meta- felsic rocks (Group (5)) are plotted in the alkaline series (Fig. 3-12). Chlorite schists (4) and albitite rocks (5) have lower K_2O (< 0.30 wt%) and higher Na_2O (> 8 wt%).

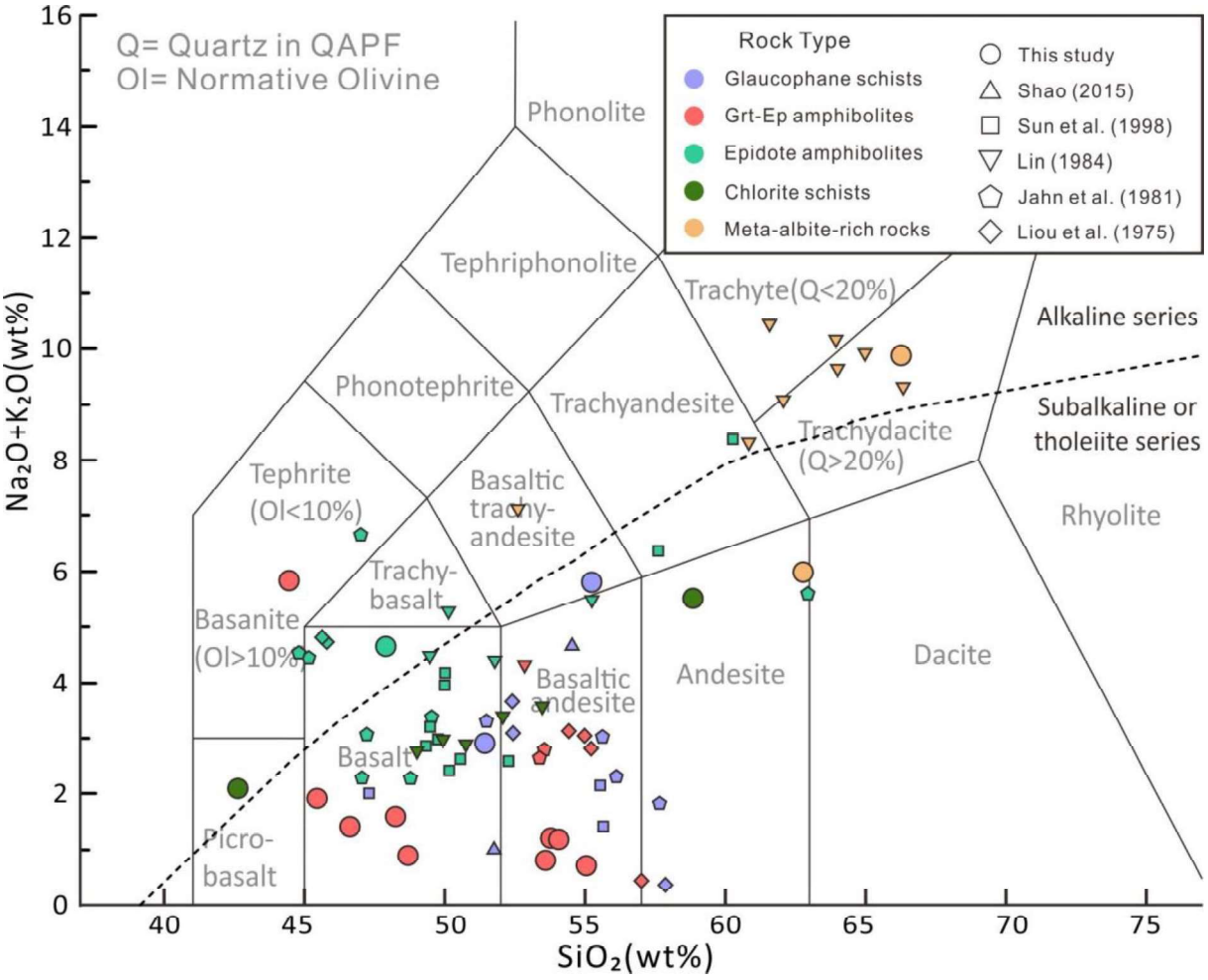

Fig. 3-12: TAS diagram SiO_2 / (Na_2O + K_2O) of Le Bas et al (1986). Samples are divided into five groups: (1) Glaucophane schists; (2) Garnet-epidote amphibolites; (3) Epidote amphibolites; (4) Chlorite schists; (5) Meta-albite rich felsic / albitite rock. Data from Liou et al. (1975), Jahn et al. (1981), Lin (1984), Sun et al. (1998) and Shao (2015) are included for comparison.

Table 3-3: Concentrations of the major element oxides of the high pressure metamorphic rocks from the Yuli Belt, Taiwan (wt.%). Major elements were measured using X–ray fluorescence (XRF). < LOD: below the limit of detection. LOI: Loss on ignition. See Appendix B- Fig. S2 for sample localities.

Sample name	Lithology	Location	SiO_2	Al_2O_3	TiO_2	CaO	K_2O	Na_2O	Fe_2O_3	MgO	MnO	P_2O_5	Total	LOI
UK09-26	chlorite schists	Wanjun	42.43	0.99	15.79	12.04	0.28	15.19	10.76	1.92	0.18	0.08	99.66	4.25
YQ17-2	chlorite albite schists	Wanjun	62.13	0.72	14.75	5.99	0.09	5.54	3.90	5.84	0.02	0.13	99.11	2.34
UK09-23	garnet-epidote amphibolites	Juisui	44.30	0.77	22.69	11.91	0.65	7.42	5.93	2.26	3.54	0.23	99.70	4.14
UK09-24	epidote amphibolites	Juisui	47.67	0.85	18.19	9.65	0.27	10.95	7.18	1.29	3.33	0.11	99.49	3.61
UK09-25	garnet-epidote amphibolites	Juisui	54.92	0.49	11.77	16.56	1.77	4.38	8.89	0.64	0.09	0.30	99.81	1.01
UK10-17	chlorite schists	Juisui	58.41	0.38	15.43	6.08	0.10	8.44	5.09	4.22	1.25	0.06	99.46	1.90
YQ17-50a	garnet-epidote amphibolites	Juisui	46.28	0.63	18.16	11.56	0.72	5.36	15.14	1.35	0.05	0.13	99.38	2.03
YQ17-50b	garnet-epidote amphibolites	Juisui	53.45	0.51	13.32	15.19	1.48	4.48	9.78	1.12	0.10	0.17	99.60	0.66
YQ17-50c	garnet-epidote amphibolites	Juisui	45.23	0.90	14.29	15.72	1.23	9.53	10.58	1.42	0.49	0.23	99.62	2.25
YQ18-06a	garnet-epidote amphibolites	Juisui	53.11	0.50	12.55	9.47	1.17	5.66	15.27	0.78	0.05	0.77	99.33	1.53
YQ18-06b	garnet-epidote amphibolites	Juisui	48.54	0.70	14.29	12.01	1.11	5.33	16.85	0.83	0.04	0.06	99.76	1.64
YQ18-06c	garnet-epidote amphibolites	Juisui	53.79	0.44	11.72	11.36	1.09	6.17	13.69	1.14	0.06	0.18	99.64	1.71
YQ18-08a	garnet-epidote amphibolites	Juisui	48.02	1.04	16.37	14.29	0.29	5.19	12.89	1.48	0.09	0.03	99.69	1.65
YQ18-TW2	glaucophane schists	Juisui	51.19	0.56	13.84	18.40	1.86	4.63	5.63	1.51	1.43	0.44	99.49	0.82
UK10-20	glaucophane schists	Juisui	54.72	0.30	15.49	14.84	1.28	4.07	2.56	1.70	3.96	0.22	99.14	0.91
YQ17-30	amphibole albitite	ChinsuiHsi	66.08	0.42	16.81	2.14	0.02	3.67	0.86	9.82	0.02	< LOD	99.84	0.85

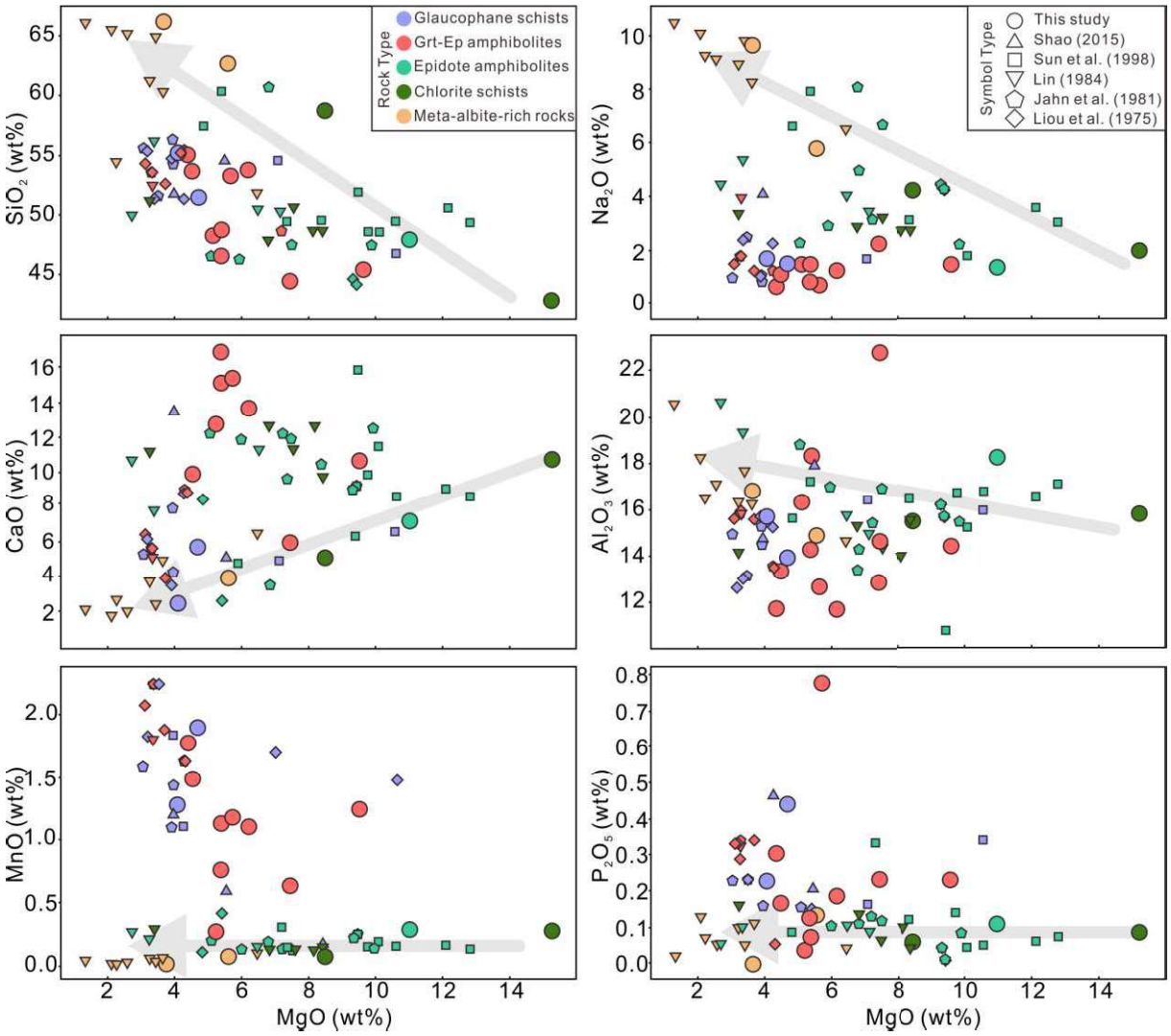

Fig. 3-13: Plots of MgO versus other major oxides (Harker diagrams). Data from Liou et al. (1975), Jahn et al. (1981), Lin (1984), Sun et al. (1998) and Shao (2015) are included for comparison. Grey arrows roughly indicate the trends from mafic suites (Group-(4) and (3)) to felsic suites (Group-(5)).

Plots of MgO versus other major oxides are shown in Fig. 3-13. Both glaucophane schists (1) and garnet-epidote amphibolites (2) with distinctly higher MnO (> 0.50 wt%), higher P_2O_5 (> 0.15 wt%) and lower Na_2O (< 2.20 wt%) have apparently accumulated larger grain size of garnet consistent with petrographic examinations (Fig. 3-11 (e)(f)(g); Fig. 3-13). Garnet-epidote amphibolites (2) also have pronouncedly higher CaO (> 12 wt%) and lower Al_2O_3 (< 13 wt%). The MnO and P_2O_5 content of epidote amphibolites (3) are lower than other mafic rock types (MnO = ca. 0.1-0.2 wt% and P_2O_5 = ca. 0.1 wt%) while the Na_2O and Al_2O_3 content are higher (Na_2O = ca. 2-8 wt% and Al_2O_3= ca. 14-18 wt%). The chlorite schists (4) are scattering plotted in the SiO_2 / (Na_2O + K_2O) diagram with a large range of SiO_2 (ca. 43-58 wt%) and MgO (ca. 3.5-16 wt%) content. In most cases, chlorite schists (4) points are seated in the area of epidote amphibolites (3) (Fig. 3-13), indicating both of rocks could share similar

Table 3-4: Trace elements of the meta-igneous rocks from the Yuli Belt, Taiwan (μg/g). (: measured by ICP-OES)*

Sample Name	UK 09-26	YQ 17-2	UK 09-23	UK 09-24	UK 09-25	UK 10-17	YQ 17-50a	YQ 17-50b	YQ 17-50c	YQ 18-06a	YQ 18-06b	YQ 18-06c	YQ 18-08a	YQ 18-TW 2	UK 10-20	YQ 17-30
V	251.10	150.00	186.10	192.00	191.60	141.40	206.00	162.40	221.30	72.67	78.20	69.40	177.00	275.00	232.30	58.40
Cr	216.90	8.00	77.00	109.70	39.90	38.60	52.02	34.90	159.40	39.88	53.20	47.10	197.50	33.80	35.20	1.48
Co	29.00	12.87	46.90	35.80	40.20	14.57	32.68	45.90	59.48	41.70	40.30	48.60	44.20	51.40	47.40	6.13
Ni	123.00	18.20	150.00	161.00	175.00	58.30	107.00	104.00	331.60	108.00	114.00	117.70	196.20	133.04	115.00	17.02
Cu	30.02	77.80	81.70	97.40	195.52	43.20	70.40	160.80	228.00	6.35	6.89	4.90	122.76	6.12	0.67	1.09
Zn	114.70	71.69	112.50	90.10	113.00	34.90	53.80	52.20	103.00	132.00	134.00	163.00	59.30	177.60	203.00	15.00
Rb	4.03	0.22	96.01	82.93	2.00	45.70	0.24	1.18	11.10	0.55	0.18	0.30	1.01	40.90	86.00	0.24
Sr*	210.30	101.40	457.00	160.60	186.30	196.40	525.00	252.60	237.93	404.19	532.00	440.00	308.30	32.52	47.50	44.00
Zr	46.00	78.50	56.80	53.70	42.90	24.67	62.00	62.40	57.30	57.10	73.00	75.65	23.70	52.96	18.26	63.00
Nb	2.51	4.77	9.82	6.30	4.67	1.15	8.55	5.77	8.70	7.80	13.90	7.59	1.57	3.65	8.31	2.30
Cs	0.04	0.04	2.43	1.00	0.59	0.64	0.04	0.68	0.81	0.04	0.02	0.05	0.03	1.39	5.49	0.91
Ba	45.70	3.67	718.00	720.00	8.10	186.60	5.39	6.00	101.46	15.10	11.90	10.00	6.56	839.30	1476.00	4.90
Hf	1.34	2.04	1.69	1.64	1.15	0.78	1.72	1.67	1.57	1.59	2.03	2.14	0.82	1.44	0.56	1.89
Ta	0.19	0.36	0.82	0.48	0.44	0.09	0.78	0.48	0.53	0.53	0.95	0.93	0.07	0.34	0.66	0.16
Pb	2.46	1.34	34.00	9.50	14.45	4.27	30.93	15.05	11.87	62.50	82.50	69.30	0.68	4.29	6.69	0.24
Th	0.22	0.93	12.83	6.59	8.73	0.59	11.80	10.56	4.85	8.82	12.32	12.15	0.14	10.56	11.20	0.48
U	0.10	0.33	2.11	1.23	1.98	0.19	1.80	1.84	0.93	1.65	2.37	2.33	0.38	2.02	1.57	0.33
La	3.13	7.54	43.99	18.96	45.52	2.81	42.17	45.56	27.60	34.40	42.20	41.41	2.31	50.80	47.82	3.00
Ce	8.16	15.30	78.71	42.70	57.82	6.51	72.09	67.07	36.20	54.50	77.00	70.80	6.43	66.70	68.80	6.27
Pr	1.29	1.92	11.32	4.90	11.37	0.91	10.76	11.40	7.34	8.43	11.03	10.53	1.09	12.88	11.94	0.87
Nd	6.73	8.35	45.70	19.71	46.90	4.27	43.60	46.50	31.72	34.20	45.00	42.60	5.99	53.10	49.14	4.24
Sm	2.25	2.15	9.77	4.28	10.00	1.23	9.30	9.92	7.30	7.22	9.58	8.90	2.19	11.33	10.50	1.33
Eu	1.05	0.95	2.25	1.22	2.49	0.44	2.16	2.40	2.00	1.67	2.26	1.95	0.96	2.66	2.43	0.36
Gd	3.28	2.57	9.40	4.24	10.40	1.54	8.97	10.00	7.90	6.92	9.26	8.52	3.28	11.30	10.31	1.63
Tb	0.59	0.45	1.43	0.69	1.55	0.26	1.37	1.52	1.24	1.04	1.38	1.28	0.61	1.67	1.50	0.27
Dy	4.18	2.98	8.90	4.38	9.97	1.70	8.40	9.48	7.90	6.43	8.61	8.00	4.28	10.21	8.96	1.74
Ho	0.95	0.64	1.82	0.91	2.01	0.37	1.67	1.90	1.63	1.30	1.71	1.60	0.93	2.06	1.79	0.35
Er	2.88	1.92	5.28	2.67	5.78	1.09	4.81	5.50	4.78	3.89	4.77	4.67	2.86	5.97	5.11	0.99
Tm	0.42	0.28	0.76	0.39	0.81	0.17	0.70	0.78	0.69	0.57	0.65	0.67	0.42	0.85	0.72	0.14
Yb	2.70	1.84	4.97	2.55	5.15	1.08	4.56	4.95	4.52	3.86	4.20	4.31	2.83	5.46	4.64	0.90
Lu	0.39	0.28	0.73	0.37	0.76	0.16	0.68	0.71	0.67	0.57	0.61	0.62	0.43	0.79	0.68	0.13
Y	24.20	16.80	48.50	23.18	50.90	9.43	42.88	47.70	40.30	34.00	42.78	41.46	23.90	49.80	44.33	8.93

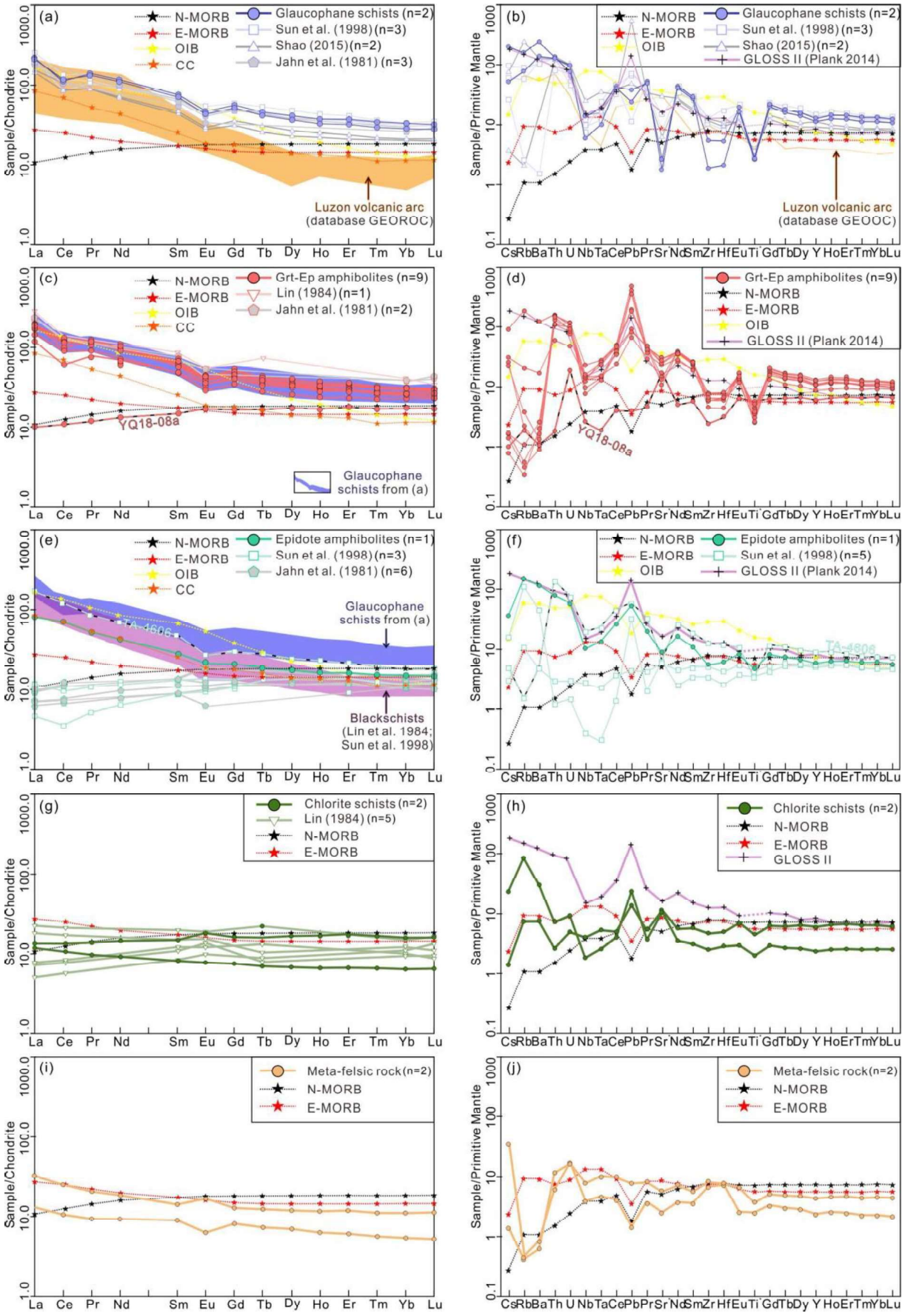
(a)
N-MORB
E-MORB
OIB
CC
Glaucophane schists (n=2)
Sun et al. (1998) (n=3)
Shao (2015) (n=2)
Jahn et al. (1981) (n=3)
Luzon volcanic arc
(database GEOROC)
Sample/Chondrite
(b)
GLOSS II (Plank 2014)
Sample/Primitive Mantle
(c)
Grt-Ep amphibolites (n=9)
Lin (1984) (n=1)
Jahn et al. (1981) (n=2)
YQ18-08a
Glaucophane
schists from (a)
(d)
(e)
Epidote amphibolites (n=1)
Jahn et al. (1981) (n=6)
TA-4606
Blackschists
(Lin et al. 1984;
Sun et al. 1998)
(f)
(g)
Chlorite schists (n=2)
Lin (1984) (n=5)
(h)
(i)
Meta-felsic rock (n=2)
(j)
La Ce Pr Nd Sm Eu Gd Tb Dy Ho Er Tm Yb Lu
Cs Rb Ba Th U Nb Ta Ce Pb Pr Sr Nd Sm Zr Hf Eu Ti Gd Tb Dy Y Ho Er Tm Yb Lu

Fig. 3-14: Chondrite-normalized REE patterns are on the left side. Data are normalized to chondrite of Sun and McDonough (1989). Primitive mantle-normalized trace element multivariation diagrams are on the right side. Data are normalized to primitive mantle of Hofmann (1988). Sr and Ti* are measurements of OES. The REE patterns of Blackschists are after Lin et al. (1984) and Sun et al. (1998). Global subducted sediments (GLOSS II) are after Plank (2014). The database GEOROC (Geochemistry of Rocks of the Oceans and Continents) of Luzon volcanic arc is from http://georoc.mpch-mainz.gwdg.de/georoc/.Trace elements data of the normal mid-ocean-ridge basalt (N-MORB), enriched mid-ocean-ridge basalt (E-MORB), oceanic-island basalt (IOB) are after Sun and McDonough (1989). Chondrite-normalized REE patterns of the continental crust (CC) are after Rudnick and Gao (2003). Yuli Belt trace elements data from Liou et al. (1975), Jahn et al. (1981), Lin (1984), Sun et al. (1998) and Shao (2015) are included for comparison. (a) and (b): Group (1), Glaucophane schists. (c) and (d): Group (2), Garnet-epidote amphibolites. (e) and (f): Group (3), Epidote amphibolites. (g) and (h): Group (4), Chlorite schists. (i) and (j): Group (5), Meta-albite rich felsic / albitite rocks. High-res images are enclosed in the supplement.*

characteristics in major elements. Albitite rocks (5) have high ($Na_2O + K_2O$) as well as SiO_2 and plot in the trachydacite field (Figs. 3-12, 3-13).

3.4.4 REE and trace element compositions

The trace element data (Table 3-4 and Figs. 3-14, 3-15) show that the analysed metamorphosed samples display distinct are earth element (REE) patterns and trace element multivariation diagrams (spider diagrams). On the Zr/4-2Nb-Y discrimination diagram (Meschede 1986) and Ti-V discrimination diagram (Shervais 1982) (Fig. 3-15), most of our samples plot both within or above the normal mid-ocean-ridge basalt (N-MORB) to back-arc basin (BAAB) array. Below, we will present and discuss the trace element in five groups, the same classification with major element compositions (Fig. 3-12).

Group (1): Glaucophane schists

Glaucophane schists samples display the lower ratio of La/Yb than the Luzon volcanic arc, although the glaucophane schists show similar light rare earth element (LREE) trends with the Luzon volcanic arc. Glaucophane schists have more enriched heavy rare earth element (HREE) above MORB values than the Luzon volcanic arc (in the yellowish background) (Fig. 3-14(a)).

Group (2): Garnet-epidote amphibolites

A suite of trace elements including Th, U, Nb, Ta, Zr, Hf, and the REE shows approximately equal concentrations in the glaucophane schists and garnet-epidote amphibolites (Fig. 3-14 (a)-(d)). A slightly negative Europium (Eu) anomaly (Eu/Eu*= avg. 0.25; Eu*=SQRT(Sm×Nd)) relative to the other REEs might indicate plagioclase is a residual solid in a reducing magma, where Eu^{2+} substitutes for calcium (Ca^{2+}) (Fig. 3-14(a)(c)) in shallow (< 40 km) partial melting of the mantle (e.g., Weill and Drake 1973). The spider diagrams of the glaucophane schists and garnet-epidote amphibolites show a similar pattern (Fig. 3-14(b)(d)) and, except for some mobile elements such as Cs, Rb, and Ba, as well as the usually immobile Sr, have similar values.

(1)

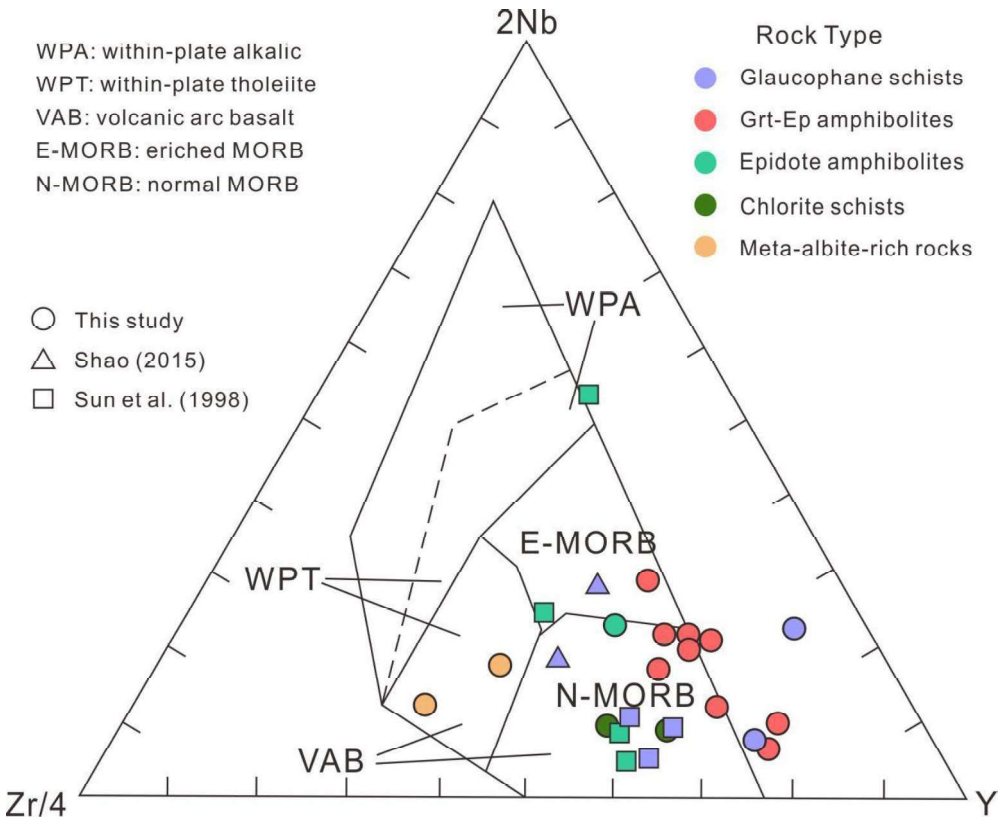

(2)

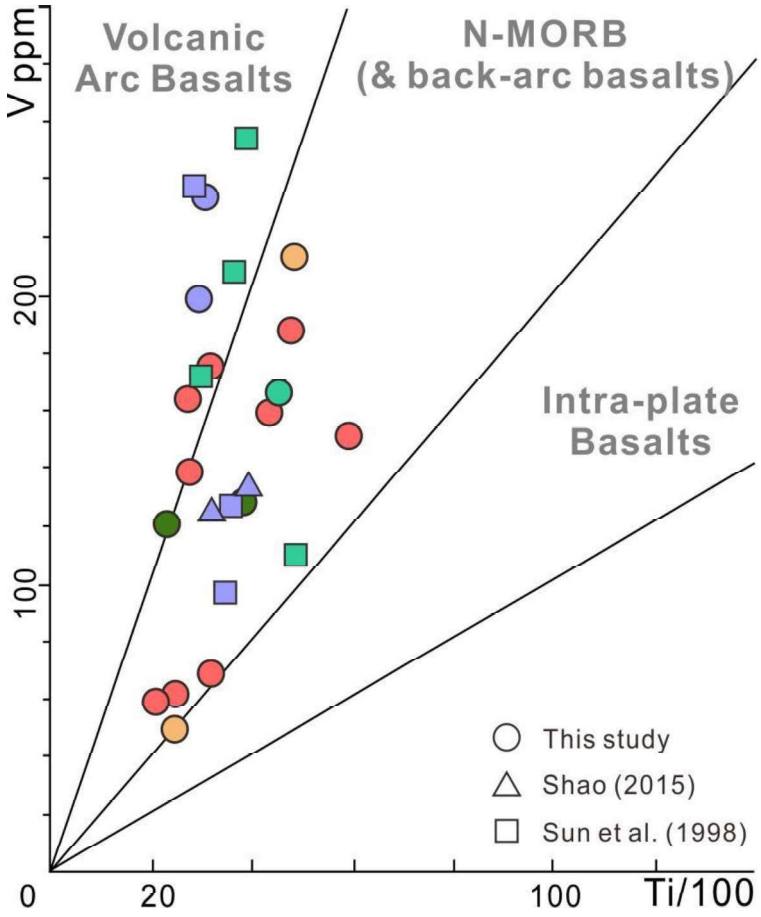

Fig. 3-15: (1) The Zr/4-2Nb-Y discrimination diagram after Meschede (1986). (2) Ti-V discrimination diagrams (Shervais, 1982) for Yuli Belt rocks of this study. Symbols as in (1). Data from Sun et al. (1998) and Shao (2015) are included for comparison.

One exception of sample YQ18-08a in the garnet-epidote amphibolites group, shows a similar REE pattern with N-MORB in Fig. 3-13(e) and is characterized by low concentrations of Nb - Ta, a typical signature of subduction-related melts (Pearce, 1982). Besides, the Zr-Hf trough in both glaucophane schists and garnet-epidote amphibolites groups may indicate a melt that assimilated continental crust. Therefore, it is an indication for supra-subduction environments.

Group (3): Epidote amphibolites

Garnet concentrates the HREE and fractionates. Both glaucophane schists and garnet-epidote amphibolites display higher HREE above MORB values than epidote amphibolites (Fig. 3-14(a)(c)(e)). Most of epidote amphibolites are characterized by relatively flat HREE patterns, similar to N-MORB. Variably elevated abundances for large-ion lithophile element (LILE) and Pb relative to N-MORB could due to the seawater hydrothermal alteration and the crustal contamination. Two exceptions of TA-4606 (Sun et al. 1998) and our sample UK 09-24 displaying the LREE enrichment and HREE depletion relative to MORB values, indicate an igneous signature, with Ta-Nb depletion in a supra-subduction environment. However, the two samples with relatively negative Eu anomaly exhibit chemical compositions similar to blackschists in the Yuli Belt and global subducted seafloor sediments (GLOSS II) (Lin et al. 1984, Sun et al. 1998, Plank 2014; Fig. 3-14 (e)(f)), considered to be strongly contaminated by an aqueous environment.

Group (4): Chlorite schists

These REE data collectively indicate that the geochemical composition of chlorite schists is similar to that of typical MORBs of the South China Sea (Fig. 3-14 (g)). However, significant enrichment in LILE, Pb, LREE, Nb and Ta relative to N-MORB despite the Nb-Ta trough in the diagram (Fig. 3-14 (h)) show chlorite schists have been influenced by hydrogenetic or hydrothermal components during subduction.

Group (5): Meta-albite rich felsic / albitite rocks

Two meta-albite rich felsic/albitite rocks with LREE enrichment support for the origin of E-MORB from the South China Sea (Figs. 3-14 (i)(j), 3-15(2)). These samples show both positive and negative Eu anomalies as actual MORB melts (e.g., Niu and O'Hara 2009). Primitive mantle normalized incompatible element distribution patterns of two samples exhibit negative anomalies in Rb, Ba and positive anomalies for Th, U (Fig. 3-14 (j)), with an indication for a fluid imprint.

3.4 Discussions

3.4.1 Structural position of the Yuli Belt high-pressure blocks

By correlating outcrop-scale observations with cross sections, we interpreted the high-pressure metamorphosed blocks to form allochthonous nappe outliers (or erosional relics) of a formerly more contiguous thrust sheet, which emplaced subducted and exhumed portions of crust and mantle on top of the lower-grade metasedimentary unit (Fig. 3-5 and 3-6). In the following, we term this fault "Juihsi Thrust" after the locality with the largest exposures of blueschist-facies rocks (Fig. 3-5). Nappe emplacement must have occurred after peak-P-T conditions in the high-pressure unit have been reached. This interpretation is supported by contrasting P-T-conditions in the blueschist-facies and the metasedimentary units (Appendix B- Fig. S1). Peak pressures and temperatures obtained for the high-pressure unit (c. 1.0 to 1.7 GPa and 500-550°C, respectively; Beyssac et al. 2008; Tsai et al., 2013; Sandmann et al. 2015; Keyser et al., 2016; Baziotis et al., 2017; Lo 2018; Appendix B- Fig. S1) are higher than those of the metasedimentary unit (0.9 GPa; Chiang 2003), although more recent work suggests substantially higher pressures, but lower temperatures for the metasediments (up to 1.5 GPa and 330-400°C; Conand et al. 2020). These contrasting P-T-conditions nourish our assumption of two tectonic units that require to be separated by a thrust. The juxtaposition of high-pressure blueschist unit and metasedimentary unit along this thrust occurred very likely during D1 or early D2; certainly before the refolding of all units during D3 and likely concomitant with late-stage retrogression at greenschist facies conditions below c. 3 kbar and 370 °C (Appendix B- Fig. S1; Fig. 3-14). This is in agreement with our cross sections with the west-dipping axial planes formed during D3 (Fig. 3-5,6,8b). D3 refolding and back-thrusting, in combination with later erosion, was responsible for the separation of high-pressure rock occurrences in map view. For the sake of completeness, we mention that the idea of the existence of such thrusts was first proposed by Yang and Wang (1985).

3.4.2 Palaeogeographic origin of the Yuli Belt and a kinematic evolutionary scheme

From geochemical considerations it has been concluded that the Yuli belt high-pressure metamorphic rock assemblage exhibits the features expected in the MORB-like basalt of the South China Sea (e.g., Group (2)YQ18-08a, Group (3), (4), and (5)), and could display the effects of metasomatism of their mantle source by slab-derived fluids and alteration from low-temperature seafloor in the subduction zone (e.g., Group (1), (2)), which are varied in LILE (e.g., Rb, Ba, and Sr) and depleted in high field strength elements (HFSE) (e.g., Nb, Ta, and Ti). Although all samples are metamorphic rock, the maximum metamorphic depth are less than 60 km (Appendix B- Fig. S1). In this depth, the equilibrium partitioning between the

metamorphic minerals is generally inhibited and the metamorphic minerals should persist the original composition of protolith (Spandler et al. 2003). Therefore, we consider the dominantly mafic to ultramafic and subordinately metasedimentary blueschist-facies tectonic blocks of the Yuli Belt to have been derived from the oceanic crust of the South China Sea. This interpretation is based on a number of arguments outlined in the following. We minted our arguments into a

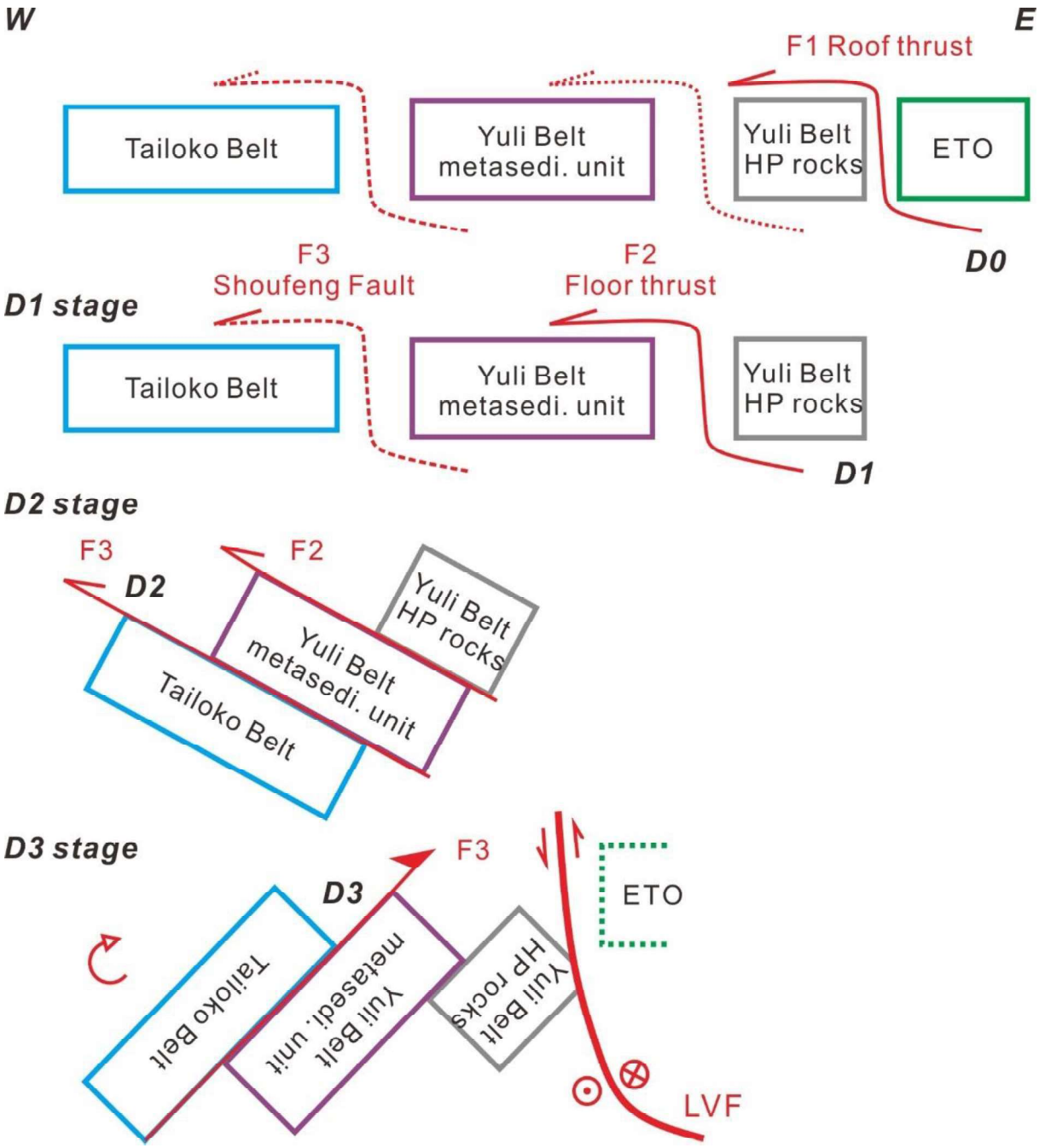

Fig. 3-16: A kinematic evolutionary "shoe box" cartoon illustrating deformation stages, starting with the suspected paleogeographic configuration. D0 stage: the subduction of the Yuli Belt HP unit along the roof thrust; D1 stage: HP metamorphic rock thrusted over the Yuli Belt metasedimentary unit along the floor thrust; D2 stage: W-ward thrusting of Yuli Belt onto Tailuko Belt along Shoufeng Fault; D3 stage: backfolding and inversion of slip sense on Shoufeng Fault.

new kinematic evolutionary three-stage scheme for the Yuli Belt (Figs. 3-16, 3-17) and into a palaeogeographic sketch of the South China Sea and the Philippine Sea for 15 Ma (Figs. 3-17, 3-18). We selected the GPlates framework of a global plate reconstruction of Wu and Suppe (2018) using a hybrid absolute reference frame that includes moving Indian/Atlantic hotspots and a true polar wander corrected paleomagnetic-based model (O'Neill et al. 2005; Seton et al. 2012), and projected the present-day as well as the 15 Ma paleogeographic reconstructions.

(1) Available protolith ages for the blueschists, constrained from U-Pb LA-ICP-MS dating of zircons, are around 15.4–16.0 Ma (Chen et al. 2017; Lo et al. 2020), making them well comparable in age with gabbros from the easterly adjacent, unmetamorphosed ETO accreted to the base of the Lichi Mélange (Hsieh et al. 2017; Lin et al. 2019; Huang et al. 2018; Table 3-1, Table 3-2 and Fig. 3-2, 3-10(B)(D)). These ages are about the youngest possible for oceanic crust issued at a mid-oceanic ridge of the South China Sea (Table 3-1), which ceased spreading at about 15.5 Ma (see Section 3.2 and Fig. 3-2). The geochemical composition of basalts and gabbros in the ETO has affinities towards MORB and/or BABB (Lin et al. 2019). Based on these geochemical data and ages, we conjecture that the most probable locus, where both the Yuli Belt blueschists and the ETO originated, was to either side of a spreading ridge of the South China Sea (Fig. 3-16a). We took this idea further by positioning the original locus of these units on a simple palaeogeographic reconstruction for 15 Ma (Fig. 3-18). Assuming that both the present-day plate convergence rate of 7-8 cm/a (Seno, 1977; Yu et al. 1997) and the NW-SE-oriented convergence direction between Eurasian and Philippine Sea plates (after Seno, 1977) were constant during the last 15 Ma, we roughly aligned the possible original palaeogeographic locations of both Yuli Belt and ETO on three positions along this trajectory (red and blue dashed stars in Fig. 3-18b). Given large uncertainties on the trend of the subducted portions of the spreading ridges (cross-hatched area in Fig. 3-18b), all three pairs of stars mark positions where South China Sea oceanic crust might have formed near a mid-oceanic ridge at c. 15 Ma. However, only the southeasternmost pair of red and blue dashed stars is in good agreement also with the amount of plate convergence that has occurred since 15 Ma, amounting to roughly 1100 km using the simple assumptions above. This "preferred" position is conspicuously close to the position of the Manila trench reconstructed by Lee and Lawer (1995; blue line in Fig. 3-18b), which we hence prefer over the two alternative reconstructions of Sibuet et al. (2002; green line in Fig. 3-18b) and Wu and Suppe (2018; red line in Fig. 3-18b), which would only be viable if substantially slower convergence rates operated, which, in turn, is considered unlikely (Wu and Suppe, 2018).

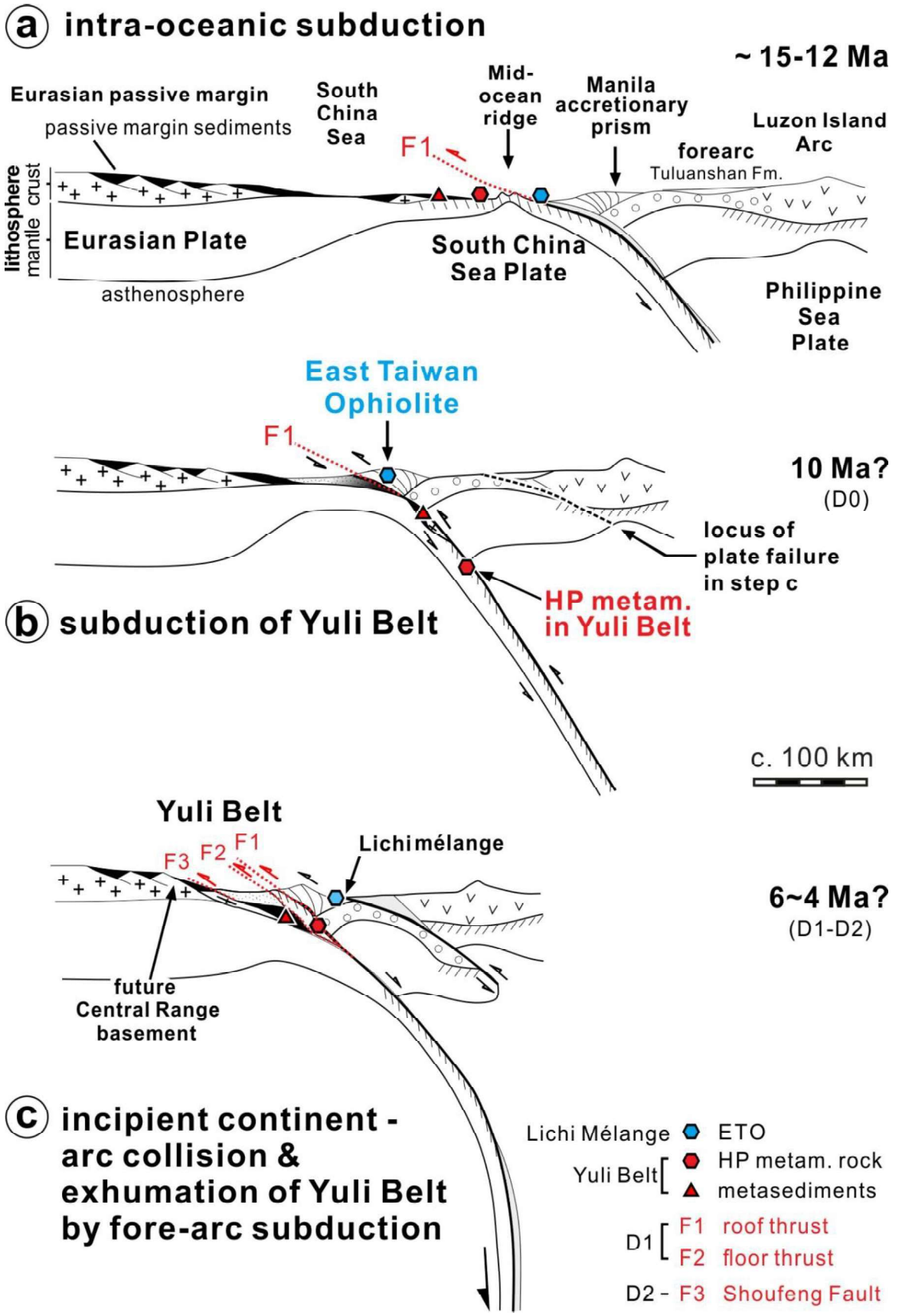

Fig. 3-17: Lithosphere-scale kinematic model to explain the origin of the Yuli Belt of Taiwan. The Yuli Belt is interpreted to have originated from a subducted and exhumed segment of the South China Sea, relying on time constraints from Chen et al. (2017) and Lin et al. (2019) for igneous protolith ages in the Yuli Belt and East Taiwan Ophiolites, respectively. See text for further discussion.

In our kinematic evolutionary sketch (Fig. 3-17), we show an intraoceanic subduction zone already operating at 15 Ma. This takes account of (i) the oldest reported ages for subduction-related magmatism in the Coastal Range dating back to the Late Oligocene (Table 3-1), (ii) maximum stratigraphic age constraints of the Tuluanshan Fm. in the Coastal Range (Fig. 3-2) as well as (iii) plate tectonic reconstructions for 15 Ma as discussed above, which show the Manila Trench at variable longitudes in the western Philippine Sea (Lee and Lawer, 1995; Sibuet et al., 2002; Wu and Suppe, 2018; Fig. 3-18b).

(2) Subduction of the oceanic crust and lithosphere forming the Yuli Belt blueschists must have commenced soon after ~15 Ma (e.g., Jahn et al. 1981; Lo and Yui, 1996), with peak metamorphic conditions reached between 15 and 10 Ma (Chen et al., 2017). At the same time, the ETO has escaped the fate of being subducted, implying that it must have been frontally accreted to the wedge forming along the Manila trench (Fig. 3-18b). We suspect that the metasedimentary unit of the Yuli Belt, with depositional ages inferred to be as young as mid-Miocene (Chen et al. 2017; Figs. 3-2 and 3), occupied a more continent-ward paleogeographic position prior to its subduction (Fig. 3-11a). Despite the absence of any geochronological data on metamorphic conditions from this unit, we further suspect that it must have closely followed the blueschist unit into subduction (Fig. 3-17b; Appendix B- Fig. S1).

(3) Exhumation of the Yuli Belt series was facilitated by the failure of the upper plate along a lithosphere-scale fault forming between the dense, negatively buoyant fore-arc lithosphere and the more buoyant magmatic Luzon arc upon the entrance of Eurasian continental lithosphere in the trench between c. 6 and 4 Ma (Chemenda et al. 2001). Subsequently, ongoing convergence led to subduction of the negatively buoyant fore-arc lithosphere by slab extraction (Froitzheim et al. 2003; Shyu et al. 2011; Sandmann et al. 2015; Fig. 3-17c), a mechanism that very efficiently reduced the overburden on top of the subducted material. We conjecture (i) that this mechanism of slab extraction was at play both for the blueschist-facies units as well as for the metasedimentary unit of the Yuli Belt and (ii) that the juxtaposition of these units along the floor thrust occurred during this stage (Fig. 3-16). Roof and floor thrust of the blueschist-facies unit define part of the suture zone between Eurasian and Philippine Sea Plates, and they likely formed during this stage of fore-arc subduction. We suggest that the easterly adjacent ETO (from which the Yuli Belt is presently separated by the LVF), should be considered to constitute the remainder of Taiwan's suture zone. Such an assembly with blueschist-facies oceanic units overlain by unmetamorphosed oceanic units is also described from the Chenaillet Ophiolite in the French-Italian Western Alps, where it is attributed to represent the suture between European and Adriatic units (e.g., Manatschal et al., 2011). Furthermore, we suspect that the juxtaposition

of the Yuli Belt series and Tailuko belt along the Shoufeng Fault could have occurred within this timespan.

Finally, we realize that it is increasingly difficult to reconcile the Lu-Hf isochron ages of 5.1 ± 1.7 Ma, considered to reflect peak-pressure conditions during blueschist-facies metamorphism (Sandmann et al. 2015) with the fact that between about 6 to 4 Ma continental lithosphere of Eurasia has entered the subduction, dating the transition from intra-oceanic subduction to continent-arc collision (Chi et al. 1981; Suppe 1984a; Fig. 3-17c). The even younger U-Pb ages on zircon rims from nephrite at Fengtien (3.3 ± 1.7 Ma; Yui et al. 2014), however, may still be geologically viable, as this method possibly dates peak-temperature conditions rather than peak-pressures. In this case, Yui et al. (2014) would have likely obtained an age at which post-collisional shortening during deformation phase D3 was at work. We conclude that further geochronological and structural work is hence needed to better constrain the timing of peak-metamorphic conditions and their structural imprint on the Taiwan orogen.

3.5 Conclusions

Three new cross-sections across Taiwan's Yuli Belt were constructed, taking new outcrop- to microscope-scale structural observations from several river-transects into account. Our observations suggest that the Yuli Belt was affected by at least three successive deformation phases (D1 to D3). We suspect that high-pressure metamorphic units were emplaced on top of metasedimentary units of Yuli Belt along a thrust during D1. This assembly was later thrust over Eurasian-derived series of the Tailuko Belt along the Shoufeng Fault during D2, suggested by (rarely preserved) downplunging stretching lineations on W- to NW-dipping foliation planes. E-vergent open to tight folds throughout the Yuli Belt with W- to NW-dipping axial planes were produced by the D3 phase, refolding earlier foliations as well as the D1 nappe contact, during which also the blueschist- facies and metasedimentary units were folded. This phase might be related to a top-E back-thrusting and a reorientation of the Shoufeng Fault from an initially E-dipping to a presently W-dipping contact, for which we present new evidence. We interpret the high-pressure metamorphic units to form erosional relics of nappe outliers of a formerly more contiguous thrust nappe that hosts part of the suture zone in Taiwan. The whole-rock geochemical fingerprint of high-pressure metamorphic rocks is in the MORB tectonic settings. Therefore, we suggest that the blueschist-facies metamorphic unit most likely represents a mid-Miocene fragment of oceanic crust and mantle issued in the South China Sea before having been subducted, exhumed and 'sandwiched' between the Tailuko Belt and the easterly adjacent Coastal Range derived from the Philippine Sea Plate.

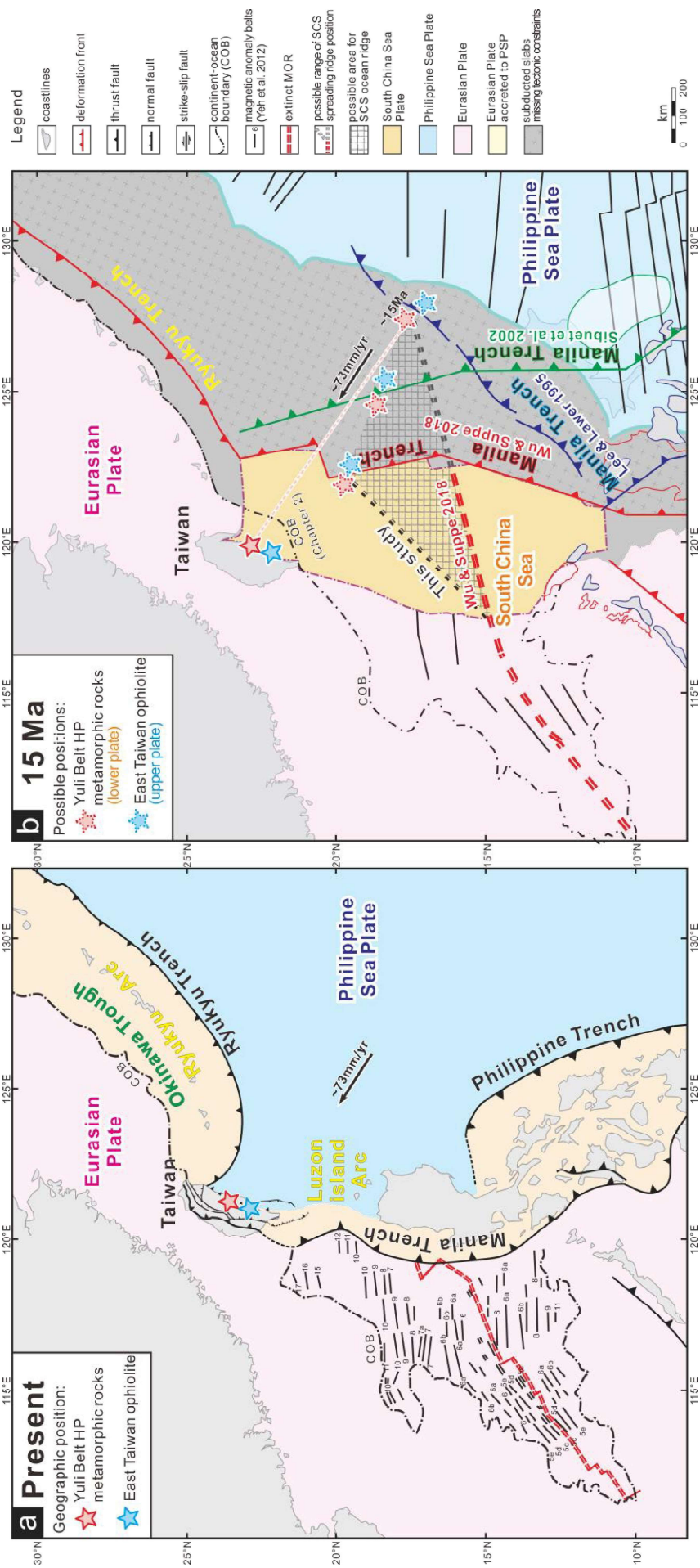

Fig. 3-18: a: Present-day plate tectonic map around Taiwan. b: Paleogeographic reconstruction for 15 Ma showing possible locations of the Yuli Belt (red star) and East Taiwan Ophiolite (blue star), the eastward-extension of the spreading ridge of the (now subducted) South China Sea as well as proposed positions of the Manila Trench at 15 Ma according to Lee and Lawer (1995), Sibuet et al. (2002) and Wu and Suppe (2018). Uncertainties in the position of the now subducted spreading ridge (checkered area) arise from the eastward projection of the azimuthal range of magnetic anomalies below the present-day position of the Manila Trench. Assuming a constant plate convergence velocity and direction (Seno, 1977) between 15 Ma and present would place YB and ETO close to the trench position suggested by Lee and Lawer (1995; blue line in Fig. 3-18b). The extent of the spreading ridge subducted beneath the Manila Trench is confirmed from seismic tomography (Yeh et al. 2012; Wu and Suppe 2018). The former continent-ocean boundary (COB) is reconstructed on the basis of shortening estimates of the three transects (Chapter 2). High-res images are enclosed in the supplement.

Chapter 4

Thermal evolution of the metamorphism in the eastern Taiwan: implications for blueschist exhumation

This manuscript is in preparation for submission.

Abstract:

The Yuli Belt in Taiwan's eastern Central Range encloses high pressure (HP) mafic–ultramafic blocks in intensely deformed greenschist-facies metasediments. It is still debated how its structures relate to those of the westerly and easterly adjacent units. We integrated new and published Raman-spectroscopic measurements on carbonaceous matter from metasedimentary successions across the Tailuko and Yuli Belts and combined these results with new cross sections. Our results suggest temperature variations of up to 150°C within the Yuli Belt itself, with lower temperatures between 400 and c. 460°C within the metasediments and up to 550° in spotted schists directly underlying the HP metamafic assemblages. No temperature gradient can be found across the Shoufeng Fault separating the Yuli and Tailuko belts in the west. The most pronounced temperature gradient exists across a fault contact between the Yuli Belt and the easterly adjacent Chulai Fm. Both Chulai Fm. and Backbone Slates to the west of the Tailuko Belt exhibit T<400°C. In combination with lithological similarities, we consider the Chulai Fm. an easternmost extension of the Backbone Slates. We suggest that the Yuli Belt was initially emplaced on top of lower-grade Paleogene successions. Later, the nappe succession was overprinted by E-vergent backfolding of the Central Range and contemporaneous backthrusting along the Shoufeng Fault, leading to the presently observed synformal structure of the Yuli Belt.

Keywords: Taiwan; Yuli Belt; geothermometer; RSCM; blueschists

Statement of significance:

Unlike the Alps and the Himalaya, where topographic growth occurred well-after the onset of submarine continental accretion, Taiwan is characterized by a much shorter time interval between these two tectonic stages. This makes the interpretation of pressure-temperature-timing data challenging. A careful inspection of metamorphic temperature trends in sedimentary successions is thus particularly important. Our results support the effectiveness of Raman spectroscopy for carbonaceous material as geothermometer for deformed greenschist-facies metasediments to provide peak metamorphic temperatures in the eastern Taiwan Central Range that are useful to constrain deformation phases.

4.1 Introduction and geological setting

The collision between the Eurasian passive continental margin and the Luzon volcanic arc of the overriding Philippine Sea Plate formed the Taiwan Central Range since ca. 4–6 Ma (e.g., Chang and Chi, 1983; Suppe, 1984a). Five roughly N-S oriented major morphotectonic units make up the Taiwan mountain belt (Fig. 4-1a). The Longitudinal Valley Fault (F4) separates units to the west derived from the Eurasian Plate, and the Coastal Range of the Philippine Sea Plate to the east. The Backbone Slates comprises a metamorphosed Cenozoic sedimentary cover unconformably overlying the Mesozoic metamorphic basement (the Tailuko Belt of the Tananao Complex) (Fig. 4-1a). The outcropping stratigraphy of the Backbone Slates consists of the prehnite–pumpellyite to greenschist facies Pilushan phyllite (incl. Heiyenshan and Tayuling formations) of Eocene (to Miocene) age as well as the prehnite–pumpellyite facies Lushan slate of Miocene age in the western range, and the greenschist facies Chulai Formation of Eocene age in the eastern range from the southern Cross-island highway to around Juisui area (e.g., Chow and Lin, 1974; Stanley et al., 1981; Ho, 1986).

The Tananao Complex crops out as a narrow belt on the eastern side of Taiwan's Central Range (Fig. 4-1a) and bears evidence of polymetamorphism and multiple deformations (e.g., Ernst and Jahn 1987). Traditional classification subdivides the Tananao Complex into the western pre-Cenozoic Tailuko Belt and the eastern Cretaceous to Miocene Yuli Belt (e.g., Ho, 1986; Chen et al., 2017), separated by the Shoufeng Fault (Yen, 1963, F3 in Fig. 4-1), a possibly mega-backthrusting fault (e.g., Zhang et al., 2020). The Tailuko Belt consists of Permian Chiuchu marbles and variegated Mesozoic Kuyuan greenschists (Liou, 1981; Fig. 4-2). The Yuli Belt contains lithologically heterogeneous blueschist-facies rocks in what is referred to as high-pressure (HP) tectonic or exotic blocks (e.g., Liou et al., 1975) surrounded by an intensely deformed schistose unit of lower metamorphic grade (Fig. 4-1b). Three larger exposures of these blocks are the Wanjun, Juisui, and Chinsui Hsi areas (Yen, 1963; Liou et al., 1975). Some petrological pressure-temperature-timing studies and structural analyses (e.g., Yang and Wang,1985; Tsai et al., 2013; Sandmann et al., 2015; Conand et al., 2020) suggest an allochthonous HP blueschist nappe (~550 °C, 10–12 kbar) emplaced on top of the lower-grade metasedimentary unit along a thrust during a first deformation phase D1 (Zhang et al., 2020). The Yuli Belt's eastern contact with the Chulai Formation of the Backbone Slates (Fig. 4-1b) is strongly deformed and the sharp boundary in terms of lithology and metamorphic grade was interpreted as an unconformity (Stanley et al., 1981; Ho, 1986). However, based on recent detrital zircons ages, from the Yuli Belt metasediments and the northern part of the Chulai Formation, as young as Upper Miocene (e.g., 11.2 ± 0.2 Ma, Mesalles et al., 2020), an

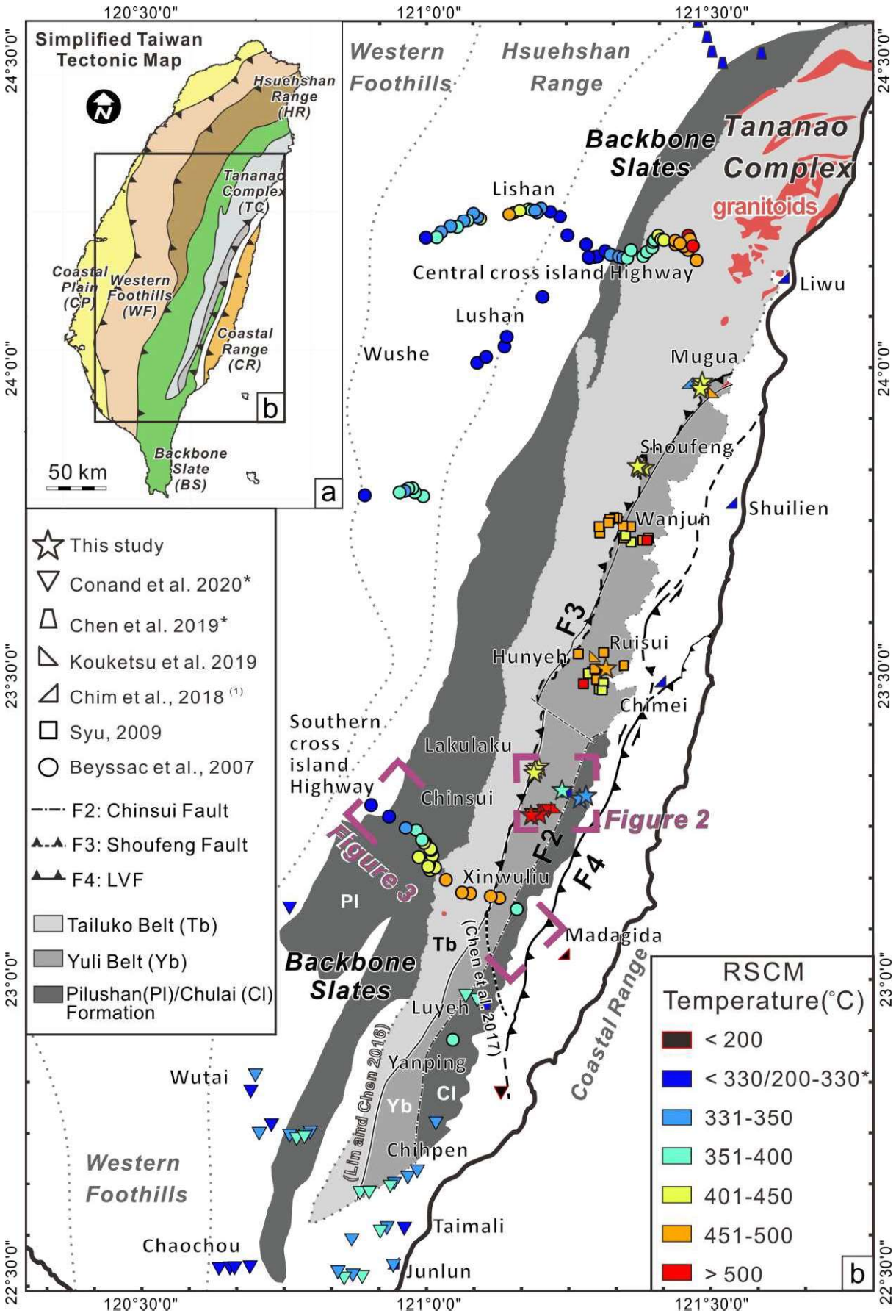
Simplified Taiwan Tectonic Map
Hsuehshan Range (HR)
Tananao Complex (TC)
Coastal Plain (CP)
Western Foothills (WF)
Coastal Range (CR)
Backbone Slate (BS)
50 km
a
b
Western Foothills
Hsuehshan Range
Backbone Slates
Tananao Complex
granitoids
Lishan
Central cross island Highway
Liwu
Lushan
Wushe
Mugua
Shoufeng
Wanjun
Shuilien
F3
Hunyeh
Ruisui
Chimei
Southern cross island Highway
Lakulaku
Chinsui
Figure 2
Figure 3
F2
F4
Xinwuliu
Madagida
PI
Tb
Backbone Slates
(Chen et al., 2017)
Luyeh
Yanping
Cl
Yb
(Lin and Chen 2016)
Coastal Range
Wutai
Chihpen
Western Foothills
Taimali
Chaochou
Junlun
This study
Conand et al. 2020*
Chen et al. 2019*
Kouketsu et al. 2019
Chim et al., 2018 (1)
Syu, 2009
Beyssac et al., 2007
F2: Chinsui Fault
F3: Shoufeng Fault
F4: LVF
Tailuko Belt (Tb)
Yuli Belt (Yb)
Pilushan(Pl)/Chulai (Cl) Formation
RSCM Temperature(°C)
< 200
< 330/200-330*
331-350
351-400
401-450
451-500
> 500
120°30'0"
121°0'0"
121°30'0"
24°30'0"
24°0'0"
23°30'0"
23°0'0"
22°30'0"

Fig. 4-1: (a) Tectonic map of Taiwan. Traditional nomenclature subdivides the Tananao Complex into the western Tailuko Belt (colored light gray) and the eastern Yuli Belt (colored dark gray) (e.g., Lin and Chen, 2016). (b) Map of peak temperatures in eastern Taiwan obtained from RSCM, compiling various sources. All RSCM were obtained using the calibration of Beyssac et al. (2002) for T>330°C and low temperatures (200°C < T < 330 °C) were obtained using Lahfid et al. (2010) marked with "". (1): Data of Chim et al., (2018) are plotted as arithmetic means of a larger population of data at the localities shown. F2: Chinsui Fault (after Lin and Chen, 2016); F3: Shoufeng Fault (with different interpretations, e.g., Lin and Chen, 2016; Chen et al., 2017); F4: Longitudinal Valley Fault (LVF) (after Shyu et al., 2005).*

alternative trace of Shoufeng Fault has been depicted and the Chulai Formation has been reinterpreted as part of the Yuli Belt (e.g., Chen et al., 2017, 2019; Conand et al., 2020; Zhang et al., 2020; Fig. 4-1b).

Raman spectroscopy of carbonaceous material (RSCM) is being increasingly used as a quantitative geothermometer to estimate maximum metamorphic temperature of the host sediments (e.g., Wopenka and Pasteris,1993; Yui et al., 1996; Beyssac et al., 2002; Lahfid et al., 2010; Henry et al. 2019). Beyssac et al. (2007) was a pilot study using RSCM at a continuous thermal gradient from the Backbone Slates to the Tananao Complex in Taiwan (Fig. 4-1b). The study encouraged a wider use of RSCM as geothermometer (e.g., Chim et al., 2018; Chen et al., 2019; Conand et al., 2020). However, most past efforts have focused on the central part of the island, and little attention has been paid to the eastern side (Fig. 4-1b). Kouketsu et al. (2019)'s three samples from the Yuli Belt suggested that the results relate not only to peak metamorphic temperature, but also to the pre-metamorphic history and the duration of metamorphic heating. Two samples taken from the Chulai Formation (in Lakulaku and Xinwuliu areas; Fig. 4-1b) have been estimated via RSCM (ca. 370°C; Beyssac et al., 2007; Chim et al., 2018). The temperature is much lower than those of the adjacent Yuli Belt (ca. 450~500°C; Fig. 4-1b), which shows a significant gap between these two units. It is likely that the contact as a fault. These results and conclusions need to be tested with a larger sample set.

The purpose of this study is to investigate the thermodynamic evolution of the metamorphism in the Yuli Belt of Taiwan based on new RSCM data combined with interpretations of the structural deformation of the Yuli Belt and adjacent units. We also discussed the potential influence of our new data on the working tectonic model of the Taiwan arc-continent collision.

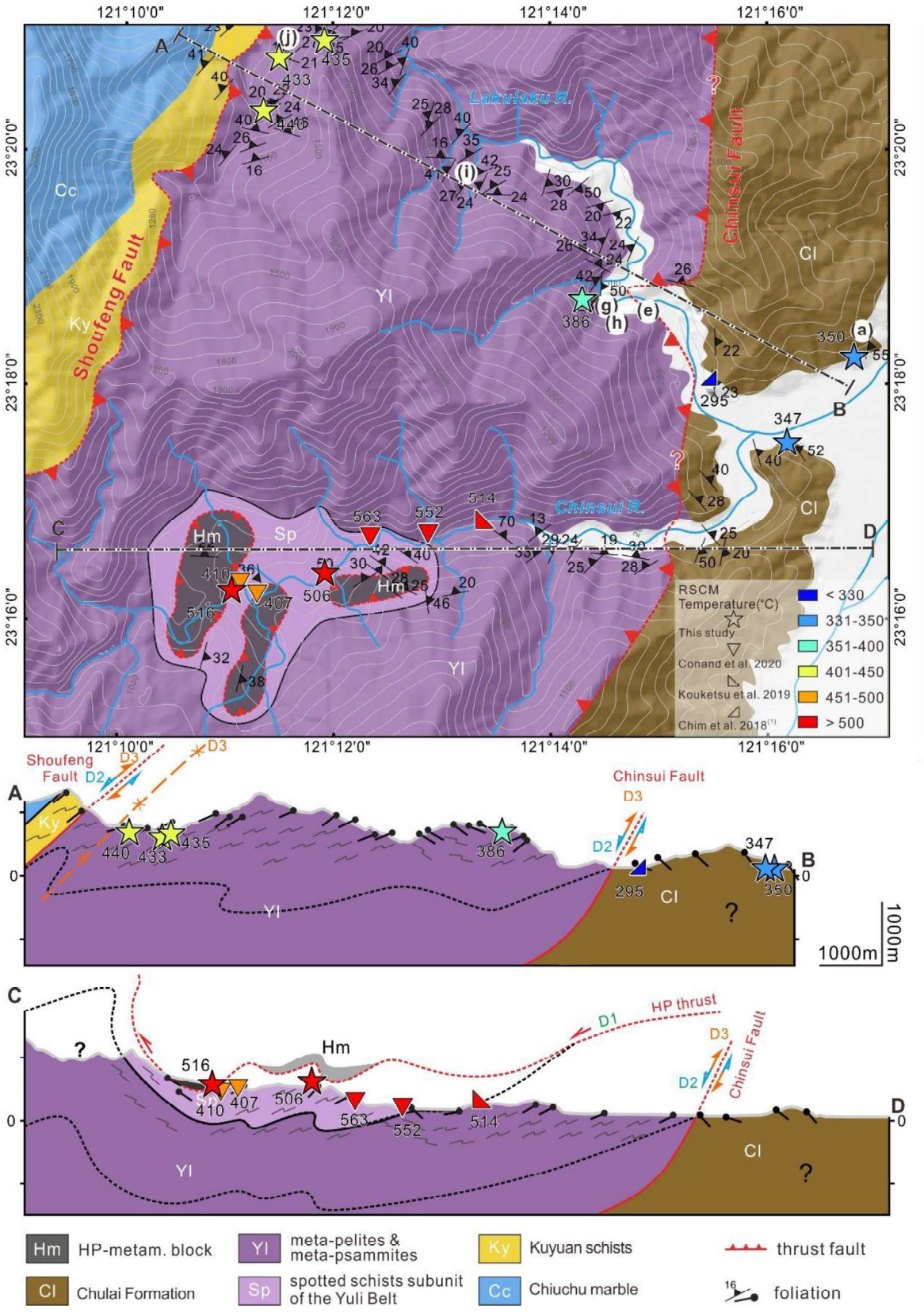

Fig. 4-2: Geological map and cross sections (A-B and C-D) in the Lakulaku Hsi and Chinsui Hsi areas. See Fig. 4-1b for location. Parentheses enclosed letters indicate the locations of outcrops in Figs. 4-4, 4-5. The high-pressure metamorphosed units formed allochthonous nappe outliers of a former thrust sheet, emplacing on top of the lower-grade metasedimentary unit.

4.2 Sampling and methodology

To fill the gap in eastern Taiwan, our data complement previous RSCM data from transects of two cross-island highways (Beyssac et al., 2007), southern Taiwan (Conand et al., 2020), northern Taiwan (Chen et al., 2019), the Coastal Range (Chim et al., 2018), and the Yuli Belt (Syu, 2009; Kouketsu et al., 2019). Temperatures over 330°C were calibrated using the equation proposed by Beyssac et al. (2002) and low temperatures (200°C < T < 330 °C) were obtained using Lahfid et al. (2010) (Fig. 4-1b). Data of Chim et al. (2018) are plotted as arithmetic means of a larger population of data at the estimated localities shown. Our sixteen black metapelites/phyllites samples were collected along selected transects in the Yuli Belt and the Chulai Formation of eastern Taiwan (Fig. 4-1b; Table 4-1; representative microscopic features, Appendix C- Fig.S1). At each sampling site, a careful examination of structural deformation was carried out to systematically measure and characterize ductile deformation by the direction of stretching lineation and associated sense of shear whenever possible (Figs. 4-2, 4-3).

RSCM was used to quantify the degree of thermal alteration of carbonaceous material (CM) within the sampled metasediments. Raman spectra were obtained using corundum polished standard petrographic thin sections, with a thickness of ca. 30 μm. RSCM analyses were performed at the Friedrich Schiller University of Jena using the Horiba LabRam HR Evolution with a focal length of 800 mm and a 532 nm Spectra Physics argon laser. Grains of CM were selected and analyzed one by one with an Olympus microscope mounted on the Raman spectrometer. 31 to 107 particles of CM (with an average of 66.4 for all samples) were collected per sample (Tables 4-1, Appendix C- Fig. S1). The spectra were baseline corrected via LabSpec Spectral Software using a linear baseline in the spectral range of 1100–1800 cm-1, and decomposed to the G-band (1580 cm–1), D1-band (1350 cm-1) and D2-band (1620 cm–1). We evaluated the crystallinity of CM using the parameter R2, which is the area ratio of D1/(G + D1 + D2). According to the calibration of Beyssac et al. (2002), the R2-ratio shows a linear correlation to peak metamorphic temperature (T) in the range of 330 °C to 640 °C. Standard errors are given for temperature with 1σ. Details on data processing and representative Raman spectra of CM in each sample are provided in supporting materials, respectively (Appendix C-Table S1). Despite the use of the same calibration method, RSCM data obtained by different authors may show slight discrepancies in view of diverse analytical setups and differences in data handling.

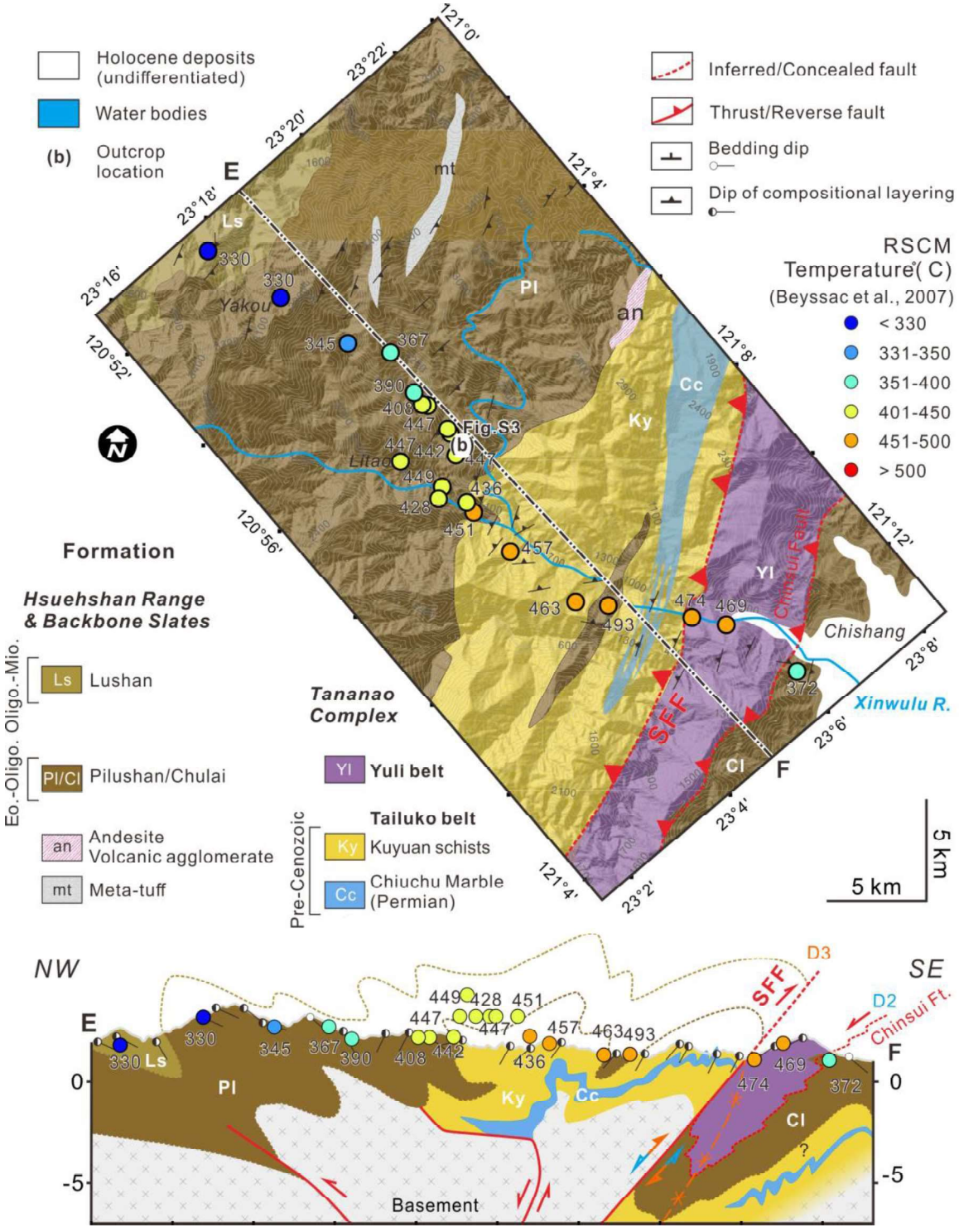

Fig. 4-3: Geological map and the cross section E-F of the Xinwuliu Hsi area. See Fig. 4-1b for location. (b): outcrop location in Fig. 4-4. The lower-grade metasedimentary unit of the Yuli Belt is interpreted to thrust on top of the Pilushan/Chulai Formation before the E-vergent refolding.

Table 4-1: Summary of sixteen RSCM data of the samples with point measurements. (Details of each measurements see Appendix C- Table S1)

Sample	Rock	Longitude	Latitude	Spectra	mean R2	sdv	peak T	1σ, °C	Equation
YQ17-3	albite mica quartz schist	121.4995	23.97566	100	0.36	0.0482	**477**	22	Beyssac 2002
YQ17-09	mica quartz schist	121.5004	23.97814	107	0.53	0.0425	**401**	19	Beyssac 2002
YQ17-10b	mica quartz schist	121.4966	23.96673	69	0.46	0.0276	**432**	13	Beyssac 2002
YQ17-12b	mica quartz schist	121.2798	23.28852	81	0.5	0.0477	**415**	22	Beyssac 2002
YQ17-15	mica quartz schist	121.2082	23.27108	61	0.66	0.0077	**347**	3	Beyssac 2002
YQ17-23a	talc schist	121.1935	23.26975	62	0.3	0.0366	**506**	16	Beyssac 2002
YQ17-28	albite quartz mica schist	121.2908	23.30152	80	0.28	0.0379	**516**	17	Beyssac 2002
YQ17-29	quartz mica schist	121.2073	23.34856	62	0.64	0.016	**350**	7	Beyssac 2002
YQ18-01a	mica quartz schist	121.2012	23.34496	31	0.45	0.0468	**435**	21	Beyssac 2002
YQ18-02	mica quartz schist	121.1989	23.3384	47	0.46	0.04	**433**	18	Beyssac 2002
YQ18-03	mica quartz schist	121.2483	23.31024	47	0.44	0.041	**440**	19	Beyssac 2002
YQ18-05	quartz mica schist	121.3964	23.83747	70	0.56	0.0483	**386**	22	Beyssac 2002
YQ18-09	mica quartz schist	121.3885	23.83799	61	0.45	0.0364	**436**	17	Beyssac 2002
YQ18-11	mica quartz schist	121.3854	23.84	57	0.47	0.0574	**427**	26	Beyssac 2002
YQ18-12	mica quartz schist	121.3851	23.84037	61	0.41	0.0779	**455**	35	Beyssac 2002
YQ18-13a	mica quartz schist	121.4995	23.97566	66	0.47	0.0347	**426**	16	Beyssac 2002

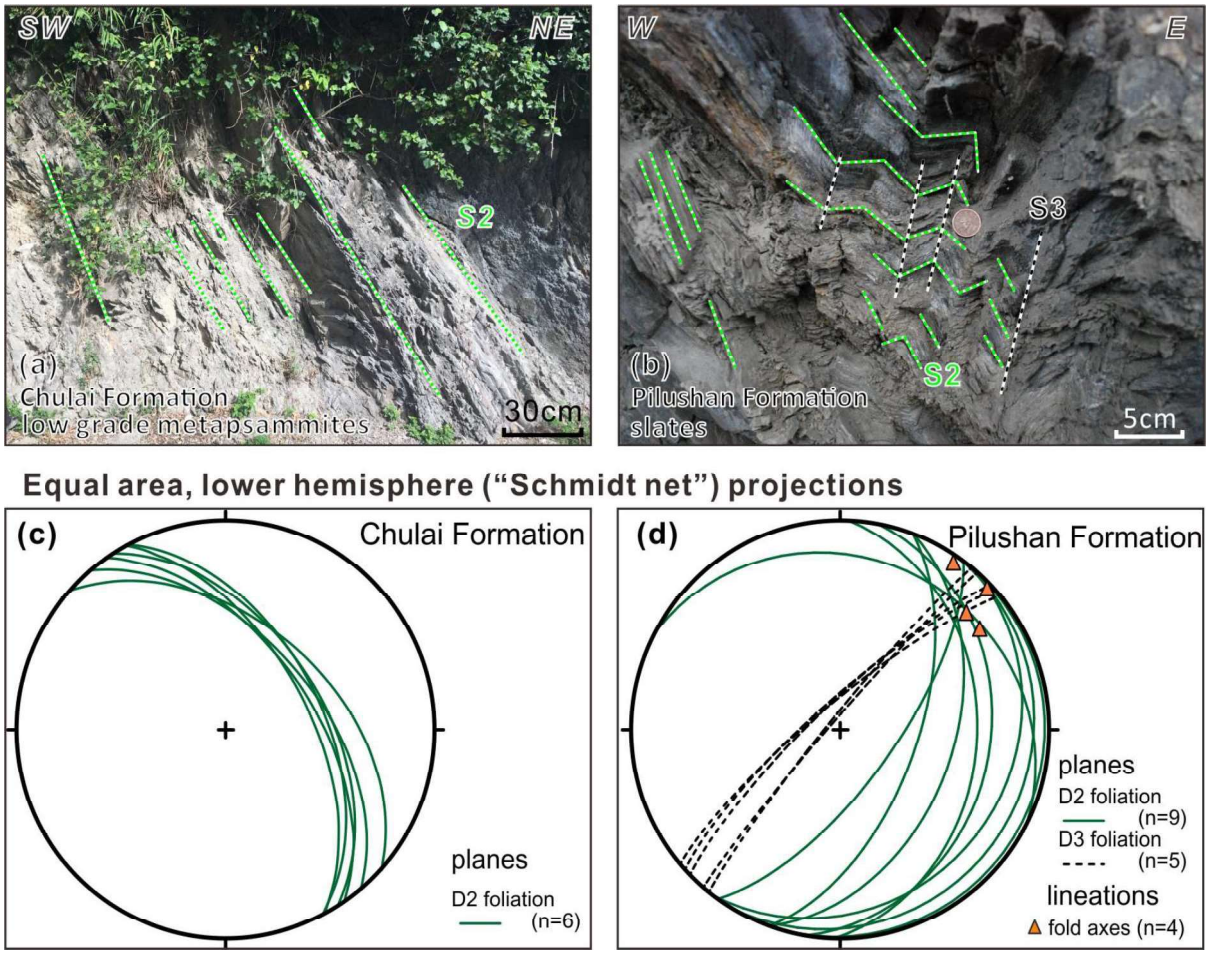

Fig. 4-4: Outcrops and equal area, lower hemisphere ("Schmidt net") projections of Chulai and Pilushan Formation within the Backbone Slates considered representative for map-scale structures.

(a) and (c): Northeast-dipping low-grade metamorphic slates and thin intercalations of sandstones (S2) in the Chulai Formation. Location: west Lakulaku river, 23.301333°N, 121.290917°E.

(b) and (d): The east-facing metamorphic foliation (slaty cleavage, S2) of quartzite slate and dark phyllites in the Pilushan Formation. The refolded axial planar cleavage (S3) dips to the west. Location: east Litao, 23.191908°N, 121.018261°E.

4.3 Results

RSCM temperature contours are generally along the NNE-strike in the eastern Taiwan Central Range (Fig. 4-7). Compared with RSCM temperatures of other major morphotectonic units in Taiwan (Fig. 4-1a), the Tananao Complex shows higher temperatures between ca. 350 and 550 °C (Fig. 4-1b). The western Tailuko Belt shows average temperatures of c. 450 °C. In its northern part that hosts numerous granitoids intrusions (Fig. 4-1b), temperatures can reach over 500 °C. The peak metamorphic temperatures along the Central and Southern cross island highways show a general eastward increasing trend in the Tailuko Belt (Figs. 4-1b, 4-3). We interpret the Tailuko Belt to be an eastward backfolding and thrusting structure in the orogenic retro-wedge, evidenced by the new developing W-dipping foliations (D3) overprinting earlier E-dipping foliated planes during crenulation (Figs. 4-3, 4-7). The eastern Yuli Belt shows generally maximum metamorphic temperatures between ca. 400 and 550 °C, which is higher than in adjacent units. The peak metamorphic temperatures in the Yuli Belt are complicated due to the intensely multi-deformed schist formations (Fig. 4-2). In places, maximum temperatures in the Yuli Belt exceed 500 °C, specifically in close proximity to three HP metamorphic exotic blocks (Figs.4-1b, 4-2). We interpret higher temperatures to indicate antiformal structures, and lower temperatures to be synforms in the mostly NW-dipping schistose unit of the Yuli Belt (Figs. 4-2, 4-3). In the Yuli Belt, the northwest-dipping dominant (D3) foliation (Fig. 4-2) refolded the earlier (D2) compositional layering (Fig. 4-4 (a) (c)), and simple shear deformed schists with top-to-the-SE/S kinematic (Fig. 4-5(i)(j)), considered to have accommodated eastward backfolding and thrusting during D3. Temperature transitions across the Shoufeng Fault (e.g., along Shoufeng Hsi and Xinwuliu Hsi, Figs. 4-1b, 3) are gradual, which is in agreement with lithological and fabric transitions in the field. Dip direction and dip of schistose foliations are mostly W- to NW in the Yuli and Tailuko belts and remain constant across the fault (Figs. 4-2, 4-3). Thus, the juxtaposition of the two belts across the Shoufeng Fault may form during an early W-directed transport (D2) before eastward backfolding and thrusting (D3).

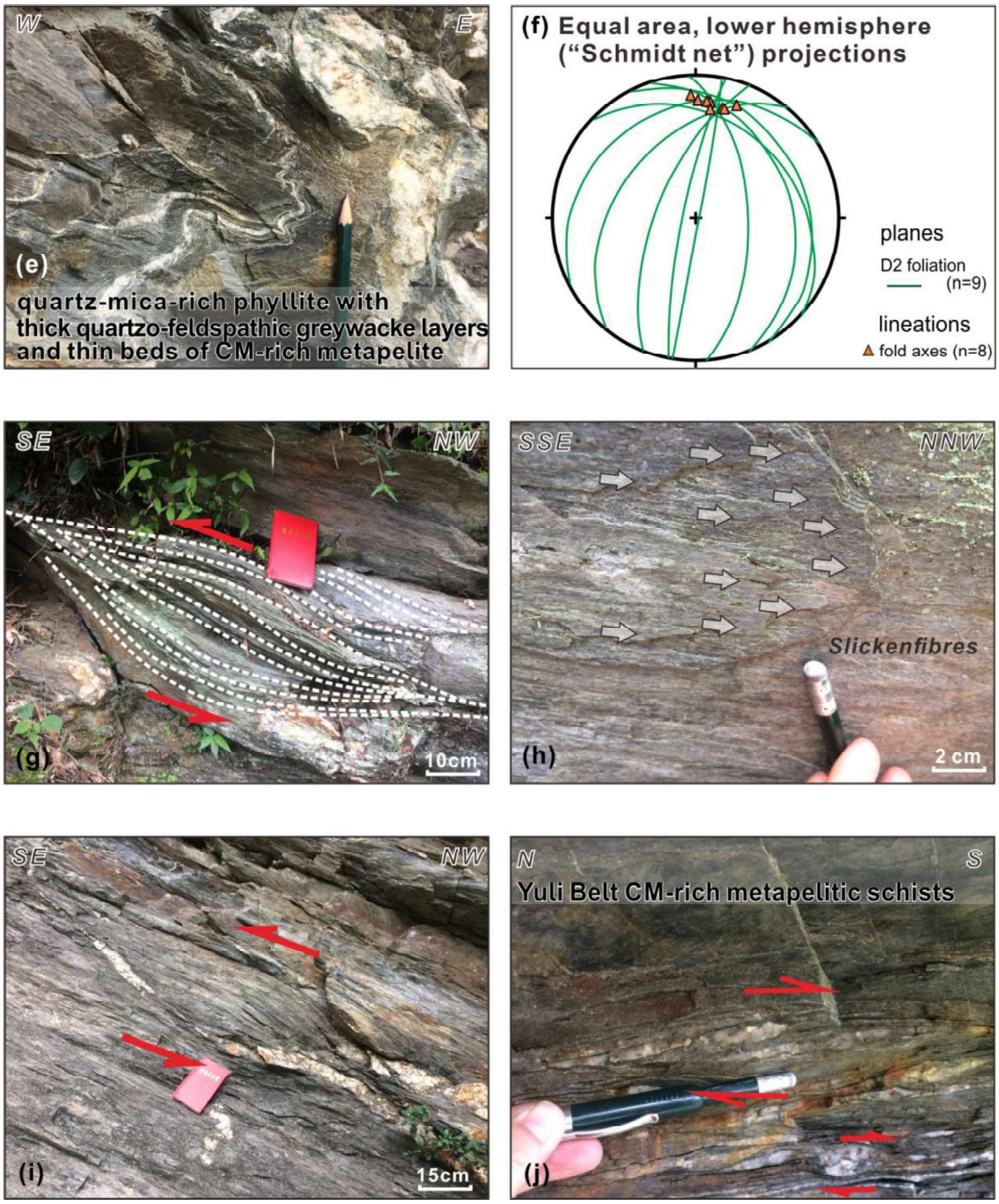

Fig. 4-5: Field photos of the Chulai Formation and the Yuli Belt in the Lakulaku area, showing example of ductile shear zone. See Fig. 4-2 for outcrop locations. (e)-(h) are from the contact between the Chulai Formation and the Yuli Belt. (i) and (j) are from the Yuli Belt.
(e) and (f): Veined metapsammitic to metapelitic sediments are intensely deformed and affected by D3 refolding with gradational textural and metamorphic change in the contact zone. Fold axes gently plunge to the north. Location: 23.309016°N, 121.252120°E.
(g): Northwest-dipping low-grade metamorphic slates and thin intercalations of sandstones in the contact zone, showing deformation structures indicative of top-to-the SE shear and layer-parallel extension. Location: 23.309450°N, 121.248937°E.
(h): Structural planes with slickensides. Black arrows indicate the moving direction of the contrary side judged from steps. Northwest-dipping dominant foliation in the contact zone with top-to-the SSE shear sense of the hanging wall. Location: 23.309450°N, 121.248937°E.
(i): Simple shear deformed Yuli Belt schists with top-to-the-SE kinematic. Location: 23.337362°N, 121.217721°E
(j): Quartz veins crosscutting foliation planes in the Yuli Belt CM-rich schists, showing deformation structures indicative of top-to-the S shear. The plunge/trend of quartz stretching lineations in quartz layers is 012/09. Location: 23.345590°N, 121.198246°E.

By contrast, samples from the Backbone Slates, including the western Pilushan Formation and the eastern Chulai Formation, contain much lower RSCM temperatures between 295 and 372 °C (Figs. 4-1b, 4-2, 4-3). The Chulai Formation is significantly different from the adjacent Yuli Belt but shares a number of key features to the Pilushan Formation. (1): The Chulai Formation shows average temperatures of c. 360 °C, within the temperature range of the Pilushan Formation, between 330 and 450°C. (2): Both Chulai and Pilushan formations contain pervasive silvery gray, quartz-rich phyllites and slates with NE/N-dipping in the field (S2 foliation in Fig.4-4; Figs. 4-2, 3). Therefore, we propose a stratigraphic correlation linking Chulai Formation and Pilushan Formation together in the Backbone Slates (Fig. 4-3). (3): The temperature difference between the Chulai Formation and the Yuli Belt reaches ca. 100 °C (e.g., in the cross sections A-B and E-F, Figs. 4-2, 4-3), indicating the contact between these two units as a fault, namely the Chuisui Fault in this study (F2; Figs. 4-1, 4-2, 4-3). The Yuli Belt schist has experienced greenschist to amphibolite facies metamorphism at deeper levels, with higher estimated temperatures than the phyllitic Chulai Formation. On the basis of surface structural data and RSCM data, we interpret the whole Yuli Belt to be a nappe that emplaced on top of the lower-grade Chulai Formation along the Chuisui Fault during a second deformation phase D2. In the field metapsammitic to metapelitic sediments of the ductile contact zone are intensely deformed, with gradational textural and metamorphic change (Fig. 4-5 (a) (b)). The eastward transport direction (D3) is observed in the contact zone, showing deformation structures indicative of top-to-the SE shear (Fig. 4-5), kinematically similar to the Shoufeng Fault. It suggests both the Yuli Belt and the Chulai Formation may experience the same deformation history after D2 deformation.

4.4 Evolution in the eastern Taiwan Central Range

The tectonic evolution and structural position of the Yuli Belt as part of the Taiwan mountain belt is a key element for to understand the preceding subduction and the ongoing arc-continent collision. Metamorphic overprinting and age relations (e.g., Sandmann et al., 2015), RSCM data (e.g., this study; Fig. 4-7), and structural analyses (e.g., Zhang et al., 2020) suggest that the eastern Taiwan Central Range formed during four successive deformation stages, termed D1, D2, D3 and D4 in the following. A kinematic evolutionary shoe-box cartoon (Figs. 4-6, 4-8) is proposed to illustrate the relationship between cooling and erosion during exhumation of the eastern Taiwan Central Range.

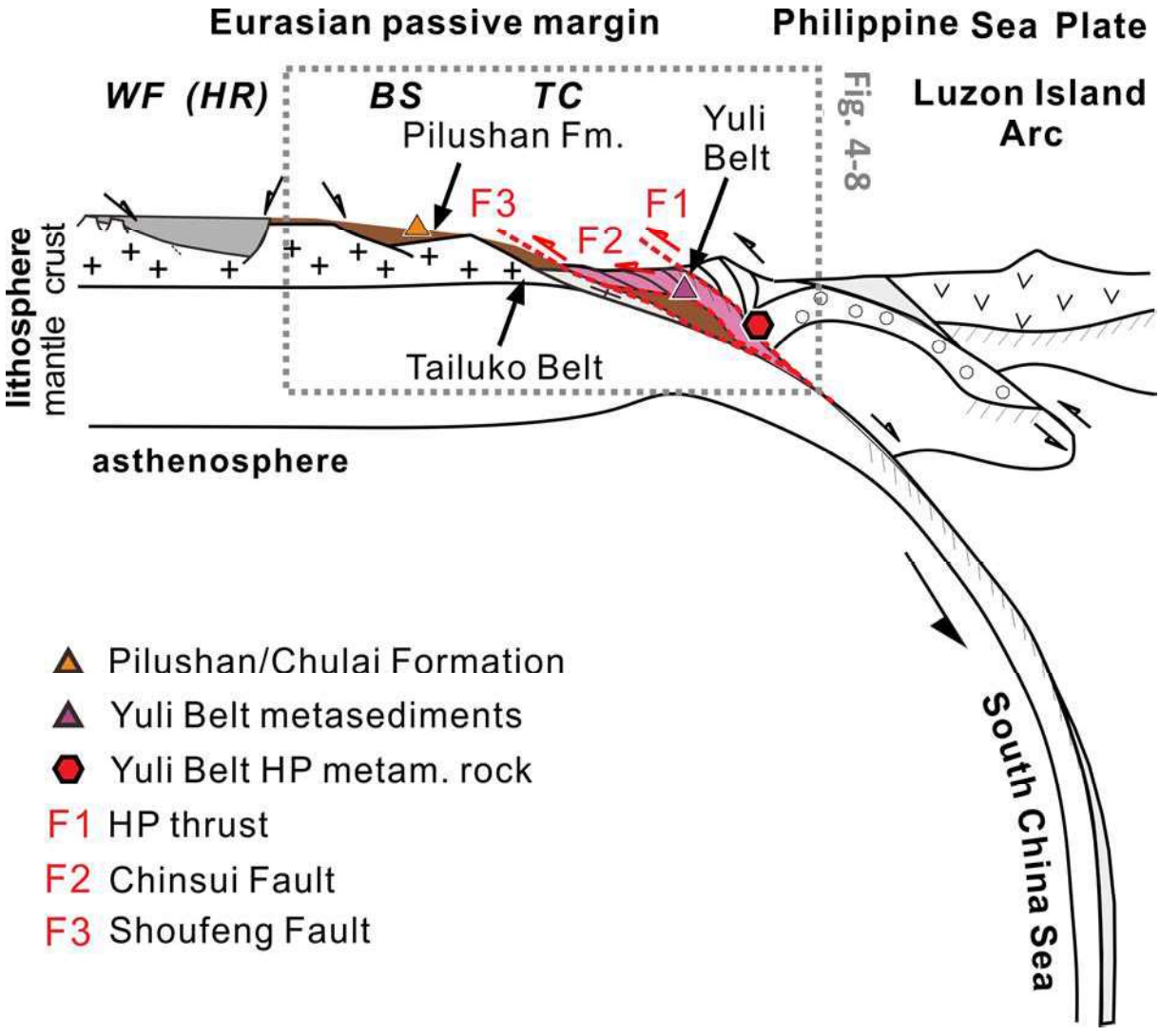

Fig. 4-6: Lithosphere-scale kinematic model to explain the origin of the Yuli Belt of Taiwan (modified after Zhang et al., 2020). WF: Western Foothill; HR: Hsuehshan Range; BS: Backbone Slates; TC: Tananao Complex. See text and Fig. 4-8 for further discussion.

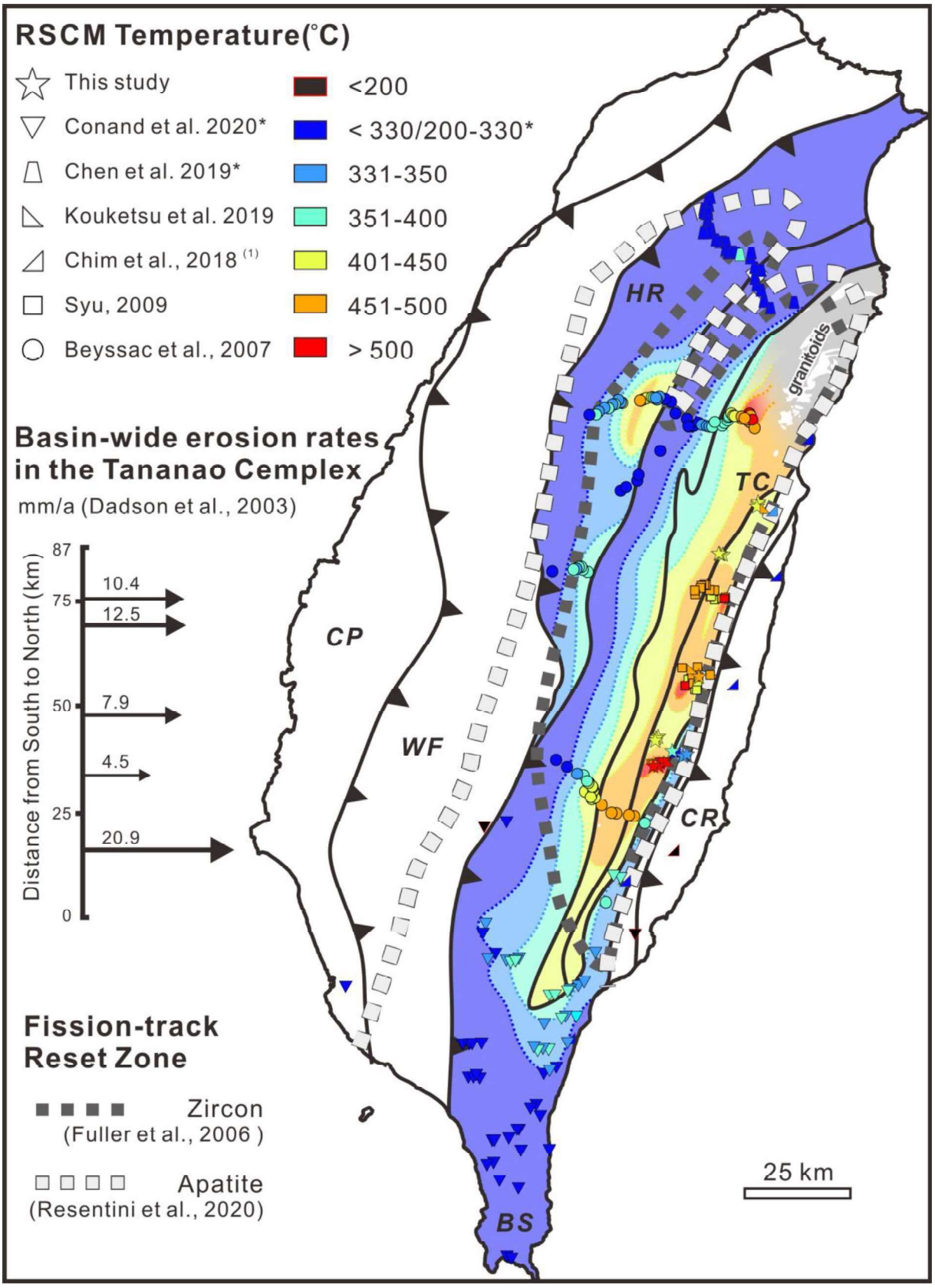

Fig. 4-7: RSCM temperature contours in the eastern Taiwan Central Range. Contours are processed by line smoothing (Gaussian Filtering, Sensitivity 3) within major morphotectonic units. Late Cretaceous granitoids intrusions are shown in the northern Tailuko Belt (Yui et al., 2009). Exposure of reset apatite and zircon fission-track ages (after Fuller et al., 2006 and Resentini et al., 2020) supports southward erosion rates are higher in the retro-side of the Taiwan orogen, as also suggested by catchments studies (after Dadson et al., 2003).

D1: HP rock exhumation phase. The HP, blueschist-facies blocks within the Yuli Belt show Mid-Miocene protolith ages (three samples weighted mean of 15.6 ± 0.3 Ma; Chen et al., 2017), about when the South China Sea ceased spreading (ca. 15.5 Ma, Taylor and Hayes, 1983; Sibuet et al., 2002) and started subducting under the Philippine Sea Plate (Huang et al., 2006). The crystallization ages perhaps provide the single most solid maximum age for Taiwan mountain building initiation. HP blocks subducted reaching peak-P-T conditions (e.g., Beyssac et al., 2008; Tsai et al., 2013) and exhumed portions of crust and mantle along the HP thrust on top of the lower-grade metasedimentary unit of the Yuli Belt (F1; Zhang et al., 2020; Fig. 4-8). The higher RSCM temperatures of the metasediments surrounding the HP blocks (Fig. 4-7) are a result of additional thermal overprint either by the HP metamorphic blocks or by a retrograde overprint under amphibolite- to higher greenschist-facies conditions along the exhuming F1 thrust. Both possibilities suggest that the post-D1 metamorphic history of the Yuli Belt and the HP metamorphosed blocks is similar.

D2: W-ward folding and thrusting phase. Recent chronological constraints argue for the Yuli Belt metasedimentary unit and the Chulai Formation share the same continental affinity zircon U-Pb age populations as young as Upper Miocene (ca. 11 Ma, Chen et al., 2017; Mesalles et al., 2020). However, different lithologies and different maximum metamorphic temperatures (Figs. 4-1, 4-7) between the Yuli Belt and the Chulai Formation contradict this interpretation. In this study, the correlation with the Eocene to Upper Miocene age has been assigned to the sediments in Chulai and Pilushan Formations. Rift-related half-grabens generally accumulated via Eocene-Miocene fluvial to outer shelf deposits over 6 km thick, and derived from the Eurasian continent (Yu et al., 2013) (Fig. 4-6). RSCM temperatures, lithological-, and fabric-transitions are constant across the Shoufeng Fault (Figs. 4-1b, 4-4; Zhang et al., 2020). This indicates that the juxtaposition of the Yuli Belt and the Tailuko Belt (unconformably covered by Pilushan Formation) across the Shoufeng Fault formed during early W-directed transport (D2 phase; Figs. 4-6, 4-8). The Yuli Belt including the former allochthonous HP metamorphic material was thrusted on top of the Pilushan/Chulai Formation along F2 (Chinsui Fault).

D3: Erosional E-ward backfolding and backthrusting phase. The Yuli Belt appears as a large synformal structure with top-to-the-SE shear at the footwall of Shoufeng Fault (F3), in contact with the Tailuko Belt to the west as part of the hanging wall of the F3 (Fig. 4-8). The majority of the HP metamorphic material was eroded during this deformation stage with the exception of small relic blocks in the center of the synformal structure (e.g., cross section C-D; Fig. 4-2). Notably the trace of the F2 contact is poorly preserved and was only reported in the Xinwuliu Hsi area along the Yuli Belt (Stanley et al., 1981). A possible explanation for this might be that the Chulai Formation underwent essentially the same deformation history as the

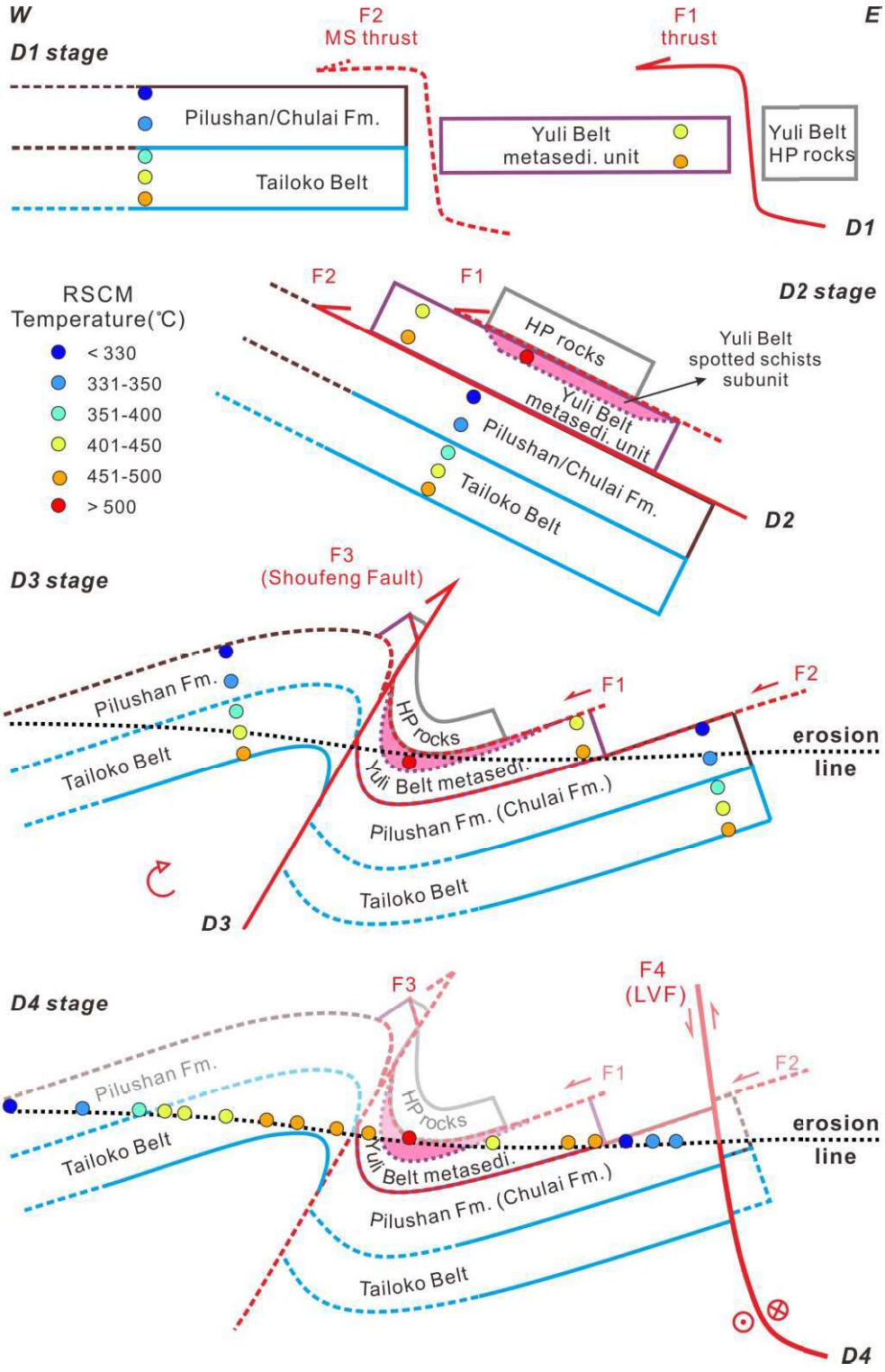

Fig. 4-8: Conceptual kinematic model to explain the Yuli Belt exhumation and structural position (modified after Zhang et al., 2020). The correlation with the Eocene to Upper Miocene age has been assigned to the sediments in Chulai and Pilushan Formations. D1 stage: high-pressure metamorphic rock thrusted over the Yuli Belt metasedimentary unit along the F1 (HP thrust); D2 stage: W-ward thrusting of Yuli Belt onto Tailuko Belt along F2 (Chinsui Fault); D3 stage: E-ward backfolding and backthrusting along F3 (Shoufeng Fault), in combination with later erosion; D4 stage: F4 (LVF, Longitudinal Valley Fault) possibly overprinted the earlier structures. See text for further discussion.

Yuli Belt (in D3-D4 phases), as indicated by sedimentary relationships and structural considerations (Ho, 1986; Fig. 4-5). Thus, the emplacement of the higher-grade metasedimentary Yuli Belt as a nappe on top of the lower-grade Chulai Formation was most likely a separate step prior to the D3 refolding and backthrusting (Figs. 4-3, 4-5). Future research should hence focus on kinematics and fault-related fabrics along the contact to test our model.

D4: Erosion phase. RSCM contours (Fig. 4-7), the continental margin, and the Luzon arc of the Philippine Sea Plate are subparallel, nourishing an initial collision that was simultaneous along the NNE-strike. Apatite and zircon fission-track ages (Fuller et al., 2006; Resentini et al., 2020) and catchments studies (Dadson et al., 2003) both imply that erosion rates in the Backbone Slates were systematic higher towards the south (Fig. 4-7). F4 (Longitudinal Valley Fault) possibly overprinted the earlier structures in combination with later erosion.

4.5 Conclusions

We applied new RSCM temperature measurements in metasedimentary rocks of the Yuli Belt and the Chulai Formation. Peak metamorphic temperatures in the greenschist-facies metasediments, when compiled with published data, support systematic spatial variations across the eastern Taiwan Central Range. The metasedimentary unit of the Yuli Belt shows higher temperatures of c. 400–550 °C than the westerly and easterly adjacent units of the Tailuko belt and the Chulai Formation. Close to allochthonous high pressure blocks, the metasediments of the Yuli Belt indicate maximum metamorphic temperatures of > 500 °C. The temperature difference between the Yuli Belt and the Chulai Formation exceeds 100 °C. Therefore, it appears more likely that the contact between the Yuli Belt and the Chulai Formation is a fault contact (F2; Chinsui Fault in this study), suggesting an overall synformal structural position of the Yuli Belt, with respect to the easterly and westerly adjacent units. We suggest that this synformal geometry, as results of backfolding during the D3 phase of the Taiwan Central Range.

Chapter 5

General Conclusions and Outlook

The aim of my PhD thesis is to better understand improperly understood aspects of the Taiwan orogeny and accretion, subduction and collision processes. In this dissertation, based on results from regional mapping and structure analysis, three crustal-scale geological cross-sections of the Taiwan mountain belt were constructed, providing quantitative estimates on the amount of shortening that the former passive margin of the South China Sea underwent prior to its involvement in arc-continent collision. Four cross sections in a local scale across the Taiwan's metamorphic Yuli Belt were constructed, taking new outcrop- to microscope-scale structural observations from several river-transects into account. Analyses of the whole-rock geochemistry study on the high-pressure rocks and analyses of the Raman spectroscopic geothermometry on the metasediments were conducted in order to constrain tectonic settings and palaeogeographic reconstructions. The following conclusions can be drawn, with respect to the three questions presented in Chapter 1.

(A) This study provides new surface geological mapping and three transects across the entire Taiwan. The structure of Taiwan orogen was interpreted to be two deformation types (D1 and D2) with three basement imbricates. D1 type is an imbricate westward fold-and-thrust system, which develops in the Coastal Plain, Western Foothills, Hsuehshan Range and Backbone Slates. D2 type is an east-facing backfolding and backthrusting system in the eastern Central Range, leading to the development of a second, vertical to steeply W-dipping younger cleavage (S2) that overprinted older nappe-stacking related foliations (S1). Three crustal scale basement imbricates (the Infra-Pilu Tunnel Thrust basement unit, the Pilu Tunnel Thrust basement, and the Shoufeng Fault basement unit) are bounded by three basal thrusts and the Longitudinal Valley Fault. Following nappe stacking accretion, these basement units were later involved in orogen-scale D2 backfolding and backthrusting in structural architecture. Based on three balanced and restored cross sections, we estimate the minimum shortening of the former passive margin of Eurasia to be ~120 km in the central and ~140 km in the south, which is consistent with the underlying unfolded passive margin tomography. Over half of the basement, on top of which the accreted material was initially sitting, has entered subduction. The restored cross sections also reveal a system of subducting rift basins on the continental shelf with bounding normal faults that have been reactivated during subduction. In the paleogeographic

maps, the Eurasian passive margin likely formed a slightly eastward-convex salient prior to plate convergence that created the Taiwan orogen.

(B) Three new cross-sections across Taiwan's Yuli Belt were constructed in a local scale, taking new outcrop- to microscope-scale structural observations from several river-transects into account. The Yuli Belt was affected by at least three successive deformation phases (namely D0 to D2). High-pressure metamorphic units were emplaced on top of metasedimentary units of Yuli Belt along a thrust during the first deformation D0. This assembly was later thrust over Eurasian-derived series of the Tailuko Belt along the Shoufeng Fault during D1, suggested by (rarely preserved) downplunging stretching lineations on W- to NW-dipping foliation planes. E-vergent open to tight folds throughout the Yuli Belt with W- to NW-dipping axial planes were produced by the D2 phase, refolding earlier foliations as well as the D0 nappe contact, during which also the blueschist- facies and metasedimentary units were folded. This phase might be related to a top-E back-thrusting and a reorientation of the Shoufeng Fault from an initially E-dipping to a presently W-dipping contact, for which we present new evidence. High-pressure metamorphic units were interpreted to form erosional relics of nappe outliers of a formerly more contiguous thrust nappe that hosts part of the suture zone in Taiwan. The whole-rock geochemical fingerprint of high-pressure metamorphic rocks is in the MORB tectonic settings of the South China Sea, and could display the effects of metasomatism of their mantle source by slab-derived fluids and alteration from low-temperature seafloor in the subduction zone. Therefore, the blueschist-facies metamorphic unit most likely represents a mid-Miocene fragment of oceanic crust and mantle issued in the South China Sea before having been subducted, exhumed and 'sandwiched' between the Tailuko Belt and the easterly adjacent Coastal Ranges derived from the Philippine Sea Plate.

(C) New Raman spectroscopy of carbonaceous material (RSCM) temperatures in from metasedimentary rocks of the Yuli Belt and the Chulai Formation were applied. Peak metamorphic temperatures in the greenschist-facies metasediments, when compiled with published data, support systematic spatial variations across the eastern Taiwan Central Range. The metasedimentary unit of the Yuli Belt shows higher temperatures of c. 400–550 °C than the westerly and easterly adjacent units of the Tailuko belt and the Chulai Formation. Close to allochthonous high pressure blocks, the metasediments of the Yuli Belt indicate maximum metamorphic temperatures of > 500 °C. The temperature difference between the Yuli Belt and the Chulai Formation exceeds 100 °C. Therefore, it appears more likely that the contact between

the Yuli Belt and the Chulai Formation is a fault contact (Chinsui Fault), suggesting an overall synformal structural position of the Yuli Belt, with respect to the easterly and westerly adjacent units. We suggest that this synformal geometry, as results of the backfolding deformation phase of the Taiwan Central Range.

There are some perspectives which are worth to be studied in the future regarding several aspects of this thesis. The most important point concerns the Yuli Belt of Taiwan. In the Yuli Belt, protolith ages of blueschists are ca. 15 Ma (e.g., Chen et al., 2017; MORB-type, this study); protolith ages of (meta)gabbros/plagiogranite are ca. 15-17 Ma (MORB-type geochemistry; Lo 2018); only one age on epidote amphibolite was estimated at ca. 79 Ma (MORB-type; Jahn et al., 1981); and no protolith age constraints from serpentinite blocks. More accurate structural and geochronological data, particularly on the ages of magmatic protoliths and of high-pressure metamorphism are necessary, in order to constrain the deformation-metamorphism relations and the exhumation mechanism of Yuli Belt blueschists. This, in turn, will facilitate our understanding of the models of fore-arc subduction.

References

Alvarez-Marron, J., Brown, D., Camanni, G., Wu, Y.-M., and Kuo-Chen, H., 2014: Structural complexities in a foreland thrust belt inherited from the shelf-slope transition: Insights from the Alishan area of Taiwan. Tectonics 33, 1322-1339.

Amante, C., and B. W. Eakins, 2009: ETOPO1 arc-minute global relief model: procedures, data sources and analysis. NOAA Technical Memorandum NESDIS NGDC-24, 25 pp.

Angelier, J., 1986: Geodynamics of the Eurasia-Philippine Sea Plate boundary: Preface. Tectonophysics 125, 9-10.

Barrier, E., and C. Muller, 1984: New observations and discussion on the origin and age of the Lichi Mélange. Memoir of the Geological Society of China, 6, 303-325.

Baziotis, I., C. H. Tsai, W. G. Ernst, B. M. Jahn, and Y. Iizuka, 2017: New P-T constraints on the Tamayen glaucophane-bearing rocks, eastern Taiwan: Perple_X modelling results and geodynamic implications. Journal of Metamorphic Geology, 35, 35-54, doi:10.1111/jmg.12218.

Beyssac, O., Goffé, B., Chopin, C. and Rouzaud, J.N., 2002: Raman spectra of carbonaceous material in metasediments: a new geothermometer. Journal of Metamorphic Geology, 20, 859–871. doi:10.1046/j.1525-1314.2002.00408.x

Beyssac, O., Negro, F., Simoes, M.Y., Chan, C. and Chen, Y. G., 2008: High-pressure metamorphism in Taiwan: from oceanic subduction to arc-continent collision. Terra Nova, 20, 118-125, doi:10.1111/j.1365-3121.2008.00796.x

Beyssac, O., Simoes, M., Avouac, J. P., Farley, K. A., Chen, Y.G., Chan, Y.C. and Goffé, B., 2007: Late Cenozoic metamorphic evolution and exhumation of Taiwan. Tectonics, 26, TC6001, doi:10.1029/2006TC002064.

Briais, A., P. Patriat, and P. Tapponnier, 1993: Updated Interpretation of Magnetic Anomalies and Seafloor Spreading Stages in the South China Sea: Implications for the Tertiary Tectonics of Southeast Asia. Journal of Geophysical Research, 98, 6299-6328. https://doi.org/10.1029/92JB02280

Biete, C., Alvarez-Marron, J., Brown, D., and Kuo-Chen, H., 2018: The structure of southwest Taiwan: The development of a fold - and - thrust belt on a margins outer shelf and slope. Tectonics, 37, 1973-1993. https://doi.org/10.1029/2017TC004910

Biq, C., 1971: Comparison of mélange tectonic in Taiwan and in some other mountain belts. Petro. Geol. Taiwan, 9, 79-106.

Bonvalot, S., Balmino, G., Briais, A., Kuhn, M., Peyrefitte, A., Vales N., R. Biancale, G. Gabalda, G. Moreaux, F. Reinquin, M. Sarrahilh, 2012: World Gravity Map. 1:50000000 map, Eds., BGI-CGMW-CNES-IRD, Paris.

Bonnefoi, C.C., Provost, A., and Albarede, F., 1995: The 'Daly gap' as a magmatic catastrophe. Nature, 378, 270–272, doi: 10.1038/378270a0.

Brown, D. and Ryan, P.D. (eds.), 2011: Arc-Continent Collision, Frontiers in Earth Sciences, 4, 477-493. DOI 10.1007/978-3-540-88558-0_17.

Brown, D., Alvarez-Marron, J., Schimmel, M., Wu, Y.M., Camanni, G., 2012: The structure and kinematics of the central Taiwan mountain belt derived from geological and seismicity data. Tectonics, 31, 10.1029/2012TC003156.

Bunsen, R., 1851: Ueber die prozesse der vulkanishen Gesteinsbildungen Islands. Annalen der Physics, 83, 197-272, doi: 10.1002/andp.18511590602.

Camanni, G., Chen, C.-H., Brown, D., Alvarez-Marron, J., Wu, Y.-M., Chen, H.-A., Huang, H.-H., Chu, H.-T., Chen, M.-M., Chang, C.-H., 2014: Basin inversion in central Taiwan and its importance for seismic hazard. Geology 42, 147-150.

Carena S., J. Suppe and H. Kao, 2002: Active detachment of Taiwan illuminated by small earthquakes and its control of first-order topography. Geology, 30, 935-938, doi: 10.1130/0091-7613(2002)030<0935:ADOTIB>2.0.CO;2

Chai, H.T., 1972: Structure and tectonic evolution of Taiwan, Amer. Jour. Sci., 272, 389-422.

Chang, C.-P., J. Angelier, and C.-Y. Huang, 2000: Origin and evolution of a mélange: the active plate boundary and suture zone of the Longitudinal Valley, Taiwan. Tectonophysics, 325, 43-62. 10.1016/S0040-1951(00)00130-X

Chang, H.-C., C.-W. Lin, M.-M. Chen, and S.-T. Lu, 1998: An Introduction to the Active Faults of Taiwan, Explanatory Text of the Active Fault Map of Taiwan (in Chinese with English abstract), Spec. Pub. Cent. Geol. Surv., 10, 103pp., Cent. Geol. Surv., Ministry Econ. Affairs, Taipei, Taiwan.

Chang, L.-S., 1969: A biostratigraphic study of the Tertiary in the Coastal Range, eastern Taiwan, based on smaller foraminifera (III: Middle part). Proc. Geol. Soc. China, 12, 89-101.

Chang, S.-S. L. and W. R. Chi, 1983. Neogene Nannoplankton biostratigraphy in Taiwan and the tectonic implications. Petroleum Geology of Taiwan, 19, 93-147.

Chen, C.-T., Chan, Y.-C., Lu, C.-Y., Simoes, M., and Beyssac, O., 2011: Nappe structure revealed by thermal constraints in the Taiwan metamorphic belt. Terra Nova, 85-91.

Chen, C.-T., Chan, Y. C., Beyssac, O., Lu, C. Y., Chen, Y. G., Malavieille, J., Kidder, S. B. and Sun, H. C., 2019: Thermal history of the Northern Taiwanese slate belt and implications for wedge growth during the Neogene arc-continent collision. Tectonics, 38, 3335–3350. https://doi.org/10.1029/2019TC005604

Chen, C.-T., Chan, Y.-C., Lo, C.-H., Malavieille, J., Lu, C.-Y., Tang, J.-T., and Lee, Y.-H., 2018: Basal accretion, a major mechanism for mountain building in Taiwan revealed in rock thermal history. Journal of Asian Earth Sciences, 152, 80-90. doi:10.1016/j.jseaes.2017.11.030

Chen, C.-H., and C.-H. Wang, 1995: Explanatory notes for the metamorphic facies map of Taiwan. Centr. Geol. Surv. Spec. Publ., 2nd ed., 51pp.

Chen, C.-H., T. F. Yang, J. l. Tien, and T. Lee, 1992: Eruption ages of northern Luzon Arc (Taiwan): based on fission-track dating. Acta Geologica Taiwanica, 30, 149-156.

Chen, W.-H., C.Y. Huang, Y.J. Lin, Q. Zhao, Y. Yan, D. Chen, X. Zhang, Q. Lan, M. Yu, 2015: Depleted deep South China Sea δ13C paleoceanographic events in response to tectonic evolution in Taiwan–Luzon Strait since Middle Miocene. Deep-Sea Res. II. http://dx.doi.org/10.1016/j.dsr2.2015.02.005

Chen, W.-S., Chung, S. L. Chou, H. Y., Zugeerbai, Z., Shao, W. Y. and Lee, Y. H., 2017: A reinterpretation of the metamorphic Yuli belt: Evidence for a middle-late Miocene accretionary prism in eastern Taiwan. Tectonics, 36, 188–206. https://doi.org/10.1002/2016TC004383

Chen, W.-S., J. J. Yeh, and S. J. Syu, 2019: Late Cenozoic exhumation and erosion of the Taiwan orogenic belt: New insights from petrographic analysis of foreland basin sediments and thermochronological dating on the metamorphic orogenic wedge. Tectonophysics, 750, 56-69, https://doi.org/10.1016/j.tecto.2018.09.003.

Chen, W.-S., K. D. Ridgway, C. S. Horng, Y. G. Chen, K. S. Shea, and M. G. Yeh, 2001: Stratigraphic architecture, magnetostratigraphy, and incised-valley systems of the Pliocene-Pleistocene collisional marine foreland basin of Taiwan. GSA Bulletin, 113, 1249-1271.

Chen, W.-S., S. L. Chung, H. Y. Chou, Z. Zugeerbai, W. Y. Shao, and Y. H. Lee, 2017: A reinterpretation of the metamorphic Yuli belt: Evidence for a middle-late Miocene accretionary prism in eastern Taiwan. Tectonics, 36, 188-206. https://doi.org/10.1002/2016TC004383

Chen, C.-H. and Wang, C.-H., 1995: Explanatory Notes for the Metamorphic Facies Map of Taiwan, 2nd edn. Special Report of Central Geological Survey 2, 51pp. Central Geological Survey, Taipei, Taiwan.

Chen, C.-H. and T.-Y. Chuang, 1989: Geology of the Southwest Central Range and a structural interpretation of the Central Range of Taiwan. Bulletin of the Central Geological Survey, 5, 1-18. (in Chinese)

Chen, Y.-L., 1995: Three-dimensional velocity structure and kinematic analysis in Taiwan area. MS thesis, National Central University, Chung-Li, 172 pp.

Chi, W. R., J. Namson, and J. Suppe, 1981: Stratigraphic record of plate interactions in the Coastal Range of Eastern Taiwan. Mem. Geol. Soc. China, 4, 155-194.

Chiang, S. F., 2003: Original and metamorphic P–T evolution of porphytroblastic albites of spotted schists in Juisui. Master thesis, National Central Univ., Taiwan, 120 pp.

Chim, L. K., Yen, J. Y., Huang, S. Y., Liou, Y. S. and Tsai, L. L., 2018. Using Raman Spectroscopy of Carbonaceous Materials to track exhumation of an active orogenic belt: An example from Eastern Taiwan. Journal of Asian Earth Sciences, 164, 248–259. https://doi.org/10.1016/j.jseaes.2018.06.030

Chow, J.T. and Lin, C. C., 1974. Geology of Taiwan. Taiwan Provincial Documentary Committee, 450 p. (in Chinese).

Chung S. L., and S. S. Sun, 1992: A new genetic model for the East Taiwan Ophiolite and its implications for Dupal domains in the Northern Hemisphere. Earth and Planetary Science Letters, 109, 133-145, https://doi.org/10.1016/0012-821X(92)90079-B.

Clark, M. B., D. M. Fisher, and C. Y. Lu, 1992: Strain variations in the Eocene and older rocks exposed along the Central and Southern cross-island highways, Taiwan. Acta Geol. Taiwanica, 30, 1-10.

Conand, C., F., Mouthereau, J., Ganne, A. T.-S., Lin, A., Lafhid, M., Daudet, L., Mesalles, S., Giletycz, and M., Bonzani, 2020: Strain partitioning and exhumation in oblique Taiwan collision: role of rift architecture and plate kinematics. Tectonics, 39, p. e2019TC005798.

Conand, C., Mouthereau, F., Ganne, J., Lin, A. T.-S., Lafhid, A., Daudet, M., Mesalles, L., Giletycz, S. and Bonzani, M., 2020. Strain partitioning and exhumation in oblique Taiwan collision: role of rift architecture and plate kinematics: Tectonics, 39, p. e2019TC005798.

Condie, K.C., 1989: Plate Tectonics and Crustal Evolution, Pergamon Press, Oxford, 476pp.

Condie, K.C., 2016: Earth as an evolving Planetary system, 3rd ed. Elsevier Academic Press, 95-96.

Crespi, J. M., Y.C., Chan, and M. S., Swaim, 1996: Synorogenic extension and exhumation of the Taiwan hinterland. Geology, 24, 247-250. doi: https://doi.org/10.1130/0091-7613(1996)024<0247:SEAEOT>2.3.CO;2

Dadson, S.J., Hovius, N., Chen, H., Dade, W.B., Hsieh, M.L., Willett, S.D., Hu, J.D., Horng, M.J., Chen, M.C., Stark, C.P., Lague, D. and Lin, J.C., 2003. Links between erosion, runoff variability and seismicity in the Taiwan orogen. Nature, 426, 648-651.

Dahlstrom, C. D. A. 1969: Balanced cross sections, Can. J. Earth Sci., 6, 743-757, doi:10.1139/e69-069.

Daly, R.A., 1925: The geology of Ascension Island. American Academy of Arts and Sciences Proceedings, v. 60, p. 1–80.

Deschamps, A., P. Monié, S. Lallemand, S. K. Hsu, and K. Y. Yeh, 2000: Evidence for Early Cretaceous oceanic crust trapped in the Philippine Sea Plate. Earth and Planetary Science Letters, 179, 503-516. https://doi.org/10.1016/S0012-821X(00)00136-9

Dewey, J.F., 1987: Suture. In: Encyclopedia of Structural Geology and Tectonics. Encyclopedia of Earth Science series. Springer, Berlin, Heidelberg. doi.org/10.1007/3-540-31080-0_115

Dorsey, R. J., 1992: Collapse of the Luzon Volcanic Arc during onset of arc-continent collision: Evidence from a Miocene-Pliocene unconformity, eastern Taiwan. Tectonics, 11, 177–191, doi:10.1029/91tc02463

Ernst, W. G., 1979: Coexisting sodic and calcic amphiboles from high-pressure metamorphic belts and the stability of barroisitic amphibole. Mineralog. Mag., 43, 269.

Ernst, W.G., Liou, J. G., and Moore, D.E., 1981: Multiple metamorphic events recorded in Tailuko amphibolites and associated rocks of the Suao Nanao area, Taiwan. Mem. Geol. Soc. China, 4, 391-441.

Ernst, W.G., C.S. Ho, and J.G. Liou, 1985: Rifting, drifting and crustal accretion in the Taiwan sector of the Asiatic continental margin. Tectonostratigraphic Terranes of the Circum-Pacific RegionD.G. Howell (Ed.), Am. Assoc. Pet. Geol., Spec. Vol., 375-389.

Ernst, W. G., and B. M. Jahn, 1987: Crustal accretion and metamorphism in Taiwan, a post-Palaeozoic mobile belt. Phil. Trans. R. Soc. Lond., 321, 129-161.

Faure, M., C., Y. Lu, and H. T. Chu, 1991: Ductile deformation and Miocene nappe-stacking in Taiwan related to motion of the Philippine Sea Plate. Tectonophysics, 198, 95-105, doi:10.1016/0040-1951(91)90134-E.

Fisher, D. M., 1999: Orogen parallel extension Eastern Central range of Taiwan. J. Geol. Soc. China-Taiwan, 42, 41-58.

Fisher, D. M., C. Y. Lu, and H. T. Chu, 2002: Taiwan Slate Belt: insights into the ductile interior of an arc-continent collision. Geol. Soc. Am. Spec. Pap., 358, 93–106. doi:10.1130/0-8137-2358-2.93

Fisher, D. M., S. Willett, E. C. Yeh, and M. B. Clark, 2007: Cleavage fronts and fans as reflections of orogen stress and kinematics in Taiwan. Geology, 35; 65-68, doi: 10.1130/G22850A.1

Fisher, D.M., Willett, S., Yeh, E.-C., Clark, M.B., 2007: Cleavage fronts and fans as reflections of orogen stress and kinematics in Taiwan. Geology 35, 65-68.

Froitzheim, N., J. Pleuger, S. Roller, and T. Nagel, 2003: Exhumation of high- and ultrahigh-pressure metamorphic rocks by slab extraction. Geology, 31, 925-928. https://doi.org/10.1130/G19748.1

Fuller, C.W., Willet, S.D., Fisher, D. and Lu, C.Y., 2006: A thermomechanical wedge model of Taiwan constrained by fission-track thermochronometry. Tectonophysics, 274, 97–115.

Gansser, A., 1964: The Geology of the Himalayas. New York: Wiley-Interscience, 289 pp.

Gansser, A., 1980: The significance of the Himalayan suture zone. Tectonophysics, 62, 37–52, doi.org/10.1016/0040-1951(80)90134-1

Gradstein, F., J. Ogg, M. Schmitz, and G. Ogg, 2012: The Geologic Time Scale, Elsevier, 1144 pp. https://doi.org/10.1016/C2011-1-08249-8

Grasemann, B., and B., Huet, 2016: Orogeny, in: Harff, J., Meschede, M., Petersen, S., Thiede, J. (Eds.), Encyclopedia of Marine Geosciences. Springer, pp. 602-610.

Groshong, R. H., 2006: 3-D Structural Geology: A Practical Guide to Quantitative Surface and Subsurface Map Interpretation. 2nd ed. Berlin, Heidelberg, New York: Springer-Verlag, 400 pp.

Henry D. G., Jarvis, I., Gillmore, G. and Stephenson, M., 2019. Raman spectroscopy as a tool to determine the thermal maturity of organic matter: Application to sedimentary, metamorphic and structural geology. Earth-Science Reviews, 198, https://doi.org/10.1016/j.earscirev.2019.102936.

Ho, C. S., 1986: A synthesis of the geologic evolution of Taiwan. Tectonophysics, 125, 1-16. https://doi.org/10.1016/0040 - 1951(86)90004 - 1

Ho, C. S., 1988: An introduction to the geology of Taiwan: explanatory text of the geological map of Taiwan, Cent Geol. Surv., Minist. of Econ. Affairs, Taipei.

Ho, G. R., 2015: The structural evolution of the Tananao Complex, Taiwan – taking examples from Hopin, Wanrung and Shouthern cross-island highway. National Taipei University of Technology. 95 pp. (in Chinese with English abstract)

Ho, G. R., and W. Lo, 2015: Structural analysis in Shoufengsi area of Tananao Complex, eastern Taiwan. Terr. Atmos. Ocean. Sci., 26, 557-569, doi: 10.3319/TAO.2015.05.15.01(TT)

Hofmann, A.W., 1988: Chemical differentiation of the Earth: the relationship between mantle, continental crust, and oceanic crust. Earth and Planetary Science Letters, 90, pp. 297-314.

Hsieh, R., G. Shellnutt, and M. W. Yeh, 2017: Age and tectonic setting of the East Taiwan Ophiolite: Implications for the growth and development of the South China Sea. Geological Magazine, 154, 441-455, doi:10.1017/S0016756816000054

Hsu, T.L., 1956: Geology of the Coastal Range, eastern Taiwan. Bull. Geol. Surv. Taiwan 8, 39-64.

Hsu, S. K., Y. Yeh, W. B. Doo, and C. H. Tsai, 2004: New Bathymetry and Magnetic Lineations Identifications in the Northernmost South China Sea and their Tectonic Implications. Mar Geophys Res, 25: 29. https://doi.org/10.1007/s11001-005-0731-7

Hsu, W.-H., T. B. Byrne, W. Ouimet, Y.-H. Lee, Y.-G. Chen, M. Soest, and K. Hodges, 2016: Pleistocene onset of rapid, punctuated exhumation in the eastern Central Range of the Taiwan orogenic belt. Geology, 44, 719–722. doi: https://doi.org/10.1130/G37914.1

Hu, Hsien-Neng and Tsan, S. F., 1984: Structural study of the Slate Formation along the South Link Railroad, Taiwan. Special Pub. Central Geol. Surv., 3, 25-43. (in Chinese)

Huang, C. Y., P. B. Yuan, and S. J. Tsao, 2006: Temporal and spatial records of active arc-continent collision in Taiwan: A synthesis. Geological Society of America Bulletin, 118, 274-288, doi:10.1130/b25527.1

Huang C. Y., Yuan P B, Lin C W, Tan, K.W., and Chang, C.-P., 2000: Geodynamic processes of Taiwan arc-continent collision and comparison with analogs in Timor, Papua New Guinea, Urals and Corsica. Tectonophy, 325: 1–21

Huang, C. Y., Yen, Y., Zhao, Q. H., and Lin, C.-T., 2012: Cenozoic stratigraphy of Taiwan: Window into rifting, stratigraphy and paleoceanography of South China Sea. Chin Sci Bull, 57, 3130-3149, doi: 10.1007/s11434-012-5349-y

Huang, C. Y., W. H. Chen, M. H. Wang, C. T. Lin, S. Yang, X. Li, and R. Harris, 2018: Juxtaposed sequence stratigraphy, temporal-spatial variations of sedimentation and development of modern-forming forearc Lichi Mélange in North Luzon Trough forearc basin onshore and offshore eastern Taiwan: An overview. Earth-Science Reviews, 182, 102-140, doi:10.1016/j.earscirev.2018.01.015

Huang, S.-T., Yang, K.-M., Ting, H.-H., Lee, C.-J., 2004: Observation of fault activity and evaluation of the earthquake potential in the Western foothills area of Taiwan, based on the synthetic analysis of subsurface data (in Traditional Chinese). Publications of the Central Geological Survey Taiwan, p. 71.

Huang, T. C., J. S. Ting, and C. Muller, 1983: A note on Pliocene microfossils from the Kenting mélange. Proceedings of the Geological Society of China, 26, 57-66.

Jahn, B. M., and J. G. Liou, 1977: Age and geochemical constraints of glaucophane schists of Taiwan. Mem. Geol. Soc. China, 2, 129-140.

Jahn, B.M., F. Martineau, J.J. Peucat, and J. Cornichet, 1986: Geochronology of the Tananao Schist complex, Taiwan, and its regional tectonic significance. Tectonophysics, 125, 103-124. https://doi.org/10.1016/0040-1951(86)90009-0

Jahn, B.M., J. G. Liou, and H. Nagasawa, 1981: High-pressure Metamorphic Rocks of Taiwan: REE Geochemistry, Rb-Sr Ages and Tectonic Implications. Mem. Geol. Soc. China, 7, 497-520.

Juang, W. S. and H. Bellon, 1986: Potassium-Argon Ages of the Tananao Schist in Taiwan. Mem. Geol. Soc. China, 7, 405-416.

Juang, W. S., 1988: Geochronology and chemical variations of late Cenozoic volcanic rocks in Taiwan. Ph.D. thesis, National Taiwan University, Taipei, 231 pp.

Juang, W. S., and J. C. Chen, 1990: Geochronology and chemical variations of volcanic rocks along the arc-continent collision zone in eastern Taiwan. Bulletin of the National Museum of Natural Sciences, 2, 89-118.

Kao, H., G. Huang, and C. Liu, 2000: Transition from oblique subduction to collision in the northern Luzon arc - Taiwan region: Constraints from bathymetry and seismic observations. Journal of Geophysical Research Solid Earth, 105, 3059 – 3079. https://doi.org/10.1029/1999JB900357

Keyser, W., C. H. Tsai, Y. Iizuka, R. Oberhänsli, and W. G. Ernst, 2016: High-pressure metamorphism in the Chinshuichi area, Yuli belt, eastern Taiwan. Tectonophysics, 692, 191-202, doi:10.1016/j.tecto.2015.09.012

Kouketsu, Y., Tsai, C.H. and Enami, M., 2019: Discovery of unusual metamorphic temperatures in the Yuli belt, eastern Taiwan: New interpretation of data by Raman carbonaceous material geothermometry. Geology, 47, 522–526. doi: https://doi.org/10.1130/G45934.1

Lahfid, A., Beyssac, O., Deville, E., Negro, F., Chopin, C. and Goffé, B., 2010: Evolution of the Raman spectrum of carbonaceous material in low-grade metasediments of the Glarus Alps (Switzerland). Terra Nova, 22: 354–360. doi:10.1111/j.1365-3121.2010.00956.x

Lallemand, S., Font, Y., Bijwaard, H., Kao, H., 2001: New insights on 3-D plates interaction near Taiwan from tomography and tectonic implications. Tectonophysics 335, 229-253.

Lan, C. Y., and J. G. Liou, 1981: Occurrence, petrology and tectonics of serpentinites and associated rodingites in the Central Range, Taiwan. Memoir of the Geological Society of China, 4, 343-389.

Lan, C. Y., B. M. Jahn, S. A. Mertzman, and T. W. Wu, 1996: Subduction-related granitic rocks of Taiwan. Journal of Southeast Asian Earth Sciences, 14, l-28. https://doi.org/10.1016/S0743-9547(96)00017-7

Lan, C. Y., and J. G. Liou, 1984: Mineral chemistry of metamorphosed oceanic rocks in the Yuli Belt of the Tananao schist, Taiwan. Memoir of the Geological Society of China, 6, 153-178.

Lee, J.-C., Chu, H.T., Angelier, J., Chan, Y.C., Hu, J.C., Lu, C.Y., and Rau, R.J., 2002: Geometry and structure of northern surface ruptures of the 1999 Mw=7.6 Chi-Chi, Taiwan earthquake: influence from inherited fold belt structures. Jour. Struct. Geol., 24, 1, 173-192.

Lee, T. Y., and L.A. Lawer, 1995: Cenozoic plate reconstruction of Southeast Asia. Tectonophysics, 251, 85-138.

Lee, Y. H., Byrne T., Wang W. H., Lo W., Rau R. J., Lu H. Y., 2015: Simultaneous mountain building in the Taiwan orogenic belt. Geology, 43, 451–454. doi: https://doi.org/10.1130/G36373.1

Letouzey, J., and Kimura, M., 1985: Okinawa Trough genesis: Structure and evolution of a back-arc basin developed in a continent. Marine Petroleum Geology, 2, 111-130.

Li, Q., G. Wu, L. Zhang, S. Yu, and S. Lei, 2017: Paleogene marine deposition records of rifting and breakup of the South China Sea: An overview. Sci. China Earth Sci. 60, 2128–2140, doi: 10.1007/s11430-016-0163-x.

Lin, A. T., and Watts, A. B., 2002: Origin of the West Taiwan basin by orogenic loading and flexure of a rifted continental margin. Journal of Geophysical Research, 107, 2185B9, doi:10.1029/2001JB000669.

Lin, A.T., Watts, A.B., and Hesselbo, S. P., 2003: Cenozoic stratigraphy and subsidence history of the South China Sea margin in the Taiwan region. Basin Res., 15, 453-478. https://doi.org/10.1046/j.1365-2117.2003.00215.x

Lin, C. T., R. Harris, W. D. Sun, and G. L. Zhang, 2019: Geochemical and geochronological constraints on the origin and emplacement of the East Taiwan Ophiolite. Geochemistry, Geophysics, Geosystems, 20, 2110-2133. https://doi.org/10.1029/2018GC007902

Lin, C. W. and Chen, W. S., 2016. Geologic Map of Tawan. Published by Geological Society of Taiwan.

Lin, M. L., C. N. Yang, and Y. Wang, 1984: Petrotectonic study on the Yuli belt of the Tananao Schist in the Chinshuichi area, eastern Taiwan. Acta Geol. Taiwanica, 22, 151-188.

Lin, M. L., 1999: Litho-stratigraphy and structural geology of the Wanjung area, eastern

Taiwan and their tectonic implications. J. Geol. Soc. China, 42, 247-267.

Liou, J. G., 1981: Petrology of metamorphosed oceanic rocks in the Central Range of Taiwan. Mem. Geol. Soc. China, 4, 291-342.

Liou, J. G., and W. G. Ernst, 1984: Summary of Phanerozoic metamorphism in Taiwan, Mem. Geol. Soc. China, 6, 133-152.

Liou, J. G., C. O. Ho and T. P. Yen, 1975: Petrology of some Glaucophane Schists and Related Rocks from Taiwan. Journal of Petrology, 16, 80-109.

Lo, C. H. and T. F. Yui, 1996: 40Ar/39Ar dating of high-pressure rocks in the Tananao basement complex. Taiwan. J. Geol. Soc. China, 39, 13-30.

Lo, C. H., T. C. Onstott, C. H. Chen, and T. Q. Lee, 1994: An assessment of 40Ar/39Ar dating for the whole-rock volcanic samples from the Luzon Arc near Taiwan. Chemical Geology, 114, 157-178. https://doi.org/10.1016/0009-2541(94)90049-3

Lo, W. H., 2018: Zircon U-Pb geochronological constraints and whole-rock geochemical characteristics of metamorphic rocks in the Chinshuichi area of the Yuli belt, eastern Taiwan. Master thesis, National DongHwa University, 177 pp.

Lo, Y. C., C. T. Chen, C. H. Lo, and S. L. Chung, 2020: Ages of ophiolitic rocks along plate suture in Taiwan orogen: Fate of the South China Sea from subduction to collision. Terrestrial, Atmospheric and Oceanic Sciences, Accepted. doi: 10.3319/TAO.2019.06.19.01

Malavieille, J., Lallemand, S.E., Dominguez, S., Deschamps, A., Lu, C.-Y., Liu, C.-S., Schnuerle, P., Angelier, J., Collot, J.Y., Deffontaines, B., Fournier, M., Hsu, S.K., Le Formal, J.P., Liu, S.Y., Sibuet, J.C., Thareau, N., Wang, F., Crew, A.A.C.i.T.S., 2002. Arc-continent collision in Taiwan: New marine observations and tectonic evolution. Geological Society of America - Special Paper 358, 187-211.

Malavieille, J., Trullenque, G., 2007. Consequences of continental subduction on forearc basin and accretionary wedge deformation in SE Taiwan: Insights from analogue modeling. Tectonophysics, doi:10.1016/j.tecto.2007.1011.1016.

Maltman A., 1990: Geological cross-sections. In: Geological maps: An Introduction. Springer, Boston, MA. https://doi.org/10.1007/978-1-4684-6662-1_5

Manatschal, G., D., Sauter, A.M., Karpoff, E., Masini, G., Mohn, Y., Lagabrielle, 2011: The Chenaillet Ophiolite in the French/Italian Alps: An ancient analogue for an Oceanic Core Complex? Lithos, 124, 169-184.

Maruyama, S., M. Cho, and J. G. Liou, 1986: Experimental investigation of blueschist greenschist transition equilibria: pressure dependence of Al2O3 contents in sodic amphiboles – a new geobarometer. In: Evans, B.W., Brown, E.H. (Eds.), Blueschists and Eclogites, 164. Geological Society of America Memoir, 1-16.

McIntosh, K., Nakamura, Y., Wang, T.-K., Shih, R.-C., Chen, A., and Liu, C.-S., 2005: Crustal-scale seismic profiles across Taiwan and the western Philippine Sea. Tectonophysics, 401, 23-54.

Mesalles, L., Mouthereau, F., Bernet, M., Chang, C.P., Lin, A.T., Fillon, C., Sengelen, X., 2014: From submarine continental accretion to arc-continental orogenic evolution: the thermal record in southern Taiwan. Geology, 42, 907-910.

Mesalles, L., Mouthereau, F., Bernet, M., Chang, C.-P., Tien-Shun Lin, A., Fillon, C., and Sengelen, X., 2014: From submarine continental accretion to arc-continent orogenic evolution: The thermal record in southern Taiwan. Geology, 42, p. 907-910.

Mesalles, L., Y.-H. Lee, T.-C. Ma, W.-L. Tsai, X.-B. Tan and H.-Y. Lee, 2020: A Late-Miocene Yuli Belt? New constraints on the eastern Central Range depositional ages. Terr. Atmos. Ocean. Sci., 31, 1-12, doi: 10.3319/ TAO.2019.06.24.01

Meschede, M., 1986: A method of discriminating between different types of Mid-Oceanic Ridge Basalts and continental tholeiites with the Nb-Zr-Y diagram. Chemical Geology, 56, 207-218.

Misch, P., 1969: Paracrystalline microboudinage of zoned grains and other criteria for synkinematic growth of metamorphic minerals. Am J Sci, 267(1), 43-63.

Mitra, S., and J. Namsom, 1989: Equal-area balancing. American Journal of Science, 289, 563–599, DOI: 10.2475/ajs.289.5.563.

Mitra, S., 1992: Balanced structural interpretations in fold and thrust belts, in S. Mitra, and G. W. Fisher, eds., Structural Geology of Fold and Thrust Belts. Johns Hopkins University Press, Maryland, p. 53-77.

Mondro, C., D. Fisher, and E-C., Yeh, 2017: Strain histories from the eastern Central Range of Taiwan: A record of advection through a collisional orogen. Tectonophysics, 705. 10.1016/j.tecto.2017.03.007.

Moores, E. M., and F. J. Vine, 1971: The Troodos Massif, Cyprus and other ophiolites as oceanic crust: evaluation and implications. Philosophical Transactions of the Royal Society of London, A268, 443-466, http://doi.org/10.1098/rsta.1971.0006

Moores, E., 1970: Ultramafics and Orogeny, with Models of the US Cordillera and the Tethys. Nature, 228, 837–842, doi:10.1038/228837a0

Mouthereau, F., Lacombe, O., Deffontaines, B., Angelier, J., Brusset, S., 2001. Deformation history of the southwestern Taiwan foreland thrust belt: insights from tectono-sedimentary analyses and balanced cross-sections. Tectonophysics 333, 293-318.

Mouthereau, F., and Lacombe, O., 2006: Inversion of the Paleogene Chinese continentalmargin and thick-skinned deformation in the Western Foreland of Taiwan. Journal of Structural Geology, 28(11), 1977-1993. https://doi.org/10.1016/j.jsg.2006.08.007

Muecke, G.K., C. Pride, P. Sarkar, 1979: Rare earth element geochemistry of regional metamorphic rocks. Phys. Chem. Earth, 11, 449-464.

Namson, J., 1983. Structure of the Western Foothills Belt, Miaoli-Hsinchu Area, Taiwan: (II) Central Part. Petroleum Geology of Taiwan 19, 51-76.

Namson, J., 1984. Structure of the Western Foothills Belt, Miaoli-Hsinchu area, Taiwan: (III) Northern Part. Petroleum Geology of Taiwan 20, 35-52.

Naylor M., and H. D. Sinclair, 2007: Punctuated thrust deformation in the context of doubly vergent thrust wedges: Implications for the localization of uplift and exhumation. Geology, 35, 559-562. https://doi.org/10.1130/G23448A.1

Niu, Y., and M.J. O'Hara, 2009: MORB mantle hosts the missing Eu (Sr, Nb, Ta and Ti) in the continental crust: New perspectives on crustal growth, crust-mantle differentiation and chemical structure of oceanic upper mantle. Lithos, 112, 1-17.

O'Neill, C., D. Müller, and B. Steinberger, 2005: On the uncertainties in hot spot reconstructions and the significance of moving hot spot reference frames. Geochem. Geophys. Geosyst., 6, Q04003, doi:10.1029/2004GC000784.

Ota, T., and Y. Kaneko, 2010: Blueschists, eclogites, and subduction zone tectonics: Insights from a review of Late Miocene blueschists and eclogites, and related young high-pressure metamorphic rocks. Gondwana Research, 18, 167-188.

Page, B. M. and C. Y. Lan, 1983: The Kenting mélange and its record of tectonic events, Mem. Geol. Soc. China, 5, 227-248.

Page, B. M., J. Suppe, 1981: The Pliocene Lichi Mélange of Taiwan: its plate tectonic and olistostromal origin. Am J Sci, 281,193-227.

Pearce, J., 1982: Trace Element Characteristics of Lavas from Destructive Plate Boundaries. In Thorpe, R.S. (ed.), Andesites: Orogenic Andesites and Related Rocks. John Wiley and Sons, Chichester, 525-548.

Pelletier, B. and J. F. Stephan, 1986: Middle Miocene deduction and late Miocene beginning of collision registered in the Hengchun peninsula: Geodynamic implications for the evolution of Taiwan. Tectonophysics, 125, 133-160. https://doi.org/10.1016/0040-1951(86)90011-9

Pelletier, B., and H. N. Hu, 1984: New structural data along two transects across the southern half of the Central Range of Taiwan. Mem. Geol. Soc. China, 6, 1-19.

Plank, T., 2014: The chemical composition of subducting sediments, in Handbook of Geochemistry, pp. 607–629 Elsevier, Amsterdam, doi:10.1016/B978-0-08-095975-7.00319.3.

Prior, D. J., R. J. Knipe, M. P. Bates, N. T. Grant, R. D. Law, G. E. Lloyd, A. Welborn, S. M. Agar, K. H. Brodie, R. H. Maddock, E. H. Rutter, S. H. White, B. T.H., C. C. Ferguson, and J. Wheeler, 1987: Orientation of specimens: Essential data for all fields of geology. Geology, 15, 829-831.

Rau, R.-J. and F.T. Wu, 1885: Tomographic imaging of lithospheric structures under Taiwan. Earth Planet. Sci. Lett., 133, 517-532.

Reed, D. L., N. Lundberg, C. H. Liu, and B.-Y. Kuo, 1992: Structural relations along the margins of the offshore Taiwan accretionary wedge: Implications for accretion and crustal kinematics. Acta Geologica Taiwanica, 30, 105-122.

Resentini, A., Malusà, M. G. and Garzanti, E., 2020. Ongoing exhumation of the Taiwan orogenic wedge revealed by detrital apatite thermochronology: The impact of effective mineral fertility and zero-track grains. Earth and Planetary Science Letters, 544, 116374.

Richard, M., H. Bellon, R. Maury, E. Barrier, W.-S. Juang, 1986: Miocene to recent calc-alkalic volcanism in eastern Taiwan: K-Ar ages and petrography. Tectonophysics, 125, 87-102, https://doi.org/10.1016/0040-1951(86)90008-9.

Rudnick, R.L., and Gao, S., 2003: Composition of the continental crust. In: Rudnick, R.L. (Ed.), Treatiseon Geochemistry. The Crust, vol. 3. Elsevier, Amsterdam, pp. 1-64.

Sandmann, S., Nagel, T.J., Froitzheim, N., Ustaszewski, K., Münker, C., 2015. Late Miocene to Early Pliocene blueschist from Taiwan and its exhumation via forearc extraction. Terra Nova, 27, 285-291.

Schmid, S.M., Pfiffner, O.A:, Froitzheim, N., Schönborn, G., Kissling, E., 1996. Geophysical-geological transect and tectonic evolution of the Swiss-Italian Alps. Tectonics, 15, 1036-1064.

Seno, T., 1977: The instantaneous rotation vector of the Philippine Sea plate relative to the Eurasian plate. Tectonophysics, 42, 209-226. https://doi.org/10.1016/0040-1951(77)90168-8

Seton, M., R. D. Müller, S. Zahirovic, C. Gaina, T. Torsvik, G. Shephard, A. Talsma, M. Gurnis, M. Turner, S. Maus, and M. Chandler, 2012: Global Continental and Ocean Basin Reconstructions since 200 Ma. Earth-Science Reviews, 113, 212–270. https://doi.org/10.1016/j.earscirev.2012.03.002

Shao, W. Y., S. L. Chung, , W. S. Chen, , H. Y. Lee, and L. W. Xie, 2015: Old continental zircons from a young oceanic arc, eastern Taiwan: Implications for Luzon subduction initiation and Asian accretionary orogeny. Geology, 43, 479-482, doi:10.1130/g36499.1

Shen, C.-C., and H.-Y. Yang, 1996: A study on paragonite in the metamorphic terrane of Taiwan (in Chinese with English abstract), Bulletin of the Central Geological Survey Taiwan, 11, 85-104.

Shen, P., H.-T. Chu, and R.-C. Jeng, 1984: Electron microscopy observations of the plagiogranite from east Taiwan ophiolite. Memoir of the Geological Society of China, 6, 211-218.

Shervais, J. W., 1982: Ti - V plots and the petrogenesis of modern and ophiolitic lavas. Earth and Planetary Science Letters, 59, 101-118. https://doi.org/10.1016/0012-821X(82)90120-0

Shyu, J. B. H., Sieh, K., Chen, Y. G. and Liu, C. S., 2005. Neotectonic architecture of Taiwan and its implications for future large earthquakes. J. Geophys. Res., 110, B08402, doi:10.1029/2004JB003251.

Shyu, J. B. H., Y.M. Wu, C. H. Chang, and H.H. Huang, 2011: Tectonic erosion and the removal of forearc lithosphere during arc-continent collision: Evidence from recent earthquake sequences and tomography results in eastern Taiwan. Journal of Asian Earth Sciences, 42, 415-422. https://doi.org/10.1016/j.jseaes.2011.05.015

Sibuet, J. C., Deffontaines, B., Hsu, S. K., Thareau, N., Le Formal, J.-P., Liu, C. S., and the ACT party, 1999: Okinawa trough backarc basin: Early tectonic and magmatic evolution. Journal of Geophysical Research, 103, 30245-30267.

Sibuet, J. C., S. K. Hsu, X. Le Pichon, J. P. Le Formal, D. Reed, G. Moore, and C. S. Liu, 2002: East Asia platetectonics since 15 Ma: constraints from the Taiwan region. Tectonophysics, 344, 103-134. https://doi.org/10.1016/S0040-1951(01)00202-5

Sibuet, J. C., Y. C. Yeh, and C. S. Lee, 2016: Geodynamics of the South China Sea. Tectonophysics, 692, 98-119. https://doi.org/10.1016/j.tecto.2016.02.022

Sibuet, J.-C., Hsu, S.-K., 2004. How was Taiwan created? Tectonophysics 379, 159-181.

Simoes, M., Beyssac, O., Chen, Y.-G., 2012. Late Cenozoic metamorphism and mountain building in Taiwan: A review. Journal of Asian Earth Sciences 46, 92-119.

Simpson, C., and S. M. Schmid, 1983: An evaluation of criteria to deduce the sense of movement in sheared rocks. Geol. Soc. Am. Bull., 94, 1281-1288.

Stanley, R. S., Hill, L. B., Chang, H. C. and Hu, H. N., 1981. A transect through the metamorphic core of the central mountains, southern Taiwan, Mem. Geol. Soc. China, 4, 443–473.

Stern, R.J., 2005. Evidence from ophiolites, blueschists, and ultrahigh-pressure metamorphic terranes that the modern episode of subduction tectonics began in Neoproterozoic time. Geology, 33, 557-560.

Spandler, C., Hermann, J., Arculus, R. and Mavrogenes J., 2003: Redistribution of trace elements during prograde metamorphism from lawsonite blueschist to eclogite facies; implications for deep subduction-zone processes. Contrib Mineral Petrol, 146, 205-222. https://doi.org/10.1007/s00410-003-0495-5

Spry, A., 1969: Metamorphic textures. 358 pp., Pergamon, Oxford.

Sun, C. H., A.D. Smith and C.H. Chen, 1998: Nd-Sr Isotopic and Geochemical Evidence on the Protoliths of Exotic Blocks in the Juisui Area, Yuli Belt, Taiwan, International Geology Review, 40, 12, 1076-1087, DOI: 10.1080/00206819809465255.

Sun, S. S., and McDonough, W. F., 1989: Chemical and isotopic systematic of oceanic basalts: Implications for mantle composition and processed. Magmatism in Ocean Basins. Geological Society of London Special Publication, 42, 313–345. https://doi.org/10.1144/GSL. SP.1989.042.01.19

Suppe, J., 1980. A retrodeformable cross section of northern Taiwan. Proceedings of the Geological Society of China 23, 46-55.

Suppe, J., 1981. Mechanics of mountain building and metamorphism in Taiwan. Memoir of the Geological Society of China 4, 67-89.

Suppe, J., 1984a, Kinematics of arc-continent collision, flipping of subduction, and back-arc spreading near Taiwan. Geological Society of China Memoir, 6, 131-146.

Suppe, J., 1984b. Seismic interpretation of the compressively reactivated normal fault near Hsinchu, Western Taiwan. Petroleum Geology of Taiwan 20, 85-96.

Suppe, J., 1986. Reactivated normal-faults in the Western Taiwan fold-and-thrust belt. Memoir of the Geological Society of China 7, 187-200.

Suppe, J., and J. G. Liou, 1979: Tectonics of the Lichi Mélange and East Taiwan Ophiolite. Memoir of the Geological Society of China, 3, 147-153.

Suppe, J., C.-Y. Lan, E. M. Hendel, and J. G. Liou, 1977: Paleogeographic interpretation of red shales within the East Taiwan Ophiolite, Petroleum Geology of Taiwan, 14, 109-120.

Suppe, J., Namson, J., 1979: Fault-bend origin of frontal folds of the Western Taiwan fold-and-thrust belt. Petroleum Geology of Taiwan 16, 1-18.

Syu, B.Y., 2009: Preliminary discussion on X-ray diffraction pattern and Raman spectrum of carbonaceous materials in metamorphic complexes in Juisui and WanJun, Taiwan. Master dissertation, National Taiwan Normal University, 59pp.

Taylor, B. and D. E. Hayes, 1983: Origin and history of South China Sea Basin, In D. E. Hayes (Ed.), The Tectonic and Geologic Evolution of Southeast Asian Seas and Islands: Part 2, Am. Geophys. Union., Washington, DC, 23-56, doi:10.1029/gm027p0023.

Teng, L.S., 1979: Petrographical study of the Neogene sandstones of the Coastal Range, eastern Taiwan. Acta Geol. Taiwan. 20, 129-156.

Teng, L.S., 1990: Geotectonic evolution of late Cenozoic arc-continent collision in Taiwan. Tectonophysics, 183, 57-76.

Teng, L.S., Wang, Y., Tang, C. H., Huang, C. Y., Huang, T. C., Yu, M. S. and Ke, A., 1991: Tectonic aspects of the Paleogene depositional basin of northern Taiwan. Proc. Geol. Soc. China, 34, 313-336.

Teng, L.S., Lin, A.T., 2004: Cenozoic tectonics of the China continental margin: insights from Taiwan. Geological Society, London, Special Publication 226, 313-332.

Teng, L.S., Wang, Y., Tang, C.-H., Huang, C.-Y., Huang, T.-C., Yu, M.-S., Ke, A., 1991: Tectonic aspects of the Paleogene depositional basin of northern Taiwan. Proceedings of the Geological Society of China 34, 313-336.

Tian, Z. - X., Y. Yan, C. - Y. Huang, X.-C. Zhang, H. - Q. Liu, M. - M. Yu, D. Yao, Y. Dilek, 2019: Geochemistry and geochronology of the accreted mafic rocks from the Hengchun Peninsula, southern Taiwan: Origin and tectonic implications. Journal of Geophysical Research: Solid Earth, 124, 2469- 2491. https://doi.org/10.1029/2018JB016562

Tillman, K.S., Byrne, T., Lu, C.-Y., 1992: Pre-collisional extensional structures from the Central Range, Taiwan: Implications for the kinematic evolution of the South China margin. Acta Geologica Taiwanica 30, 11-26.

Tsai, C.-H., Iizuka, Y., Ernst, W.G., 2013: Diverse mineral compositions, textures, and metamorphic P–T conditions of the glaucophane-bearing rocks in the Tamayen mélange, Yuli belt, eastern Taiwan. Journal of Asian Earth Sciences 63, 218-233.

Tsai, Y.-B., Ten, T.L., Chiu, J.M., Liu, H.L., 1977: Tectonic implications of the seismicity in the Taiwan region. Memoir of the Geological Society of China 2, 13-41.

Tsao, S., E. Law, H. C. Ho, Y. H. Lee, W. T. Jiang, and C. H. Chen, 1996: The geological significances of K–Ar ages of metapelites from the Central Range, Taiwan. Bulletin of the Central Geological Survey (Taiwan), 11, 37-84.

Ustaszewski, K., Wu, Y.-M., Suppe, J., Huang, H.-H., Chang, C.-H., Carena, S., 2012: Crust-mantle boundaries in the Taiwan-Luzon arc-continent collision system determined from local earthquake tomography and 1D models: Implications for the mode of subduction polarity reversal. Tectonophysics 578, 31-49.

von Hagke, C., Philippon, M., Avouac, J.-P., Gurnis, M., 2016: Origin and time evolution of subduction polarity reversal from plate kinematics of Southeast Asia. Geology 44, 659-662.

Wan, K., S. Xia, J. Cao, J. Sun, and H. Xu, 2017: Deep seismic structure of the northeastern South China Sea: Origin of a high-velocity layer in the lower crust, J. Geophys. Res. Solid Earth, 122, 2831–2858, doi:10.1002/2016JB013481.

Wang, Y., 1992: The geological map of Taiwan scale1:50,000, Yuli sheet. Central Geological Survey, MOEA.

Wang, Y., C.H. Tsai, L. Zhou, Y. Qiu, and G. Sun, 2017: Reassessment of the Mesozoic metasedimentary rocks and tectonic setting of Taiwan and the adjacent continental margin of eastern Asia. Geological Magazine, 154, 1127-1154.

Wang, Z., Zhao, D., Wang, J., and Kao, H., 2006: Tomographic evidence for the Eurasian lithosphere subducting beneath south Taiwan. Geophysical Research Letters, 33, L18306, doi: 18310.11029/12006GL027166.

Watkins, K. P., 1983: Petrogenesis of Dalradian albite porphyroblast schists. Journal of the Geological Society, 140, 601-618. doi:10.1144/gsjgs.140.4.0601

Weill, D. F., and M. J. Drake, 1973: Europium Anomaly in Plagioclase Feldspar: Experimental Results and Semiquantitative Model. Science, 180, 1059-1060. doi:10.1126/science.180.4090.1059

Whitney, D. L., and B. W. Evans, 2010: Abbreviations for names of rock-forming minerals. American mineralogist, 95, 185-187. https://doi.org/10.2138/am.2010.3371

Willett, S., Fisher, D.M., Fuller, C.W., Yeh, E.-C., Lu, C.-Y., 2003. Erosion rates and orogenic-wedge kinematics in Taiwan inferred from fission-track thermochronometry. Geology 31, 945-948.

Wintsch, R.P., Yang, H.-J., Li, X.-H., Tung, K.-A., 2011: Geochronologic evidence for a cold arc–continent collision: The Taiwan orogeny. Lithos 125, 236-248.

Wopenka, B. and Pasteris, J.D., 1993: Structural characterization of kerogens to granulitefacies graphite: Applicability of Raman microprobe spectroscopy. American Mineralogist, 78,533–577.

Wu, Y.-M., C.-H. Chang, L. Zhao, T.-L. Teng, and M. Nakamura, 2008a: A Comprehensive Relocation of Earthquakes in Taiwan from 1991 to 2005, Bulletin of the Seismological Society of America, 98(3), 1471-1481.

Wu, Y.-M., L. Zhao, C.-H. Chang, and Y.-J. Hsu, 2008b: Focal mechanism determination in Taiwan by genetic algorithm, Bulletin of the Seismological Society of America, 98(2), 651-661.

Wu, J., Suppe, J., Lu, R., and Kanda, R., 2016: Philippine Sea and East Asian plate tectonics since 52 Ma constrained by new subducted slab reconstruction methods: Journal of Geophysical Research. Solid Earth, 121, 4670-4741.

Wu, J., and J. Suppe, 2018: Proto-South China Sea Plate Tectonics Using Subducted Slab Constraints from Tomography. Journal of Earth Science, 29, 1304-1318. doi:10.1007/s12583-017-0813-x

Yang, C.-N., and Y. Wang, 1985: Petrotectonic study on the Yuli belt of the Tananao Schist in the Juisui area, eastern Taiwan. Acta Geol. Taiwanica, 23, 153-180.

Yang, H.-Y., and S.-J. Lin, 1982: The porphyroblastic garnet and the garnet-hornblende-epidote-paragonite schist from Tamayenshan, Juisui, Eastern Taiwan, Proceedings of the Geological Society of China, 25, 82-87.

Yang, K.-M., Huang, S.-T., Wu, J.-C., Ting, H.-H., Mei, W.-W., 2006: Review and New Insights on Foreland Tectonics in Western Taiwan. International Geology Review, Vol. 48, 910–941.

Yang, K.-M., Huang, S.-T., Wu, J.-C., Ting, H.-H., Mei, W.-W., Lee, M., Hsu, H.H., Lee, C.J., 2007. 3D Geometry of the Chelungpu Thrust system in Central Taiwan: Its implications for Active Tectonics. Terrestrial, Atmospheric and Oceanic Sciences 18, 143-181.

Yang, K.-M., Rau, R.-J., Chang, H.-Y., Hseih, C.-Y., Ting, H.-H., Huang, S.-T., Wu, J-C, and Tang, Y-J, 2016: The role of basement-involved normal faults in the recent tectonics of western Taiwan. Geological Magazine, 153, 1166–1191. https://doi.org/10.1017/S0016756816000637

Yang, T. F., J. l. Tien, C. H. Chen, T. Lee, and R. S. Punongbayan, 1995: Fission-track dating of volcanics in the northern part of the Taiwan-Luzon Arc: eruption ages and evidence for crustal contamination. Journal of Southeast Asian Earth Sciences, 11, 81-93. https://doi.org/10.1016/0743-9547(94)00041-C

Yeh, E. C., 2004: Structural evolution of slates belts: examples from Tawain and eastern Pennsylvania. The Pennsylvania State University, 207pp.

Yeh, Y. C., J. C. Sibuet, S. K. Hsu, and C. S. Liu, 2012: Tectonic evolution of the Northeastern South China Sea from seismic interpretation. Journal of Geophysical Research, 115, 307–326, doi:10.1029/2009jb006354

Yen, T. P., 1959: The minerals of the Tananao Schist of Taiwan. Bull. Geol. Surv. Taiwan, 11, 1-53.

Yen, T. P., 1963. The metamorphic belts within the Tananao schist terrane of Taiwan. Proc. Geol. Soc. China, 6, 72–74.

Yen, T. P., 1966: Glaucophane schists of Taiwan. Proceedings of the Geological Society of China, 9, 70-83.

Yi, T. C., Z. Y. Chen, and C.W. Lin, 2012: The geological map of Taiwan scale 1:50,000, Guangfu sheet. Central Geological Survey, MOEA.

Yu, H. S. and Y. W. Chou, 2001: Characteristics and development of the flexural forebulge and basal unconformity of Western Taiwan Foreland Basin. Tectonophysics, 333, 277-291. https://doi.org/10.1016/S0040-1951(00)00279-1

Yu, N.T., Teng, L.S., Chen, W.S., Yue, L.F. and Chen, M.M., 2013: Early post-rift sequence stratigraphy of a Mid-Tertiary rift basin in Taiwan: insights into a siliciclastic fill-up wedge. Sediment. Geol., 286–287, 39–57.

Yu, S. B., H. Y. Chen, and L. C. Kuo, 1997: Velocity field of GPS stations in the Taiwan area. Tectonophysics, 274, 41-59. https://doi.org/10.1016/S0040 - 1951(96)00297 - 1

Yue, L.-F., Suppe, J., Hung, J.-H., 2005: Structural geology of a classic thrust belt earthquake: the 1999 Chi-Chi earthquake Taiwan (Mw=7.6). Journal of Structural Geology 27, 2058-2083.

Yui, T. F., Okamoto, K., Usuki, T., Lan, C. Y., Chu, H. T. and Liou, J. G., 2009: Late Triassic–Late Cretaceous accretion/subduction in the Taiwan region along the eastern margin of South China – evidence from zircon SHRIMP dating. International Geology Review, 51, 304-328, DOI: 10.1080/00206810802636369

Yui, T. F., T. Usuki, C. Y. Chen, A. Ishida, Y. Sano, K. Suga, Y. Lizuka, and C. T. Chen, 2014: Dating thin zircon rims by NanoSIMS: the Fengtien nephrite (Taiwan) is the youngest jade on Earth. International Geology Review, 56, 1932-1944, doi:10.1080/00206814.2014.972994

Yui, T.F. and C.H. Lo, 1989: High-pressure metamorphosed ophiolitic rocks from the Wanjung area, Taiwan. Proc. Geol. Soc. China, 32, 47-62.

Yui, T.F., Huang, E. and Xu, J., 1996: Raman spectrum of carbonaceous material: a possible metamorphic grade indicator for low-grade metamorphic rocks. J. metamorphic Geol., 14, 115–124.

Yui, T.F., K. Maki, C. Y. Lan, T. Hirata, H. T. Chu, Y. Kon, T. D. Yokoyama, B. M. Jahn, and W. G. Ernst, 2012: Detrital zircons from the Tananao metamorphic complex of Taiwan: Implications for sediment provenance and Mesozoic tectonics. Tectonophysics, 541-543, 31-42. https://doi.org/10.1016/j.tecto.2012.03.013.

Zhang, Y., Tsai, C.-T., Froitzheim, N., Ustaszewski, K., 2020: The Yuli Belt in Taiwan: part of the suture zone separating Eurasian and Philippine Sea plates. Terr. Atmos. Ocean. Sci., in press. DOI: 10.3319/TAO.2020.06.28.01

Appendix A (Chapter 2)

Figure S1:

Deep crustal interpretation on the cross section across Central Cross-island Highway of Taiwan (A-A') based on the Vp tomography (Wu Y.-M. et al., 2008a). Crust-mantle interfaces constrained from a 3D-model employing seismological data after Ustaszewski et al. (2012). See Fig. 2-2 for section trace A-A'.

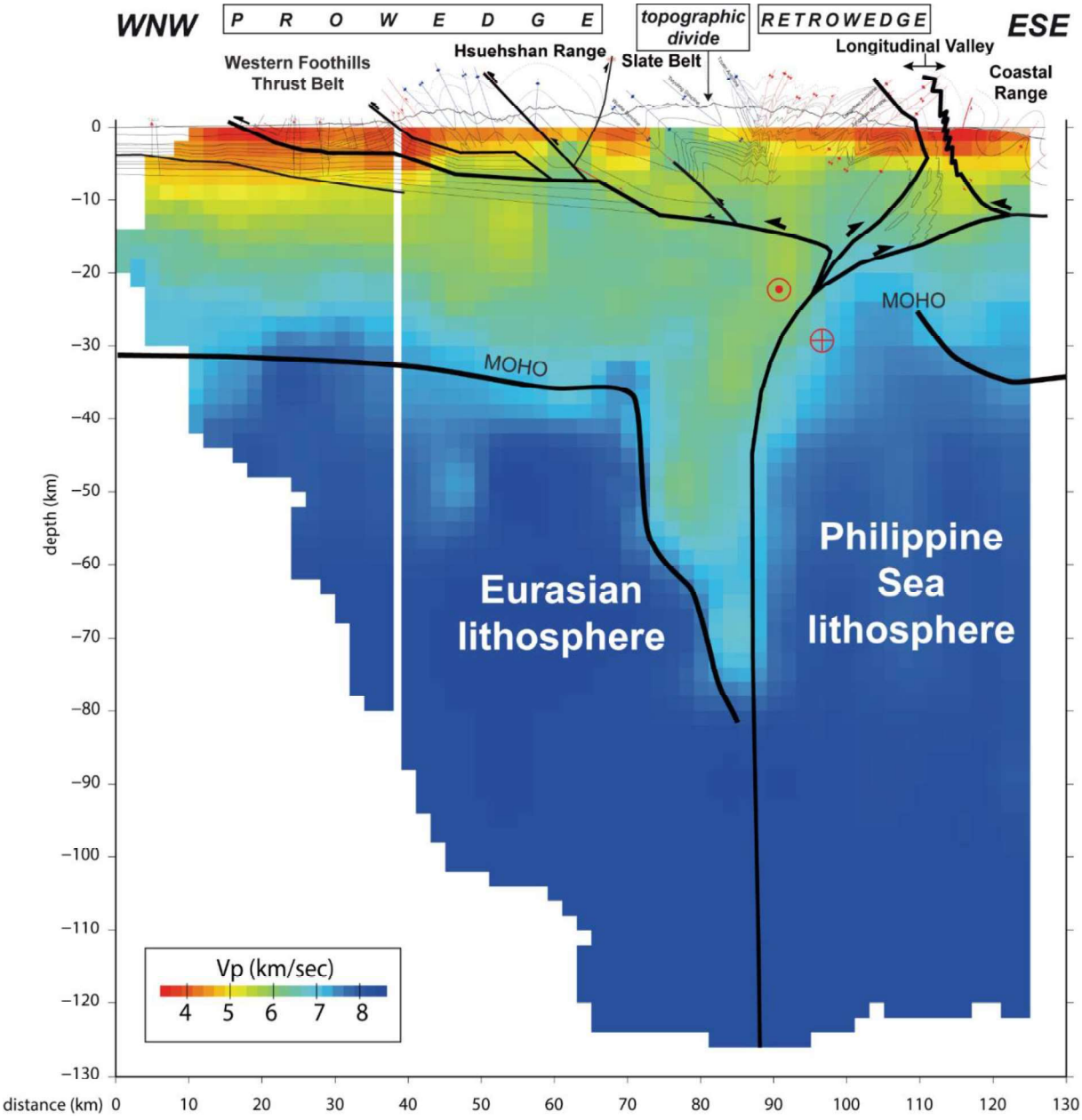

Figure S2:

Deep crustal interpretation on the cross section across central Taiwan (B-B') based on the Vp tomography (Wu Y.-M. et al., 2008a). Crust-mantle interfaces constrained from a 3D-model employing seismological data after Ustaszewski et al. (2012). See Fig. 2-2 for section trace B-B'.

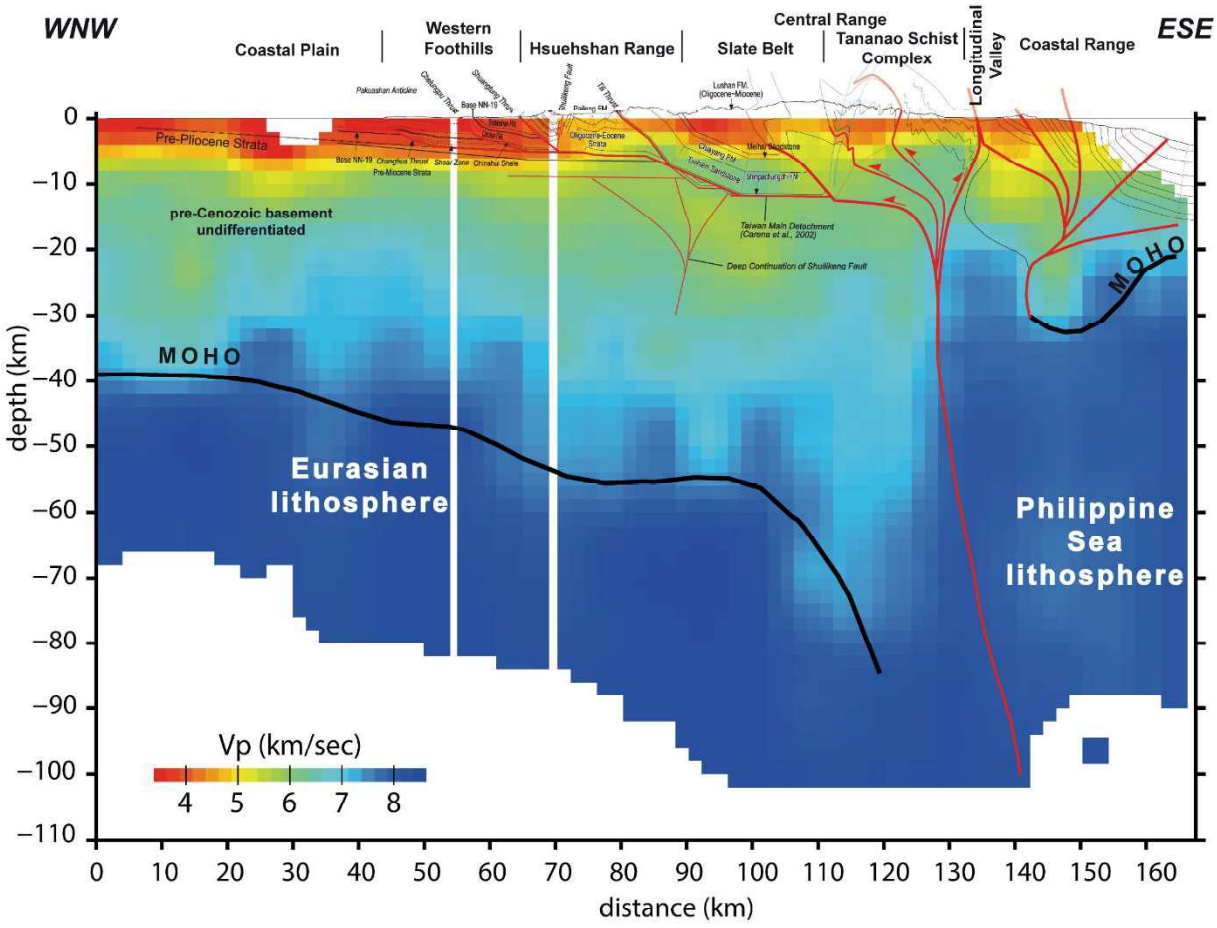

Figure S3:

Deep crustal interpretation on the cross section cross Southern Cross-island Highway of Taiwan (C-C') based on the Vp tomography (Wu Y.-M. et al., 2008a). Crust-mantle interfaces constrained from a 3D-model employing seismological data after Ustaszewski et al. (2012). See Fig. 2-2 for section trace C-C'.

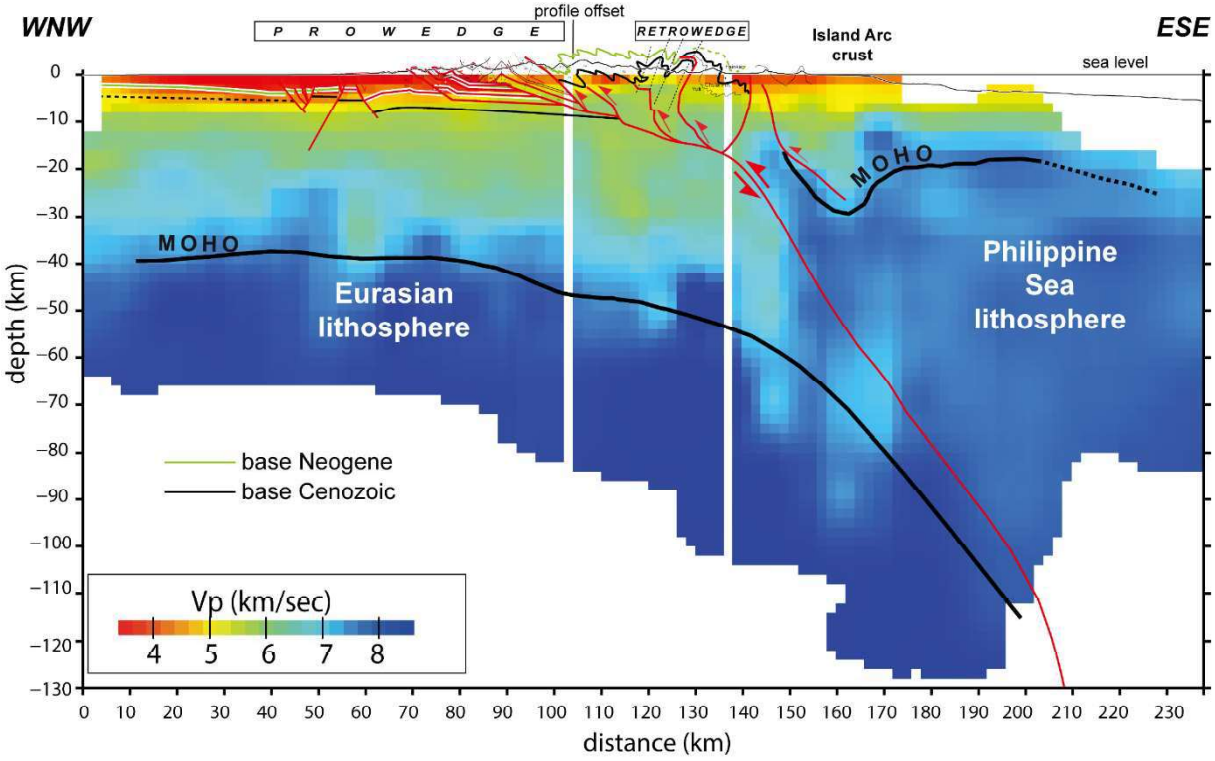

Figure S4:

Correlation of stratigraphic divisions of Taiwan (modified after Yen 1963; Chi et al., 1981; Chang and Chi, 1983). The stratigraphic names, facies, and regional unconformities have been correlated from north to south. Fm.: formation; Ss.: sandstone; Sh.: shale; Red dots: volcanic stratigraphic sequence.

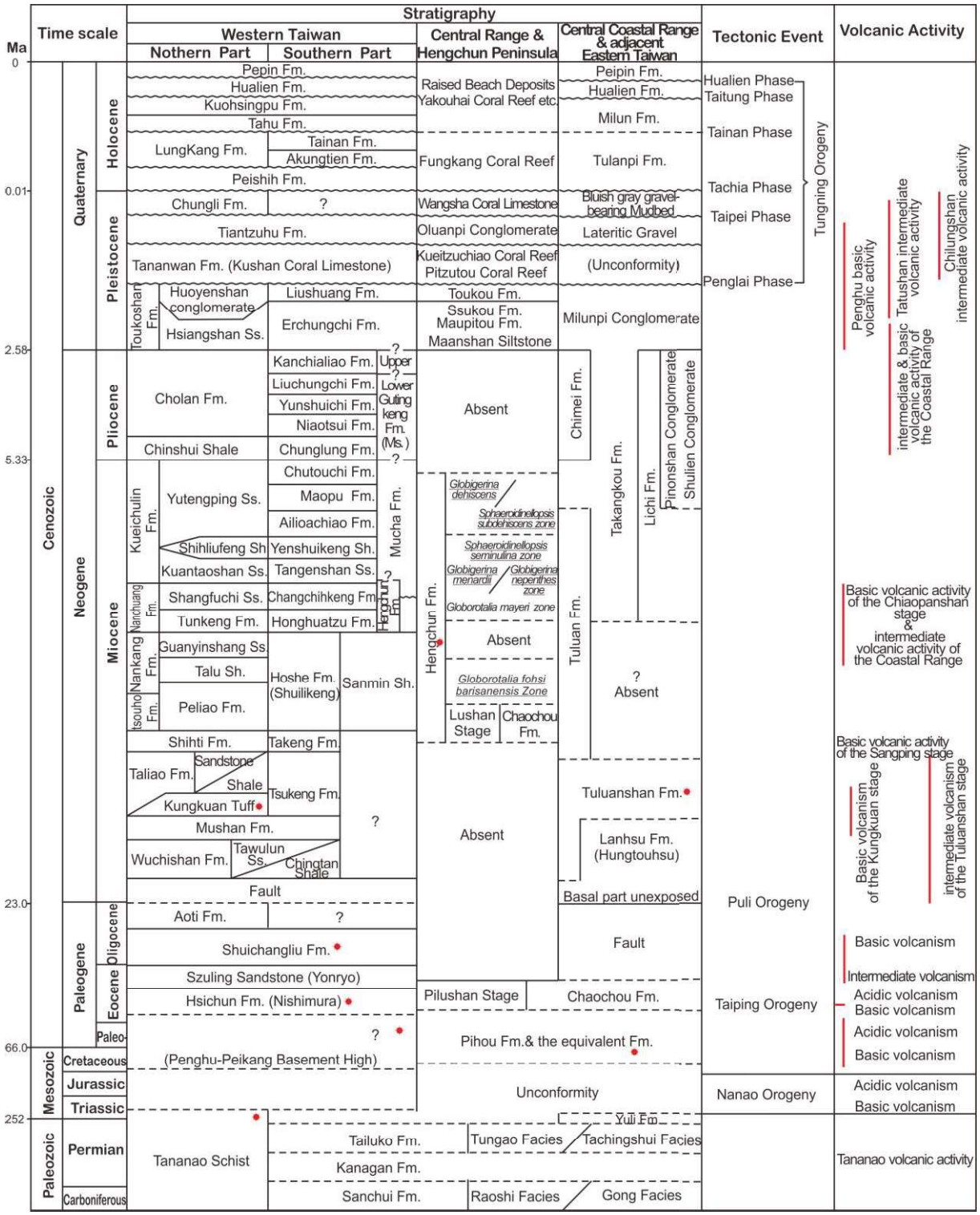

Appendix B (Chapter 3)

Figure S1:

P-T diagram (simplified after Maruyama et al. 1986) showing calculated metamorphic conditions and P-T-t paths suggested for high-pressure rocks in the Yuli belt with various metamorphic parageneses, as well as for a chlorite-mica schist from the metasedimentary unit (bold path-8). Type-I (Amp + Qz + Ep + Gar+ Chl + Rt/Ttn; Type-II: Pg + Amp + Qz + Ep + Gar + Chl + Ttn + Bt + Mag), Type-III (Amp + Qz + Ab + Ep + Gar + Rt + Hem + Ttn), and Type-IV (Amp +Ep + Pg+ Qz + Ab) are from Tsai et al. (2013). Mineral abbreviations follow those of Whitney and Evans (2010). Other abbreviations are Zeo, zeolite facies, PP, prehnite-pumpellyite facies; PA, pumpellyite–actinolite facies; PrA, prehnite-actinolite facies; GS, greenschist facies; EA, epidote-amphibolite facies; AM, amphibolite facies; BS, blueschist facies; AEC, amphibole eclogite facies. Sources: (1) Baziotis et al. 2017; (2) Tsai et al. 2013; (3) Sandmann et al. 2015; (4) Beyssac et al. 2008; (5) Lan et al. 1996; (6) Lo 2018; (7) Chiang 2003; (8) Conand et al. 2020.

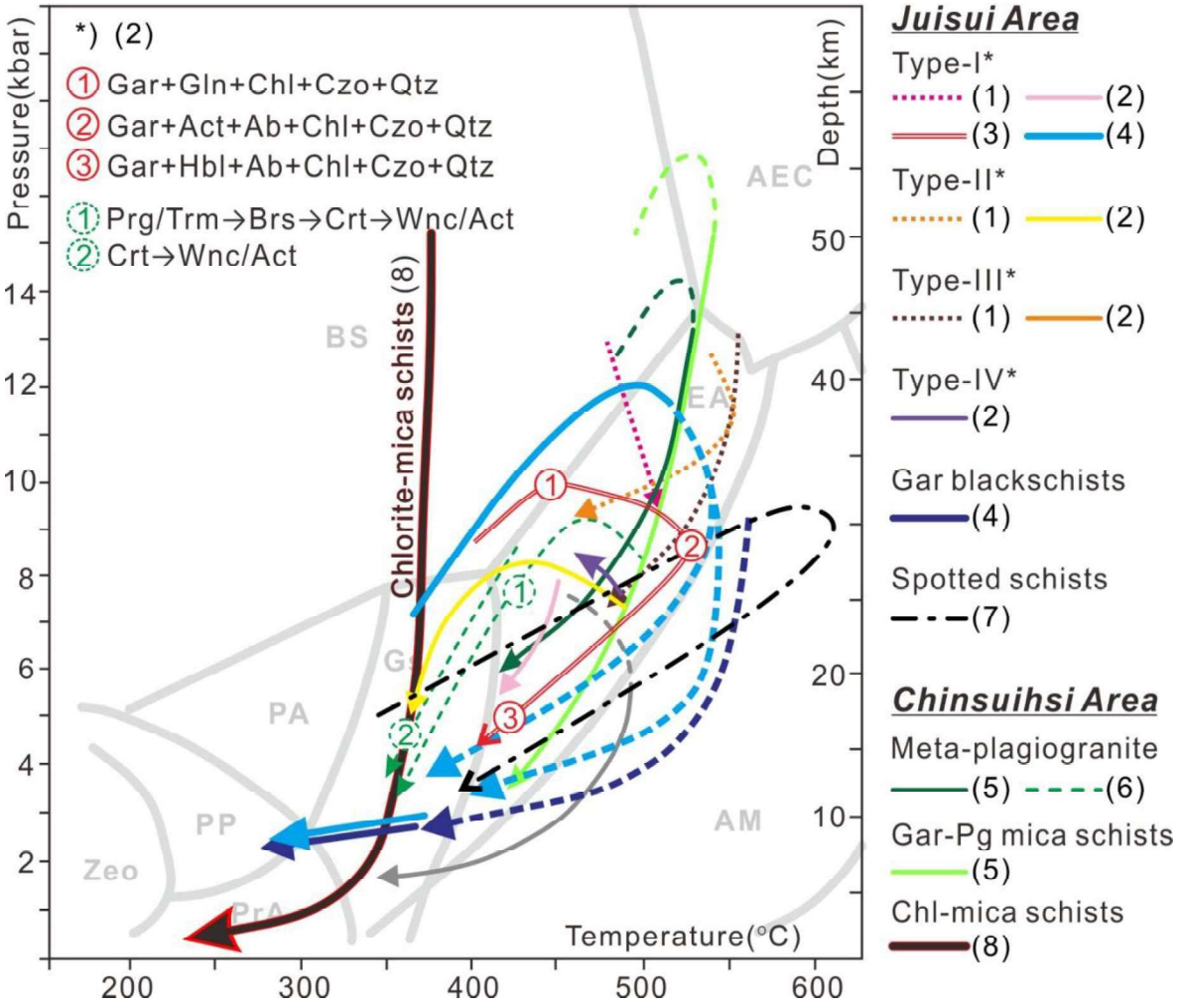

Figure S2:

The samples localities of the whole-rock geochemistry analysis.

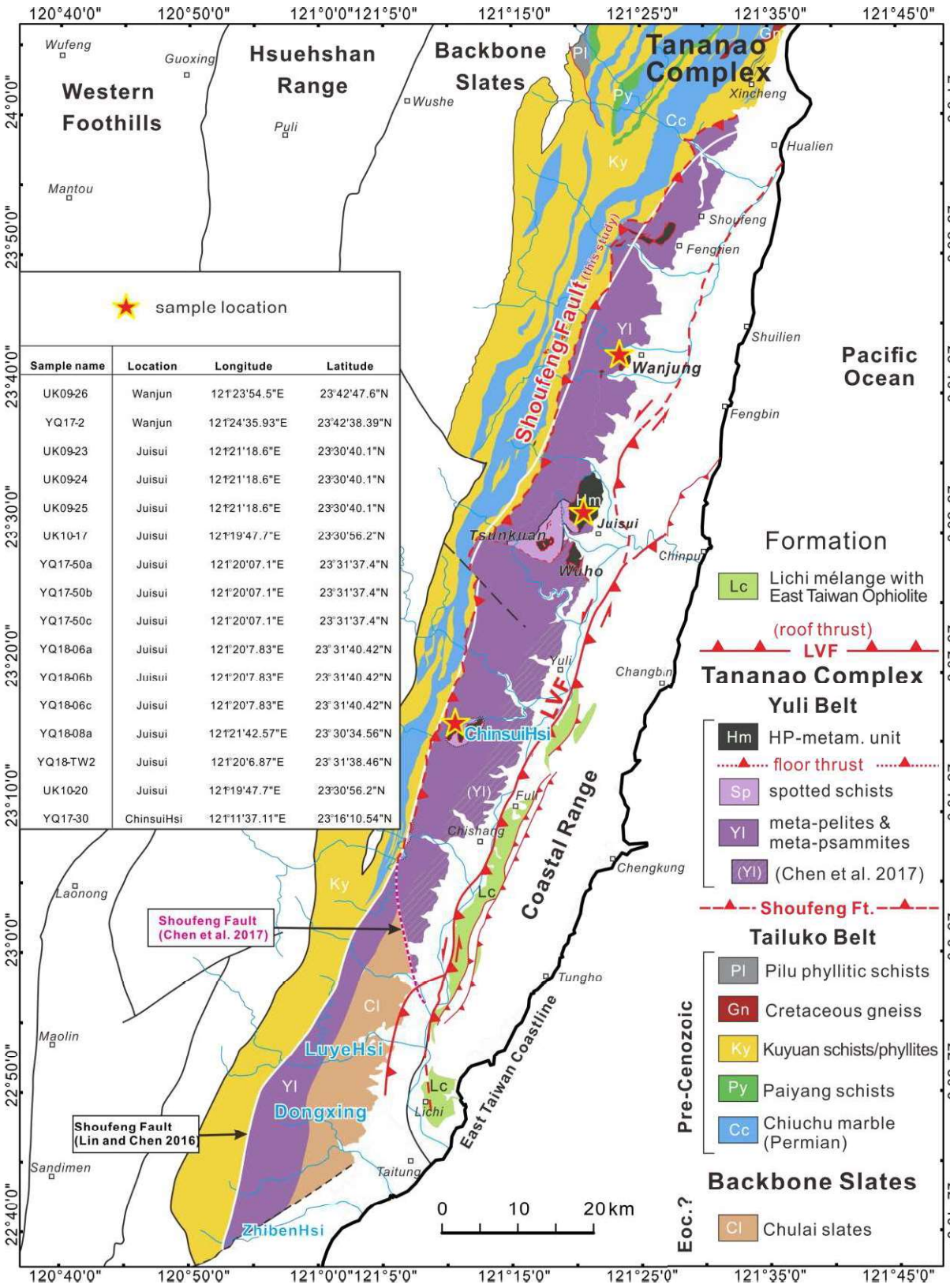

Table S1:

Summary of deformation phases of the Yuli Belt metasediments from previous studies

Reference	Area	Method	Deformation phases & age (if any)
Stanley et al. 1981	Southern Cross island highway	Schistosity and folding crosscutting relationships; Lithological correlations	**S1** = Cryptic **S2** = Penetrative axial surface **F2**= West vergent folds and faults **S3** = NE strike; W dipping; Crenulation cleavage **F3** = East verging; hinge plunge NE **S4** = NE strike; NW dip; **F4** = minor folds deforming **F5 & F6** = kink folds; variable orientation; flexing of dominant schistosity
Pelletier and Hu, 1984	Southern Cross Island Highway; East & South Taiwan	Structural analysis	**F0** = southward directed slumps **D1** = EW to NW-SE compression; **S1**=Axial planar **T1** = west vergent thrust **F2** = kink-folds verging to the East, backfolding **S2** = Crenulation cleavage **F3** = North verging, E-W axis
Hu and Tsan 1984	Southeastern Taiwan, Central Range	Structural and sedimentological analysis	**F0** = NS (EW depositional folds) **S2** = NWW-SEE (NS-overturned tight folds & cleavage) **D3** = bending of S2 cleavage
Faure et al 1991	Central & Southern cross island highway	Microstructural analysis & synthesis of previous works	**S1** = fracture cleavage (in the W. slate belt) **F1** = overturned to the west (in slate belt) **L1**= non-coaxial, top to the NW shear sense **D2** =3.5 Ma (Pelletier and Stephan, 1986) **F2** = overturned to the E., axis trend 100N (back folding); **S2** =axial planar crenulation **F3** = axis S dipping **D4** = Normal faulting
Clark et al. 1992	Northern & Southern Cross Island Highway	Microstructural analysis (syntectonic fibrous growth orientation)	**D1**; **D2**; **D3**=**D2**; **D4** of Stanley et al., 1981 **S1** = dipping ~40SE; **L1** = updip; Clockwise rotation of elements + asymmetric folds and boudins → non-coaxial (simple shear) **S2** = crenulation cleavage with fanning structure **F2** = west vergent folds & axis dipping ~35° to the NE **L2** = indicate fold-axis parallel extension & left-lateral shear **Normal Faults**= σ 3 plunge towards the NE, parallel to S2 **S3** = crenulation cleavage dipping NW, locally transposing S2 (in the east)
Fisher 1999 & Fisher et al. 2002	Easternmost Backbone Slates	Structural and microstructural analysis	**S2** = local crenulation, moderately W dipping **F2** = axis gentle NE plunging. **L2** = moderately NE dipping **Normal Faults**= late W-dipping
Yeh 2004	Eastern Central Range	Structural and microstructural analysis	**S0** = 37/096, overturned **S1** = 31/075 strong pervasive slaty cleavage **S2** = 36/308 pervasive foliation **F2** = kink-folds verging to the East; backfolding **S3** = 27/215, slaty cleavage **F3** = kink-folds verging to the North; fold axis 21/025 **S4** = weak crenulation cleavage **Normal Faults**= 45/045, 45/205, top-to-NE/SW shear
Ho and Lo 2015	Shoufeng Hsi (Wanjung area)	Structural and microstructural analysis	**S1** = commonly destroyed; in the microlithon **S2** = moderately NW dipping **F2** = east-vergence isoclinal folding **S3** = sub-horizontal axial plane cleavage **F3** = recumbent folds; fold hinge plunge NW
Ho 2015	Southern Cross Island Highway	Structural and microstructural analysis	**S1**; **S2**; **S3** of Ho and Lo 2005 **Normal Faults**
Mondro et al. 2017	Eastern Central Range (Eocene slates)	Syntectonic fibrous growth orientation	**S2** of Fisher et al. 2002 bulk coaxial strain and lateral extrusion effects

Appendix C (Chapter 4)

Table S1: RSCM data of the sixteen samples with point measurements. All peak metamorphic temperatures (T) were obtained using the calibration of Beyssac et al. (2002).

int: band intensity; FWHM: full width half maximum; R1= (D1/G) (peak height ratio); R2=D1/(G+D1+D2) area

Sample 1: YQ17-3

ID	D1_int	D1_FWHM	D1_area	G_int	G_FWHM	G_area	D2_int	D2_FWHM	D2_area	R1	R2	T
1	999	42	61508	3007	22	101733	291	15	6726	0.33	0.36	476
2	447	46	31407	1610	21	51961	145	14	3093	0.28	0.36	476
3	619	45	37532	2169	22	70960	219	14	3249	0.29	0.34	488
4	752	44	45229	2467	21	79076	221	14	3847	0.30	0.35	480
5	874	44	52360	2997	21	95259	288	12	4661	0.29	0.34	485
6	897	45	55343	2751	24	99746	259	15	4143	0.33	0.35	483
7	812	44	49054	3145	21	101260	261	12	5027	0.26	0.32	497
8	774	45	46091	2776	21	89314	227	16	4568	0.28	0.33	491
9	513	46	30879	1695	22	56519	174	15	3772	0.30	0.34	487
10	516	43	33966	1884	20	57501	207	26	5671	0.27	0.35	482
11	488	44	29478	1811	20	56430	191	11	2769	0.27	0.33	490
12	436	45	28266	1638	21	52855	177	11	2887	0.27	0.34	488
13	681	45	40256	2295	21	72372	227	13	3607	0.30	0.35	483
14	648	44	37493	2484	20	77092	207	13	2940	0.26	0.32	496
15	675	46	44216	2420	22	80765	223	15	5070	0.28	0.34	486
16	681	47	42915	2323	21	74090	200	14	3785	0.29	0.36	479
17	510	45	33531	1730	21	56413	156	12	2665	0.29	0.36	476
18	600	45	39388	1508	23	52335	158	16	2959	0.40	0.42	452
19	579	43	34966	1991	20	60285	182	15	4281	0.29	0.35	481
20	492	51	38711	1763	22	59652	141	25	5444	0.28	0.37	471
21	548	44	37581	1635	22	53979	172	19	3995	0.34	0.39	462
22	542	49	39445	1883	21	60793	163	20	3622	0.29	0.38	468
23	445	47	32092	1351	22	46477	125	14	2500	0.33	0.40	461
24	492	48	35606	1731	21	55081	195	13	3530	0.28	0.38	469
25	487	46	34555	2009	20	61520	214	12	3477	0.24	0.35	483
26	690	49	52237	2471	21	80644	246	16	5282	0.28	0.38	469
27	913	50	68404	3630	23	128812	279	15	5042	0.25	0.34	487
28	884	59	80209	2726	24	103112	287	32	14163	0.32	0.41	456
29	623	53	50540	1603	24	59429	282	22	9819	0.39	0.42	449
30	457	55	38732	1668	23	60482	135	14	2877	0.27	0.38	468
31	345	48	24337	2016	21	65847	101	11	1227	0.17	0.27	520
32	569	50	44120	1893	24	69669	155	14	3157	0.30	0.38	469
33	386	47	28181	1440	21	47171	106	27	4510	0.27	0.35	480
34	606	44	40877	2133	22	69929	187	21	4548	0.28	0.35	480
35	595	47	41332	2231	22	76287	176	17	3384	0.27	0.34	486
36	748	48	46693	3038	23	104628	189	18	3585	0.25	0.30	504
37	937	44	56824	3007	22	97657	282	16	5553	0.31	0.36	479
38	736	40	42594	2022	21	64741	215	14	3239	0.36	0.39	466
39	440	48	32549	1814	23	64151	164	20	5205	0.24	0.32	496
40	719	42	42613	2038	22	68614	200	21	4512	0.35	0.37	473
41	590	47	42863	2118	21	68912	255	13	5123	0.28	0.37	474
42	633	47	45316	1349	25	52259	217	31	10523	0.47	0.42	450
43	409	46	28866	2518	21	82204	137	16	2299	0.16	0.25	525
44	449	54	36928	1252	23	43825	112	13	1598	0.36	0.45	437
45	759	46	45455	2700	22	89962	271	16	5818	0.28	0.32	495
46	759	45	46307	2589	21	83421	233	12	3522	0.29	0.35	483
47	519	44	32727	1767	21	57419	160	13	2595	0.29	0.35	480
48	385	56	33251	1092	22	37904	109	17	2946	0.35	0.45	437
49	433	52	34351	1410	21	46588	125	14	2769	0.31	0.41	454
50	718	49	54112	2446	21	78512	209	14	4680	0.29	0.39	462
51	603	47	43723	1926	22	60844	175	21	5636	0.31	0.40	460
52	342	44	21091	1402	20	42910	116	20	2470	0.24	0.32	497
53	412	47	30123	2037	22	68182	148	11	2506	0.20	0.30	505
54	641	56	54696	2003	22	68496	251	15	5828	0.32	0.42	448
55	825	53	67046	2695	22	92114	271	14	5942	0.31	0.41	456
56	734	46	47340	3501	23	120776	169	19	3590	0.21	0.28	516
57	752	45	45794	2847	21	92583	246	13	3452	0.26	0.32	494
58	723	51	56150	2166	23	75986	187	22	6308	0.33	0.41	456
59	586	48	40928	2088	22	71213	170	14	2565	0.28	0.36	479

60	447	43	27286	1672	19	50083	126	16	2889	0.27	0.34	486
61	1212	62	114596	3781	22	131232	304	19	8795	0.32	0.45	436
62	386	46	23182	1488	21	48120	90	18	1719	0.26	0.32	497
63	665	47	47197	2156	22	72413	205	18	5339	0.31	0.38	469
64	348	43	23079	1546	21	50827	142	12	2509	0.23	0.30	504
65	433	60	40065	2119	22	71643	133	32	6543	0.20	0.34	487
66	465	45	30073	1735	20	54077	155	16	2590	0.27	0.35	483
67	565	46	37123	1964	21	65446	156	15	2510	0.29	0.35	480
68	756	58	67304	2324	22	79317	240	17	6165	0.33	0.44	441
69	639	44	42651	2403	20	70492	237	28	6941	0.27	0.36	479
70	741	46	47256	2747	21	87849	226	14	3990	0.27	0.34	486
71	810	52	64880	1776	23	64569	223	15	4984	0.46	0.48	421
72	870	89	117454	1910	26	78214	260	27	10712	0.46	0.57	382
73	1044	44	63484	3952	21	127022	368	15	7698	0.26	0.32	495
74	676	44	45469	2475	21	79466	262	13	4379	0.27	0.35	481
75	760	47	48841	3088	21	98808	248	17	5375	0.25	0.32	496
76	454	45	28288	2166	21	68537	166	14	2548	0.21	0.28	511
77	650	46	41101	2249	21	72067	161	18	3406	0.29	0.35	481
78	470	47	34267	1775	23	63411	183	15	4384	0.26	0.34	488
79	461	52	36787	1195	22	40813	99	16	1674	0.39	0.46	430
80	438	45	30459	1397	22	43866	153	22	3648	0.31	0.39	463
81	704	42	43072	2413	21	76810	217	20	4563	0.29	0.35	484
82	658	43	43223	2704	20	84882	207	15	4958	0.24	0.32	493
83	558	55	47285	2001	22	69110	195	11	2893	0.28	0.40	461
84	719	46	44166	2499	22	80775	201	19	3982	0.29	0.34	485
85	567	44	38476	2155	21	69068	170	24	4424	0.26	0.34	485
86	728	42	46565	1905	24	64132	263	33	9243	0.38	0.39	464
87	478	46	32868	1628	20	51035	166	16	4236	0.29	0.37	471
88	679	47	45733	2236	22	76677	254	15	5109	0.30	0.36	478
89	801	63	76873	2333	25	90131	253	16	4544	0.34	0.45	437
90	629	46	36490	2897	20	87726	248	11	3450	0.22	0.29	511
91	543	54	45167	1658	23	60243	217	17	5699	0.33	0.41	456
92	1046	67	107029	3086	24	117030	367	32	17942	0.34	0.44	440
93	849	43	50388	2407	21	74922	261	14	4866	0.35	0.39	465
94	974	40	54350	2494	22	81694	281	11	4632	0.39	0.39	465
95	770	43	46074	2688	21	85185	262	14	5400	0.29	0.34	488
96	553	46	39206	1819	20	57574	202	17	5403	0.30	0.38	466
97	602	46	41613	1978	22	67454	200	13	4084	0.30	0.37	474
98	607	47	36646	2451	20	76182	183	18	4108	0.25	0.31	498
99	1075	42	64215	3010	22	101459	306	16	7045	0.36	0.37	472
100	912	45	59001	3792	21	121640	268	15	4549	0.24	0.32	496

Sample 2: YQ17-09

ID	D1_int	D1_FWHM	D1_area	G_int	G_FWHM	G_area	D2_int	D2_FWHM	D2_area	R1	R2	T
1	715	41	45592	726	32	35642	107	29	3348	0.98	0.54	396
2	1173	45	81172	1722	34	88865	214	23	5312	0.68	0.46	430
3	819	41	52121	1011	34	50153	137	25	3660	0.81	0.49	417
4	1306	43	86719	1353	36	74563	214	22	5002	0.97	0.52	404
5	336	42	21789	416	34	20431	36	32	1243	0.81	0.50	413
6	535	42	32615	351	37	18851	59	24	1500	1.52	0.62	361
7	993	46	69653	1410	34	73592	157	21	3488	0.70	0.47	425
8	652	44	44012	778	31	36726	152	28	5186	0.84	0.51	408
9	823	44	56412	695	37	39423	122	25	3806	1.18	0.57	383
10	540	43	35718	536	35	28644	67	25	1798	1.01	0.54	395
11	403	45	27668	296	36	15802	53	26	1463	1.36	0.62	361
12	475	41	30052	425	29	19196	107	35	4752	1.12	0.56	388
13	409	38	24153	403	34	20187	27	27	775	1.02	0.54	397
14	710	43	46348	729	34	37737	114	28	3364	0.97	0.53	400
15	1306	44	86086	2763	32	124139	265	25	6903	0.47	0.40	461
16	2223	43	142839	2261	34	116623	319	24	8187	0.98	0.53	398
17	1031	42	66928	1015	33	51737	175	27	5103	1.02	0.54	395
18	1459	40	91111	1230	34	64433	192	25	5020	1.19	0.57	383
19	898	42	56966	1267	32	58695	162	25	4321	0.71	0.47	425
20	807	41	51495	700	33	35029	149	25	3971	1.15	0.57	382
21	924	46	65591	799	41	50037	136	20	2964	1.16	0.55	389
22	299	40	18375	375	32	17418	52	25	1378	0.80	0.49	416
23	419	40	25877	371	33	18740	86	31	3570	1.13	0.54	397
24	1945	49	148003	2149	41	135359	206	22	4854	0.90	0.51	407
25	908	42	58259	769	33	39088	163	33	6536	1.18	0.56	386
26	1265	41	80809	1030	33	51122	235	26	6415	1.23	0.58	375
27	494	43	31157	578	34	29389	76	22	1767	0.85	0.50	413
28	728	41	44791	1029	31	45895	176	26	4802	0.71	0.47	428
29	600	40	36617	617	31	28441	153	23	4947	0.97	0.52	403

30	2094	44	141743	2566	37	144328	239	25	9137	0.82	0.48	423
31	369	43	24514	437	30	20490	88	28	2876	0.84	0.51	408
32	1483	43	93068	1271	36	65848	220	23	5437	1.17	0.57	383
33	891	43	54129	1036	35	50772	142	25	3813	0.86	0.50	414
34	1478	43	95254	1591	34	79053	228	26	6320	0.93	0.53	401
35	720	40	44476	881	32	41163	134	22	3114	0.82	0.50	413
36	3048	58	270362	5430	42	351864	504	29	20842	0.56	0.42	450
37	1797	43	111340	1854	34	91086	289	23	7066	0.97	0.53	399
38	1272	43	81776	1175	36	61863	174	27	4926	1.08	0.55	391
39	524	37	29343	474	31	21556	85	20	1834	1.11	0.56	388
40	1248	42	71856	1148	33	55346	205	23	5123	1.09	0.54	394
41	1020	37	55564	909	33	41926	149	21	3370	1.12	0.55	390
42	2001	45	126219	3138	34	153121	343	23	8380	0.64	0.44	441
43	1975	41	126428	1815	36	99784	101	34	4530	1.09	0.55	392
44	960	42	62546	809	34	42240	176	23	4555	1.19	0.57	381
45	968	41	61460	1148	34	57670	123	26	3353	0.84	0.50	413
46	460	43	29190	556	32	26888	69	29	2125	0.83	0.50	413
47	1590	41	98594	1301	37	69944	228	24	5845	1.22	0.57	384
48	813	43	53416	1140	35	58039	89	21	1968	0.71	0.47	427
49	1033	41	64349	1112	31	50348	199	30	6318	0.93	0.53	399
50	1319	41	83228	1196	31	56635	283	26	7869	1.10	0.56	385
51	551	42	35317	388	37	20553	110	26	2995	1.42	0.60	368
52	639	44	43581	575	33	29019	166	35	6213	1.11	0.55	389
53	344	41	21550	349	34	17050	70	35	2643	0.98	0.52	403
54	477	46	33345	484	39	26661	83	24	2102	0.99	0.54	397
55	585	42	37902	512	34	25768	105	32	3574	1.14	0.56	385
56	672	43	44316	589	32	28858	157	30	5030	1.14	0.57	383
57	700	43	45831	733	34	37490	121	29	4231	0.96	0.52	403
58	432	42	26707	805	31	36027	99	23	2394	0.54	0.41	454
59	714	42	45857	926	33	47169	113	23	2716	0.77	0.48	423
60	737	42	47616	771	35	38279	144	22	3382	0.96	0.53	398
61	321	42	20891	488	31	22785	64	24	1678	0.66	0.46	431
62	961	46	64363	1003	36	53095	133	30	4296	0.96	0.53	400
63	547	43	36537	627	32	29631	102	29	3171	0.87	0.53	401
64	287	41	18332	325	34	15794	39	25	1065	0.88	0.52	404
65	538	45	36290	540	34	27391	87	27	2549	1.00	0.55	392
66	966	45	65911	886	36	48202	146	25	3938	1.09	0.56	387
67	638	39	38212	677	32	32639	104	21	2368	0.94	0.52	404
68	925	44	60483	890	35	45097	156	25	4211	1.04	0.55	390
69	812	43	53639	936	32	45385	150	25	3957	0.87	0.52	404
70	736	46	49886	599	36	32773	104	28	3145	1.23	0.58	376
71	644	44	41251	624	37	33554	73	21	1616	1.03	0.54	395
72	559	43	36169	564	31	26334	97	33	3438	0.99	0.55	391
73	172	38	10086	158	34	7047	24	24	600	1.09	0.57	382
74	221	46	14311	205	36	9935	40	21	916	1.08	0.57	382
75	212	45	13277	251	30	10944	40	20	870	0.84	0.53	400
76	226	42	13641	252	34	13124	33	18	615	0.90	0.50	414
77	372	45	25963	391	35	19965	66	25	1739	0.95	0.54	393
78	1895	45	124009	2242	36	119117	287	27	8267	0.85	0.49	417
79	758	40	45677	721	35	35482	105	26	2888	1.05	0.54	394
80	290	39	17123	307	32	14788	51	25	1344	0.94	0.51	407
81	428	43	28047	463	36	24012	76	23	1876	0.92	0.52	404
82	382	42	24955	319	37	16576	73	26	2027	1.20	0.57	380
83	1046	43	68055	971	35	50210	159	27	4621	1.08	0.55	389
84	431	42	28252	462	32	22493	76	29	2391	0.93	0.53	399
85	501	42	32708	618	32	29476	102	28	3000	0.81	0.50	413
86	480	44	32724	733	31	32790	117	33	4040	0.66	0.47	427
87	1416	41	87816	1170	36	61835	234	25	6184	1.21	0.56	385
88	471	42	29820	423	33	20846	74	28	2187	1.11	0.56	384
89	588	40	35653	509	33	24830	97	30	3138	1.16	0.56	386
90	510	38	29941	550	32	25777	75	25	1992	0.93	0.52	405
91	408	37	22151	457	29	19296	58	21	1262	0.89	0.52	405
92	589	40	35272	457	36	22532	87	25	2336	1.29	0.59	374
93	1086	43	68528	1051	33	52100	172	23	4192	1.03	0.55	391
94	916	40	53477	964	32	45386	132	23	3207	0.95	0.52	403
95	369	38	21067	486	30	21378	58	25	1536	0.76	0.48	423
96	554	38	32230	720	31	33051	73	21	1651	0.77	0.48	422
97	366	38	19702	442	31	19189	63	24	1589	0.83	0.49	420
98	266	38	15427	301	31	13866	38	22	863	0.88	0.51	408
99	201	45	13898	404	32	20160	34	13	687	0.50	0.40	459
100	816	43	51774	977	34	47995	159	20	3456	0.84	0.50	413
101	413	41	25756	598	32	27504	80	21	1827	0.69	0.47	428
102	1009	41	62830	840	31	38704	204	27	5926	1.20	0.58	375
103	669	41	42368	600	35	30874	120	25	3241	1.12	0.55	389
104	521	42	33806	535	32	25285	142	26	3861	0.97	0.54	397
105	805	43	50958	722	36	37558	121	26	3307	1.12	0.55	388

106	655	46	46342	568	39	32697	99	22	2367	1.15	0.57	382
107	659	41	42203	501	34	25322	115	32	3862	1.32	0.59	372

Sample 3: YQ17-10b

ID	D1_int	D1_FWHM	D1_area	G_int	G_FWHM	G_area	D2_int	D2_FWHM	D2_area	R1	R2	T
1	1243	40	77128	1839	30	84712	326	18	6263	0.68	0.46	432
2	1623	46	115557	2716	33	139378	245	16	4227	0.60	0.45	438
3	2786	44	189554	3973	36	223022	261	25	6814	0.70	0.45	435
4	994	40	59396	1604	30	70792	225	22	5289	0.62	0.44	442
5	1062	52	84267	2140	36	118093	208	25	5556	0.50	0.41	457
6	987	39	59105	1567	30	69374	237	19	4699	0.63	0.44	439
7	1423	40	85233	1753	31	78854	317	22	7384	0.81	0.50	415
8	666	40	39185	933	32	42348	141	21	3084	0.71	0.46	430
9	857	45	59073	1244	36	69103	122	17	2177	0.69	0.45	435
10	1209	41	69598	1623	33	74865	194	23	4703	0.74	0.47	429
11	773	43	48906	1364	30	60054	150	24	3833	0.57	0.43	444
12	587	38	34300	1026	30	45471	127	22	2956	0.57	0.41	452
13	865	39	49444	1470	31	65044	202	21	4533	0.59	0.42	452
14	695	41	41463	972	33	45052	122	26	3321	0.71	0.46	431
15	1590	44	95387	2225	34	106216	228	26	6325	0.71	0.46	432
16	909	43	60606	1494	34	75608	148	21	3363	0.61	0.43	443
17	663	41	39631	969	33	44989	135	20	2855	0.68	0.45	435
18	634	43	38261	1121	32	50624	124	22	2981	0.57	0.42	451
19	1421	45	98701	2312	33	118746	194	19	3953	0.61	0.45	438
20	576	41	35847	916	32	43162	110	20	2356	0.63	0.44	441
21	1556	44	95271	2239	34	106838	271	22	6398	0.70	0.46	433
22	473	42	28938	678	33	31622	94	21	2154	0.70	0.46	431
23	959	44	61527	1411	34	68098	163	23	3930	0.68	0.46	431
24	2128	51	165894	2767	40	170035	126	22	2990	0.77	0.49	418
25	1341	46	94996	2191	34	115834	224	21	5017	0.61	0.44	441
26	466	41	27596	656	30	28888	106	22	2507	0.71	0.47	428
27	1208	45	83100	1796	33	92342	170	19	3454	0.67	0.46	430
28	766	41	47986	1272	29	55608	183	18	3516	0.60	0.45	437
29	837	44	56154	1256	33	63634	130	17	2412	0.67	0.46	432
30	1589	62	151048	2470	41	157412	160	5	873	0.64	0.49	419
31	1428	42	83185	2005	33	93867	231	24	5785	0.71	0.45	434
32	2261	40	138418	4006	30	176576	540	19	11186	0.56	0.42	448
33	623	44	42658	896	35	47711	112	17	2031	0.70	0.46	431
34	1356	42	87866	2499	30	115307	251	21	5730	0.54	0.42	450
35	1796	46	128589	2860	35	154504	224	19	4610	0.63	0.45	438
36	1113	41	64747	1595	33	74028	192	25	5037	0.70	0.45	436
37	618	39	36068	1005	31	44207	116	23	2864	0.62	0.43	444
38	1223	40	74352	1992	32	91222	263	23	6356	0.61	0.43	444
39	843	45	58163	1335	35	67409	134	24	3381	0.63	0.45	436
40	577	41	35252	1128	30	49898	140	19	2789	0.51	0.40	459
41	1413	41	81667	1882	34	88619	252	23	6083	0.75	0.46	430
42	652	43	39226	1002	33	45715	140	21	3203	0.65	0.45	439
43	828	41	49183	1393	32	62992	162	21	3553	0.59	0.42	448
44	933	40	54738	1507	30	65993	209	21	4566	0.62	0.44	442
45	888	45	58955	949	34	47287	166	21	3774	0.94	0.54	397
46	696	45	48643	1039	32	50273	118	24	3010	0.67	0.48	424
47	1246	50	96086	1571	41	98161	159	26	4374	0.79	0.48	421
48	676	42	39009	912	33	41858	144	21	3174	0.74	0.46	430
49	1156	46	75099	1303	38	70776	169	24	4271	0.89	0.50	413
50	873	45	59040	1189	34	59571	145	26	3961	0.73	0.48	422
51	515	44	35006	698	34	35223	81	23	1949	0.74	0.48	420
52	864	45	59273	1108	35	56450	132	25	3464	0.78	0.50	415
53	702	44	47105	838	33	41767	117	22	2796	0.84	0.51	407
54	840	45	52622	1242	34	58852	173	23	4180	0.68	0.45	434
55	760	42	47035	936	34	45776	133	21	2958	0.81	0.49	418
56	714	43	47799	1046	34	52956	120	24	3027	0.68	0.46	431
57	665	45	45133	825	35	42226	109	24	2732	0.81	0.50	413
58	589	44	39553	795	34	39724	101	21	2234	0.74	0.49	420
59	639	45	43926	864	34	42870	109	23	2614	0.74	0.49	417
60	524	44	34485	765	33	37725	85	23	2124	0.68	0.46	430
61	564	45	38467	837	34	41592	93	26	2582	0.67	0.47	429
62	1209	46	74203	1790	34	83933	225	23	5459	0.68	0.45	435
63	630	45	41983	913	35	45613	123	21	2793	0.69	0.46	430
64	887	45	55431	1365	34	64741	179	22	4168	0.65	0.45	438
65	720	45	49420	1467	32	66915	132	24	3337	0.49	0.41	453
66	585	44	37232	770	36	40809	108	19	2198	0.76	0.46	430
67	1091	42	66007	1439	34	67560	194	23	4761	0.76	0.48	424
68	804	45	49096	1109	35	53094	159	24	4048	0.72	0.46	431

69	891	45	59800	962	34	48813	156	22	3727	0.93	0.53	399

Sample 4: YQ17-12b

ID	D1_int	D1_FWHM	D1_area	G_int	G_FWHM	G_area	D2_int	D2_FWHM	D2_area	R1	R2	T
1	870	43	54928	1150	33	54440	161	22	3699	0.76	0.49	420
2	686	42	39076	1074	32	48642	133	22	3045	0.64	0.43	445
3	343	41	20667	539	31	23944	57	23	1388	0.64	0.45	437
4	1495	44	101423	1780	35	96829	228	23	5692	0.84	0.50	415
5	845	41	50987	1040	33	50393	119	22	2837	0.81	0.49	418
6	1142	42	74438	806	37	45945	188	21	4798	1.42	0.59	370
7	793	39	48391	758	33	37554	142	23	3506	1.05	0.54	395
8	593	41	35694	716	34	37371	78	20	1647	0.83	0.48	424
9	1900	49	142539	2063	43	135704	211	18	3999	0.92	0.51	411
10	259	40	15609	389	30	17698	27	24	677	0.67	0.46	432
11	710	41	43917	621	32	30238	124	28	3676	1.14	0.56	384
12	1876	44	126624	1886	36	104372	260	23	6369	0.99	0.53	398
13	584	44	40077	466	39	28086	79	25	2085	1.25	0.57	381
14	1781	44	121993	1090	45	74898	202	55	16934	1.63	0.57	381
15	1603	42	103840	1463	35	77891	228	22	5401	1.10	0.55	389
16	1156	39	69150	1761	32	82105	192	21	4273	0.66	0.44	439
17	257	44	16802	354	33	17328	34	23	825	0.73	0.48	422
18	359	41	22546	377	36	19507	55	25	1451	0.95	0.52	405
19	825	42	49480	846	33	41034	132	20	2800	0.98	0.53	400
20	1151	44	74276	1380	34	68453	183	24	4688	0.83	0.50	412
21	2865	42	187177	2749	37	155314	338	24	8703	1.04	0.53	398
22	569	41	34657	754	30	34353	87	21	1943	0.75	0.49	419
23	363	42	20662	461	31	20841	54	24	1344	0.79	0.48	422
24	239	41	15167	301	33	14333	37	20	775	0.80	0.50	413
25	740	41	43796	834	33	40091	105	27	3001	0.89	0.50	412
26	1775	42	115190	2264	34	118822	249	18	5645	0.78	0.48	422
27	652	43	42551	770	34	40767	94	26	2567	0.85	0.50	416
28	259	44	16154	296	35	15370	50	20	1070	0.88	0.50	415
29	807	42	47243	915	34	44352	126	22	2888	0.88	0.50	413
30	416	43	25608	484	35	25643	41	21	900	0.86	0.49	418
31	447	41	25636	282	35	14179	80	22	1829	1.58	0.62	361
32	1365	45	91690	1378	35	73466	212	24	5340	0.99	0.54	396
33	509	43	30803	714	33	34369	87	21	1934	0.71	0.46	432
34	1839	35	97411	1055	32	50956	283	21	6323	1.74	0.63	354
35	440	41	26708	627	33	29806	62	18	1196	0.70	0.46	430
36	1471	42	91330	1749	33	86968	195	23	4709	0.84	0.50	414
37	331	40	19529	440	34	21404	51	21	1121	0.75	0.46	430
38	765	44	50993	1054	33	51965	144	22	3429	0.73	0.48	423
39	594	41	35127	915	34	42756	93	25	2516	0.65	0.44	442
40	944	40	55628	1297	32	60407	143	20	3096	0.73	0.47	429
41	1611	42	98782	2412	31	109944	245	21	5488	0.67	0.46	431
42	862	42	52345	1473	32	66594	152	20	3177	0.59	0.43	446
43	578	44	37213	717	34	34834	102	23	2572	0.81	0.50	414
44	304	41	17950	375	32	17458	59	23	1457	0.81	0.49	419
45	253	40	14994	312	33	14766	44	20	925	0.81	0.49	419
46	451	46	30780	622	33	31799	59	18	1106	0.73	0.48	421
47	830	43	52999	1153	34	56504	136	25	3654	0.72	0.47	428
48	614	40	38226	758	33	37538	87	20	1861	0.81	0.49	417
49	874	42	53978	1078	34	52984	140	23	3372	0.81	0.49	418
50	578	39	33631	729	32	34226	70	25	1870	0.79	0.48	422
51	1328	39	79457	1034	35	53418	220	22	5252	1.28	0.58	379
52	448	39	26681	663	32	30396	87	22	2041	0.68	0.45	436
53	701	43	41252	1359	31	58926	142	22	3353	0.52	0.40	460
54	1852	42	119003	2289	35	115084	282	23	6960	0.81	0.49	416
55	950	39	55704	946	32	44061	181	21	4088	1.00	0.54	397
56	1200	39	70719	1018	34	51597	167	24	4221	1.18	0.56	387
57	332	40	20374	388	32	18610	61	19	1389	0.86	0.50	411
58	418	41	26274	389	34	19882	66	22	1908	1.07	0.55	392
59	751	40	44003	987	35	49394	103	26	2822	0.76	0.46	433
60	742	41	45313	698	35	36617	95	23	2286	1.06	0.54	396
61	1292	53	104854	1525	43	100695	141	19	2826	0.85	0.50	412
62	966	42	60004	864	34	41860	182	22	4305	1.12	0.57	384
63	369	40	21959	450	33	20974	60	26	1668	0.82	0.49	417
64	1332	51	103926	1698	38	100091	330	28	14458	0.78	0.48	425
65	647	43	41343	1042	32	48911	113	22	2631	0.62	0.45	438
66	1081	45	71912	1633	34	80045	191	24	4945	0.66	0.46	432
67	632	48	44764	931	35	46737	126	23	3116	0.68	0.47	426

68	465	44	29078	720	32	33512	92	21	2095	0.65	0.45	436
69	796	42	48755	1112	31	50691	135	25	3540	0.72	0.47	426
70	1671	46	118955	2200	37	125376	228	19	5120	0.76	0.48	424
71	1013	40	60791	1415	32	66950	151	21	3315	0.72	0.46	430
72	1019	41	60678	959	32	46239	182	22	4245	1.06	0.55	393
73	903	43	57008	933	34	45456	179	24	4587	0.97	0.53	399
74	1466	41	91102	1227	35	64226	213	22	4991	1.20	0.57	382
75	414	46	26585	843	30	37717	74	27	2116	0.49	0.40	459
76	518	45	34358	871	31	39477	114	24	2914	0.60	0.45	437
77	457	41	27566	609	32	29598	67	21	1514	0.75	0.47	427
78	1046	44	70617	1389	33	70155	204	23	5181	0.75	0.48	421
79	877	43	57950	618	35	33136	123	25	3218	1.42	0.61	361
80	505	42	32619	471	33	24060	70	23	1686	1.07	0.56	387
81	800	46	56584	759	36	41977	102	20	2115	1.05	0.56	385

Sample 5: YQ17-15

ID	D1_int	D1_FWHM	D1_area	G_int	G_FWHM	G_area	D2_int	D2_FWHM	D2_area	R1	R2	T
1	295	52	23408	160	45	10870	54	28	1619	1.84	0.65	344
2	615	50	47337	338	44	22684	114	35	4246	1.82	0.64	351
3	797	52	63583	412	47	29100	172	36	6617	1.93	0.64	350
4	641	53	51991	295	48	21499	156	39	6408	2.17	0.65	345
5	585	52	46313	279	45	19096	137	37	5402	2.10	0.65	343
6	326	52	26179	161	46	11399	69	37	2765	2.02	0.65	346
7	435	51	32986	234	44	15759	85	34	3081	1.86	0.64	351
8	390	50	29111	209	44	13776	73	32	2471	1.87	0.64	349
9	414	54	33930	199	47	14258	103	39	4238	2.08	0.65	347
10	795	54	66317	329	56	28109	192	45	9213	2.41	0.64	350
11	599	51	46219	308	44	20487	127	32	4346	1.94	0.65	345
12	666	53	54292	305	47	21849	159	38	6512	2.18	0.66	342
13	902	58	79788	398	52	31353	250	40	10568	2.27	0.66	343
14	730	50	55508	349	45	23412	154	35	5788	2.09	0.66	343
15	730	50	55440	357	45	24391	148	39	6095	2.04	0.65	347
16	796	53	64378	370	48	27348	176	39	7364	2.15	0.65	345
17	1185	49	89030	674	44	45580	195	27	5605	1.76	0.63	352
18	539	50	40761	285	43	18305	107	31	3541	1.89	0.65	345
19	494	53	39222	241	48	17775	107	39	4390	2.05	0.64	350
20	389	51	29798	216	44	14429	76	30	2465	1.80	0.64	351
21	830	52	66454	427	45	29458	174	32	5846	1.94	0.65	344
22	763	52	60606	335	47	23723	184	39	7662	2.28	0.66	341
23	563	54	46189	275	46	19225	139	35	5222	2.05	0.65	343
24	460	54	38281	218	51	17129	107	40	4591	2.11	0.64	351
25	808	53	65339	443	46	31316	140	35	5165	1.82	0.64	349
26	936	51	72822	476	45	32542	191	36	7404	1.97	0.65	347
27	557	52	42618	310	47	20341	108	30	3456	1.80	0.64	349
28	643	49	46812	348	40	21352	140	32	4819	1.85	0.64	349
29	539	50	41753	270	46	18920	114	38	4661	2.00	0.64	350
30	620	53	49630	292	48	21319	137	40	5852	2.12	0.65	347
31	617	53	49409	259	55	21784	135	43	6152	2.38	0.64	350
32	529	51	41375	281	44	18858	96	31	3139	1.88	0.65	344
33	729	50	56168	380	45	26019	150	37	5947	1.92	0.64	351
34	815	52	65255	391	45	26931	187	36	7128	2.08	0.66	342
35	705	59	63320	286	56	24289	216	42	9625	2.46	0.65	345
36	791	52	62844	398	45	27154	166	32	5632	1.99	0.66	342
37	761	54	62783	348	53	28287	187	45	8870	2.19	0.63	355
38	768	53	62195	313	52	24790	195	43	8883	2.45	0.65	346
39	656	51	50938	310	45	21396	150	37	5858	2.11	0.65	345
40	726	51	56444	354	44	24159	163	37	6417	2.05	0.65	346
41	874	54	71965	435	46	30662	204	35	7652	2.01	0.65	344
42	474	51	37239	229	45	15727	99	38	3980	2.07	0.65	343
43	844	51	65351	411	45	27937	192	35	7108	2.05	0.65	345
44	701	52	54024	390	42	24962	128	33	4523	1.80	0.65	347
45	764	51	60382	422	43	28003	157	31	5217	1.81	0.65	347
46	689	53	55918	354	44	24001	166	37	6452	1.95	0.65	346
47	777	50	60157	373	47	26957	185	40	7949	2.08	0.63	353
48	664	52	53347	386	51	27427	76	31	2490	1.72	0.64	349
49	899	51	70973	421	49	31507	197	41	8541	2.14	0.64	350
50	799	52	61905	391	44	26433	191	36	7249	2.04	0.65	346

51	645	55	54038	311	48	22934	166	39	6890	2.07	0.64	348
52	1101	52	88253	534	45	36994	218	34	7877	2.06	0.66	339
53	632	49	47355	352	43	23241	112	32	3839	1.80	0.64	352
54	1087	51	85862	576	45	40006	228	33	8022	1.89	0.64	349
55	1056	51	81226	600	46	41248	165	29	5108	1.76	0.64	351
56	702	55	59247	336	47	24356	163	36	6143	2.09	0.66	341
57	824	54	68094	393	49	29237	211	39	8797	2.10	0.64	349
58	784	49	58873	424	43	27587	158	31	5221	1.85	0.64	349
59	779	52	61666	398	45	27560	186	39	7758	1.96	0.64	352
60	1022	50	78767	517	45	35516	234	38	9433	1.97	0.64	351
61	611	53	49167	327	44	22284	118	34	4249	1.87	0.65	345

Sample 6: YQ17-23a

ID	D1_int	D1_FWHM	D1_area	G_int	G_FWHM	G_area	D2_int	D2_FWHM	D2_area	R1	R2	T
1	38	44	2387	136	22	4272	12	27	340	0.28	0.34	486
2	54	47	2930	266	21	8204	15	19	291	0.20	0.26	524
3	34	47	2105	150	21	4819	10	14	190	0.23	0.30	506
4	108	45	5856	446	21	14027	38	11	537	0.24	0.29	511
5	34	46	1966	138	22	4606	9	20	194	0.25	0.29	509
6	64	47	3809	335	24	11531	18	22	412	0.19	0.24	531
7	46	46	3309	194	21	6015	17	29	527	0.24	0.34	488
8	76	45	4124	325	21	10142	26	11	391	0.23	0.28	513
9	49	45	2903	236	21	7211	10	30	302	0.21	0.28	514
10	95	46	5278	352	21	11145	28	15	452	0.27	0.31	499
11	101	47	5677	508	22	17099	29	13	400	0.20	0.24	530
12	89	45	4722	493	21	15111	24	15	388	0.18	0.23	535
13	104	46	5832	400	22	12742	30	16	523	0.26	0.31	502
14	64	46	3576	284	20	8603	19	13	263	0.22	0.29	510
15	88	45	4811	372	20	11028	28	11	473	0.24	0.29	507
16	64	46	3671	259	22	8422	17	16	291	0.25	0.30	506
17	56	45	3427	246	21	7729	19	17	369	0.23	0.30	506
18	65	45	3735	234	21	7220	18	18	339	0.28	0.33	491
19	42	47	2967	192	21	6121	14	12	232	0.22	0.32	496
20	88	46	4962	428	20	13161	26	15	421	0.21	0.27	519
21	58	46	3328	216	21	6653	14	13	276	0.27	0.32	493
22	71	46	3909	253	22	7975	17	24	427	0.28	0.32	497
23	115	45	6359	492	20	14768	41	12	684	0.23	0.29	508
24	109	45	5924	653	20	19949	33	12	434	0.17	0.23	539
25	96	45	5439	420	20	12952	26	16	455	0.23	0.29	510
26	124	46	6810	685	20	21104	41	11	538	0.18	0.24	532
27	103	46	5684	442	20	13505	34	10	380	0.23	0.29	509
28	79	50	5685	352	22	11758	28	25	773	0.22	0.31	499
29	82	49	6080	320	21	10018	22	16	366	0.26	0.37	473
30	61	47	3562	344	19	10382	19	10	195	0.18	0.25	526
31	101	44	5575	380	22	12370	30	11	475	0.26	0.30	503
32	41	48	2267	134	21	4234	11	21	257	0.31	0.34	488
33	65	46	3492	251	21	7868	24	8	300	0.26	0.30	505
34	42	47	2417	162	23	5433	12	10	186	0.26	0.30	504
35	87	46	4871	375	22	12141	28	13	467	0.23	0.28	514
36	103	45	5974	274	21	8848	25	20	529	0.38	0.39	464
37	121	46	6680	622	21	19598	47	11	688	0.19	0.25	528
38	122	45	6718	479	21	15016	43	11	695	0.25	0.30	505
39	123	45	6671	656	20	20051	36	13	494	0.19	0.25	529
40	83	47	4648	448	22	14650	15	24	393	0.18	0.24	534
41	103	45	5882	390	21	12467	27	19	531	0.26	0.31	499
42	154	47	9153	571	22	19050	42	18	818	0.27	0.32	497
43	65	46	3644	167	23	5618	15	21	334	0.39	0.38	468
44	114	45	6651	408	22	13162	25	30	792	0.28	0.32	494
45	25	47	1678	182	21	5477	7	27	215	0.14	0.23	537
46	44	46	2389	180	21	5748	12	17	216	0.24	0.29	511
47	34	47	2187	165	23	5553	10	22	227	0.21	0.27	516
48	54	46	3179	191	22	6194	14	20	284	0.28	0.33	491
49	99	46	5455	386	22	12257	27	20	569	0.26	0.30	505
50	105	45	5975	467	21	14552	26	18	495	0.23	0.28	512
51	51	46	3235	207	21	6511	14	24	352	0.25	0.32	495
52	62	45	3844	226	22	7180	16	24	395	0.27	0.34	488
53	57	46	3310	222	23	7519	15	20	314	0.26	0.30	506
54	119	44	6647	367	22	12176	32	15	513	0.32	0.34	485
55	61	47	3439	245	22	7885	15	19	291	0.25	0.30	506
56	38	46	2300	119	22	3884	11	23	270	0.32	0.36	479
57	44	44	2740	147	23	4807	13	33	465	0.30	0.34	485
58	81	46	4609	290	22	9242	24	17	432	0.28	0.32	494
59	110	45	6062	528	21	16394	35	12	509	0.21	0.26	521

60	87	46	4976	327	21	10432	28	12	451	0.27	0.31	498
61	123	46	6871	522	20	16104	37	13	601	0.24	0.29	508
62	38	46	2250	180	19	5454	11	16	190	0.21	0.29	511

Sample 7: YQ17-28

ID	D1_int	D1_FWHM	D1_area	G_int	G_FWHM	G_area	D2_int	D2_FWHM	D2_area	R1	R2	T
1	164	42	9360	874	18	24485	37	12	479	0.19	0.27	517
2	165	44	10857	793	19	23818	55	11	623	0.21	0.31	501
3	162	46	11563	830	19	23871	80	26	2241	0.20	0.31	501
4	168	42	10759	836	19	24321	72	29	2205	0.20	0.29	510
5	193	44	10855	928	21	29103	30	20	626	0.21	0.27	519
6	264	42	15387	1288	19	37055	92	12	1364	0.20	0.29	511
7	86	45	5959	338	20	10019	38	25	1023	0.25	0.35	482
8	190	44	9836	882	19	25338	41	12	523	0.22	0.28	516
9	178	46	11872	661	20	20081	47	21	1031	0.27	0.36	477
10	114	45	7867	677	18	19058	63	25	1645	0.17	0.28	516
11	152	46	9737	774	20	22687	47	10	486	0.20	0.30	506
12	154	45	10401	775	21	24493	52	28	1518	0.20	0.29	511
13	174	43	8948	691	19	19935	53	11	618	0.25	0.30	503
14	140	44	8237	759	20	22879	40	11	472	0.18	0.26	522
15	115	44	7862	581	20	18017	35	24	899	0.20	0.29	507
16	220	45	13023	1031	19	30148	107	9	1308	0.21	0.29	508
17	139	46	9201	1007	19	28910	34	30	1105	0.14	0.23	534
18	131	45	8983	548	19	14939	47	24	1207	0.24	0.36	478
19	136	43	7867	706	19	21206	49	10	528	0.19	0.27	520
20	159	47	11525	725	19	19914	58	25	1575	0.22	0.35	482
21	166	44	10190	946	20	29324	54	12	887	0.18	0.25	526
22	142	46	10144	709	19	20550	53	23	1298	0.20	0.32	497
23	174	43	10133	888	20	26282	72	8	786	0.20	0.27	517
24	187	44	12691	1027	20	31504	64	21	1447	0.18	0.28	514
25	202	46	11814	960	22	31377	36	20	766	0.21	0.27	519
26	162	43	9509	778	20	23272	56	12	874	0.21	0.28	512
27	181	48	13279	846	20	26240	45	10	483	0.21	0.33	490
28	160	43	10201	753	21	23630	39	26	1071	0.21	0.29	508
29	199	44	11930	757	21	23798	48	18	907	0.26	0.33	493
30	100	45	5523	643	19	18460	35	10	371	0.16	0.23	538
31	101	42	5399	637	18	17444	36	11	439	0.16	0.23	535
32	82	42	5153	441	19	12887	24	25	633	0.19	0.28	515
33	111	40	6911	565	18	14700	67	24	1696	0.20	0.30	506
34	160	43	8617	785	18	22202	32	21	723	0.20	0.27	517
35	301	45	16035	1781	20	53900	56	15	874	0.17	0.23	538
36	137	43	8851	797	19	23468	57	10	814	0.17	0.27	519
37	196	42	10438	1114	18	30578	70	9	794	0.18	0.25	527
38	145	46	8439	1100	22	35842	42	13	668	0.13	0.19	556
39	110	44	6169	629	20	18804	35	11	422	0.18	0.24	530
40	210	43	11725	1193	18	33628	90	8	1076	0.18	0.25	526
41	301	44	15447	2008	19	57484	114	10	1162	0.15	0.21	546
42	170	52	13620	913	19	25943	87	21	1942	0.19	0.33	492
43	150	43	9447	799	20	24034	43	17	775	0.19	0.28	516
44	98	43	6183	533	20	16038	25	13	351	0.18	0.27	516
45	106	46	7507	546	19	15726	39	28	1145	0.19	0.31	501
46	104	44	5440	640	20	18813	36	9	357	0.16	0.22	540
47	256	43	13788	1580	19	45073	61	12	791	0.16	0.23	536
48	201	43	10794	1259	18	34889	69	10	844	0.16	0.23	535
49	174	42	10057	1194	19	34247	77	10	1002	0.15	0.22	540
50	236	44	13291	1102	20	32715	76	10	1039	0.21	0.28	512
51	117	42	7666	688	19	19253	46	28	1371	0.17	0.27	518
52	184	43	10145	717	19	20417	60	8	782	0.26	0.32	494
53	224	43	12459	1065	18	29363	72	11	858	0.21	0.29	508
54	142	42	8238	865	19	24905	64	9	888	0.16	0.24	531
55	176	44	10417	1070	20	31586	96	9	1249	0.16	0.24	531
56	137	43	7287	707	19	20912	41	13	566	0.19	0.25	526
57	81	44	4332	489	20	14821	23	12	290	0.17	0.22	540
58	152	43	9145	759	20	22718	65	9	851	0.20	0.28	514
59	179	43	10244	1346	18	37221	53	9	531	0.13	0.21	544
60	193	43	11863	970	20	28548	71	12	1286	0.20	0.28	512
61	77	43	4852	462	19	12956	23	28	684	0.17	0.26	522
62	143	43	9506	614	20	17680	58	23	1388	0.23	0.33	490
63	184	43	11557	756	19	21987	50	20	1104	0.24	0.33	489
64	197	43	10857	1066	19	31460	67	10	855	0.18	0.25	527
65	103	42	5906	606	20	17856	29	18	563	0.17	0.24	531
66	107	40	6556	582	19	17061	37	22	986	0.18	0.27	520
67	143	42	9303	563	18	15490	46	24	1163	0.25	0.36	478

68	102	43	6741	473	19	13265	33	28	970	0.21	0.32	495
69	124	43	7186	620	19	18306	32	15	503	0.20	0.28	515
70	120	43	7872	708	20	20681	43	26	1182	0.17	0.26	521
71	151	44	7770	825	19	23632	46	10	501	0.18	0.24	530
72	200	42	10892	1051	20	31771	69	9	831	0.19	0.25	527
73	132	42	7891	725	19	21103	47	9	684	0.18	0.27	520
74	123	43	8025	611	20	18200	39	11	696	0.20	0.30	505
75	210	43	11916	1192	19	34878	74	10	918	0.18	0.25	527
76	235	45	13811	1206	22	38462	48	17	863	0.19	0.26	523
77	195	42	10871	1145	19	32821	57	9	659	0.17	0.25	529
78	182	45	10451	877	20	26760	49	10	519	0.21	0.28	515
79	118	50	9066	610	18	16920	52	24	1321	0.19	0.33	490
80	205	43	11433	1198	20	35949	53	15	832	0.17	0.24	533

Sample 8: YQ17-29

ID	D1_int	D1_FWHM	D1_area	G_int	G_FWHM	G_area	D2_int	D2_FWHM	D2_area	R1	R2	T
1	1160	49	84923	709	46	47564	166	27	4845	1.64	0.62	360
2	1247	50	92505	712	43	45364	231	30	7351	1.75	0.64	351
3	2031	57	176889	834	60	75799	485	46	23694	2.44	0.64	350
4	1050	50	78092	514	43	34081	244	36	9235	2.04	0.64	348
5	837	54	68368	389	47	28219	200	42	8855	2.15	0.65	346
6	1263	49	91931	679	41	42309	295	33	10242	1.86	0.64	351
7	1694	53	134773	675	48	46855	378	39	15621	2.51	0.68	330
8	3451	50	261149	2114	43	140846	577	29	18059	1.63	0.62	358
9	1609	50	122125	921	42	59605	283	33	9810	1.75	0.64	351
10	1380	48	99462	735	41	46805	235	33	8341	1.88	0.64	348
11	1199	47	83411	683	41	40716	222	28	6624	1.76	0.64	351
12	1941	54	157482	928	47	66943	476	39	19886	2.09	0.64	348
13	1255	53	101571	715	43	47744	222	33	7765	1.75	0.65	347
14	2212	50	168089	1270	43	84779	389	30	12452	1.74	0.63	353
15	2701	50	208261	1522	45	104469	453	35	16966	1.78	0.63	354
16	2161	51	168852	1016	47	73232	450	40	19153	2.13	0.65	347
17	2715	59	245687	1011	61	90348	755	45	36088	2.68	0.66	341
18	3447	53	276715	1695	46	119254	612	39	25667	2.03	0.66	342
19	1148	53	92760	648	51	48161	142	30	4443	1.77	0.64	351
20	2059	47	148485	999	42	65100	376	35	14094	2.06	0.65	344
21	2360	48	169124	1275	43	84145	393	32	13371	1.85	0.63	352
22	1855	50	138796	1010	45	68248	295	30	9490	1.84	0.64	349
23	1470	49	110413	839	41	52375	340	33	12039	1.75	0.63	354
24	1804	54	145739	744	51	58331	458	44	21346	2.42	0.65	347
25	1511	58	134577	1024	40	63135	410	39	16813	1.48	0.63	356
26	2032	56	175321	889	51	67254	488	41	21168	2.29	0.66	339
27	1661	55	139135	1120	41	71195	320	34	11748	1.48	0.63	356
28	1039	49	78020	761	36	42243	209	32	7170	1.37	0.61	362
29	1410	54	115868	832	40	50939	392	41	17153	1.69	0.63	354
30	1174	52	90745	737	39	43902	247	34	8849	1.59	0.63	353
31	1855	56	158590	676	58	59550	495	44	23241	2.74	0.66	342
32	998	52	77980	421	51	32555	255	43	11689	2.37	0.64	351
33	1105	48	78477	779	37	44196	202	32	6792	1.42	0.61	365
34	1080	54	88567	499	50	38384	258	42	11491	2.16	0.64	350
35	1532	48	111847	822	43	53344	276	26	7706	1.86	0.65	347
36	2223	54	184806	1186	48	86557	396	39	16292	1.88	0.64	349
37	1901	59	170463	819	56	69786	509	44	24048	2.32	0.64	348
38	2910	55	243869	1241	54	103194	566	45	27395	2.34	0.65	345
39	790	48	52227	435	46	25949	119	26	3288	1.82	0.64	349
40	2327	58	204430	880	54	70227	552	43	25042	2.64	0.68	331
41	1805	52	135437	1118	49	77366	210	23	5161	1.61	0.62	358
42	1467	51	112450	865	44	57910	253	29	7785	1.70	0.63	354
43	1990	50	150686	956	44	62348	433	36	16633	2.08	0.66	342
44	2695	52	215635	1180	47	83761	578	39	24171	2.28	0.67	338
45	920	48	62967	556	43	34076	182	26	4976	1.65	0.62	360
46	1324	54	109015	699	46	49262	281	37	11024	1.89	0.64	348
47	763	48	53967	443	47	30404	113	23	2759	1.72	0.62	359
48	1922	49	144908	1272	38	74262	407	34	14691	1.51	0.62	359
49	1429	56	120664	748	48	54765	315	37	12468	1.91	0.64	349
50	1284	52	95693	729	48	48191	168	27	4828	1.76	0.64	348
51	2239	57	191998	1017	50	74567	521	38	21081	2.20	0.67	337
52	1271	49	95310	622	45	42307	193	31	6281	2.04	0.66	340
53	3322	54	277437	1446	54	119130	725	46	35567	2.30	0.64	349
54	3539	52	285335	1759	45	121729	893	37	35555	2.01	0.64	348
55	1206	51	89040	746	50	50999	123	25	3229	1.62	0.62	358
56	2338	59	212083	1122	56	95743	535	46	26283	2.08	0.63	352
57	812	50	60194	417	48	29032	103	28	3087	1.95	0.65	344

58	1993	52	153763	1058	46	74217	360	33	12687	1.88	0.64	350
59	1310	50	98054	713	43	45327	257	31	8522	1.84	0.65	347
60	1409	55	115624	655	52	51597	294	43	13596	2.15	0.64	350
61	2254	51	170457	1424	44	93086	380	32	13011	1.58	0.62	361
62	740	47	53676	449	48	32347	97	25	2569	1.65	0.61	365

Sample 9: YQ18-01a

ID	D1_int	D1_FWHM	D1_area	G_int	G_FWHM	G_area	D2_int	D2_FWHM	D2_area	R1	R2	T
1	276	42	15564	374	32	15752	62	23	1502	0.74	0.47	425
2	666	42	43171	690	32	31823	130	34	6743	0.97	0.53	401
3	385	40	22468	685	29	28189	91	28	2666	0.56	0.42	449
4	434	39	25025	564	32	25825	80	23	1925	0.77	0.47	425
5	766	41	42765	1060	32	47010	166	22	3959	0.72	0.46	433
6	526	41	28158	675	33	29507	117	22	2758	0.78	0.47	429
7	468	36	26090	533	31	23289	106	23	2645	0.88	0.50	413
8	560	40	30701	828	32	36929	100	21	2279	0.68	0.44	441
9	353	41	19312	594	31	25241	76	26	2104	0.60	0.41	453
10	452	40	25667	565	32	24883	93	25	2494	0.80	0.48	421
11	414	39	24800	740	27	28686	142	23	3496	0.56	0.44	443
12	733	42	42880	1127	33	50151	147	23	3567	0.65	0.44	439
13	264	39	13928	316	32	13702	55	21	1209	0.83	0.48	421
14	387	41	21078	475	33	20665	79	24	2026	0.81	0.48	422
15	301	39	17418	374	32	16292	67	25	1816	0.81	0.49	418
16	270	42	14039	864	21	27312	69	35	2525	0.31	0.32	495
17	835	42	47749	1669	30	69868	161	25	4260	0.50	0.39	463
18	576	41	35036	940	24	34125	174	22	4117	0.61	0.48	423
19	802	40	43377	964	33	43554	149	23	3602	0.83	0.48	423
20	538	38	31061	653	31	28088	122	24	3135	0.82	0.50	414
21	229	40	13625	325	33	14184	49	24	1242	0.70	0.47	428
22	400	40	24462	542	30	22686	110	28	3256	0.74	0.49	420
23	458	41	25185	920	30	37555	93	23	2317	0.50	0.39	465
24	742	41	41001	1500	29	61215	120	23	2895	0.50	0.39	464
25	378	40	21982	986	25	36053	116	21	2573	0.38	0.36	476
26	454	41	25972	649	32	29243	93	28	2766	0.70	0.45	437
27	521	40	29522	728	33	33427	104	21	2365	0.72	0.45	435
28	297	38	16437	462	30	19372	56	24	1407	0.64	0.44	440
29	433	39	26039	452	29	18230	163	27	4704	0.96	0.53	399
30	389	39	20928	680	25	24706	131	16	2199	0.57	0.44	442
31	695	42	45557	1585	22	53835	259	17	4682	0.44	0.44	442

Sample 11: YQ18-03

ID	D1_int	D1_FWHM	D1_area	G_int	G_FWHM	G_area	D2_int	D2_FWHM	D2_area	R1	R2	T
1	578	47	41765	1925	24	71630	191	14	2912	0.30	0.36	478
2	212	37	12013	633	23	21440	76	24	1937	0.33	0.34	487
3	209	39	12634	430	21	13952	85	19	1754	0.49	0.45	438
4	391	42	25269	538	29	24048	129	18	2416	0.73	0.49	419
5	147	38	8570	349	19	9400	101	26	2764	0.42	0.41	453
6	180	38	10609	285	22	9317	177	18	4650	0.63	0.43	445
7	128	35	6893	192	28	8273	33	19	948	0.67	0.43	446
8	251	39	15134	475	23	16109	175	25	4605	0.53	0.42	449
9	177	46	12623	282	29	12651	63	28	1859	0.63	0.47	429
10	132	38	7690	200	28	8511	89	21	2450	0.66	0.41	453
11	267	41	16862	513	27	21309	119	24	3114	0.52	0.41	455
12	168	40	10423	252	24	9327	112	24	3672	0.67	0.45	439
13	180	42	11793	452	21	14911	92	27	2610	0.40	0.40	458
14	375	37	21445	534	28	22654	89	28	2616	0.70	0.46	432
15	191	39	11561	253	25	8361	142	22	4063	0.76	0.48	422
16	250	36	13812	456	20	13406	153	26	4266	0.55	0.44	441
17	121	41	7598	265	25	10367	51	21	1119	0.46	0.40	460
18	385	40	23724	510	33	24853	76	23	1989	0.76	0.47	428
19	176	35	9580	289	26	11828	54	18	1211	0.61	0.42	448
20	203	48	15025	421	26	16959	88	21	2008	0.48	0.44	440
21	451	35	22076	704	27	26370	72	22	1680	0.64	0.44	441
22	117	41	7404	171	25	6212	67	18	1827	0.68	0.48	423
23	336	39	19492	668	27	26117	60	24	1519	0.50	0.41	453
24	672	40	38961	1118	31	50763	120	23	2989	0.60	0.42	450
25	515	40	30435	748	27	30724	155	19	3210	0.69	0.47	426
26	203	40	12701	271	30	11055	58	29	1753	0.75	0.50	414
27	186	41	11661	258	25	9943	88	28	2880	0.72	0.48	424

28	216	37	12347	274	31	12127	60	25	1603	0.79	0.47	426
29	185	40	11533	259	32	11512	62	18	1174	0.71	0.48	424
30	94	31	4463	138	24	4985	73	18	2070	0.68	0.39	465
31	251	43	16720	393	26	15903	75	28	2216	0.64	0.48	423
32	1750	37	86149	3686	26	135480	288	22	6808	0.47	0.38	469
33	215	36	12003	299	27	12157	49	34	1752	0.72	0.46	430
34	317	37	18073	448	28	18196	99	23	2449	0.71	0.47	429
35	362	35	19676	396	27	15754	99	26	2680	0.91	0.52	406
36	260	43	17048	421	25	16380	115	24	3088	0.62	0.47	429
37	553	43	32951	1420	30	59883	113	25	3019	0.39	0.34	485
38	351	41	22407	646	21	21310	142	22	3358	0.54	0.48	424
39	139	38	8100	188	27	7746	85	21	1940	0.74	0.46	434
40	221	42	14306	327	27	13245	85	24	2187	0.68	0.48	422
41	382	37	22084	573	27	23396	116	26	3179	0.67	0.45	434
42	258	37	14374	368	31	16212	58	28	1714	0.70	0.45	439
43	266	38	15521	387	28	15443	68	22	1605	0.69	0.48	424
44	181	41	11388	384	25	15153	80	20	1717	0.47	0.40	458
45	257	35	13956	489	28	20552	71	24	1797	0.53	0.38	466
46	247	37	14287	354	26	13748	85	26	2367	0.70	0.47	427
47	635	24	23871	321	45	22409	132	22	3085	1.98	0.48	421

Sample 12: YQ18-05

ID	D1_int	D1_FWHM	D1_area	G_int	G_FWHM	G_area	D2_int	D2_FWHM	D2_area	R1	R2	T
1	385	43	25629	414	28	15474	176	26	4804	0.93	0.56	387
2	189	55	14184	338	14	7426	129	58	7994	0.56	0.48	423
3	264	40	16179	168	30	5525	135	24	4219	1.57	0.62	357
4	2216	48	162748	1243	39	74174	429	36	16419	1.78	0.64	349
5	1074	41	68417	833	34	39220	250	28	7334	1.29	0.60	370
6	469	46	30021	305	38	15127	119	34	5861	1.54	0.59	373
7	1505	43	94470	1153	34	57190	271	29	8491	1.31	0.59	373
8	234	37	13408	183	25	6492	155	21	4027	1.28	0.56	386
9	285	44	19201	194	31	8825	141	27	4953	1.47	0.58	376
10	556	48	41380	466	35	22578	228	29	7072	1.19	0.58	376
11	421	49	30034	409	28	17586	121	33	4204	1.03	0.58	377
12	1173	40	66533	1089	34	50646	219	25	5774	1.08	0.54	395
13	401	47	28776	349	32	17295	132	33	4614	1.15	0.57	383
14	467	33	23958	517	25	18006	166	23	4011	0.90	0.52	404
15	373	48	27333	373	33	18863	89	24	2302	1.00	0.56	385
16	524	40	31531	415	30	17785	178	22	4188	1.26	0.59	373
17	430	45	29636	366	37	20986	91	27	2598	1.17	0.56	388
18	524	48	38973	537	32	23990	162	26	4533	0.97	0.58	378
19	503	44	34215	447	32	20582	199	25	7408	1.12	0.55	391
20	1522	36	80539	1851	29	76570	447	21	9808	0.82	0.48	421
21	515	42	33367	220	30	6966	304	22	9932	2.34	0.66	339
22	860	40	50294	1027	32	47930	226	22	5936	0.84	0.48	421
23	795	39	47386	667	33	31178	243	23	5932	1.19	0.56	386
24	1090	57	95402	1151	37	66443	247	28	7479	0.95	0.56	385
25	877	43	58014	893	31	41680	244	29	7561	0.98	0.54	395
26	1135	46	80861	431	38	23272	351	36	13277	2.63	0.69	328
27	532	35	25843	759	29	31530	123	20	2564	0.70	0.43	445
28	609	40	37518	310	29	11762	249	29	7572	1.97	0.66	341
29	501	48	35893	457	37	21353	137	22	3241	1.10	0.59	371
30	438	36	23224	607	29	26078	111	19	2936	0.72	0.44	439
31	951	38	56346	1004	30	43806	321	23	8273	0.95	0.52	405
32	604	49	43136	484	33	23857	190	29	5913	1.25	0.59	372
33	701	44	43467	558	33	25917	173	27	4902	1.26	0.59	375
34	738	46	51905	500	33	24284	271	31	9346	1.48	0.61	365
35	610	41	38715	542	31	23312	249	26	6996	1.13	0.56	386
36	523	39	30581	425	31	16702	172	27	4934	1.23	0.59	375
37	803	36	44698	730	29	31350	248	22	5881	1.10	0.55	393
38	723	37	41314	631	29	25522	245	24	6323	1.15	0.56	384
39	1071	39	63979	830	30	36979	344	20	7425	1.29	0.59	372
40	735	43	44911	398	36	17691	178	30	5693	1.85	0.66	342
41	429	39	26129	397	29	15261	214	24	5387	1.08	0.56	387
42	1175	34	60774	1114	28	43796	329	21	7522	1.05	0.54	394
43	1200	40	68882	1058	35	50178	274	22	6268	1.13	0.55	391
44	405	43	24947	371	37	17222	91	23	2248	1.09	0.56	385
45	981	37	55639	756	30	32191	337	21	7604	1.30	0.58	376
46	415	43	27785	259	31	12456	188	34	6707	1.60	0.59	372
47	1095	37	56524	1279	30	54277	252	20	5411	0.86	0.49	420
48	868	39	46265	803	33	35367	179	23	4363	1.08	0.54	396
49	936	36	48556	1059	30	45075	235	21	5510	0.88	0.49	418
50	411	38	21385	478	30	20260	93	21	2104	0.86	0.49	419
51	512	36	25424	572	29	23183	110	21	2408	0.90	0.50	414
52	869	36	43243	987	30	41739	197	21	4334	0.88	0.48	421

53	2393	36	128035	2289	28	95120	596	19	11891	1.05	0.54	393
54	1468	45	102247	1186	36	65544	278	25	7350	1.24	0.58	375
55	1427	41	89858	1196	32	55411	389	21	8524	1.19	0.58	375
56	1283	40	79790	985	31	47246	415	21	9301	1.30	0.59	375
57	1697	40	104084	1599	33	75305	418	20	9029	1.06	0.55	390
58	1413	49	107201	1117	36	61300	494	16	8482	1.27	0.61	365
59	719	38	42045	629	36	34849	173	17	3676	1.14	0.52	404
60	776	39	42739	780	33	34844	163	22	3791	1.00	0.53	402
61	1206	42	72842	928	37	47003	210	23	5084	1.30	0.58	376
62	1253	39	73386	1137	32	52025	336	20	7018	1.10	0.55	389
63	1289	46	91896	1072	40	65252	215	26	5886	1.20	0.56	385
64	1125	52	86475	943	39	55090	271	36	10493	1.19	0.57	382
65	686	43	45080	604	34	31849	110	25	2982	1.13	0.56	384
66	1648	40	101492	1321	34	64327	454	20	9671	1.25	0.58	378
67	951	44	61514	814	35	41582	198	28	5833	1.17	0.56	384
68	2076	44	140895	2053	35	108761	471	24	12006	1.01	0.54	396
69	644	41	38074	625	35	30975	146	21	3294	1.03	0.53	402
70	1475	38	81202	1515	31	66677	347	22	8225	0.97	0.52	404

Sample 14: YQ18-11

ID	D1_int	D1_FWHM	D1_area	G_int	G_FWHM	G_area	D2_int	D2_FWHM	D2_area	R1	R2	T
1	999	42	61508	3007	22	101733	291	15	6726	0.33	0.36	476
1	593	43	38984	1682	30	73437	142	20	3025	0.35	0.34	487
2	696	53	56897	925	36	50857	178	29	7930	0.75	0.49	417
3	704	42	45743	934	28	41122	201	22	4804	0.75	0.50	414
4	322	39	19465	475	30	21635	66	20	1423	0.68	0.46	433
5	361	42	23538	848	27	35106	87	12	1439	0.43	0.39	463
6	451	44	29810	1477	27	57795	130	20	2840	0.31	0.33	491
7	903	39	54865	1422	25	54536	313	18	6054	0.63	0.48	425
8	193	41	12250	280	31	13369	40	23	947	0.69	0.46	431
9	396	43	26116	480	33	24688	61	14	920	0.83	0.50	411
10	249	44	16912	355	28	15375	79	15	1689	0.70	0.50	415
11	782	38	42799	1056	30	44955	196	22	4554	0.74	0.46	430
12	183	59	16502	411	32	20108	59	19	1428	0.45	0.43	444
13	1010	39	60285	1253	31	59592	177	23	4231	0.81	0.49	420
14	413	59	37202	1713	26	69181	122	19	3683	0.24	0.34	487
15	600	43	39806	914	26	36257	183	19	5337	0.66	0.49	418
16	997	41	62428	1176	32	58972	151	22	3594	0.85	0.50	414
17	488	42	31888	708	33	35203	98	24	2488	0.69	0.46	432
18	1108	42	71583	1554	29	70507	288	17	5874	0.71	0.48	421
19	1534	40	91602	1916	31	87262	265	23	6414	0.80	0.49	416
20	749	43	49297	1382	29	61417	154	20	3400	0.54	0.43	444
21	1658	48	121669	2203	34	114118	352	16	8551	0.75	0.50	414
22	298	41	18810	448	29	20219	68	21	1564	0.67	0.46	430
23	1196	39	70850	2050	28	87586	216	18	4148	0.58	0.44	443
24	512	43	34027	1353	28	58959	321	19	6447	0.38	0.34	485
25	465	42	29940	585	26	23691	150	20	4202	0.79	0.52	405
26	1096	61	101633	1662	33	83854	365	24	13253	0.66	0.51	408
27	1375	44	92570	1534	30	72283	342	15	6383	0.90	0.54	395
28	1342	40	80398	1698	32	81008	305	19	6244	0.79	0.48	423
29	413	41	26260	461	29	20838	78	15	1437	0.90	0.54	395
30	724	43	47999	1135	28	48832	177	15	4007	0.64	0.48	424
31	388	40	23935	688	25	26405	132	14	2796	0.56	0.45	436
32	958	46	67934	1244	33	63580	194	26	7849	0.77	0.49	419
33	468	39	28044	801	32	37815	83	21	1805	0.58	0.41	452
34	551	42	35522	579	30	26746	127	21	3281	0.95	0.54	394
35	721	41	45362	1128	30	51894	144	20	3822	0.64	0.45	437
36	268	36	15089	408	23	14652	96	23	2687	0.66	0.47	429
37	119	51	9304	137	38	7992	8	12	107	0.86	0.53	398
38	215	47	15682	377	33	18931	74	13	1270	0.57	0.44	442
39	101	61	9490	143	30	6624	29	50	2159	0.71	0.52	405
40	163	168	39850	127	0	32	223	64	20154	1.28	0.66	339
41	543	43	35791	763	29	34459	182	14	3411	0.71	0.49	420
42	536	45	34540	934	29	40770	103	22	2382	0.57	0.44	439
43	703	44	47784	1011	25	39418	268	14	4839	0.70	0.52	405
44	428	38	25445	514	30	23892	63	24	1591	0.83	0.50	414
45	869	39	51045	1096	32	53351	132	23	3191	0.79	0.47	425
46	547	46	39112	928	28	40427	160	22	3952	0.59	0.47	428
47	530	43	35500	760	28	32431	172	19	4981	0.70	0.49	419
48	401	39	24317	568	33	28975	73	15	1733	0.71	0.44	440
49	287	44	19651	496	33	24986	73	23	2645	0.58	0.42	452
50	387	40	24222	541	30	25045	95	18	1804	0.72	0.47	425
51	712	41	44558	874	32	41590	149	23	3604	0.81	0.50	415
52	447	40	26233	606	32	28162	69	25	1820	0.74	0.47	429
53	350	34	18430	487	32	23858	42	16	689	0.72	0.43	446
54	240	40	14852	293	30	13589	59	20	1247	0.82	0.50	413

55	332	66	33580	447	37	25347	112	32	5513	0.74	0.52	404
56	1464	50	112145	2056	29	92146	547	17	14262	0.71	0.51	408

Sample 15: YQ18-12

ID	D1_int	D1_FWHM	D1_area	G_int	G_FWHM	G_area	D2_int	D2_FWHM	D2_area	R1	R2	T
1	449	45	28812	1108	28	46579	83	22	1915	0.41	0.37	471
2	95	46	5998	253	28	10946	20	15	457	0.37	0.34	484
3	73	45	4708	168	27	6882	33	13	681	0.44	0.38	466
4	112	45	6562	534	26	19418	22	28	653	0.21	0.25	529
5	296	43	18957	515	27	20992	68	23	1675	0.58	0.46	434
6	212	45	12781	756	28	29226	42	25	1109	0.28	0.30	506
7	177	41	10785	269	34	12811	33	25	849	0.66	0.44	440
8	670	41	40482	888	29	39975	114	22	2624	0.75	0.49	419
9	249	39	14865	312	30	14561	45	22	1049	0.80	0.49	419
10	138	38	8076	208	31	9309	28	25	732	0.66	0.45	438
11	211	39	12884	315	30	14728	38	21	931	0.67	0.45	436
12	189	44	11997	1106	24	38066	49	30	1544	0.17	0.23	535
13	244	39	13319	630	27	23521	57	23	1388	0.39	0.35	482
14	870	37	45746	1235	29	53070	141	19	2951	0.70	0.45	436
15	196	39	11852	286	30	13303	34	17	871	0.69	0.46	434
16	207	41	12316	346	30	14933	41	25	1098	0.60	0.43	443
17	172	43	9408	777	26	28988	45	25	1193	0.22	0.24	533
18	514	42	33599	908	31	43721	75	19	1521	0.57	0.43	447
19	345	37	18521	565	28	21482	70	25	1862	0.61	0.44	440
20	344	44	23154	577	30	27173	61	22	1443	0.60	0.45	438
21	641	37	36110	719	29	31544	99	23	2461	0.89	0.52	407
22	201	37	11401	349	27	13515	28	20	600	0.58	0.45	438
23	257	40	15370	572	30	24467	50	24	1281	0.45	0.37	471
24	245	39	14139	255	31	11303	37	22	843	0.96	0.54	396
25	134	42	8249	164	30	7250	22	26	591	0.82	0.51	408
26	277	40	15102	535	29	21542	44	22	997	0.52	0.40	458
27	626	42	34633	1164	30	47698	110	23	2737	0.54	0.41	456
28	232	41	14040	335	31	15511	37	25	965	0.69	0.46	432
29	246	43	14969	410	30	17871	42	28	1261	0.60	0.44	441
30	228	41	13072	715	26	26292	47	23	1125	0.32	0.32	494
31	191	40	11722	269	29	11947	30	28	890	0.71	0.48	424
32	583	37	32482	829	29	35284	96	18	1848	0.70	0.47	429
33	491	38	26862	582	31	25398	79	24	2020	0.84	0.49	416
34	345	40	18485	415	31	17395	68	22	1621	0.83	0.49	417
35	277	39	16838	577	29	24182	56	24	1466	0.48	0.40	461
36	252	39	15338	376	30	17683	46	19	944	0.67	0.45	436
37	558	41	32841	580	33	27695	84	22	1967	0.96	0.53	402
38	265	38	15312	369	30	16046	45	20	987	0.72	0.47	426
39	227	39	12817	300	31	13215	38	22	886	0.76	0.48	424
40	118	34	6224	171	28	6993	20	18	389	0.69	0.46	433
41	98	40	6040	154	28	6332	17	26	462	0.64	0.47	427
42	137	40	8402	227	30	9994	28	27	794	0.60	0.44	442
43	225	38	12122	453	26	16906	58	27	1635	0.50	0.40	461
44	212	45	12041	1049	27	38867	51	27	1440	0.20	0.23	536
45	1341	43	89843	1798	36	99042	83	24	2141	0.75	0.47	427
46	448	38	22425	1182	25	40788	125	24	3168	0.38	0.34	487
47	115	45	7612	324	28	12681	34	27	962	0.36	0.36	478
48	90	33	4582	214	25	7361	19	27	559	0.42	0.37	474
49	350	40	16657	1310	27	47441	70	25	1882	0.27	0.25	526
50	381	41	21362	1070	27	40614	84	23	2020	0.36	0.33	489
51	423	37	20401	1043	28	38937	87	22	1982	0.41	0.33	490
52	185	37	10081	399	27	15740	40	29	1211	0.46	0.37	471
53	183	40	10978	412	27	16161	33	26	928	0.44	0.39	463
54	170	39	9778	253	25	9963	42	42	1863	0.67	0.45	435
55	553	37	27700	1100	28	42095	123	24	3084	0.50	0.38	468
56	264	36	14627	625	25	23228	72	30	2253	0.42	0.36	475
57	285	40	15148	466	30	19391	46	24	1181	0.61	0.42	448
58	357	40	20080	494	31	20984	65	25	1744	0.72	0.47	428
59	236	42	11543	941	28	35448	38	24	963	0.25	0.24	531
60	129	40	6765	248	28	9825	23	26	632	0.52	0.39	462
61	352	39	20179	528	28	22292	60	22	1430	0.67	0.46	432

Sample 16: YQ18-13a

ID	D1_int	D1_FWHM	D1_area	G_int	G_FWHM	G_area	D2_int	D2_FWHM	D2_area	R1	R2	T
1	570	37	32362	633	28	26858	161	23	4171	0.90	0.51	409
2	368	35	20184	409	30	18465	122	25	3282	0.90	0.48	422
3	1156	43	76923	1639	26	65268	398	17	8262	0.70	0.51	408

4	2072	45	142851	3635	26	149043	571	13	11486	0.57	0.47	427
5	1351	41	82373	1868	29	81625	311	19	6213	0.72	0.48	421
6	1870	42	122038	2636	26	107159	606	17	10985	0.71	0.51	410
7	824	38	48142	1115	28	48965	196	19	4019	0.74	0.48	424
8	666	36	36670	794	28	33658	161	19	3264	0.84	0.50	414
9	295	32	14822	342	28	14736	98	25	2635	0.86	0.46	432
10	671	38	39434	876	28	37249	157	17	2903	0.77	0.50	416
11	1092	37	61665	1489	26	58415	307	17	5550	0.73	0.49	418
12	677	38	39342	791	27	33063	180	21	4075	0.86	0.51	407
13	889	38	52683	1058	27	43891	209	18	4117	0.84	0.52	403
14	758	40	47270	975	28	41523	205	17	4372	0.78	0.51	410
15	363	42	23717	497	27	19725	107	24	2698	0.73	0.51	407
16	782	46	54832	1074	26	43158	277	18	5223	0.73	0.53	399
17	496	39	30110	682	28	29564	116	26	3247	0.73	0.48	423
18	567	40	35140	773	32	37899	103	18	1984	0.73	0.47	428
19	554	38	32005	748	32	33278	123	24	3201	0.74	0.47	428
20	924	41	57605	1268	31	59873	185	20	3960	0.73	0.47	425
21	760	39	44955	1020	31	48203	136	18	2807	0.74	0.47	428
22	1315	45	91429	1830	29	81113	429	15	8886	0.72	0.50	412
23	818	39	49314	1287	26	52552	235	18	4595	0.64	0.46	430
24	394	41	24845	551	27	22723	103	18	2026	0.72	0.50	413
25	683	39	40649	850	29	37920	170	17	3005	0.80	0.50	414
26	583	38	33972	762	28	32497	155	20	3334	0.77	0.49	420
27	655	45	45047	831	29	37154	231	35	12620	0.79	0.48	425
28	979	42	62478	1122	32	54012	162	23	3997	0.87	0.52	405
29	973	41	62049	1445	28	62153	297	16	5127	0.67	0.48	423
30	889	40	49357	1683	27	66586	183	19	3762	0.53	0.41	453
31	1195	36	66545	1558	28	63487	181	19	3731	0.77	0.50	415
32	404	36	20944	792	24	26386	103	21	2330	0.51	0.42	449
33	453	36	24873	810	24	30168	114	27	3225	0.56	0.43	447
34	365	36	20294	717	26	27558	77	26	2172	0.51	0.41	456
35	416	38	24685	831	24	30806	117	23	2814	0.50	0.42	448
36	298	35	15938	592	26	20825	137	23	3348	0.50	0.40	460
37	966	37	54050	1532	27	59146	183	23	4465	0.63	0.46	432
38	721	41	45662	1073	24	32878	340	33	17347	0.67	0.48	424
39	1375	40	77150	2520	29	106362	174	22	4074	0.55	0.41	454
40	587	38	34118	1228	28	51355	93	24	2358	0.48	0.39	464
41	767	39	46710	1587	28	64519	225	19	4544	0.48	0.40	457
42	1167	39	62386	1854	29	76868	170	22	3951	0.63	0.44	443
43	420	35	22985	620	25	23352	85	22	2015	0.68	0.48	425
44	1306	34	67494	1536	27	61451	198	21	4453	0.85	0.51	411
45	460	36	25889	501	36	27761	104	9	1090	0.92	0.47	426
46	565	40	32144	592	32	27485	100	22	2301	0.95	0.52	405
47	616	41	35652	837	31	37550	131	21	2877	0.74	0.47	428
48	1290	39	78028	1578	31	75987	237	21	5294	0.82	0.49	418
49	1688	42	108345	2641	26	107255	528	17	13996	0.64	0.47	426
50	814	39	48713	1556	25	59986	247	16	4247	0.52	0.43	445
51	814	39	49557	1298	26	52298	275	17	5037	0.63	0.46	430
52	1378	41	86662	1724	28	73982	367	17	7091	0.80	0.52	406
53	675	39	39706	769	31	35046	165	26	4593	0.88	0.50	413
54	978	40	57732	1199	32	54771	213	21	4686	0.82	0.49	417
55	682	40	41377	1171	27	48860	184	17	3501	0.58	0.44	440
56	1085	38	64056	1546	31	73889	220	18	4137	0.70	0.45	436
57	1208	40	74674	2270	28	95563	324	17	5948	0.53	0.42	448
58	589	41	36591	976	31	45657	108	22	2547	0.60	0.43	445
59	1242	40	75699	1479	30	66605	299	21	6745	0.84	0.51	410
60	874	42	55990	1143	32	53679	192	21	4375	0.76	0.49	418
61	594	40	36368	812	29	35646	152	20	3243	0.73	0.48	421
62	871	36	47096	1130	28	44857	140	24	3536	0.77	0.49	417
63	1166	36	62753	1885	26	73662	210	21	4708	0.62	0.44	439
64	937	36	50356	1179	28	47288	147	22	3497	0.79	0.50	414
65	961	36	51640	1332	28	54328	145	22	3339	0.72	0.47	426
66	401	38	23533	629	28	25504	113	19	2723	0.64	0.45	434

Figure S1:

Representative microscopic features of black schists. Images on the left are in plane-polarized light, and on the right are in cross-polarized light. Abbreviations: Ab = albite; Cal = calcite; CM = carbonaceous material; Chl = chlorite; Ep = epidote; Qz = quartz; Tlc = =talc; Tin = titanite; Wm = white mica.

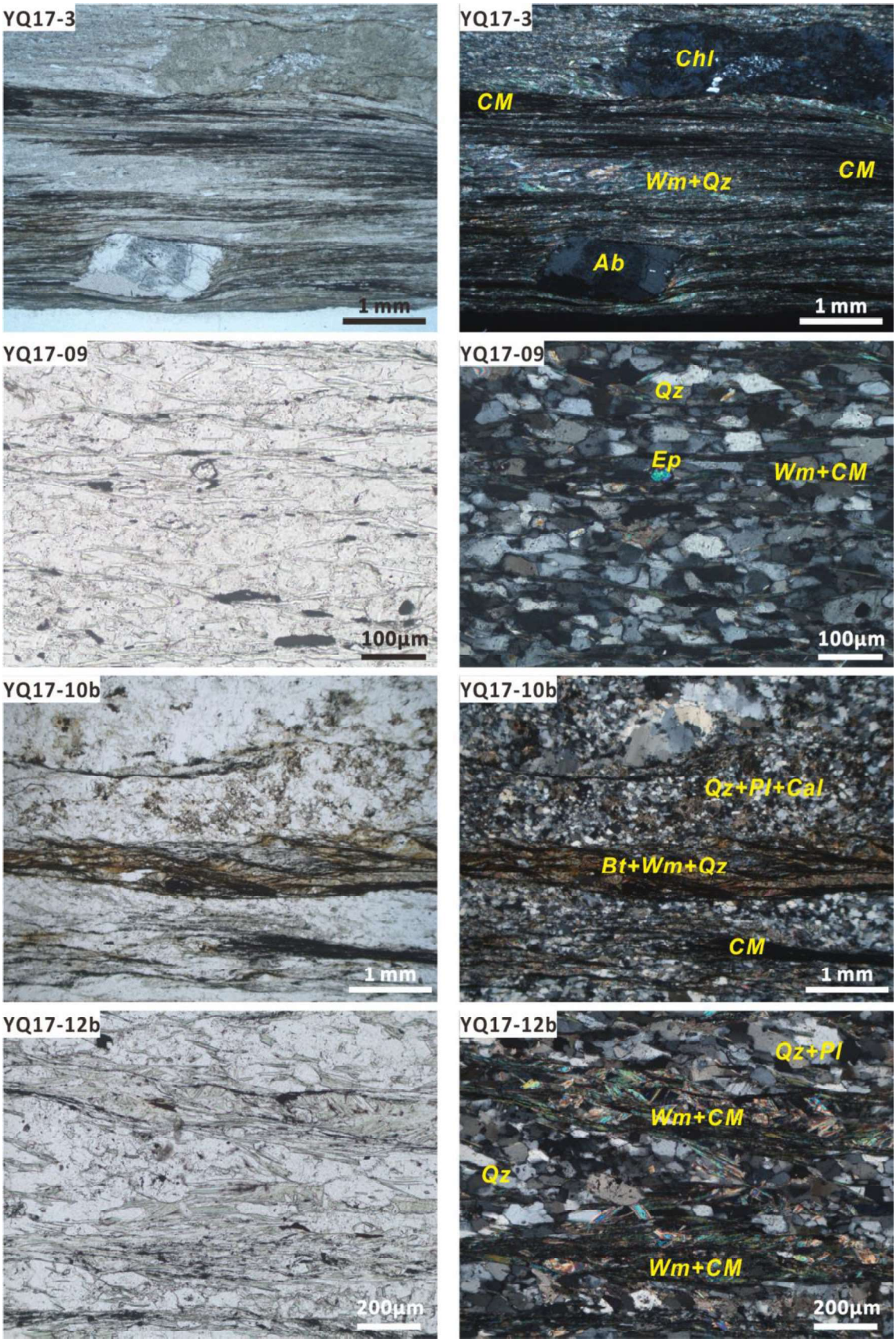

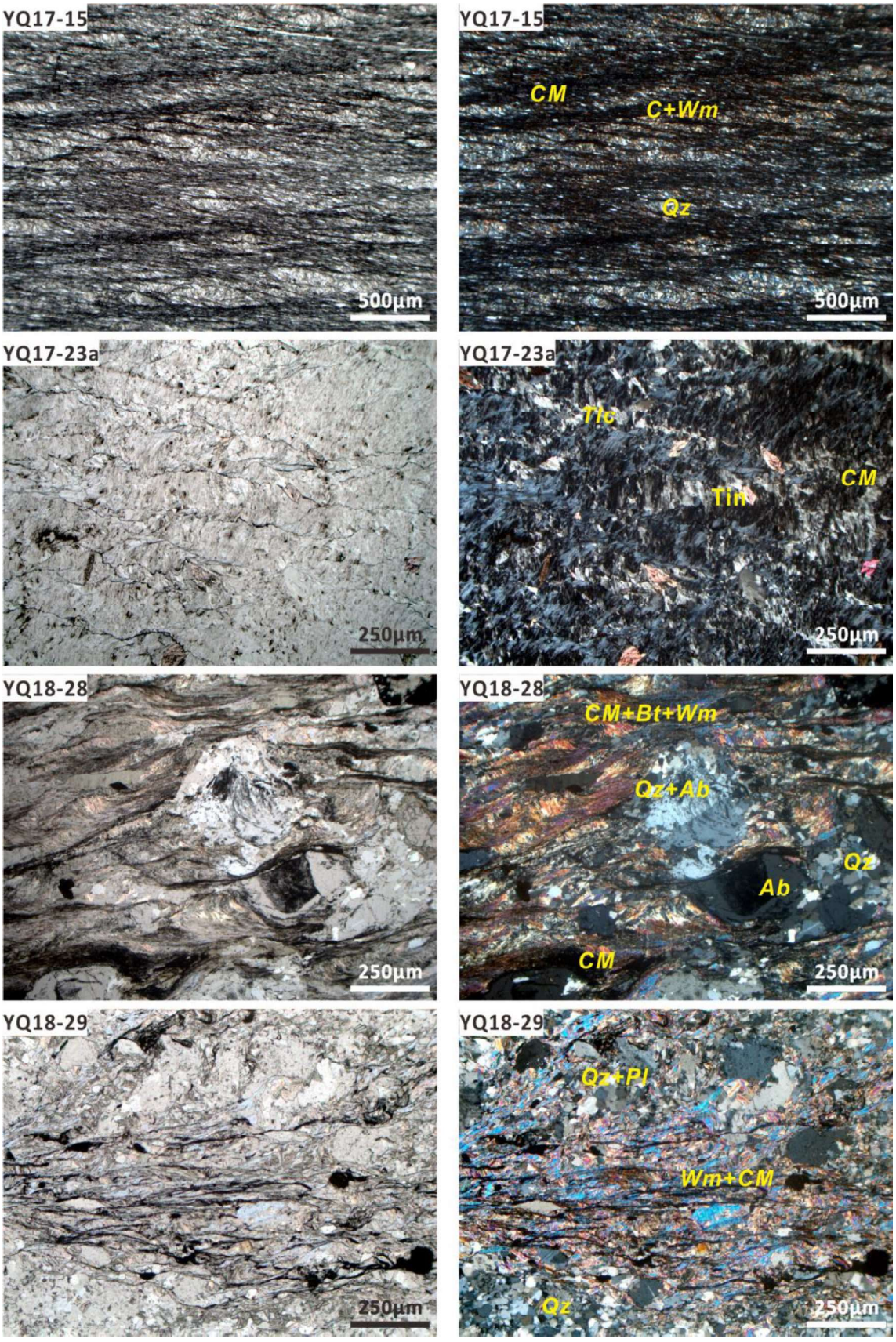
YQ17-15
500μm
YQ17-15
CM
C+Wm
Qz
500μm
YQ17-23a
250μm
YQ17-23a
Tlc
Tin
CM
250μm
YQ18-28
250μm
YQ18-28
CM+Bt+Wm
Qz+Ab
Qz
Ab
CM
250μm
YQ18-29
250μm
YQ18-29
Qz+Pl
Wm+CM
Qz
250μm

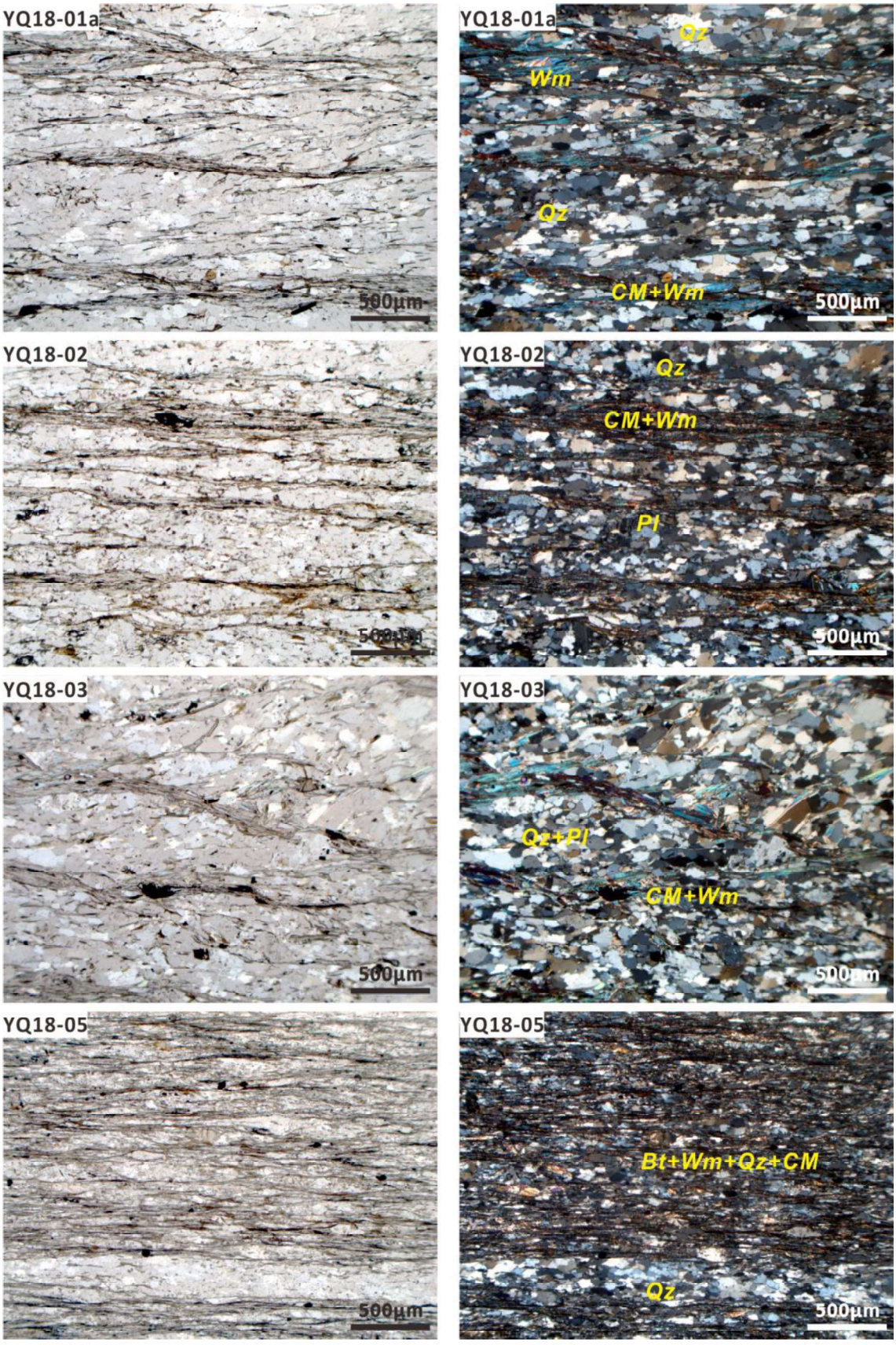
YQ18-01a
500μm
YQ18-01a
Qz
Wm
Qz
CM+Wm
500μm
YQ18-02
500μm
YQ18-02
Qz
CM+Wm
Pl
500μm
YQ18-03
500μm
YQ18-03
Qz+Pl
CM+Wm
500μm
YQ18-05
500μm
YQ18-05
Bt+Wm+Qz+CM
Qz
500μm

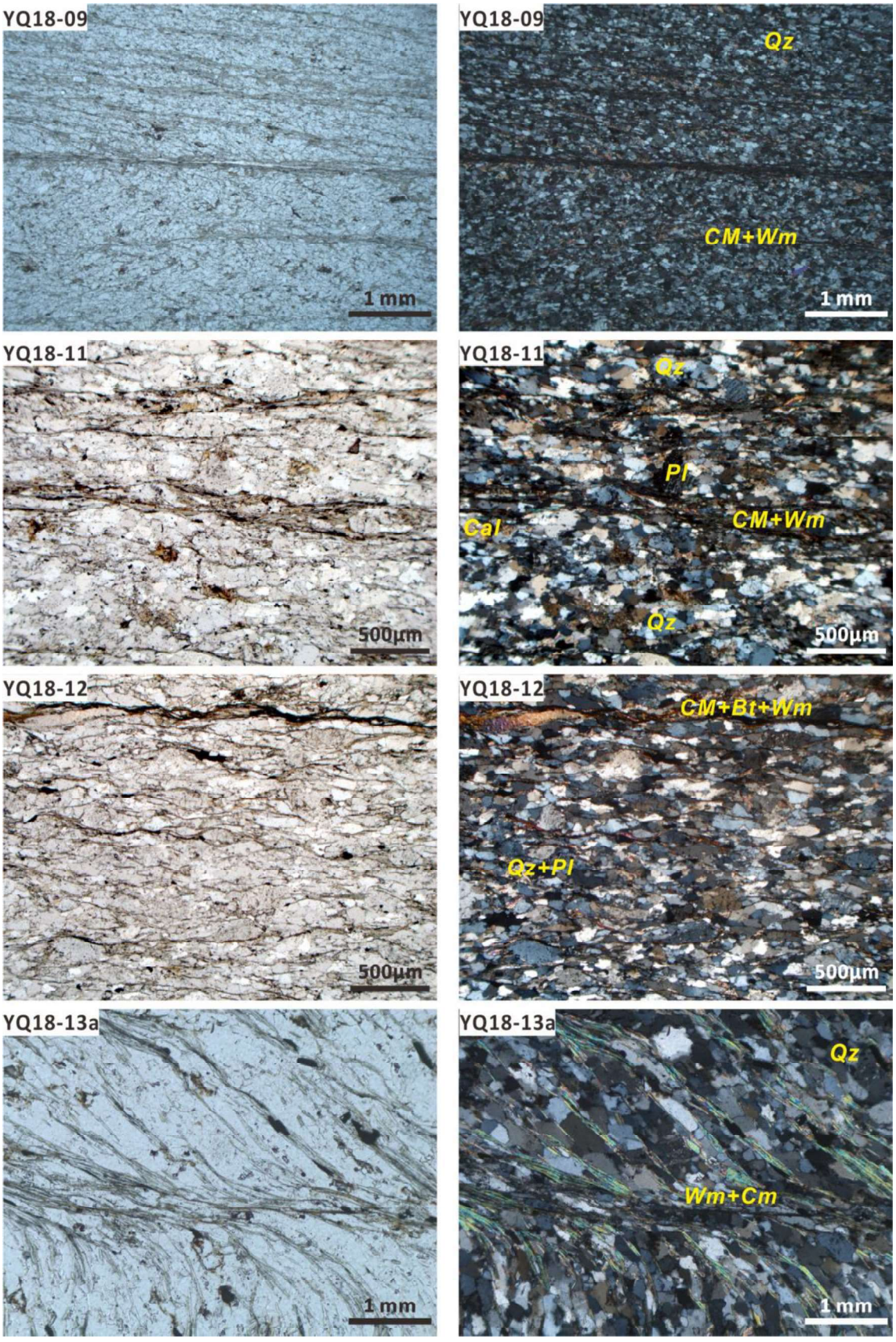
YQ18-09
1 mm
YQ18-09
Qz
CM+Wm
1 mm
YQ18-11
500µm
YQ18-11
Qz
Pl
Cal
CM+Wm
Qz
500µm
YQ18-12
500µm
YQ18-12
CM+Bt+Wm
Qz+Pl
500µm
YQ18-13a
1 mm
YQ18-13a
Qz
Wm+Cm
1 mm

Appendix D (Digital supplemental material)

The digital supplemental material in the attached CD-R is complementary to this dissertation. It provides a GIS database with Taiwan maps, Digital Elevation Models (DEM), and outcrop data, field work reports, MOVE databases with cross sections, Raman measurements with representative spectra, and whole-rock geochemistry data. It also includes the published RSCM (Raman spectroscopy of carbonaceous material) data, Luzon arc geochemistry data for comparison.

File order:

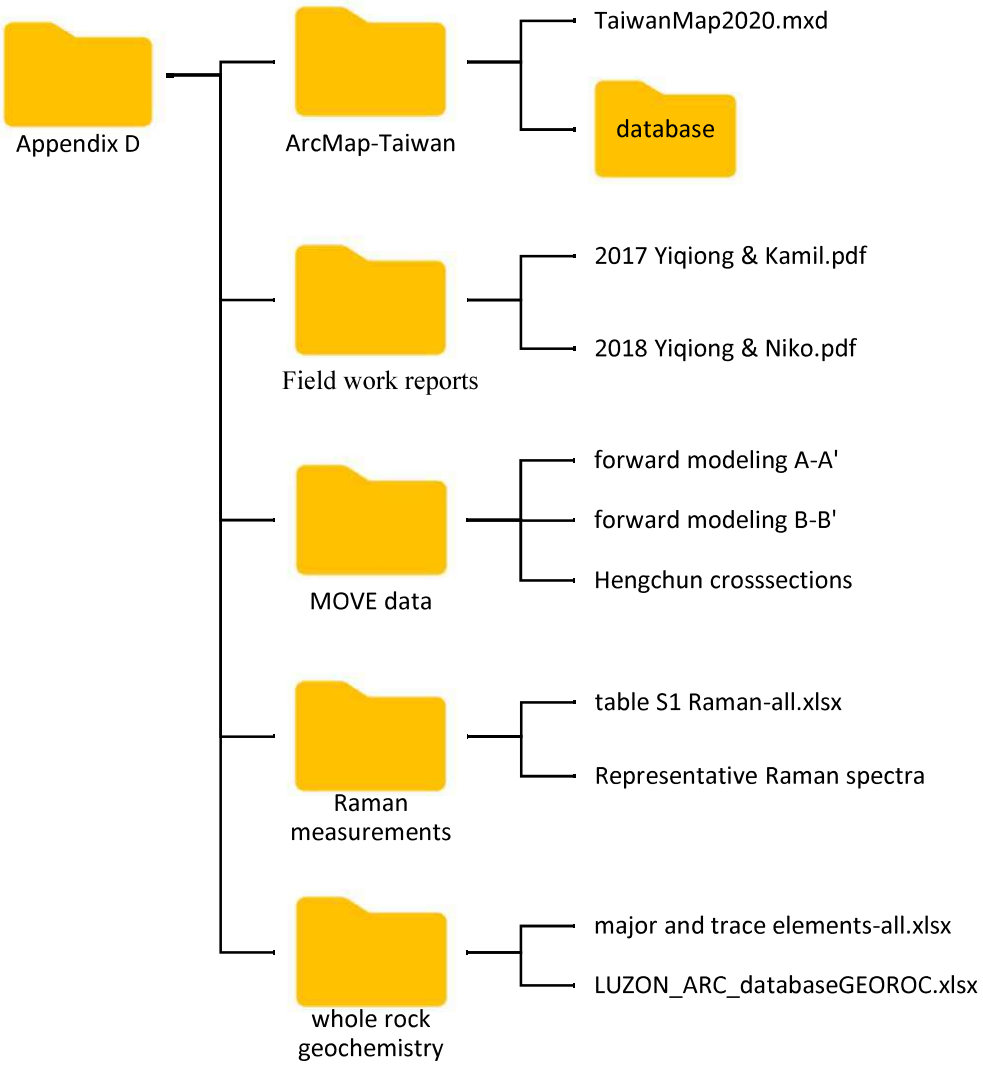

Descriptions:

The GIS database of this dissertation contains maps of Taiwan (in the scales of 1:500 000 and 1:50 000), DEM data of Taiwan and surrounding areas (with the spatial resolution of 40 metres),

outcrop data (with field measurements of several times in Taiwan from 2008 to 2018), and sample location. Our RSCM temperature data as well as the published data (e.g., Beyssac et al., 2007; Conand et al., 2020; Chim et al., 2018; Syu, 2009; Kouketsu et al., 2019) are also provided in the GIS database as a supplement for Chapter 4.

I took two times of field works in Taiwan with my PhD supervisor Prof. Dr. Kamil Ustaszewski, in the year of 2017 and with my second supervisor Prof. Dr. Nikolaus Froitzheim in the year of 2018. The field work reports provide the itinerary of daily trips, outcrop locations, measurements, maps, photos with descriptions. The reports are as supplements for Chapters 2, 3, and 4.

MOVE databases consist of three modelings. (1): Forward modelling of the cross section across Central Cross-island Highway of Taiwan (A-A') in Chapter 2. (2): Forward modelling of the cross section across central Taiwan (B-B') in Chapter 2. (3): Maps, cross sections and measurement database of the Hengchun Peninsula are an independent section of my PhD research work which is not presented in this dissertation.

The whole-rock geochemistry data contains major elements and selected trace elements. Both were measured using X–ray fluorescence (XRF) and, after total digestion, inductively coupled plasma-optical emission spectrometry (ICP–OES) and inductively coupled plasma–mass spectrometry (ICP–MS) at the Institute of Geological Sciences at the Friedrich-Schiller University Jena. The Luzon volcanic arc geochemistry data were taken from the database GEOROC (Geochemistry of Rocks of the Oceans and Continents; http://georoc.mpch-mainz.gwdg.de/georoc/) for comparison.

The dissertation-related published publication is also enclosed in the CD-R:

Zhang, Y., Tsai, C.-H., Froitzheim, N., Ustaszewski, K. (2020): The Yuli Belt in Taiwan: part of the suture zone separating Eurasian and Philippine Sea plates. Terrestrial, Atmospheric and Oceanic Sciences, 31, 415-435, doi: 10.3319/TAO.2020.06.28.01

Acknowledgements

First, I would like to sincerely thank **Prof. Dr. Kamil Ustaszewski**, my supervisor, for providing me this interesting work. I still remember our first skype-meeting on 24.11.2015, regarding the Taiwan project and the CSC application, at which time he was the reason that I decided to come to Jena. After these four years, I am completely convinced that I made a good decision and what I learnt is far beyond my expectation. His generous supervision made me feel comfortable in pursuing different subjects, and during my research, his immense knowledge and constant encouragement profoundly influenced and inspired me. With his generous patience, I can gradually grow up and broaden my view in the field of structural geology.

I am especially indebted to **Prof. Dr. Nikolaus Froitzheim** from Rheinische Friedrich-Wilhelms-Universität Bonn and **Prof. Dr. Chin-Ho Tsai** from National Dong Hwa University, Taiwan. They supervised me in the fieldwork and during the paper submissions not only as scientific-project partners, but also as generous friends. I also wish to acknowledge Master students (**Chiao Liu**, **Wen-Han Lo**, **Chih-Ying Yeh**, **Dominikus Deka Dewangga**, and **Yu-Wei Chang**) from National Dong Hwa University for fieldwork assistance.

Many thanks also go to my colleagues (**Dr. Christoph Grützner**, **Philipp Balling**, **Georg Löwe**, **Benjamin Schmitz**, **Mjahid M. Zebari**, **Chris Salomon**, **Madeline Richter**, **Dr. Taufeeq Dhansay** and **Dr. Payman Navabpour**) in the JST working group for their kindness and constant emotional support. I greatly appreciate them who offered the guidance and support over the years. Moreover, I thank **Dr. Kilian Pollok**, **Prof. Dr. Lothar Viereck**, **Dr. Sami Nabhan**, **Dr. Stefan Kiefer**, and **Dr. Arno Märten** for valuable discussions on lab experiments. I thank **Frank Linde**, **Sandra Urban**, **Michael Ude**, and **Dr. Dirk Merten** for sample preparations. The great working environment established the crucial basis of all the research works. I wish the nice memories would always last and continue in the IGW building.

The final words of thanks must be reserved for my **family**. My boyfriend Hongpu Zhou supported me whenever I needed him, and I thank you with all my heart. I would like to thank my parents for supporting me spiritually throughout my life. No matter where I am, on the way to chase my dream, they are always the strongest backing of mine.

This dissertation and my doctor study were funded by the Deutsche Forschungsgemeinschaft (DFG; grant 380155214) as well as the China Scholarship Council (CSC; number 201606400062).

Selbstständigkeitserklärung

Ich erkläre, dass ich die vorliegende Arbeit selbständig und unter Verwendung der angegebenen Hilfsmittel, persönlichen Mitteilungen und Quellen angefertigt habe.

Jena, den 10. Sep. 2020 Yiqiong Zhang